Physio-Biochemical Properties of Water Hyacinth based Bio-materials and its Application in Soil Amendment

Thesis

submitted in partial fulfillment of the requirements
of the degree of

DOCTOR OF PHILOSOPHY

by

SANANDAM BORDOLOI

Roll No. 156104017

Department of Civil Engineering
Indian Institute of Technology Guwahati
Guwahati - 781039, India

June 2019

Dedicated to my beloved mother

CERTIFICATE

This is to certify that the thesis entitled **"Physio-biochemical Properties of Water hyacinth based Bio-materials and its application in Soil Amendment"** submitted by Sanandam Bordoloi to the Indian Institute of Technology Guwahati, for the award of the degree of Doctor of Philosophy (PhD) in Civil Engineering is a record of bonafide research work carried out by him under my supervision and guidance. The thesis work, in my opinion, has reached the requisite standard fulfilling the requirement for the degree of Doctor of Philosophy.

The results contained in this thesis have not been submitted in part or full to any other University or Institute for award of any degree or diploma.

IIT Guwahati

Date:

Dr. Sreedeep Sekharan
Professor
Department of Civil Engineering
Indian Institute of Technology Guwahati
Guwahati- 781039
India

STATEMENT

I do hereby declare that the matter embodied in this thesis is the result of investigations carried out by me in the department of Civil Engineering, Indian Institute of Technology Guwahati (IITG), Guwahati, Assam, India.

In keeping with the general practice of reporting scientific observations, due acknowledgements have been made wherever the work described is based on the findings of other investigators.

IIT Guwahati
Date:

Sanandam Bordoloi

ACKNOWLEDGEMENTS

The major work of completing this research work was made possible with continuous guidance and support of my supervisor Dr. Sreedeep Sekharan. His insight, motivation and direction have helped me navigate the doctoral tenure with ease. Special thanks are given to my former co-supervisor Dr. Ankit Garg during his tenure in IITG with whom I continue to draw technical insight and guidance. I am grateful to my doctoral committee members Dr. Anil Kumar Mishra, Dr. Ravi Karangat, and Dr. Prasenjit Khanikar for their valuable suggestions and encouragement at every stage of this research work.

I am indebted to my family members: father Chandra Kanta Bordoloi, mother Himani Devi Bordoloi, brothers Subhangam and Sarangam Bordoloi, sister-in-law Prity Sarmah, niece Umica Bordoloi for their support and encouragement during my PhD tenure. I am especially filled with gratitude for my mother who has beard great adversity during my PhD tenure; yet has encouraged me to pursue this lifelong dream of mine.

Special thanks need to be mentioned for my research colleagues- Vinay Kumar Gadi and Rojimul Hussain, who have constantly encouraged and worked side-by-side in our research endeavors. I would like to acknowledge the love, friendship and support of my colleagues in Indian Institute of Technology Guwahati. They are: Dr. Sudheer, Mr. Bhaskar, Ms. Saswati, Ms. Monikongkona, Mr. Harsha, Mr. Sagar, Mr. Himanshu, Mr. Shivam, Mr. Chandrabhanu, Mr. Janarul, Mr. Abhishekh, Mr. Atma Prakash, Mr. Deepak, Mr. Anant, Ms. Saswati B, Ms. Rohini and Mr. Pradeep. Kind regards to Mr. Suriya who has assisted in the proof check of the thesis. I am really thankful to Mr. Hariram Upadhay and Mr. Samarjyoti Kalita for their help in carrying out laboratory experiments.

I am also filled with gratitude to all the faculty members, staff members of Civil engineering department, IIT Guwahati and to all those who have been related to this study, either directly or indirectly, in smooth completion of the project work. I am thankful to Central Instruments Facility (CIF) of IITG for providing research facility which helped in the study.

Sanandam Bordoloi

Contents

Abstract

Escalating cost of petroleum based geo-synthetic products and concern for environment have motivated researchers to explore alternate natural based geo-amendments. Lignocellulose based natural fibers, geotextiles and biochar derived from plant have been explored as alternative soil amendment material. *Eichorrnia Crasipes* popularly known as water hyacinth (WH) is one of the world's most invasive plant species which causes various ecological problems as well as blocks water bodies. The management of this weed produces a lot of waste bio-mass with relatively no usage. The current study finds motivation from the aforementioned problem of waste management and need for eco-friendly amendment material; to explore WH as a potential bio-material in the form of discrete fibers, geotextiles and biochar.

All the biomaterials fabricated from WH were characterized for its inherent bio-chemical composition, physical properties, surface morphology, thermal response and functional groups. The soil- WH fiber composite as randomly distributed fiber reinforced soil (RDFS) and geotextiles were tested for its mechanical strength using a series of Unconfined compressive strength (UCS) and California Bearing ratio (CBR) test respectively. UCS tests were done in comparison with other two conventional natural fibers (jute and coir). The mechanical strength of soil-biochar composite in terms of UCS was investigated for biochars derived from WH and peanut shell. The hydraulic performance was assessed based on soil water retention capacity (SWRC), desiccation crack potential and infiltration for soil-WH fiber composite. The vegetation potential along with SWRC and desiccation potential for soil-WH fiber composite was explored by conducting induced drought conditions. A basic bio-degradation assessment of WH fiber in embedded soil was conducted considering changes in bio-chemical composition, soil-fiber composite strength and microbial activity. The improvement in mechanical strength of soil-nanoparticle treated WH fiber has been investigated by conducting UCS, CBR and direct shear strength test.

For WH fiber, the optimum fiber content in the soil with respect to compressive strength was obtained as 0.75% and for other natural fibers considered in this study are at 1%. The UCS of fiber amended soil was found to be directly proportional to the amount of cellulose and hemicellulose present in the fibers. Among the three fibers tested, jute and WH showcased the highest water retention capability because of the presence of high hemicellulose content. Among the fibers tested, coir showcased higher crack resistance due to its multifilament nature and high lignin content. Among the natural fibers, WH showcased the highest increase in infiltration characteristics as compared to jute and coir. Vegetated soil on compacted soil-WH fiber composite showcased a decrease in desiccation potential by 55.5% and 25% as compared to bare soil and vegetated soil without fiber inclusion, respectively. The warp and weft pattern WH geotextile facilitated a higher tensile strength along with higher CBR value. The compressive strength of soil-WH biochar composite is less than bare soil at all compaction states. Water retention capacity increased from 29.5± 0.89 % to 48.45± 0.59 % for bare soil to WH biochar amended soil respectively and the increase is proportional with WH BC percentage (2-15%). Furthermore, inclusion of WH BC results in a gradual decrease of crack intensity factor from 7% to 2.8%. During the one-year buried time in soil, the UCS of all natural fiber amended soil decreased almost linearly. However, after a year of burial time the UCS of fiber reinforced soil was at least 1.68 times greater to that of unreinforced soil. Among all the soil-fiber composites, jute reinforced soil showcased the highest drop from its initial state (22.72%) followed by coir (16.67%) and WH (14.70%). The results from this study identified an appropriate mold ratio greater than or equal to 3.5 for conducting mini-disk infiltrometer measurements in laboratory columns.

Keywords: biomaterial, water hyacinth, natural fibers, biochar, water retention, crack

List of Figures

List of Tables

Nomenclature

E_r -Measured Evaporation

E_{tr} -Measured Evapotranspiration

$\mathcal{E}_{pb}$ -Peak strain corresponding to peak stress for bare soil

$\mathcal{E}_{pr}$, -Peak strain corresponding to peak stress for reinforced soil

k_{h0} - near saturated hydraulic conductivity

vG – van Genuchten parameter

θ -Volumetric water content

$\Theta(\psi)$ -Volumetric water content at suction ψ

Θr -Residual volumetric water content

Θs -Volumetric water content at saturation

σ_{pb} – Peak stress for bare soil

σ_{pr}, -peak stress for reinforced soil

σ_{ultb} – Ultimate stress for bare soil

σ_{ultr}, -Ultimate stress for reinforced soil

Ψ -Matric suction

Abbreviation

ASTM – American Society of Testing and Materials

BC -Biochar

BS -Bare soil

CGT – Circular pattern woven geotextile

CIF- Crack intensity factor

DC -Drying cycle

FDA -Fluorescein diacetae assay

FESEM - Field Emission Scanning Electron Microscope

FL- Fiber length

FP-Fiber percentage

FTIR – Fourier-transform infrared spectroscopy

GD -Grass density

LLG-Limited Life Geotextile

MDD- Maximum dry density

MDI –Mini-disk infiltrometer

MPSF - Mobilized peak strain factor

NDI - Normalized ductility index

OMC- Optimum moisture ratio

PE- Peanut shell

PLR –Peak load ratio

RDFS- Randomly Distributed Fiber-reinforced soil

SC -Stomatal conductance

SG -Soil + Grass

SGWH -Soil + Grass +WH

SIF -Strength improvement factor

SL -Shoot length

UCS-Unconfined compressive test

USCS- Unified soil classification system

WH- Water Hyacinth

WWGT –Warp and weft pattern woven geotextile

Chapter 1

Introduction

1.1 General

Soil reinforcement is a noble method for improving the mechanical characteristics. High cost of petroleum based geo-synthetic products and concern for environment have motivated researchers to explore alternate natural geo-reinforcements. Under the purview of natural geo-reinforcement, discrete fibers and limited life geotextiles (LLGs), manufactured from coir, bamboo, sisal and jute has been studied in the past (Methacanon et al. 2010). These plant based fiber and LLGs are feasible for amending surface soils which require initial strength whereas final strength can be achieved by vegetation (Gadi et al. 2016) or subsequent consolidation of soil (Nsiah and Schaaf 2019). Furthermore, plant based pyrolysis by-product, also known as "biochar" has been explored for amendment of surface soil for cover system (Ni et al. 2018, Reddy et al. 2015a). Biochar amended soil (BAS) has been recently found conducive as surface cover soil helping plant growth and methane oxidation.

Eichorrnia Crasipes (Fig.1.1a), popularly known as water hyacinth (WH) is an aquatic weed, that causes several environmental issues such as physical interference in fishing, navigation, irrigation systems, increased sedimentation and blockage in canals due to its fast growth (17.5 metric tons/hectare/day; Shoeb and Singh 2000). It also invades fresh water habitats and competes almost all neighboring species growing in their vicinity thereby decreasing biodiversity (Crafter et al. 1992). Control of this weed has been found to be a perennial task and it requires physical removal of the species on a regular basis resulting in unutilized waste bio-mass (Malik et al. 2010). Owing to its suitable bio-chemical composition and morphology, the current study investigates the feasibility of WH in geo-environmental applications as biomaterial (discrete fibers, LLGs and biochar). The conversion of WH to suitable bio-material and usage in green infrastructure and agriculture (Fig.1.1b) represents a more sustainable strategy for management of this invasive weed. Apart from characterization and hydro-mechanical investigation of soil-biomaterial, the study also investigates the vegetation potential and initial bio-degradation of discrete fibers.

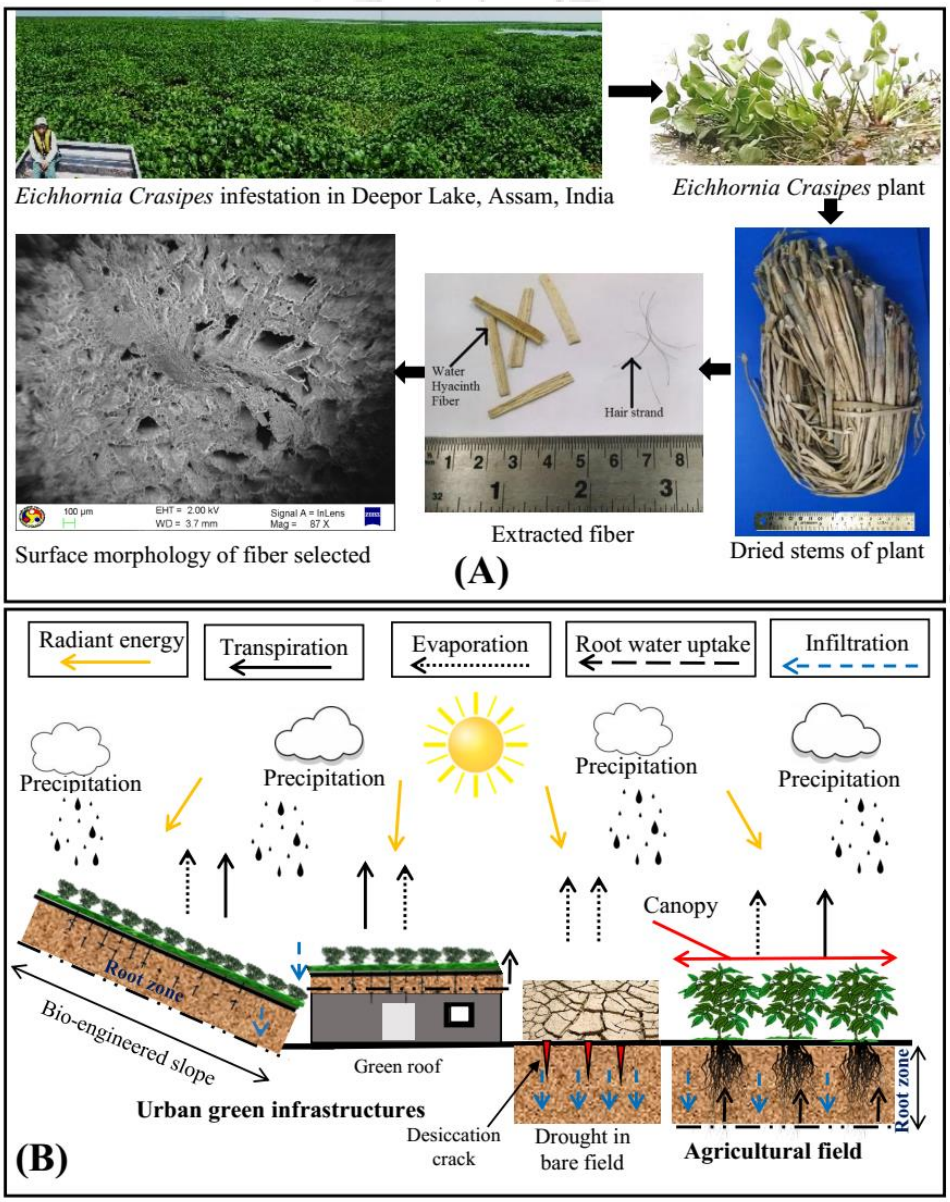

Fig. 1.1 Schematic representation of (a) conversion of invasive weed to natural fibers; (b) Potential application in urban green infrastructure and agricultural land

Initially, all the biomaterials made from WH were characterized for its inherent bio-chemical composition, physical properties, surface morphology, thermal response, functional groups, etc. The soil-fiber composite as randomly distributed fiber reinforced soil (RDFS) has been tested for unconfined compressive strength (UCS) tests and California bearing ratio (CBR) test. The material performance with other two conventional fibers (jute and coir) has also been investigated. The mechanical strength in terms of UCS has been investigated for water hyacinth BC and juxtaposed with peanut shell BC. The hydraulic performance was studied by assessing the soil water retention capacity (SWRC), desiccation potential and infiltration for soil-WH fiber composite alongside jute and coir. The vegetation potential along with SWRC and desiccation potential for soil-WH fiber composite was studied by conducting induced drought conditions. A basic bio-degradation assessment of WH fiber in embedded soil has been conducted. The consequent change in bio-chemical composition, effect on soil-fiber composite strength and microbial activity has also been done. The fibers were treated to minimize moisture absorption and enhancing mechanical strength by impregnating nano-particles on fiber surface. The improvement in mechanical strength of soil-treated WH fiber has been investigated by conducting UCS, CBR and direct shear strength test.

1.2 Motivation of the thesis

Natural fibers reported in the literature are mostly agricultural products, which have extensive alternative uses in automobile industry (Leao et al. 1998), ship rigging (to haul large loads at docksides and mines) (Sarsby 2007), paper manufacturing industry (Ververis et al. 2004) as well as sails and fishing nets (Anon 1927). The economic value and sustainability of LLG/discrete fibers/biochar would increase manifold, if it is manufactured from environmentally harmful plant species that do not find much applications in other industries. Such a need has motivated this research to explore the utility of world's most invasive weed species-WH, in geo-environmental applications as well as facilitating avenue for waste management. There are no studies that have measured the water retention and infiltration characteristics of natural fiber composite. Furthermore, the vegetation potential of compacted-natural fiber composite can also help in gauging its use in bio-engineered stabilization works.

1.3 Organization of the thesis

The thesis consists of nine chapters. Chapter 1 deals with the introduction of the whole thesis along with the motivation of the study. The major approaches used to solve them were mentioned. In Chapter 2, a thorough literature review on natural fibers is done. A brief review on desiccation cracking in vegetated soil and biochar amended soil has been discussed. In Chapter 3, the materials used in the current study was described along with some salient experimental methods required in the study. Chapter 4 encapsulates the experiments undertaken with soil-biomaterial composite incorporating natural fibers, geotextiles and WH biochar to gauge its mechanical performance. Chapter 5 investigates the infiltration, soil water retention characteristics (SWRC) and desiccation potential of soil-natural fiber composite by conducting reduce scale column tests. The SWRC and desiccation potential of soil-WH BC at different biochar percentage was tested. Chapter 6 explores the vegetation potential of compacted soil-WH fiber composite considering plant parameter effects. Chapter 7 showcases the bio-degradation of natural fibers (WH, jute and coir) and correlates its influence on soil-microbial activity and UCS of soil-natural fiber composite. Furthermore, fibers were coated with nano-particles using a simple chemical treatment method and its efficacy as a subgrade material was investigated. Finally, the conclusion and major outcomes from the present study are reported in Chapter 8. Chapter 9 finally highlights the limitations and future scopes from this study.

It is to be noted that comparisons with other bio-materials was done wherever feasible and depending on the availability of data from the literature or those generated as part of this study. The tests for biomaterials other than WH was not performed uniformly across all chapters.

Chapter 2

Literature review

2.1 General

An understanding of the physical, chemical and biological aspects of lignocellulose based bio-material is essential to gauge its feasibility as an amendment material in geo-environmental application. Focus has been laid on these aspects by systematically reviewing the use of natural fibers in geotechnical engineering by juxtaposing the work from geotechnical perspective with that of material science, plant science and chemistry. Biomaterial from lignocellulose has been discussed with respect to discrete fibers, geotextiles and biochar. The application of these biomaterial for developing vegetation commonly used in cover system is also discussed. Allied problem of desiccation crack in vegetated soil is also discussed in context with plant parameters and unsaturated soil mechanics. A brief background on biochar is also provided in context to geo-environmental infrastructure. Based on this review, some key research gaps and the future scope of research have been highlighted.

2.2 Physio-biochemical properties of natural fibers and their application in soil reinforcement

The behavior of soil–natural fiber composite is dependent on the biochemical, physical, and mechanical properties of natural fibers. These natural-fiber properties are inherently different from those of conventional synthetic fibers, in which mechanical properties essentially govern the soil-fiber composite behavior. Very few geotechnical applications using natural geo-reinforcement materials have taken into consideration the biochemical and physical properties of the fiber. Moreover, there is rarely any systematic assessment and compilation of the work encompassing the application of natural fibers in soil reinforcement. This section summarizes the use of natural fibers in soil reinforcement. The section explores the importance and impact of natural-fiber properties on the performance of natural fibers in subsoil conditions. The treatment methodologies used in natural fibers to increase their longevity and reinforcement capabilities are also discussed.

2.2.1 Introduction

Soil generally exhibits low tensile strength and its engineering properties varies with the environmental conditions (e.g. shear strength depends on water content present in soil) (Ling et al 2003). With rapid urbanization, coupled with decrease in availability of good construction sites, there is need for utilizing sites even with poor engineering properties. Major focus has been directed towards the improvement of soil using reinforcing techniques. Soil reinforcement techniques improves the engineering properties such as shear strength, compressibility and hydraulic conductivity, thereby increasing the bearing capacity, ductility and decreasing the settlement of soil (Vidal 1969). Reinforced soil can be considered as a composite material, formed by mixing soil with tension resistant elements (sheet, strips, nets, fabric) for reducing tensile strain and increasing shear strength (Saran 2010). In the past, a large array of tensile inclusions ranging from low-modulus polymeric materials to high tensile strength metallic sheets was used to reinforce soil (Gray and Al-Refai 1986). Generally, reinforcing methods of using piles, stone columns, soil nailing, chemical inclusion and fiber reinforcement have been used with synthetic man made materials (Abtahi et al. 2009, Cantoni 1989, Hughes 1975, Bruce and Jewell 1986, Gray and Al-Refeai 1986). Among these techniques, fiber reinforcement has been implemented due to its inherent advantages of strength isotropy, increased ductility and economy (Babu and Vasudevan 2008).

Fiber reinforcement in soil is generally designated as randomly distributed fiber reinforced soil (RDFS). RDFS is among the recent ground improving techniques, where fibers of desired property and quantity, are mixed randomly and compacted in-situ. The uses of planar reinforcement (e.g. metal strips, sheets of synthetic fabric) that are used in geotechnical engineering possess an inherent plane of weakness that is developed parallel to oriented reinforcement (Maher and Gray 1990). On the other hand, the randomness of RDFS fibers provides a homogeneous mass where strength isotropy is maintained. RDFS has gained popularity due to its role in enhancing soil ductility, increasing shear strength and improving post peak strength (Tang et al. 2010). These soil-fiber composite mixture mimics the behavior of plant roots, contributing to soil stability by adding strength to near-surface soil (Greenwood 2004). Other applications of RDFS are in erosion control, facilitation of vegetation development and reducing shrinkage in case of expansive soil (Saran 2010).

The inclusion of these fibers in soils improves its load-deformation response by interacting with the soil particles mechanically, via surface friction and interlocking. The interlocking leads to stress transfer mechanism, whereby the stress from the soil is transmitted to the discrete inclusions by mobilizing the tensile strength of the fiber. This mobilization is depicted in Fig. 2.1, where an idealized illustration of soil-fiber composite mechanism for a single fiber is considered (Fig. 2.1(a-b)). Upon loading, the normal stresses from the soil on the fiber results in fiber deformation, which induce mobilization of tensile stress and consequently imparts greater strength (Tang et al. 2007). As seen in Fig. 2.1 (c), the fiber is enwrapped by inter locked or inter bond soil particles, which contribute to bond strength and friction between the fiber and soil matrix (Tang et al. 2010). During shearing, soil particle rearrangement and rotation (Fig. 2.1(e)) strongly affect the interfacial friction. Frost and Han (1999) have reported that high interfacial resistance to shear is developed in more inter-locked soil particles, as compared to the case of lesser interlocking. Apart from these mechanisms, the bonding force between soil particle-fiber (solid-solid phase) and pore water-fiber (liquid-solid phase) also contribute to interfacial shear strength, but such force varies with gradation of soil (Tang et al. 2010). Moreover, suction due to capillary water developed (Fredlund and Rahardjo 1993, Garg and Ng 2015, Garg et al. 2015) in voids between soil and fiber particles can also increase shear strength of the soil-fiber composite.

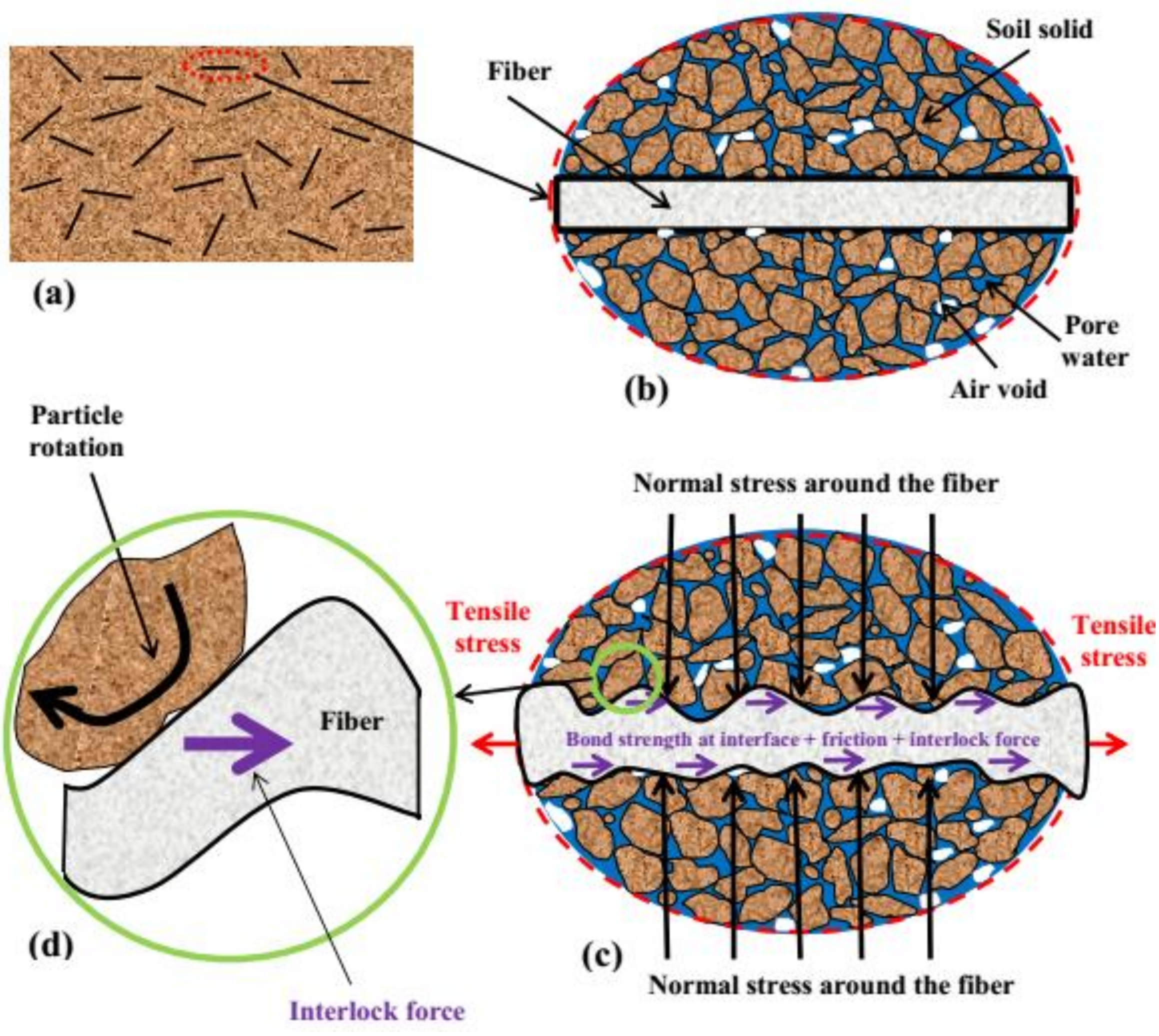

Fig. 2.1 Idealized illustration of RDFS (modified after Tang et al. 2007b, Tang et al. 2010) (a) Soil fiber composite (b-c) Individual fiber response to unloaded and loaded conditions respectively (d) Mechanism of particle rotation that induce interlock and surface friction forces in fiber

Growing awareness of sustainable construction materials have recently shifted the focus towards the use of natural fibers in soil reinforcement (Bledzki and Gassan 1998, John and Thomas 2007, Dasaka and Sumesh 2011, Vadivambal et al. 2015). A shift from conventional synthetic fibers has undertaken, as they are by-products of petroleum having limited resource (Wambua et al. 2003). This shift over to natural-fibers as fillers/reinforcement has already gained momentum in the field of plastic composites, due to their flexibility during processing, high specific stiffness and low cost (volumetric basis). The worldwide capacity of such plastic composites saw an increase from 0.36 million metric tons in 2007 to 2.33 million metric ton by 2013; and is expected to increase to 3.45 million metric tons by 2020 (Shen et al. 2009). The market for natural geotextiles/fibers is also growing at a high pace, with worldwide sales of over 14 million square meters in 1990 (English 1995). Natural fiber reinforced soil can be considered as a soil-fiber composite with enhanced properties, also termed as "Eco-composite" (Hejazi et al. 2011). Such eco-friendly composites are found to be feasible for applications, where they are meant to serve only for the initial stage after construction, and the final strength is attained by vegetation or soil consolidation (Subaida et al. 2008). With more and more renewable natural fibers discovered and used for diverse applications, this century is predicted as "the cellulosic century" according to Faruk et al. (2012).

The use of natural fibers in soil reinforcement has been extensively done. However, there is rarely any systematic assessment and compilation of the work encompassing such natural fibers in geotechnical applications. Most of the studies that have been done to understand soil-fiber composite behavior, consider the mechanical properties of such synthetic or natural fibers.

However, natural fibers - also termed as lingo-cellulose material, is composed of intricate biochemical components which determine its functioning as a reinforcing material (Methacanon et al. 2010). They are composed of complex bio-polymers which determine the strength, ductility and durability of the fiber. Based on the arrangement and relative percentage of these bio-polymers, natural fibers have distinct physical properties (such as crystallinity index and microfibrillar angle) as that found in synthetic fibers. The performance of natural fibers in sub-soil conditions is also dependent on soil conditions such as soil type, soil microbial activity and strength as well as water retention of soil. The current work explores the linkage and the importance between the natural fiber properties and its impact on the performance of fiber in sub-soil conditions (Fig. 2.2). Additionally, this work is a state of the art review on the utility of natural plant fibers in the field of soil reinforcement. The work lays out existing treatment methodologies on natural fibers, in order to increase its longevity and improve its reinforcement capabilities. Based on the discussion, the review attempts to outlay some key research gaps between geotechnical engineering understanding of the soil-natural fiber composite and inherent natural fiber properties.

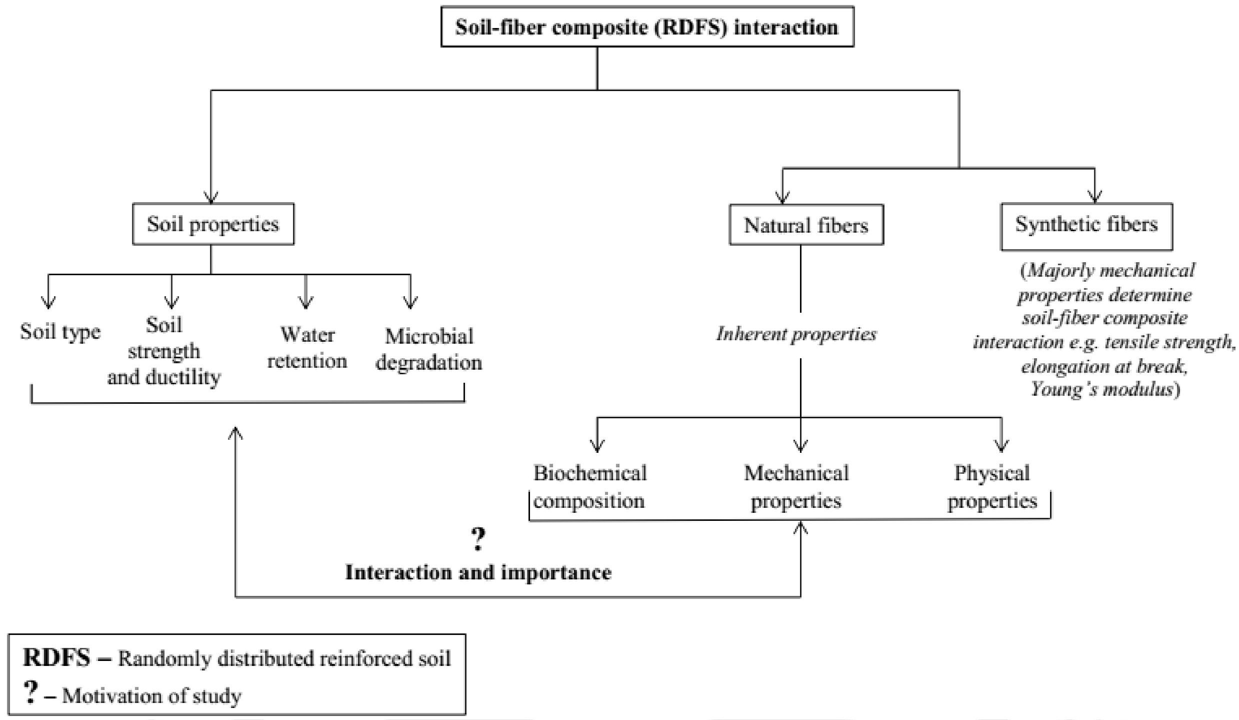

Fig. 2.2 Importance of linkage between soil properties and natural fiber properties to understand the soil-natural fiber composite

2.2.2 Soil-natural fiber composite application

The plant fibers used for soil reinforcement is shown in Fig. 2.3. The plant fibers used for soil reinforcement is classified into three categories based on their economic use: crop species, non-crop species and weed species. The individual species and its role in soil reinforcement are discussed in this section. The discussion is based on its origin, current applications, and its use in soil reinforcement. Under soil reinforcement, RDFS has been majorly discussed followed by its application as soil blocks and LLGs.

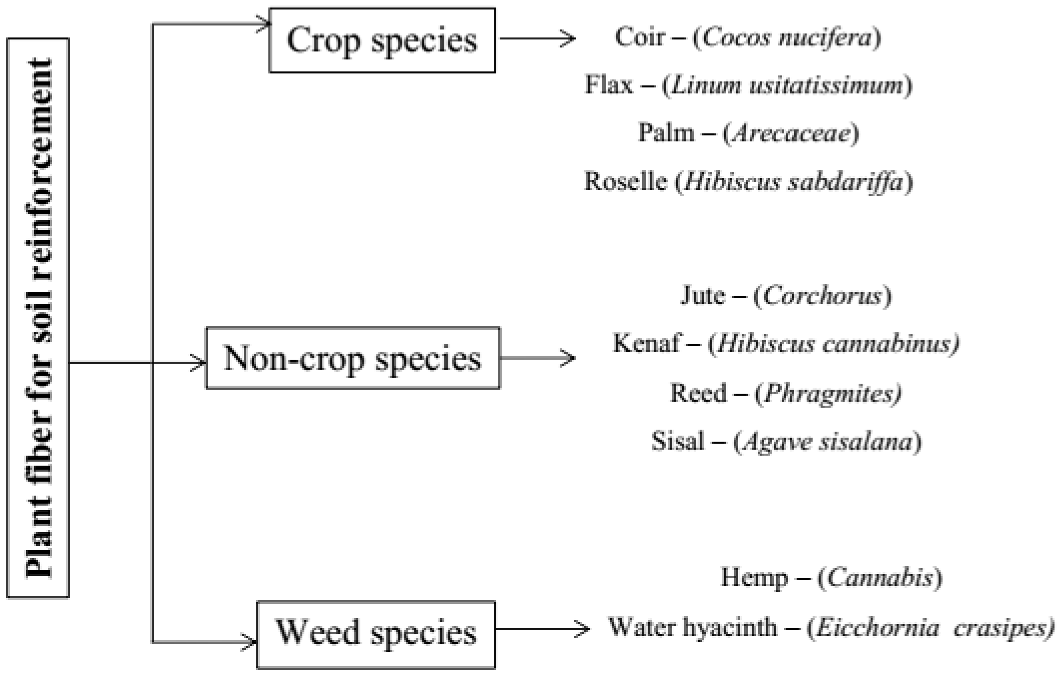

Fig. 2.3 Classification of fibers used in soil reinforcement

(A) *Fibers from crop species*

Coir

Coir fiber, derived from coconut fruit shell is also known as *Cocos Nucifera.* It is distributed throughout the tropical and subtropical regions of the world, and shows remarkable adaption to a wide range of soil types (Chan and Elevitch 2006). It has a low potential of invading other species and coconut husk fibers has been extensively used as a handicraft material, ship hauling, soil reinforcement and in soft construction building material. It is reported that 10% of all husks are utilized for fiber extraction, to meet the growing demand of coir related products (Faruk et al 2012). Coir is suitable to be used in-field due its resistance to degradation owing to higher percentage of lignin. The in-field service life of coir is reported as 4 to 10 years (Rowell et al.

2000). Coir is one of the most popular natural fibers used for soil reinforcement. A significant advantage of using coir fiber is that it retains much of its tensile strength when wet, which makes it ideal to be used in soils.

Coir has been used to reinforce clay soil in many instances. Tri-axial compression test was used to investigate the stress-strain response of kaolinite clay with inclusion of discrete coir fibers (Dasaka and Sumesh 2011). Coir fiber is found to be advantageous in reinforcing soil, especially at (1.5-2) % of dry weight of soil. At 1.5% of fiber content, there is a twice fold increase in compressive strength with respect to bare soil. A significant non-linear increase in cohesion and friction values was observed with increase in fiber content from 0.1% to 2%. Ductility of the soil was found to improve with inclusion of coir fiber with an increase in post peak strength. Babu and Vasudevan (2008) conducted tri-axial shear test and reported that the addition of coir fiber (from 1-2%) increases both strength and stiffness of clay soil used in the study. Deviator stress at failure was found to increase up to 3.5 times with respect to unreinforced soil. The cohesion (c) and friction angle (ϕ) of reinforced soil increases as compared to unreinforced soil. A series of unconfined compressive strength (UCS) test were carried to see the effect of coir fiber addition on marine clay (Sebastian et al. 2011). Fiber length ranging from (10 – 30 mm) and fiber percentage (0.2% – 1.5%) were used to ascertain the stress-strain response of soil-fiber composite. Shear strength increased with addition of fiber up to optimum fiber percentage (0.8%) resulting in a fourfold increase in strength. Optimum fiber length in the study was found to be 20 mm. Lime coupled with coir fiber was used to improve soil strength for black cotton soil (Ramesh et al. 2010). Optimum fiber content (1%) for aspect ratio of 20 was recommended in reinforcing black cotton soil. Thus in clay soil due to coir fiber addition, the range of strength increase varies from 2 to 4 times from the initial strength. This variation arises out of difference in test type, soil type and also due to fiber dimensions.

To determine its applicability in subgrade soil, California bearing ratio (CBR) tests were conducted on silty loam soil (Kumar et al. 2015). Test results shows a significant increase in CBR value with fiber inclusions, thus decreasing subgrade thickness and reducing cost of project. Chauhan et al. (2008) used optimum percentage of fly ash with coir fiber for reinforcing silty sand. UCS and tri-axial compression test were done on fly ash-coir fiber soil composite. With increase in fiber content (0.5% – 2%), there was a significant increase in UCS up to 0.75% and it remains constant thereafter. The study suggests that coir fiber reinforced soil showed better resilient response and higher UCS as compared to polypropylene fiber for the same testing conditions.

The use of coir fibers in manufacturing earth blocks for housing was studied in the recent past (Khedari et al. 2004 (a, b), Danso et al. 2015). The study reveals the efficacy of using such fibers to construct mud house with materials having low thermal conductivity, light weight and with enhanced mechanical properties. They act as binder materials and render properties useful for cool living conditions, using local low cost materials as compared to other costly building materials. Use of varied geo reinforcing products (Geocoir® 400,700 and 900) made of coir fibers has gained commercial attraction (Belton industries). A series of laboratory (Subaida et al. 2008, 2009), numerical (Mwasha 2009) and field investigation (Lekha 2004) have established coir as one of the most popular LLGs used. Field investigation was carried out by Lekha (2004) to monitor soil erosion in a coir LLG reinforced slope coupled with lemon grass seedling for a period of 1 year. The research established that there is a substantial improvement in organic carbon, soil water content of the soil, soil moisture retention capacity of soil and vegetative growth. However, a similar field investigation using coir LLG with hydro seeding (various species), resulted in deterioration of vegetation cover as compared to unreinforced soil. These contradictory results may be due to high slope angle of the studied embankment, method of sowing and also type of vegetation species.

Flax

Flax (Linum usitatissimum) is grown in temperate regions and is one of the oldest textile fibers known to mankind. This fiber is generally used in higher value–added linen textile markets. The specific tensile strength of flax fibers is comparable to synthetic E-glass fibers (Harriette et al. 2004). Although, hardly any full scale studies on flax fiber RDFS has been conducted till date, its application as rammed earth material, soil–cement composite and potential geotextile have been discussed in the past (Segetin et al. 2007, Sarsby et al. 2007, Cheah and Morgan 2009, Anand 2008).

Phormium tenax, a New Zealand based flax species, has been studied to improve soil-cement composite by testing it under flexural and compressive strength test apparatus (Segetin et al. 2007). In an attempt to increase the interfacial strength between fiber and soil-cement mixture, flax fibers were coated with enamel paint. Fiber length (70 mm and 85 mm) and fiber percentage (0.6% and 0.8%) were uniformly mixed with the composite and cured. The composite blocks showed significant improvement in terms of ductility and relative improvement in compressive strength as compared to unreinforced soil-cement composite. Based on results, the optimum fiber percentage is advocated to be 0.60%. Sarsby (2007) has conducted parametric study on flax based limited life geotextiles (LLG) and put forth time-strength envelopes in his study. The results indicate the application of flax LLGs, particularly in soft clay embankments post natural disasters

(Tsunami, Cyclones, etc.). Cheah and Morgan (2009) have reported the use of flax fibers in construction of earth rammed housing system called "Uku". They are low cost building, made from local flax fiber stabilized earth blocks and specifically designed for indigenous people of Aotearoa, New Zealand. Mwasha (2009) reported that the use of coir (warp)-flax (weft) combined geotextile increases the tensile strength of pure coir (both warp and weft) geotextile by 3 times (from 19.67 to 60.97 (kN/m)). Different combinations of flax (warp) and sisal (weft) geotextiles were tested (Anand 2008). Results indicate the efficacy of its use as LLG, due to its high tensile strength, high elongation at break and tensile modulus.

Oil palm

Oil palm lays under the genus "*Elaeis*" and comprises two species of the *Arecacea* or palm family (Faruk et al. 2012). Notable properties of these fibers such as low cost, lightweight, easy availability, durability, tensile strength and resistance to degradation makes it an alternative reinforcing material in coastal and arid regions (Yusoff et al. 2010). A lot of studies were performed to explore the efficacy of palm fibers in soil and earth block reinforcement. LLG made out of palm fibers was extensively used and monitored for soil conservation measures (Davies et al. 2006, Bhattacharyya et al. 2009, Bhattacharyya et al. 2011).

Oil palm fiber has been used to reinforce silty sand soil in the recent past. Marandi et al. (2008) investigated RDFS with palm fibers using UCS and CBR tests. Fiber contents (0.25%, 0.50%, 0.75%, 1.00%, 1.50%, 2.00% and 2.50%) and lengths of 20 and 40 mm were investigated on silty sand soil. Soil strength was found to have improved as the fiber length increased, with peak strength occurring at fiber ratio of (2.0% – 2.5%) for fiber length of 40 mm. The increase of

CBR values was observed with increasing fiber percentage for a particular fiber length. Tri-axial compression test (both drained and undrained condition) was performed on silty sand RDFS reinforced with oil palm fibers (Ahmad et al. 2010). Palm fibers of three different lengths (15 mm, 30 mm and 45 mm) at two different compositions (0.25% and 0.5%), was tested to evaluate the response of shear strength of the soil-fiber composite. The results show that with addition of fibers there is a significant increase in peak shear strength as well as strain at failure (improved ductility). The shear strength parameters (c and ϕ) were improved by the inclusion of fibers. Increase in fiber content resulted in linear improvement in "c" values and increase in fiber length resulted in higher "ϕ" values. The increment in "ϕ" value (60) for palm fiber reinforced sand is greater than with respect to coir fiber reinforced sand at 0.5% fiber inclusion, for the same testing conditions (Babu and Vasudevan 2008, Ahmad et al. 2010).

Studies on palm fiber inclusion in clay soils have been done. A study conducted by Jamellodin et al. (2010) investigated the effect of inclusion of oil palm fiber in reinforcing soft clay using tri-axial compression results. A significant improvement in the failure deviator stress and shear strength parameters (c and ϕ) was reported. There is a drop in maximum dry density (MDD) and optimum moisture content (OMC), with increase in fiber percentage. Studies on the swelling, cracking and mechanical properties were done using palm reinforced clay (Azagedan et al. 2012). The results reported that swelling increased with higher fiber content values (0.25%, 0.50% and 1%). However, the mechanical properties upon drying are considerably improved due to fiber reinforcement. The cracking of the soil was found to increase with fiber content, but this trend is not in accordance with similar study on synthetic polypropylene fiber reinforced silty clay (Tang et al. 2012).

Oil palm fibers were utilized for the manufacture of low-cost earth blocks (Ismail and Yaacob 2011, Yalley and Kwan 2013). Ismail and Yaacoob (2011) have reported that an increase in fiber content decreases the overall density of the blocks. Optimum fiber content was reported to be 3% in terms of compressive strength of blocks. The results indicate no appreciable increase in moisture absorption of these blocks with increasing fiber content. In another study, Yalley and Kwan (2013), noted an increase in compressive strength of blocks due to the inclusion of palm fibers. For palm fiber inclusion of 1.5%, the compressive strength increased by 28.50%. The use of palm based LLGS was extensively studied (Booth et al. 2005, Davies et al. 2006) and applied in field conditions (Bhattacharyya et al. 2009, Bhattacharyya et al. 2011). Based on field experiment results, the use of palm LLGs on bare soil significantly reduced soil splash height by 51% and splash erosion by 90% (Bhattacharyya et al. 2009).

Roselle

Roselle is a perennial medicinal plant belonging to the genus "Hibiscus" and is popularly known as "Hibiscus sabdariffa" (Chewonarin et al. 1998). Among various natural fibers, roselle fibers have traditionally been used as high-strength ropes and floor mats. Roselle has high tensile strength and moderate impact strength comparable to conventional soil reinforcement fibers such as jute, hemp, sisal and kenaf (Thiruchitrambalam et al. 2010). A recent study (Methacanon et al. 2010) has advocated the use of Roselle as a soil reinforcing material. The results are based on a series of tests such as mechanical tests, single cell morphology, biochemical composition, accelerated weathering test etc. on similar natural fibers (water hyacinth, sisal and reed). Roselle fibers are found to be suitable for weaving geotextiles due to its relatively high tensile strength and durability as compared to other tested fibers.

(B) Fibers from non-crop species

Jute

Jute is derived from plants under the genus *Corchorus*. Bangladesh, India and China are the leading producers of jute fibers. Among all the natural fibers, it is the cheapest and with highest production volume (Faruk et al 2012). Jute, with a growing cycle ranging from 120 -150 days has an average yield of 2,200 kg/ha (Rowell and Stout 2007). Jute fiber has been used in the field as RDFS and woven product used in soil subgrade reinforcement (Hejazi et al. 2012).

Aggarwal and Sharma (2011) have studied jute fiber reinforced clay soil application in subgrade construction using CBR and compaction tests. Jute fibers were found to be effective in increasing the CBR value from 1.8 to 5.5, which reduces the subgrade thickness by 35%. The inclusion of fiber resulted in decrease of MDD and increase of OMC for the subgrade material, but the change was not significant.

Use of jute fiber in reinforcing silty soil has been extensively done using a series of CBR and UCS test. Kumar et al (2015) have done comparative study of RDFS reinforced silty loam soil with both jute and coir, using a series of CBR test. For aspect ratio (L/D = 20 to 100), the CBR values of jute was reported to be higher as compared with those of coir fibers. The increase in strength can be attributed to superior mechanical property of jute due to its higher cellulose content, low microfibrillar angle, Young's modulus and tensile strength. The significance of these properties is discussed in later sections. Effect of freeze- thaw cycles have been investigated on jute fiber reinforced clayey silt soil with and without additional admixtures (lime and steel fiber) (Gullu and Khudir 2014). A series of UCS tests were performed by subjecting the soil-fiber composite to a maximum of 3 freeze-thaw cycles. It was found that the jute fiber was instrumental in increasing the strength of soil. A marginal reduction in strength was noted when the soil-fiber composite was subjected to freeze-thaw cycles. The study recommended using 4% lime coupled with 0.75% jute fiber and 0.25% steel fiber as the optimal combination for soil reinforcement, which resulted in higher strength and ductility.

Jute fibers were used extensively with soil, gypsum, clay and lime to manufacture earthen blocks for adobe and masonry based constructions (Ramaswamy et al. 1983, Islam and Iwashita 2010, Danso et al. 2014). Jute fibers ingrained in concrete were found to be effective in reducing shrinkage and increasing ductility. Impact and fracture toughness characteristics were improved, thus rendering them useful against earthquake motions (Ramaswamy et al. 1983, Islam and Iwashita 2010). LLGs made from jute fibers were used for soil erosion control (Islam 2013, Álvarez-Mozos et al. 2014 a, b) and soil reinforcement (Bera et al. 2009, Basu et al. 2009). Jute LLGs provide better adaptability for vegetation growth as compared to coir LLGs for the same field conditions (Álvarez-Mozos et al. 2014 b). The inclusion of jute LLG has been reported to increase the UCS of fly ash soil (Bera et al. 2009).

Kenaf

There are about 300 species of kenaf which fall under the genus "Hibiscus". Its growing cycle being 150 to 180 days, the average yield of kenaf is reported to be 1700 kg/ha (Rowell and Stout 2007). Renewed interest in the use of kenaf bast fiber stems from its adaptation to varying soil and climatic conditions (Rowell and Stout 2007, Faruk et al. 2012). Kenaf as a synthetic composite reinforcing agent, has gained considerable attention in the recent past (Akil et al. 2011, Shekeil et al. 2014), however its application in RDFS is limited.

The effect of kenaf fiber (*Hibiscus cannabinus*) inclusions on earth blocks was recently investigated by Millogo (2015). Kenaf fibers (3 mm long) with fiber content ranging from 0.20 % to 0.80 % were used to reinforce earth blocks. The incorporation of kenaf fibers reduced the development and propagation of cracks in the earth blocks. Such blocks also resulted in increase of tensile ductility. Geotextiles made from kenaf fibers was used for soil reinforcement (Chaiyaput et al. 2014, Artidteang et al. 2012). Kenaf LLG reinforced embankment was monitored and compared with numerical modelling for a period of 250 days (Chaiyaput et al. 2014). The results indicate the applicability of kenaf LLG for short term embankment reinforcement on soft clay. The performance of soil buried kenaf fiber reinforced polyurethane composites was studied for a period of 80 days (Sapuan 2013). The effect of moisture absorption on mechanical properties (tensile strength and flexural strength) was tested at 20, 40, 60 and 80 days. Although there was no significant change in flexural strength of the composite, a reduction in tensile strength was observed after 80 days. Similar results were reported in case of unsaturated polyester composites reinforced with kenaf fibers (Rashdi et al. 2009).

Reed

Reed is inherent of the genus "*Phragmites*" and is popular in soil reinforcement for its relatively stable properties, uniform diameter and relatively low modulus, which makes it ideal for extensible reinforcements (Gray and Ohashi 1983). Laboratory direct shear test were performed by Gray and Ohashi (1983) with reed fibers. It was noted that the increase in area ratio of fibers, caused a progressive rise in peak strength and post peak strength reduction at higher shear displacements. Initial fiber orientation along the shear surface was varied at 30^0, 60^0, 90^0 and 120^0, to account for the fiber orientation effect on soil strength characteristics. Initial orientation of 60^0 showed the relative highest improvement in shear strength. Shear strength improvement of RDFS with reed fibers were investigated for dense and loose sands. In case of loose sands, larger strains were required to reach peak shear stress. Reed fibers of specified length (13 mm, 25 mm and 38 mm), diameter (1.25 mm and 1.75 mm) and fiber percentage (0.2%, 0.5%, 1% and 2%) were added to uniform medium grained sand for performing tri-axial compression test (Gray and Al-Refai 1986). With rise in fiber content, there was a visible increase in peak shear strength and major principal stress at failure. With increase in aspect ratio (length of fiber/diameter of fiber), there is a rise in major principal stress at failure. Additional tests on Muskegon dune sand was done using reed fibers and rubber fibers using tri-axial compressive strength test (Maher and Gray 1990). Reed fiber reinforced soil showed a visible increase in major principal stress with confining stress. Reed fiber RDFS was found to give higher shear stresses as compared to rubber fiber RDFS. A theoretical model was proposed to validate the experimental results. Owing to its availability, low-cost and moisture absorption of reed, Methacanon et al. (2010) suggests its use in soil erosion control measures. In their study, elongation at break for reed fibers was found to be same as for kenaf fibers (18%), which indicate its possible application for soil reinforcement.

Sisal

Sisal fiber as a reinforcing material has gained popularity on account of its low cost, lightweight, high specific strength, easy availability and high modulus. It is a hard fiber and derived from the plant "*Agave sisalana*" (Li et al. 2000). Brazil, Indonesia and East African countries are the leading producers of sisal in the world (Giridhar and Rao 1986). Sisal fibers are reported to retain (25%-35%) of its tensile strength after a period of 12 months, when subjected to cyclic drying and wetting in salt water (Sarsby 2007). Methacanon et al. (2010) have done an in-depth study on the fiber properties of sisal fibers including biochemical composition test, mechanical loading tests, moisture absorption test, thermo-gravimetric analysis (TGA) test and accelerated weathering test. Their results indicate the efficacy of sisal fibers for soil reinforcement and as geotextiles.

Ghavami et al. (1999) investigated the addition of sisal fibers on the stress-strain response of a composite soil material at water content of 28% and 30%. Addition of sisal fibers resulted in significant increase in ductility of soil without much increase in compressive strength. This result may be attributed to excess proportion of fibers used which may lead to pockets of low density. Also the authors in this study have not reported the soil type used which is very important to understand the ductility of the composite. A series of compaction and undrained tri-axial tests were performed on RDFS reinforced clayey silt soil with sisal fibers with four different lengths (10 mm, 15 mm, 20 mm and 25 mm) (Prabakar and Sridhar 2002). The fiber percentage was varied at 0.25%, 0.50%, 0.75% and 1% respectively. Increase in fiber length and fiber percentage resulted in a linear decrease in MDD and OMC. Cohesion of the soil had negligible variation with fiber length. Optimum fiber percentage resulted at 0.75% for cohesion parameter. Optimum fiber length and percentage in terms of angle of internal friction was found to be at 20 mm and 0.75%, respectively. Tensile strength of fibers was monitored for a period of 30 to 210 days, for both coir and sisal fibers submerged under water to study its durability. The sisal fiber showcased tensile strength three times higher than that of coir for the entire test durations, indicating superior mechanical properties under saturated condition. Similar work done (Wu et al. 2014) on silty clay soil, indicate an improvement in the strength, deformation and shear failure characteristics of soil due to inclusion of sisal fibers.

A recent study by Martins et al. (2014) on soil-cement-sisal fiber composite has proven the efficacy of sisal fiber inclusion on mechanical parameters of the composite. Under compression, a significant improvement on the post-peak strength, toughness and strain capacity was reported. The curing of the composite resulted in increase of compressive strength (from 3.3 MPa to 7.5 MPa). The application of sisal fibers in the fabrication of earth blocks and consequent enhancement of mechanical properties was reported (Mesbah et al. 2004, Namago 2006, Danso et al. 2015). Sisal improved the properties (bending, abrasion resistance, water absorption and erosion) of earthen blocks made by bahareque technique (Mattone 2005). Anand (2008) investigated the use of LLGs made from a combination of sisal and flax fibers through a series of weaving patterns and consequent mechanical tests on the LLGs. The results indicated its potential use as a LLG, pertaining to its effective properties such as high tensile strength, elongation at break and tensile modulus.

(C) Fibers from weed species

Hemp

Hemp is a bast fiber belonging to the family of "Cannabis" and is an annual plant that grows in temperate climates. As a non-food agricultural species, it is currently under the subject of a European Union subside and new initiatives are underway for their further development in Europe (Faruk et al. 2012). Although there are no reported studies as RDFS, it is widely used in the manufacture of earthen blocks (Islam and Iwashita 2010, Danso et al. 2014). The compressive strength of hemp reinforced adobe earth blocks was found to be comparable with jute reinforced adobe block. Hemp fibers were used in the form of geotextile for the retention of pesticides in agricultural watersheds (Boutron et al. 2009). Batch studies (adsorption and desorption tests) on jute, hemp and linen were conducted for three pesticides. It was noted that hemp with its adsorption percentage of 80% at equilibrium was the most effective fiber that can retain pesticides. This would obviously have its impact in agricultural field for nutrient retention as well. Application of hemp fibers as a non-woven geotextile was patented by Roure (2013) that can be used for reinforcing slopes and embankments.

Water hyacinth

Water hyacinth (Eichhornia crassipes) is an uncompromising aquatic weed and has garnered worldwide attention due to its fast spread and congested growth, leading to serious problems in navigation, irrigation and hydro-power schemes. Inherent to Brazil and other South American countries, water hyacinth can now be readily found in most countries located between 40^0N and 40^0S (Sarika et al. 2014). In the past few decades, research activity on its biological control and consequent favorable utilization of the species was undertaken. Malik et al. (2006) in his review work, has highlighted the use of water hyacinth in bio gas production and wastewater treatment, which is applicable to rural as well as industrial problems (Malik et al. 2006). However, the use of water hyacinth in soil reinforcement has gained atttraction very recently (Methacanon et al. 2010, Maneecharoen et al. 2013, Dileep et al. 2013).

Methacanon et al. (2010) discussed the efficacy of using water hyacinth (WH) as a soil reinforcing material. Based on series of tests, the authors have advocated the application of WH fiber/geotextile in soil erosion prevention. Although WH has relatively low strength than conventional fibers used in soil reinforcement (jute, sisal, etc.), they are advocated for soil erosion measures due to their easy availability, low-cost, high elongation at break, higher water absorption and more importantly due to the efficient use of an invasive weed. These properties make it more conducive for supporting vegetation growth, reduce raindrop impact, lessen runoff velocity and also render soil fertility on its degradation.

Effect of WH fiber inclusion in paddy clay was investigated by Dileep et al. (2013) by a series of compaction, CBR and UCS test. The soil-WH composite resulted in a decrease in optimum moisture content and maximum dry density with increase in fiber content. With increase in fiber content from 0% to 0.50%, there is a significant rise in compressive strength after which it remains practically constant. The improvement in CBR values was also observed up to 0.50% after which it remained constant.

(D) Summary of natural fibers used as soil-natural fiber composite mixture

Table 2.1 summarizes the application of natural fibers in soil reinforcement used in the form of soil-natural fiber composite mixture. Its application as earth block material composite and LLG has also been mentioned. Among crop species, coir and oil palm fibers was extensively used in soil reinforcement applications. Coir as soil-natural fiber composite mixture was extensively implemented in field applications. Laboratory investigations were conducted in different types of soil and results indicate that coir inclusion enhances the engineering parameters of soil (friction angle, energy absorption capacity, resilient modulus, UCS, residual shear stress, ductility, etc.). For palm based soil-natural fiber composite mixture, with increase in fiber length, there is rise in cohesion and frictional angle as compared to unreinforced soil. Additionally, LLGs made from palm fibers, have garnered popularity in splash erosion resistance projects in the United Kingdom (Davies et al. 2006, Bhattacharyya et al. 2009). Flax and roselle have gained recent attention as potential natural fibers for RDFS. Although, no proper geotechnical investigation was conducted till date on flax and roselle based RDFS, the test conducted on its fibers indicates its potential applicability as RDFS. The flax fiber inclusion on earth blocks was found to enhance its engineering properties (Cheah and Morgan 2009).

Among non-crop species, jute is the most popular fiber applied in soil reinforcement. It has been widely studied in geotechnical applications as RDFS and LLG. Inclusion of jute fiber increases peak strength, ductility and reduces the MDD of the soil. Based on CBR tests conducted on the same soil, jute reinforced RDFS is more appropriate as subgrade material as compared to coir RDFS. Jute LLG was found to be more popular due to its effectiveness in the propagation of vegetation cover and providing resistance to soil erosion (Ayuba and Olorunnaiye 2014). The jute LLG performance was superior to that of coir LLG when it was used for bioengineered slope stability (Álvarez-Mozos et al. 2014). Reed and sisal fibers have also garnered considerable attention as RDFS with increase in the shear strength of the soil. LLG made from sisal fibers has also been studied in the recent past (Anand 2008, Mwasha and Petersen 2010). Kenaf LLGs have been studied, both in field and laboratory, for its application in soil reinforcement measures. However, relatively few tests were undertaken to understand its application as RDFS.

Amid the abundant and readily available weed species, relatively few studies were undertaken to understand its use in soil reinforcement. Its potential as RDFS has recently gained attention and preliminary tests on weeds like hemp and water hyacinth was conducted to find its application in soil reinforcement. Hemp, as fiber inclusion was tested for soil-fiber blocks and also as natural geotextile in adsorption of pesticides. Water hyacinth, being a noxious weed, its application as an alternative reinforcing material is encouraging. Recent tests indicate its efficacy as RDFS (Dileep et al. 2013) and also in soil erosion control (Maneecharoen et al. 2013).

Table 2.1 Summary of researches performed on natural fibers as RDFS

Fiber type	Soil type Tested for RDFS (USCS)	Fiber length (FL) mm and Fiber percentage (FP) %	Test method	Use as Earth block	Use as LLG	Key conclusions	References
Coir	1) SP 2) SM 3) CL 4) CH (Marine clay) 5) CL (Fine grained) 6) CH (Black cotton) 7)CL (Cohesive)	**1)** FL (10-30) FP (0.5-2.5) **2)** FL (80) FP (0.5-2) **3)** FL(15-25) FP (0.1-0.6) **4)** FL(10-30) FP(0.2-1.5) **5)** FL(50-200) FP(0.5-2) **6)** FL(20) FP(0.5-1.5) **7)** FL(15-25) FP(0.1-0.6)	TT[1,2,5] UCS[2,3,4,5,6] PL[3] CBR[7]	✓	✓	- Linear increase in friction angle with addition of coir fiber (1%-2.5%) for SP. - With addition of coir fiber up to 2.5%, energy absorption capacity increases for SP. - For SM soil, coir RDFS shows higher resilient modulus and UCS as compared to polypropylene (PP) fiber. - For field PL test on CL soil, both coir and PP increased the ultimate load of soil to 70kN and 80kN. - For CH soil (marine clay), optimum FP is 0.8%. - Peak deviator stress for CL (Fine grained) soil increases in case of coir reinforced soil. - In CH soil (black cotton) optimum FP is 4%, and addition of lime with fiber increases ductility. -Maximum residual shear stress is exhibited by 0.8% PF, for CL (cohesive soil).	Ghavami et al. 1999, Khedari et al. 2004*, Lekha 2004*, Babu and Vasudevan 2008, Chauhan et al. 2008, Subaida et al. 2008, Subaida et al. 2009, Ramesh et al. 2010, Sebastian et al. 2011, Dasaka and Sumesh 2011, Kar et al. 2012, Dutta et al. 2012, Kar et al. 2014,
Flax	N/A	N/A	UTM	✓	✓	- Flax fiber reinforced soil has not been reported.	Sarsby 2007, Segetin et al. 2007, Cheah and Morgan 2009

						- Its application is done extensively for earth blocks and increases the compressive strength of the composite. -For Harakeke earth blocks, optimum FP is 0.6%. - Significant improvement in ductility of soil-cement-fiber composites is seen for earth blocks. - Beneficial in low cost-UKU buildings. - Applicable as LLG in soft clay embankment reinforcement.	
Oil palm	1) ML 2) SM 3) N/A (Cohesive) 4) CH 5) ML	**1)** FL (30) FP (0.25-1) **2)** FL (15,30,45) FP (0.25, 0.5) **3)** FL (NA) FP (0.25 – 1) **4)** FL (1 -16) FP (5 -20) **5)** FL (270) FP (0.5 – 1.5)	UCS[1,3] ST[1] TT[2] PT[3,5] DS[4] CT[4] CBR[5]	✓	✓	- With increase in FP (0.25% – 1%), UCS rise is observed for ML soil. - No quantifiable trend in shrinkage characteristics with inclusion of fiber for ML soil. - With increase in fiber length, there is rise in cohesion and frictional angle. 0.5% fiber showed better mechanical response for SM soil. - For cohesive soil discussed, there is a drop in dry density and OMC, with increase in FP (0.25 – 1). With increase in FP, frictional angle decreases and cohesion increases. - For CH soil, significant improvement in the failure deviator stress, shear strength parameters (c and ϕ). - For ML soil, with increase in palm FP there is an increase in CBR value. At lower content, their performance is equivalent to polypropylene fiber.	Davies et al. 2006, Bhattacharyya et al. 2009, Ahmad et al. 2010, Jamellodin et al. 2010, Bhattacharyya et al. 2010, Azadegan et al. 2012, Al Adili et al. 2013, El-Maaty et al. 2016

						- Palm LLGs have garnered popularity in splash erosion resistance projects.	
Roselle	N/A	N/A	AW TS MA	x	x	- Based on accelerated weathering (AW) test, Tensile strength (TS) test and Moisture absorption (MA) test, roselle has been recommended as potential LLG. Retains 50% of its tensile strength after 4 weeks of AW. No change in elongation at break after 4 weeks of AW.	Methacanon et al. 2010*
Jute	1) CL 2) ML 3) ML (Silt)	**1)** FL (100) FP (0.2 - 1) **2)** FL (20 -100) FP (0 – 5) **3)** FL (20 -100) FP (0 – 5)	PT[1] CBR[1,2] UCS[3]	✓	✓	- Jute RDFS reduces the MDD and increases the OMC of CL soil. Optimum FP is (0.6%-0.8%). - CBR value increases with incremental fiber reinforcement for all L/D ratios and functions better than coir reinforced RDFS. - Optimum PF is 0.5% for ML (Silt) soil.	Ramaswamy et al. 1983, Islam and Iwashita 2010, Aggarwal and Sharma 2010 Güllü and Khudir 2014, Kumar et al. 2015, Pavani et al. 2016, Bera et al. 2009
Kenaf	CL	FL (3) FP (0.2 – 0.8)	Hydrau -lic press	✓	✓	- UCS increased to an optimum value near 0.4 PF and then decreased. - Inclusion of fiber prevents the propagation of cracks in earth blocks. - Kenaf reinforced earth block improves ductility in tension of the blocks.	Chaiyaput et al. 2014, Millogo et al. 2015*
Reed	1) Sand[a] 2) Sand[b] 3) SM	1) 3 to 22 in numbers 2) FL (13,25,38)	DS[1,3] TT[2] CT[3]	x	x	- For sand[a], increase in fiber leads to a progressive rise in peak strength and post peak strength reduction at higher	Gray and Ohashi 1983, Gray and Al-

		FP (0.2 - 2) 3) FL (NA) FP (5-25)				strains. Optimum orientation angle of fibers is 60^0. - For sand[b], rise in FP increases peak shear strength and major principal stress at failure. - For SM soil, optimum FP was found to be 10%.	Refeai 1986, Al Adili et al. 2012
Sisal	1) CL 2)ML	**1)** FL (10 -25) <u>FP (0.25 - 1)</u> **2)** FL (5 -15) <u>FP (0.5 – 1.5)</u>	TT[1,2] PT[1]	✓	✓	- Increase in FL and FP results in linear decrease of MDD and OMC. - Optimum FP for cohesion is 0.75%. Optimum FL and FP in terms of angle of internal friction was found at 20 mm and 0.75% respectively. - For ML soil, peak strength, ductility and cohesion are improved with fiber addition.	Prabakar and Sridhar 2002, Namango 2006, Mwasha and Petersen 2010*, Wu et al. 2014
Hemp	N/A	N/A	N/A	✓	✓	- With adsorption percentage of 80% at equilibrium, it can be used in landfill projects - Hemp fiber has been used to make a patented geotextile.	Boutron et al. 2009*, Islam and Iwashita 2010, Roure and Geco 2012
Water Hyacinth	1) ML	**1)** FL (20 – 57) <u>FP (0.25 – 1)</u> **2)** FL (28) FP(0.5 – 1)	PT[1] CBR[1]	x	✓	- For ML soil, fiber inclusion results in decrease in OMC and MDD with increase in FP. Optimum FP for CBR is 0.5%. - For SM soil, it resulted in a low drop in peak strength and increases the ductility.	Maneecharoen et al. 2013, Dileep et al. 2015

TT- Triaxial compression test, UCS – Unconfined compressive test, PL –Plate load test, CBR – California bearing ratio, UTM – Universal testing machine, PT- Proctor test, ST – Swell test, AW-Accelerated weathering test, TS- Tensile strength test, MA- Moisture absorption test, DS – Direct shear test, CT- Consolidation test, * - Biochemical composition of fiber investigated

2.2.3 Physio-biochemical properties of natural fibers

(A) Fiber structure and composition

Natural fibers derived from plants are referred to as cellulosic and lignocellulosic fibers (Siqueira et al. 2010) and constitutes cellulose, hemicellulose and lignin (Abdul et al. 2013). These components serve to form the cellulose superstructure in the form of a matrix (Khalil et al. 2015). A typical representation of such fiber is shown in Fig. 2.4 (a) and Fig. 2.4 (c). Each fiber has an intricate layered structure (Wathen 2006), which consists of three different layers- middle lamella (ML), primary wall (P) and secondary wall (S). Middle lamella and primary wall are together known as combined middle lamella. The secondary wall is divided into three layers- S1, S2 and S3. The thick middle layer (S2) of the secondary wall determines the mechanical properties of the natural fiber (Azwa et al. 2012). This S2 layer consists of a series of helically wound cellular microfibrils (represented by black lines in Fig. 2.4 (a)) formed from long chain cellulose molecules. Lignin and hemicelluloses in these layers acts as a matrix (represented by white portion in Fig. 2.4 (a)), while microfibrils (made up of cellulose molecules) acts as fibers (Azwa et al. 2012). The strength of natural fibers can be attributed to the rigidity and high molecular weight of cellulose chains (due to intermolecular and intramolecular hydrogen bonding) (Nguyen et al. 1981). The general distribution of cellulose, hemicellulose and lignin in a lignocellulose fiber has been represented in Fig. 2.4 (b). From the figure, it is evident that S2 layer has the highest percentage of cellulose and the combined middle lamella (P + ML) has the highest percentage of lignin. The individual contribution of cellulose, hemicellulose and lignin to a natural fiber are discussed in the following section.

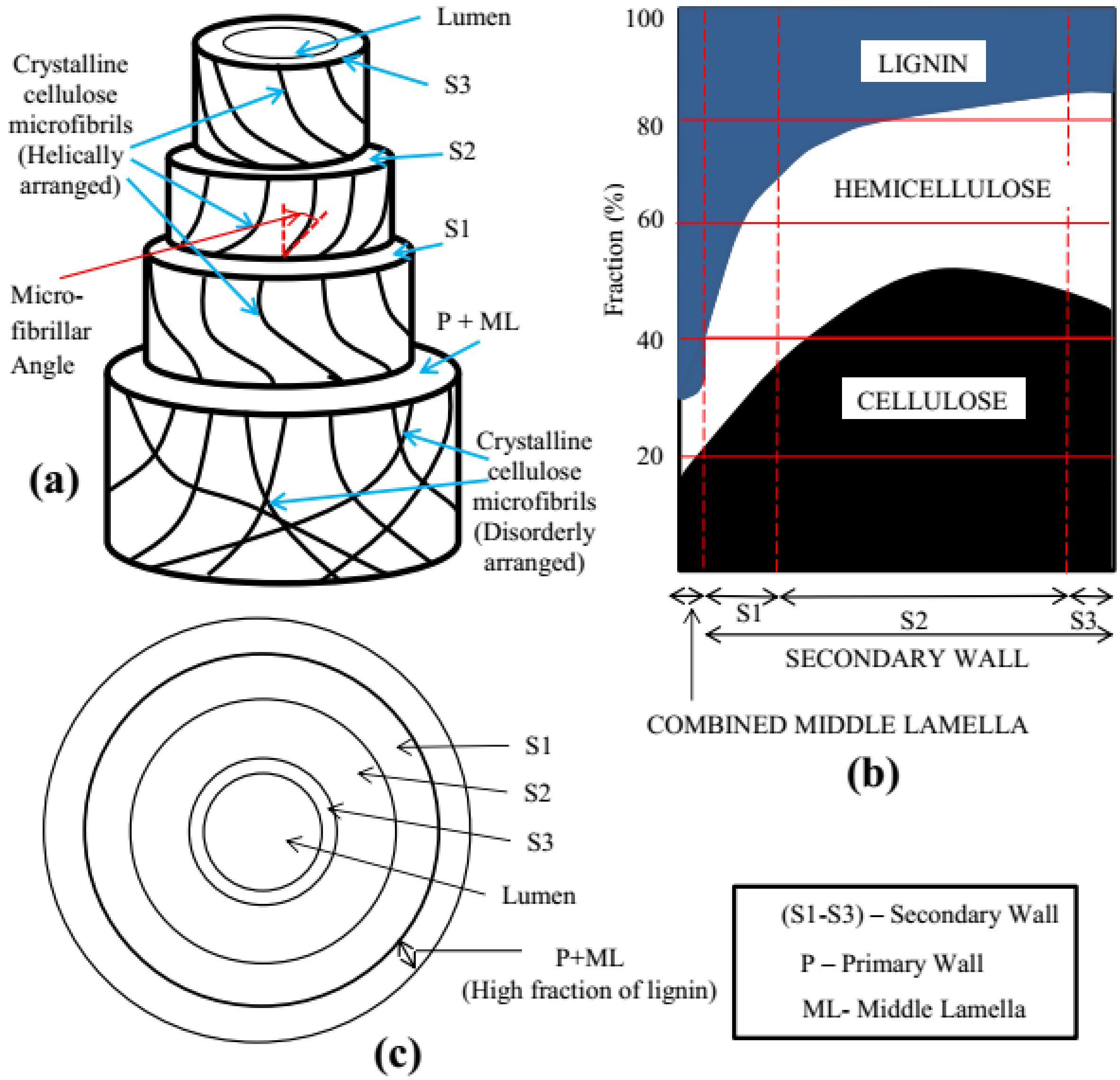

Fig. 2.4 Hypothetical arrangement of different layers in (a) Lignocellulose fibers (after John and Thomas 2008); (b) Relative composition of lignin, cellulose and hemicellulose in lignocellulose fibers (after Jensen 1977) and (c) Jute (after Mwaikambo 2009)

Cellulose

Cellulose is the main strength contributing component to lignocellulosic materials. It is a long linear polymer, composed of glucose units joined together by β-1, 4 glycosidic bonds (Khalil et al. 2014). Cellulose is made up of polymer chains consisting of glucose units which remain linked together by highly resistant hydrogen bonds (Delmer and Amor 1995). The cellulose chains group together in a hemicellulose matrix and the entire structure collectively form a microfibril (refer Fig. 2.5). Numerous microfibrils are arranged in a helical structure (refer Fig. 2.4 (a)), to form a macrofibril (Fig. 2.5). Plant fibril matrix is ultimately formed by such group of macrofibrils (Martins et al. 2011). The strength and stiffness of fibers is dependent on the crystallinity or the crystallinity index (CI) and microfibrillar angle (MFA) of the cellulose microfibrils (Mwaikambo 2009). CI is used to describe the relative percentage of crystalline material in cellulose. The microfibrils have amorphous and crystalline regions and their relative composition determines the strength of natural fiber (Zhou and Wu 2012). The crystalline region is highly ordered and packed with a strong complex intra and intermolecular hydrogen bond network (Khalil et al. 2015). MFA is the average angle between fiber axis and the microfibrils as shown in Fig. 2.4 (b). Smaller angle of MFA leads to higher fiber strength and stiffness whereas a larger angle yields to higher ductility (Azwa et al. 2012). The study by Gassan et al. (2001) has correlated the elastic modulus of material with the MFA of the fiber. With lower MFA, the elastic modulus of the fiber was found observed to decrease. Morton and Hearle (1975) have noted that the fibers with higher cellulose content can be stronger than those with low cellulose content, provided their MFA is small. For example, cotton with MFA of 20^o-30^o and cellulose content of over 90 %, exhibits lower mechanical properties as compared to hemp and flax fibers (MFA $\leq 7^o$ and cellulose content about 80%) (Morton and Hearle 1975, Mwaikambo 2002).

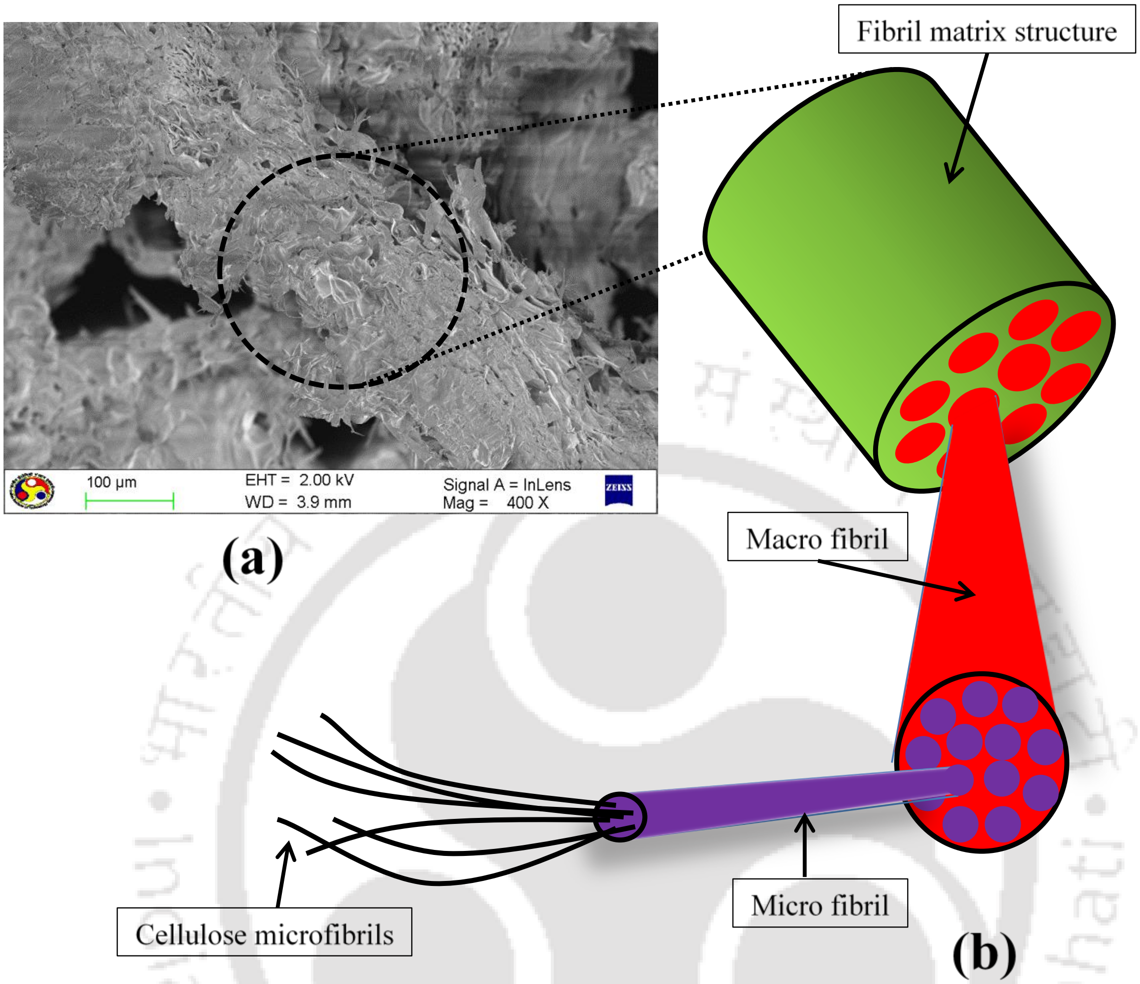

Fig. 2.5 Pictorial description of (a) *Eicchornia crasipes* fiber using FE-SEM; (b) Arrangement of cellulose microfibrils in a fibril matrix structure (after **Khalil et al. 2014**)

Hemicellulose

Hemicelluloses are made up of low molecular weight cell wall polysaccharides associated to cellulose formed up from various pentose sugars (Methacanon et al. 2010). The major role of hemicelluloses in the fiber cell walls is of cross linkage between cellulose fibril aggregate by forming complexes with lignin (Khalil et al. 2014). Furthermore, they act as an adhesive filler material in the cavities between the microfibrils. The individual contribution of hemicellulose to fiber strength is not entirely established. Spiegelberg (1966) in his study of hemicellulose, found that with decrease in hemicellulose; the tensile strength, elastic modulus and work to rupture fibers reduces. For moist fibers, hemicellulose functions as an effective stress-transfer matrix (Kersavage 1973). Rowell and Stout (2007) have found that hemicellulose is mainly responsible for moisture absorption, as its hydroxyl groups are much more accessible to water.

Lignin

Lignin, a complex phenolic polymer, with high molecular weight is important for mechanical support, water transport and resistance to biodegradation (Khalil et al. 2014). It works as a strengthening material between the cellulose and microfibrils, and also provides protection against attack by pathogens (Bjerre 1997, Moore and Jung 2001). Lignin forms between neighboring cells in middle lamella, connecting them tightly into a tissue. It then spreads into cell wall encapsulating the hemicelluloses and bonding the cellulose fibrils (Reddy and Yang 2005). Lignin is of specific importance, as it enhances resistance to microbial degradation in soils (Methacanon et al. 2010). The insolubility and complexity of the lignin polymer resists its degradation by microorganisms (Campbell and Sederoff 1996). Lignin varies in composition and quantity within the same plant. The percentage composition variation can vary within populations of plants of the same species. For instance, within the genus "Pinus", the average content of lignin can range from 25% (Pinus monticola) to 30% (Pinus palustris) (Campbell and Sederoff 1996). Lignins have been employed as a low-cost means of dust control in the recent past (Hawkins et al. 2006, Schilling et al. 2006).

(B) Chemical composition and mechanical properties of fiber used for soil

Table 2.2 Chemical composition of dried fiber used for soil reinforcement

Fiber	Cellulose (%)	Hemicellulose (%)	Lignin (%)	Ash (%)	Reference
Coir	43.4 - 53	14.7	38.3 – 40.7	2	Satyanarayana et al. 2007, Azwa et al. 2013
Kenaf	42 - 57	21.5	8 - 15	3.7	Ververis et al. 2004, Akil et al. 2011
Flax	62-72	18.6 – 20.6	2-5	———	Satyanarayana et al. 2009, Akil et al. 2011
Jute	60-64.4	22.1	15.9	1	Satyanarayana et al. 2007, Bledzki et al. 1999
Oil palm	50-65	21.9	10 - 19	0.5 - 2	Umikalsom et al. 1997, Jacob et al. 2004
Reed	33 - 47.4	18.7	17 - 19.81	4.65 - 5	Ververis et al. 2004, Methacanon et al. 2010
Sisal	60-75.2	5.63 – 14	8-14	0.8	Satyanarayana et al. 2007, Satyanarayana et al. 2009, Methacanon et al. 2010
Hemp	70 - 74	17.9 – 22.4	3.7 – 5.7	0.8	Li et al. 2007, Akil et al. 2011
Roselle	70.20	7.21	14.91	0.72	Methacanon et al. 2010

Table 2.2 summarizes the biochemical composition of natural fibers used for soil reinforcement. Cellulose content is found highest in non-crop species like sisal and roselle and in weed species such as hemp. Hemp and flax exhibits the highest amount of hemicellulose. Coir possessing the highest relative amount of lignin is one of the most popular fibers used for soil reinforcement, as it is highly resistant to biodegradation (Ghavami et al. 1998, Khedari et al. 2003,

Lekha 2003, Khedari et al. 2004, Chahuan et al. 2008, Babu and Vasudevan 2008, Subaida et al. 2008, Dasaka and Sumesh 2011). Ash content provides the natural capacity of plants for metal adsorption. It is a measure of the mineral content and other inorganic matter in any biomass.

Table 2.3 Physical and mechanical properties of dried fiber used for soil reinforcement

Fiber	Density (kg/m^{-3})	Microfibrillar angle (ϴ)	Crystallinity (%)	Water absorption (%)	Young's Modulus (GPa)	Ultimate tensile strength (MPa)	Elongation at break (%)	Reference
Coir	1390-1520	30 - 51	27 - 43	130 - 180	6	100 - 220	12 – 51.4	Cook 1984, Pavithran et al. 1987, Reddy and Yang 2005, Satyanarayana et al. 2007, K.E.F.I 2016
Kenaf	1500	9 - 15	____	____	18-53	176 - 930	1.6	Aji et al. 2009, Akil et al. 2011, K.E.F.I 2016
Flax	1500	5 - 10	80	____	27.6-80	345 - 1500	1.2 – 2.7	Cook 1984, Satyanarayana et al. 2009
Jute	1300 - 1450	17.1	____	____	10 - 30	393 – 800	1.5 – 1.8	Satyanarayana et al. 2007
Oil palm	463	42	79 - 87	____	26.5	100 - 400	19	Cook 1984, Ahmad et al. 2010, Azwa et al. 2013, Haafiz et al. 2013
Reed	490	____	____	100	____	200	14	De Baets 2008, Methacanon et al. 2010, Azwa et al. 2013,
Sisal	700-1330	10-20	72.2	56-230	17 - 22	160 - 680	3.64 – 13	Cook 1984, Pavithran et al. 1987, Ghavami et al. 1999, Reddy and Yang 2005, Methacanon et al. 2010, Azwa et al. 2013,
Hemp	1470	2 - 6.2	____	8	70	550–900	1.6	Cook 1984, Wambua et al. 2003, Vadivambal 2015

Roselle	750 - 800	——	——	40 - 50	2.8	108-184	5-11	Azwa et al. 2013, Haafiz et al. 2013
Water hyacinth	800	——	——	32	——	625	13.6	Wambua et al. 2003, Ahmad et al. 2010, Abral et al. 2014

Water hyacinth possessing highest ash percentage has been widely used for heavy metal retention (Alvarado et al. 2008, Mahamdai and Nharingo 2009, Chunkao et al. 2011). The physical and mechanical properties of natural fibers for soil reinforcement are tabulated in Table 2.3. The highest tensile strength is exhibited by kenaf, flax and hemp which possess low MFA coupled with relatively high amount of cellulose. Flax with the highest amount of CI among those fibers (Kenaf, flax and hemp) showcased the highest tensile strength. However, the variation in tensile strength is quite high for kenaf and flax which may be attributed to genetic difference.

2.2.4 Moisture absorption, degradation and treatment of natural fiber

(A) Moisture absorption of natural fibers

Natural fibers, being porous in nature, are well established to be hydrophilic in nature and are susceptible to moisture absorption (Stone and Scallan 1966). Soil fiber under sub-surface conditions is subjected to alternate cycles of wetting and drying. The morphology, as well as the chemical structure, plays a predominant role in the swelling of natural fibers (McKenzie and Yuritta 1979). Natural fibers change their dimensions (mostly at microscopic level) with moisture content variation. Cell wall of such fibers, contain hydroxyl and other oxygen containing groups, which attract moisture through hydrogen bonding (Rowell and Banks 1985). Cellulose and hemicellulose absorb up to 4-5 times more water than lignin at saturated conditions (Cousins 1978). The counter ions of the anionic groups within the fiber wall are very significant to fiber swelling (Scallan 1983). The relation of fiber swelling and the counter ions is due to a dependency of osmotic pressure inside the fibers. Water is sucked into fibers to reduce osmotic pressure. The effect of fiber swell on soil fiber composite has been reported to have resulted in the preferential flow of water through the composite and also effect the adhesion in soil-fiber interface (Ghavami et al. 1998, Hejazi et al. 2012, Azadegan et al. 2012, Ismail and Yaacob 2011). The swelling of fibers affects the adhesion of soil-fiber interface, due to periods of swelling and shrinkage, corresponding to cycles of wetting and drying. This swell, however is dependent on the fiber bio-chemical composition and fiber porosity (Methacanon et al. 2010, Scallan 1983). Figure 6 represents a schematic representation of the interaction of moisture with natural fiber- soil composite. After compaction of the soil-fiber composite, if there is a heavy spell of precipitation, high absorption of water would make the individual fiber to swell, consequently pushing the soil matrix (at the micro level) (Ghavami et al. 1998). On further drying (corresponding to drought conditions), the fiber shrinks and results in the formation of air pockets along the soil-fiber interface. These pockets form pathways for preferential flow of water on subsequent precipitation cycle thus possibly increasing the infiltration of water through the composite. A study of palm fiber inclusion on mud soil (Ismail and Yaacob 2011), have reported the increase in permeability for mud bricks as compared to unreinforced bricks. Dimensional changes due to fiber swell leads to decrease in friction angle of the composite (Azadegan et al. 2012). Thus, in addition to improve the bonding characteristics of the fiber with soil, there is also a need to possibly treat the fibers, so as to minimize water transfer between soil matrix and fibers. Some possible treatment has been discussed in the later section.

The preferential flow through fiber reinforced soil can be compared to that of rooted soil. Natural fibers can be considered as dead roots (Saran 2010), and they can act as conducting pipes for preferential flow (Azadegan et al. 2012, Johnson and Lehmann 2006). Dye tracer experiments were conducted to establish the formation of preferential flow through roots, and its subsequent increase in infiltration rate (Bramley et al. 2003). Although, infiltration studies on soil fiber composite was done on synthetic fiber reinforced soil (Miller and Rifai 2004), rarely any studies have been conducted on natural fiber reinforced soil. Methacanon et al. (2010) have found that natural fibers show a considerate increase in tensile strength and elongation at break, when wet as compared to dry state. The increase in tensile strength can be attributed to moisture in the fiber influencing the degree of crystallinity and MFA of the fibers (Reddy and Young 2005). The increase in elongation at break can be due to the adsorbed water molecules acting as a lubricant, such that the fibers could slide over one another during stretching, resulting in increased extension (Methacanon et al. 2010).

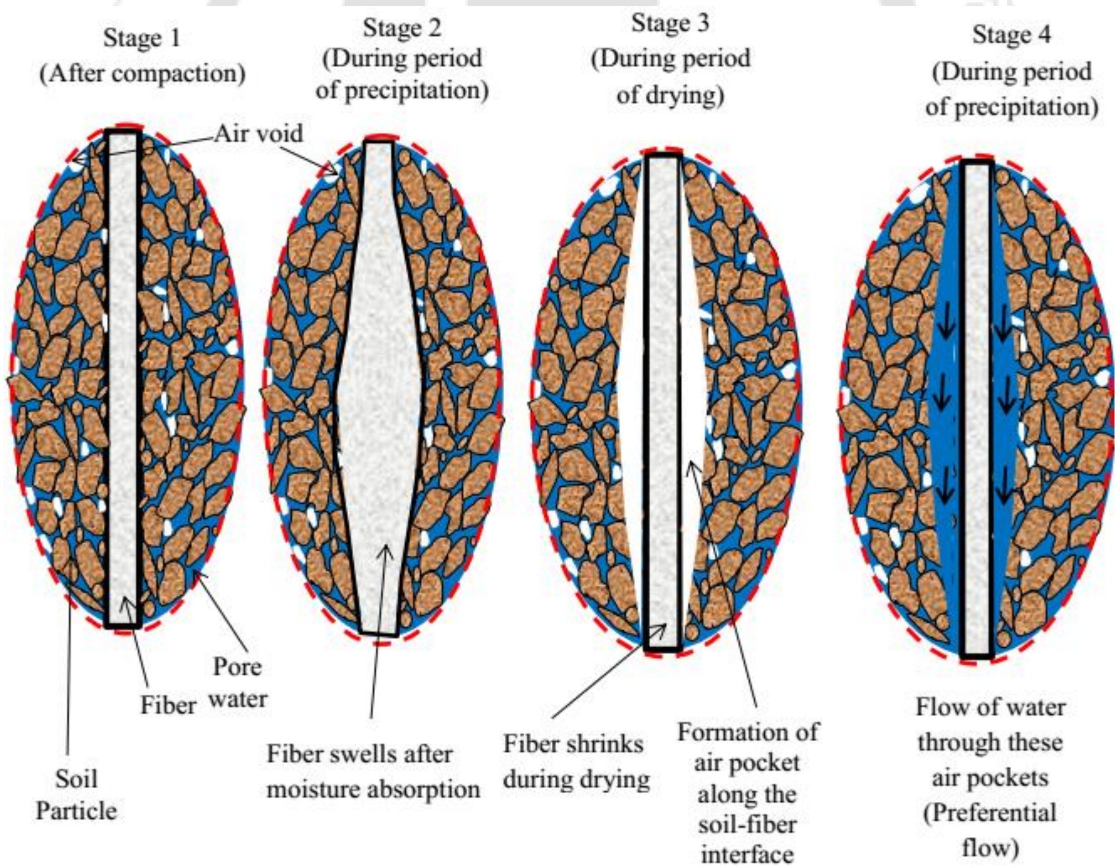

Fig. 2.6 Schematic representation of the interaction of moisture with natural fiber-soil composite

(B) Fiber degradation

Figure 2.7 represents cell wall polymers responsible for strength, moisture absorption and degradation properties. Moisture absorption and degradation of fibers are detrimental to its lifespan as reinforcing material. Thermal decomposition is usually endothermic, as heat is required to break chemical bonds in the compound undergoing decomposition. Each cell wall polymer is degraded by a variety of microorganisms which produce a battery of enzymes that leads to gradual biodegradation (Pérez et al. 2002). However, higher hemicellulose content results in higher moisture absorption, providing favorable conditions for microorganisms to act on the fiber (Methacanon et al. 2010, Beg and Pickering 2008). Thus, high percentage of hemicellulose in a fiber makes the fiber susceptible for thermal and biological degradation, moisture absorption and flammability. Biodegradation occurs under aerobic and anaerobic conditions and can be determined using Eq. 2.1 and Eq. 2.2 respectively (Holliger and Zehnder 1996, Widdel and Rabus 2001). For aerobic biodegradation, the lignocellulose polymer formed by carbons, breaks up into residue carbon polymer and release carbon with CO_2 and H_2O. With anaerobic degradation, there is additional emission of methane (CH_4) along with residue carbon, CO_2 and H_2O. Ultraviolet degradation of fibers is susceptible with higher content of lignin. An accelerated weathering test (exposed to UV ray coupled with moisture in cycles) on four natural fibers (sisal, roselle, reed and water hyacinth) has been carried out, to gauge its effect on mechanical properties, such as tensile strength and elongation at break, for a continuous period of five weeks (Methacanon et al. 2010). The tensile strength decrease is significantly high (approximately 50%) for sisal, reed and Roselle after the five-week duration. However, the decrease in tensile strength is negligible for water hyacinth at 20% of initial strength. The effect of such accelerated weathering has negligible effect on the elongation at break of the fibers.

$$C\ polymer + O_2 \rightarrow C\ residue + C\ biomass + CO_2 + H_2O \quad (2.1)$$

$$C\ polymer \rightarrow C\ residue + C\ biomass + CO_2 + CH_4 + H_2O \quad (2.2)$$

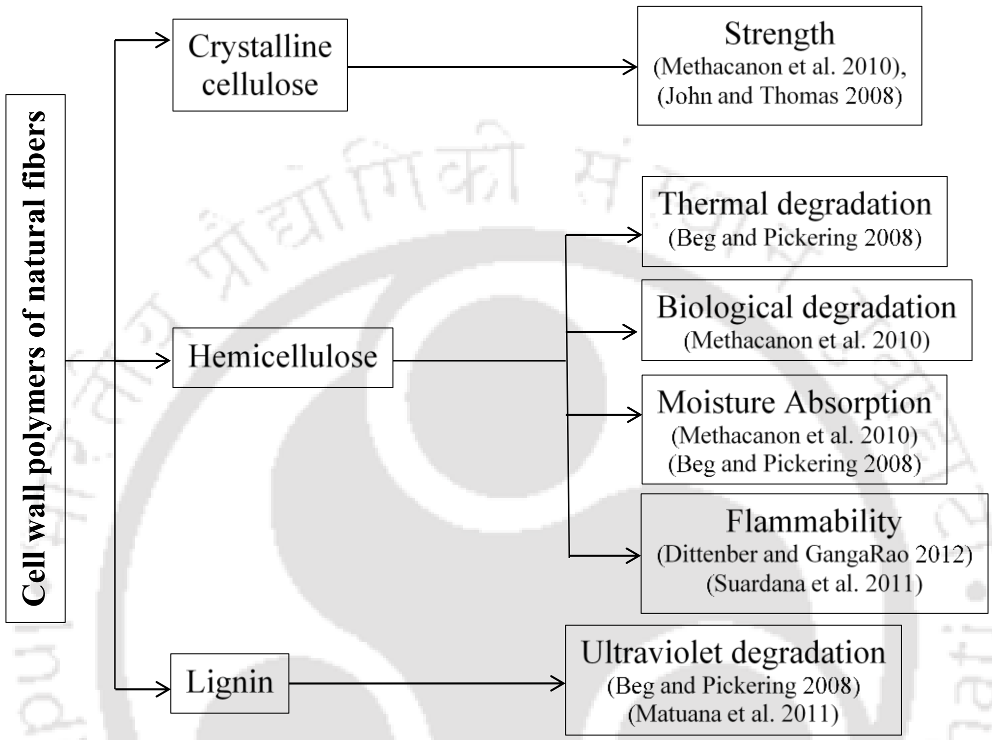

Fig. 2.7 Cell wall polymers responsible for strength, moisture absorption and degradation properties

(C) Fiber treatment

Treatment of natural fibers, aimed at improving the adhesion and reducing the moisture absorption with the surrounding matrix, was investigated by a number of researchers. The major chemical modifications used in natural fiber treatment (Li et al. 2007) are alkali treatment, silane treatment, acetylation treatment, benzolyation of fibers and permanganate treatment as discussed below.

Alkali treatment

Alkaline treatment disrupts the hydrogen bonding in the fiber network structure, thereby increasing surface roughness of the fiber. However, this treatment removes a certain amount of lignin. Equation 2.3 represents the aqueous sodium hydroxide (NaOH) addition to natural fiber, which promotes the ionization of the hydroxyl group to the alkoxide and directly influences the cellulosic fibril (Agrawal et al. 2010, Jähn et al. 2002). It is reported that alkaline treatment increases surface roughness resulting in better mechanical interlocking between fibers and surrounding matrix (Valadez et al. 1999). This treatment is extensively used in RDFS (Gu et al. 2009, Dutta et al. 2012, Rawal and Sayeed 2014).

$$\text{Fiber –OH + NaOH} \longrightarrow \text{Fiber –O –Na} + H_2O \quad (2.3)$$

Silane treatment

Silane with chemical formula SiH_4, reduces the number of cellulose hydroxyl groups in the fiber–matrix interface (Li et al. 2007). The hydrocarbon chains provided by the application of silane restrain the swelling of the fiber. The reaction schemes are given by Equations 2.4 and 2.5 (Agrawal et al. 2010).

$$CH_2CHSi(OC_2H_5)_3 \xrightarrow{H_2O} CH_2CHSi(OH)_3 + 3C_2H_5OH \quad (2.4)$$

$$CH_2CHSi(OH)_3 + \text{Fiber – OH} \longrightarrow CH_2CHSi(OH)_2O\text{–Fiber} + H_2O \quad (2.5)$$

Acetylation of natural fibers

Introducing an acetyl functional group ($CH3COO^{-}$) into an organic compound is a well-known esterification method which causes plasticization of lignocellulosic fibers. Chemical modification of such fibers, with acetic anhydride (CH3-C(=O)-O-C(=O)-CH3) substitutes the polymer hydroxyl groups of the fiber cell wall with acetyl groups, and making the cell wall hydrophobic (Hill et al. 1998). The general equation for acetyl treatment is represented by Equation 2.6.

$$\text{Fiber}-OH + CH_3-C(=O)-O-C(=O)-CH_3 \longrightarrow \text{Fiber}-OCOCH_3 + CH_3COOH \quad (2.6)$$

Treatment of sisal fiber by acetylation is reported to improve the fiber–matrix adhesion (Mishra et al. 2003). After the treatment, sisal fiber became very rough and with higher voids provided better mechanical interlocking.

Benzolyation treatment

Benzolyation treatment includes benzoyl ($C_6H_5C=O$) group and decreases the hydrophilic nature of the treated fiber. The reaction between the cellulosic hydroxyl group of the fiber and benzoyl chloride is shown in Equations 2.7 and 2.8 (Joseph 2000).

$$\text{Fiber}-OH + NaOH \longrightarrow \text{Fiber}-O^{+}Na^{-} + H_2O \quad (2.7)$$

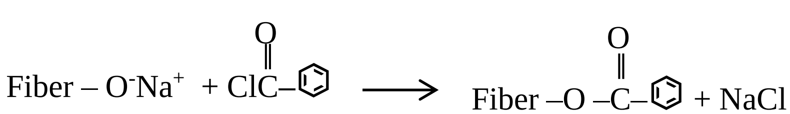

(2.8)

Benzoylation of fiber can highly improve its application in soil-fiber composite by considerably increasing the composite strength, decreasing fiber water absorption and improving its thermal stability.

Permanganate treatment

Permanganate ($MnO4^-$) treatment leads to the formation of cellulose radical by $MnO3^-$ ion formation. Subsequently, highly reactive $Mn3^+$ ions are responsible for initiating graft co-polymerization and are represented in Equations 2.9 and 2.10 (Frederick and Norman 2004).

$$\text{Cellulose–H} + KMnO_4 \longrightarrow \text{Cellulose –H–O–}\overset{\overset{\displaystyle O}{\|}}{\underset{\underset{\displaystyle O}{\|}}{Mn}}\text{–OK}^+ \qquad (2.9)$$

$$\text{Cellulose–H–O–}\overset{\overset{\displaystyle O}{\|}}{\underset{\underset{\displaystyle O}{\|}}{Mn}}\text{–OK}^+ \longrightarrow \text{Cellulose + H–O–}\overset{\overset{\displaystyle O}{\|}}{\underset{\underset{\displaystyle O}{\|}}{Mn}}\text{–OK}^+ \qquad (2.10)$$

It is reported that due to permanganate treatment, the hydrophilic tendency of sisal fibers decreases (Paul et al. 1997). Table 2.4 summarizes the various treatment applied to natural fibers in soil reinforcement. Natural fibers used as RDFS or LLGs were treated using various chemical treatment (NaOH, CCl_4,) coating (Polyurethane, Enamel paint, Bitumen, Polythene, Acrylic butadiene styrene) and ultrasonic impact. The key conclusions are discussed with respect to its performance as a reinforcing material properties as well as its performance as a soil-fiber composite.

Table 2.4 Summary of treatment applied to natural fibers in soil reinforcement

Fiber	Treatment	General objectives	Key conclusions	References
Coir	1- NaOH and CCl_4 4- Nanomodification 5- Ultrasonic impact	- Improve fiber interfacial bonding - Decrease degradation - Increase strength - Increase hydroxyl group in fiber	- For fiber treated with NaOH and CCl_4 in a clay soil, there is a significant improvement in strength and ductility of the clay-fiber composite. Higher peak strength and strain was observed for CCl_4, as compared to NaOH treatment. - For nano-modified fibers, there is a significant improvement in cohesion and internal friction as compared to untreated soil. - Ultrasonic impact treated fibers showcased higher cellulose content as compared to untreated fiber.	Gu 2009, Dutta et al. 2012, Renouard et al. 2014, Anggraini et al. 2016
Kenaf	Polyurethane coating	- Reduce water absorption - Decrease effect of radiation	- Higher deformations or stresses in both coated and non-coated LLGs reinforced embankments were observed.	Chaiyaput et al. 2014
Flax	1- Ultrasonic impact 2- Enamel paint coating	- Reduce the transfer of water between the matrix and the fiber	- Ultrasonic impact reduces the cellulose content of the fiber - Enamel coat forms a heavy coating and is relatively hard to mix. The strength and ductility of the composite is not significantly improved with such coating.	Segetin et al. 2007, Renouard et al. 2014
Jute	1 - Bitumen coating 2- NaOH 3 – Alkali-steam 4 – Polythene coat	- Protection from microbial attack - Enhance surface roughness - Increase strength	- Bitumen coated LLGs derived from coir fiber, has been tested at fully saturated river slope. After 550 days, the coir LLG retains 30% of its strength and reported to be functional. Also the CBR values increases	Sanyal and Chakraborty 1994, Mwaikambo and Ansell 2002,Aggarwal and Sharma 2010, Rawal and Sayeed 2014,

			from 2.5 (untreated fiber reinforced) to 7.36 (treated fiber inclusion). - NaOH treatment on LLGs enhances surface. Significant increase in tensile strength and secant modulus is observed for treated LLGs as compared to untreated ones. - The steam method increases the tensile strength and elongation at break - Polythene coated fiber RDFS improved CBR 2.8 times	
Oil palm	Acrylic butadiene styrene thermoplastic	- Reduce hydrophilic nature of fiber	- Coated fibers increase the shear strength of the soil as coating increase the diameter and surface area of the fibre, and consequently, interface friction of fiber and soil increases.	Ahmad et al. 2010
Reed	NA	NA	NA	NA
Sisal	Emulsified bitumen coating	- Repel water	- Introduction of emulsified bitumen reduced water absorption of fibers significantly. But, introduction of emulsion did not enhance the bonding between the soil and fibers. Significantly improvement in durability is reported.	Ghavami et al. 1999
Hemp	Ultrasonic impact	- Increase durability	- There is no effect in the amorphous cellulose composition of treated fibers. However, ultrasonic exposed fiber shows a certain decrease in crystalline cellulose.	Renouard et al. 2014
Roselle	NA	NA	NA	NA
Water hyacinth	NA	NA	NA	NA

2.2.5 Gap areas and future scope of natural fiber in geotechnical engineering

Research on soil-natural fiber composite is gaining popularity for soil reinforcement owing to its low cost, coupled with dwindling petroleum resources and increasing ecological considerations. This review initially attempts to provide a state of the art on the use of natural fibers in soil reinforcement measures. One of the primary objectives of the current review is to put forth the importance of bio-chemical and physical properties of the natural fiber in understanding the fiber application as geo-reinforcement material. These inherent properties of a natural fiber have been discussed extensively and their individual contribution to the fiber is detailed. Based on the interdependency between the soil conditions and these properties, some case studies have been discussed in the context of moisture absorption, fiber degradation as well as possible treatment methodologies. Based on the discussion in previous sections, there is scope in further exploring the soil-natural fiber composite interaction and the review lays out some key prospective studies.

From Table 2.1, it is evident that many fibers (flax, roselle, hemp) bear potential as a fiber in RDFS, as seen by its application in earth block studies and LLGs. The application of these species in fiber reinforcement has not been studied till date. As discussed in section 2.2.3, the biochemical composition plays a major role, in the functioning of a lignocellulose fiber as reinforcing material. However, very few studies in geotechnical engineering have investigated the biochemical properties of a fiber, as shown in Table 2.1. The incorporation of biochemical property of a fiber better helps understand the mechanical response of a fiber upon loading. Surface roughness of fiber is also a property that is rarely investigated. It is important as it helps to increase the soil-fiber friction by soil particle interlocking and thus contribute to the general strength of the composite (refer Fig. 2.1).

Preliminary studies have been undertaken to study the effect of natural LLG on the vegetation growth of the surrounding soil (Lekha 2003, Álvarez-Mozos et al. 2014). However, there has been no comprehensive study undertaken to understand the role of natural fiber on the vegetation growth, which can sustainably and permanently reinforce soil against erosion, especially in road embankments. Such a coupled study on the interaction of fiber with vegetation growth, taking into consideration the microbiological content of soil can be applied in the design of bioengineered slopes (Morgan and Rickson 2003, Gadi et al. 2106). Although, the biochemical composition (percentage of lignin) gives a relative indication of the degradation time of the fiber/ LLGs, there is need to carry out studies that can model the life period of such lignocellulose materials in sub-soil conditions.

Lignocellulose fibers absorb water and expand at least at a micro-level (Refer Fig. 2.6). The formation of preferential flow path of water can increase the infiltration rate of such fiber reinforced soil. However, relatively very few studies have been undertaken to determine infiltration of such natural fiber reinforced soils. Monitoring the infiltration rate of such soils helps in developing models to predict runoff and surface erosion of such infrastructure. As lignocellulose fibers tend to absorb moisture, it is likely that the inclusion of fibers might influence the soil water retention property of the soil. Water retention property of a soil is represented by the soil water retention characteristic curve (SWRC), which is the relationship between the water content and the soil suction. As per the author’s knowledge, rarely any studies on WRCC of fiber reinforced soil have been conducted. The knowledge of WRCC further will help in determining the suitability of vegetation growth in such fiber reinforced soils (Gadi et al. 2016). Relatively few studies have adopted chemical treatment measures in the field of geotechnical engineering. As shown in section 2.2.4, the use of chemical modification to the fiber surface may further extend the life period of natural fibers, along with improving its mechanical properties.

Table 2.5 summarizes the cost of some natural fibers as compared to commercially used glass fibers used for soil reinforcement (Maher and Gray 1990, Michalowski and Zhao 1996, Novich et al. 2000). From the Table, it is evident that most of the naturally derived fibers reduce the material cost significantly. A comprehensive life cycle cost analysis can highlight the economy of such green infrastructures (Bianchini and Hewage 2012). The use of ligno-cellulosic fibers in soil reinforcement applications can help generate jobs in both rural and urban areas, with addition to reducing waste, thus contributing to a sustainable environment. However, more studies, as highlighted above are required on product development and performance evaluation of these green infrastructures, including the effect of environmental aging to further improve the use of natural fibers in geotechnical applications.

Table 2.5 Summary of cost of natural fibers as compared to artificial glass fiber (**Dittenber and GangaRao 2012**)

Fiber type		Glass	Coir	Flax	Hemp	Jute	Kenaf	Sisal
Cost per kg weight	Minimum cost (in dollars)	3.25	0.45	1.55	1.65	0.36	0.70	0.72
	Maximum cost (in dollars)	1.60	0.23	0.35	0.36	0.325	0.36	0.37
Cost per unit length of fibers able to resist tensile load of 100 kN	Minimum cost (in dollars)	0.12	0.11	0.40	0.65	0.60	0.60	0.75
	Maximum cost (in dollars)	0.42	0.67	0.67	0.92	0.17	0.41	0.28

2.3 Effect of vegetation on desiccation cracks

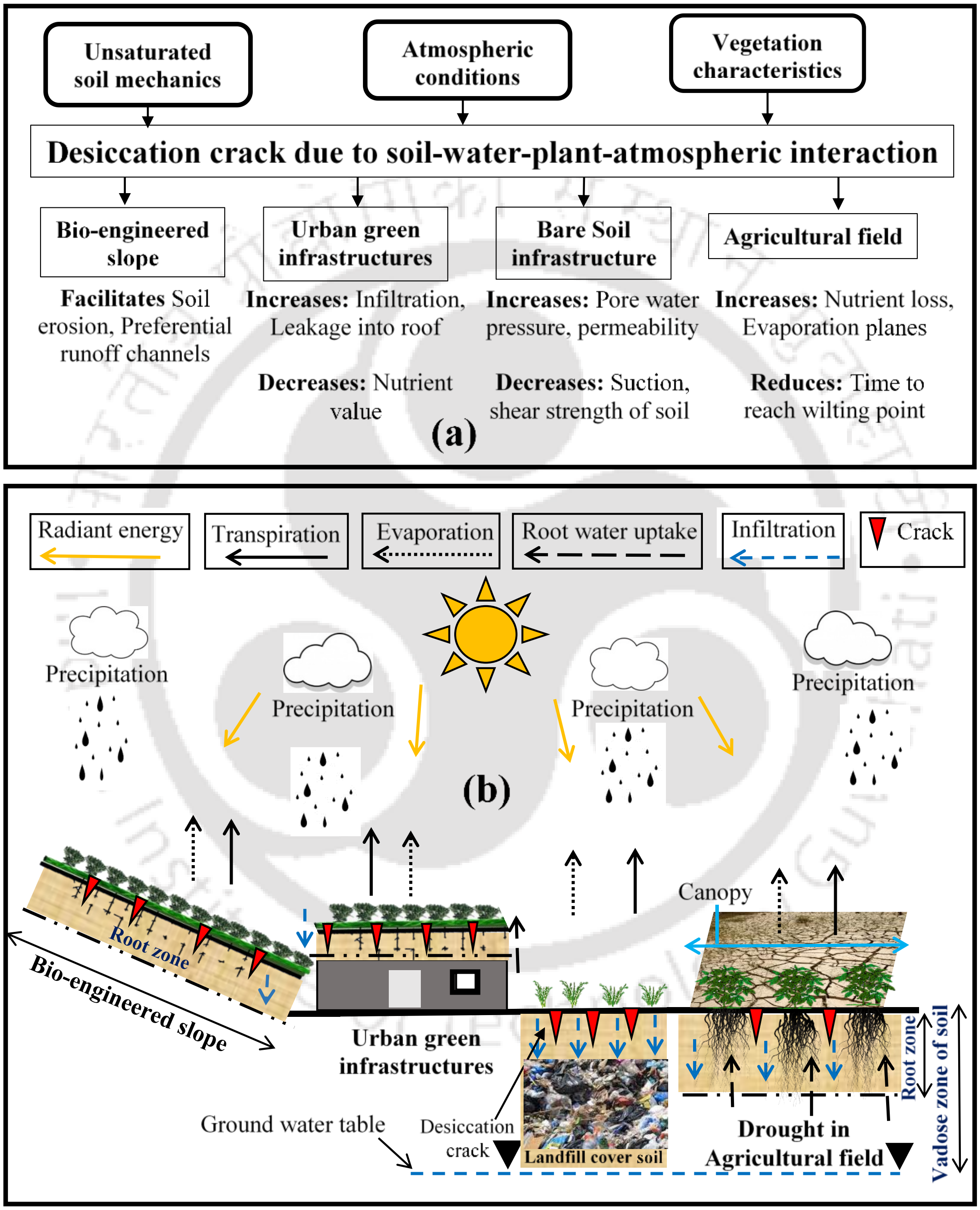

Fig. 2.8 Schematic (a-b) relationship of desiccation cracks with soil-air-water-plant interaction and its application in engineering infrastructure and agricultural field

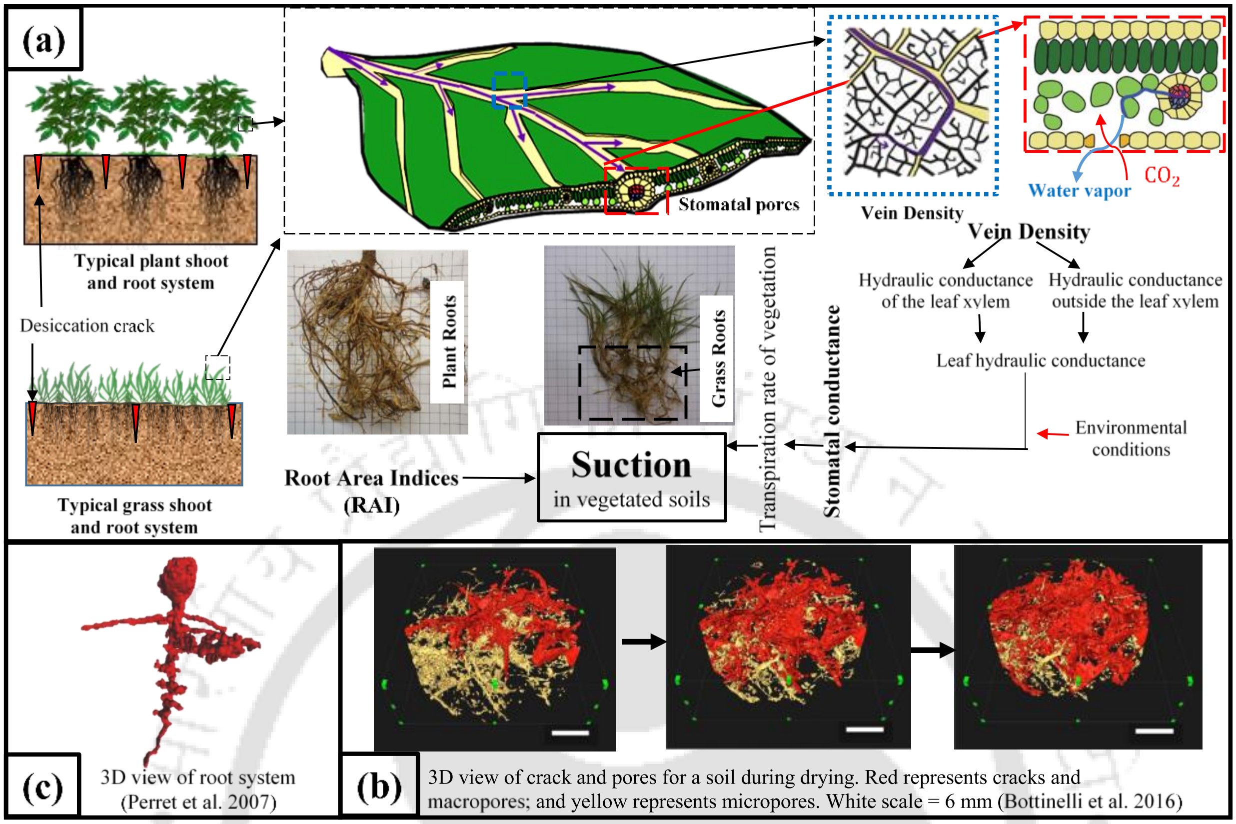

Fig. 2.9 Relationship (a) of root and shoot parameters with soil suction (after Scoffoni et al. 2016 and Ni et al. 2016); (b-c) Nondestructive tomography to investigate subsoil root and crack propagation

The presence of desiccation cracks upon drying in soils is of considerable concern in geotechnical engineering infrastructures. Desiccation cracks are widely seen in agricultural and engineered soils (Shokri et al. 2015). In agriculture soil, these cracks lead to unrestrained nutrient loss, facilitates pathway to harmful pesticides into ground water table and exacerbates formation of evaporation planes (Peng et al. 2016). These phenomena potentially reduce the time needed for plant species to reach wilting point in vegetated soil. Negative effects of desiccation cracks on the functioning of engineered infrastructures such as embankment slopes (Juang et al. 1998, Chang et al. 2011, Jiang et al. 2014, Chen and Zhang 2014, Li et al. 2015), dam failure (Talbot and Deal 1993), landfill liner (Li et al. 2016), green infrastructures (Gadi et al. 2016) have been documented extensively. Fig. 2.8 showcases the effects of desiccation which progressively deteriorates engineered infrastructures through high infiltration, soil erosion and pore-water pressure, etc. The formation and propagation of surface desiccation cracks involves coupled reasons including unsaturated soil mechanics (suction-moisture dynamics, initial compaction state), atmospheric conditions and vegetation characteristics. A comprehensive understanding of soil-air-water-plant interaction is necessary to understand and characterize desiccation cracks (Gadi et al. 2016) especially in vegetated infrastructures.

Recent studies have shown that the presence of vegetation (Fig. 2.9 (a)) can affect desiccation crack propagation significantly (Li et al. 2016, Song et al. 2017). Evapotranspiration-induced root-water-uptake affects the moisture dynamics of the vadose zone (Ni et al. 2018, Smethurst et al. 2015). It has been shown that induced soil suction in vegetated soils can be up to 4 times higher than that the bare soil (Ng et al. 2016). This process may potentially exacerbate crack propagation. In addition, roots can promote cracks by restricting self-healing of cracks (Zhan et al. 2007, Sinnathamby et al. 2014). Due to the reinforcement of grass roots, the swelling of a relatively expansive soil upon wetting is hindered and the closing of the open cracks and fissures will hence be delayed (Zhan et al. 2007). They also found that evapotranspiration of grass will induce a high soil suction deep in the soil layers, which will facilitate crack development and prevent self-healing of cracks. Infiltration rates in grassed soils was thus found to be twice that in the bare ground (Zhan et al. 2007). It has been reported that roots can proliferate in cracks (Ghestem et al. 2011) and further exacerbate plane of weakness where cracks propagate. On the contrary, plant roots can also restrict desiccation cracking by performing like random fibers in soil (Li et al. 2016, Zhou et al. 2009), especially in the early stage of the drying and wetting cycles. This is because the larger shear strength of rooted systems restricts the cracking in soils. Such observations were also reported in clayey soils by Song et al. (2017), who found that the presence of Bermuda grass in the soil restricted the crack development during wetting and drying cycles. Hence, *Cynodon dactylon* with fibrous root system was suggested to be used in landfill covers to reduce infiltration. From the discussion above, it can be concluded that it is still arguable whether plant roots restrict soil cracking or not.

Recent studies (Gadi et al. 2016, Gadi et al. 2017) revealed that crack intensity factor (CIF) was highly dependent on plant parameters, such as stomatal conductance, photosynthetic yield, evapotranspiration and vegetation density. CIF is defined as the area ratio of cracked section to the total section of soil. Scoffoni et al. (2016) based on field monitoring of 30 different species of *Viburnum*, correlated that photosynthetic activity of a plant directly effects the plant hydraulic system (transpiration). They proposed a fundamental theory based on measured stomatal conductance, photosynthetic activity and environmental factors (Fig. 2.9(b)). The theory proposed in the study, states that photosynthetic activity directly affects plant induced suction due to transpiration which might additionally increases tensile forces in root zone. However, for a non-crop grass species, there was no evidence of effect of photosynthetic yield on suction of soil-root composite and consequent cracking. Hence, this property may vary based on plant species. Stomatal conductance (Gadi et al. 2017) controls the abilities of plant transpiring and consequent inducing suction; it can indirectly affect soil crack propagation. Comparing the stomatal conductance for two species (*Vigna unguiculate and Axonopus compressus*) with different values under same soil and irrigation conditions, it is seen that surface cracking in the soil was directly proportional to its stomatal conductance. When using shoot length to quantify CIF, it is interesting to note that CIF increases with the growth of shoot length, up to a threshold length (400 mm) for a crop species, cowpea (*Vigna unguiculate*). In addition, CIF increased with Leaf area index (LAI) to a certain threshold value of 0.56, after which there was no change in CIF. Increase in plant density restricts further rise in CIF after a certain threshold density is met. Other root parameters such as root area index (RAI) and root biochemical variation with depth and their consequent effect on suction and tensile strength of soil-root composite has been recently discussed (Ng et al., 2016; Boldrin et al., 2017). Bottinelli et al. (2016) and Perret et al. (2007) have used an expensive approach of cathode ray tomography to delineate the variation of cracks and plant roots with growing plant age in low compacted soil (Fig. 2.9 (b-c)).

Soil cracking is also reported to be affected by plant cover distribution (Dasog et al. 1988) and species type (Mitchell and van Genuchten 1992). There are some basic studies concerning the influence of crops on cracking geometry (Johnston and Hill 1944, Johnson, 1962, Fox 1964). They found that large cracks mainly developed midway between crop rows, where the water content was the highest. The crack would become wider when the inter-row spacing increased (Johnson 1962). Cucci et al. (2017) investigated the spatial distribution of roots and cracks in two clay soils cropped with sunflower. They found that the volume of cracks in the soil grown with flower at 0.4 m spacing was almost 8 times higher than the values on the bare soil and 2.5 times higher than the one grown at 0.8 m between rows. An optimum inter-row spacing of 0.6 m was suggested in terms of root density, soil moisture and crack size. The formation of inter-row cracks was attributed to the anchoring of soil to the crop roots (Fox 1964). In addition to this, the bidirectional water movement caused by the spread of roots under the rows could potentially facilitate the crack propagation between rows (Sharma and Verma 1977, Mitchell and van Genuchten 1992, Dasog and Shashidhara 1993). However, none of the previous studies has separated these two effects of roots on crack formation. The inter-row cracks tended to be linear and parallel to the rows under the condition of active transpiration by crop species. However, the crack distribution became isotropic when crop transpiration was absent (Yoshida and Adachi 2001a, b). This is dominated by the distribution of the soil mechanical strength against the tensile stress (Yoshida and Adachi, 2001b). In this situation, the presence of crop roots and tracks of agricultural vehicles are the two of the most important determinants of the crack geometry particularly in field cases. It has been concluded that the distribution of soil water content (or soil suction) by root water uptake affected the location and geometry of inter-row cracks (Yoshida and Adachi 2004). The crack distribution between rows is influenced by the uptake of water and nutrients that normally occurs in the soil depth close to root surface, which ranges from 2 to 8 mm (Yamaguchi and Tanaka 1989). Especially, the influence of nutrient concentration and its consequent effect on desiccation has been rarely quantified. Depending on the nutrient salinity, varied types of crack patterns are observed (Pauchard et al. 1999). At lower salinities a regular pattern of radial cracks was seen to develop all around the drop edge in this study. Furthermore, at intermediate salinities, disordered patterns were observed, while at large salinities a unique circular crack appears. However, this study was conducted on a colloidal suspension rather a natural soil. A recent study (Zhang et al. 2017) on pure clay (bentonite) has showed that there is a significant effect of salt concentration which induces and alters cracking morphology and patterns. There were few theoretical and numerical studies investigating the tensile strength generation between rows due to evapotranspiration (Nieber 1982, Yoshida and Adachi 2004). They found that when soil suction is about to rise, the horizontal tensile strength has its peaks. The peaks would move towards the center of the inter-row and the magnitude increase as suction continues to increase. The distribution of tensile stress has either single or double peaks between rows. Thus, it is still not clear the spatial and temporal variability of cracks for different plantation fields, irrigation schedule, species type which needs to be studied for mitigating soil desiccation cracking in arid regions.

2.3.1 Gap areas and future scope of desiccation cracks in vegetated soil

For vegetated soil, the early plant establishment period is of primary concern in terms of mitigating desiccation cracks especially in case of landfill liners and bio-engineered slopes. In recent research, major focus has been given in relating suction induced in root zone with cracking (Song et al. 2017, Li et al. 2016). However, there is rarely any studies that relate temporal variations in a species shoot parameters such as plant age, stomatal conductance, stem sap flow which essentially governs the plant hydraulics and thus desiccation cracking in vegetated soil. The plant hydraulics along with plantation patterns will govern the induced suction in vegetated infrastructure. This variability in suction patterns will affect the desiccation cracks in vegetated infrastructure as previously discussed. Thus, for engineered vegetated infrastructure there is a need to explore these parameters to regulate irrigation schemes and understand plant age effects for varied species and plantation conditions, so that cracks can be minimized.

2.4 Biochar amended soil for geo-environmental application

Biochar (BC) is made from biomass by a process called pyrolysis. Pyrolysis/gasification is a physiochemical process associated with thermal decomposition of organic or lignocellulose matter at relatively high temperatures under deficit of oxygen and limited supply of air or gases (Shackley et al. 2012, Yang et al. 2018, Liu et al. 2018, De Bhowmick et al. 2018). The process results in bio-fuel after condensation and the solid residue left is the BC. Many experimental studies have demonstrated use of BC addition as a soil reform measure because of its reported potential for refinement of soil degradation and support for larger crop yields (Lehmann and Joseph 2015, Ahmed and Hameed 2018, Belmonte et al. 2018). In an agricultural point of view, BC provides a secure habitat for microbial activity which is important for crop production to bloom. Because of its high organic carbon content, BC tends to serve as a soil conditioner to improve properties like physiochemical and biological properties of soils. As there is increase in organic carbon content, soil water retention capacity also increases. Addition of BC causes decrement in bulk density and an increment in water content at wilting point, and total pore volume (Abel et al. 2013). BC is made from biomass (plant or animal waste). Biomass is often a by-product or waste which eventually decomposes and releases CO_2. Conversion of biomass into BC will reduce emission of CO_2 to the atmosphere since a lot of carbon is trapped in BC. Thus, production of biochar is considered to be a cleaner one, since waste which otherwise would decompose is now converted to BC and used for a sustainable cause.

BC increases the water retention capacity of soils when amended with coarse grained soils and is suitable for geo-environmental applications (Yargicoglu and Reddy 2015, Yargicoglu and Reddy 2017, Bashir et al. 2018, Paetsch et al. 2018, Zama et al. 2018, Ji et al. 2018, Shen et al. 2018). BC addition and its role on soil water retention has mainly been investigated in studies (Abel et al. 2013, Wong et al. 2017, Paetsch et al. 2018). Wong et al. (2018) quantified water retention characteristics at the very low water suction range (i.e., near residual water content) or high soil suction (48.49–124.56 MPa) (dry condition) without considering entire suction range. The water retention property of soil-biochar composite from near-saturated (i.e, 10 kPa) till wilting point (1000-2000 kPa; Feddes et al. 1978) has been rarely studied. This particular range is important as it covers the typical ranges of water potential observed in most plant bearing soils under natural weather conditions and thus, is the most relevant for plant growth. Biochar amended soil (BAS) has been advocated for use in such landfill systems in the recent past (Reddy et al. 2015, Jayawardhana et al. 2016, Ni et al. 2018, Weber and Quicker 2018). Addition of biochar in soil can improve the physical properties of soil like pore size distribution, porosity, bulk density, saturated hydraulic conductivity, surface area and water retention (Abel et al. 2013, Ulyett et al. 2014, Rodriguez-Vila et al., 2018). Due to high surface area of biochar, process of oxidation of Methane (CH_4) gas into carbon di oxide (CO_2) can be enhanced by adding the biochar in landfill cover (Sadasivam and Reddy 2015a, b).

Recently, Paetsch et al. (2018) investigated water retention capacity at different equilibrium water content values of soil and soil-biochar composite. In their study, the measurement of suction and water content were based on equilibrium condition established through pressure plate extractor technique without considering natural drying conditions. Further, any details of measurement of soil suction in their study was not reported. Investigation of cracking in soil was missing in these studies. It is well-known that soil undergoing wetting-drying cycles can develop cracks. This is also the case for soil-based cover materials such as those used at landfills or reclaimed metal contaminated sites or bio-engineered slopes (Li et al. 2016, Yargicoglu and Reddy 2017). Desiccation or surface cracks initiates due to evaporation from the ground surface which is a resultant of high surface suction (tensile forces) developed in the soil matrix (Gadi et al. 2017, 2018). Increased surface cracking may lead to elevated methane gas emissions to the atmosphere through landfill covers (Czepiel et al. 1996), increase soil erodibility (Indraratna et al. 2008), result in elevated nutrient loss (especially phosphorous) in agricultural soil (mostly during events of heavy rain on initially dry soils) and also increase in permeability of soil (Li et al. 2011).

As far as authors are aware, only very few studies (Lu et al. 2014) have considered the impact of BC addition to soil on crack formation and unsaturated soil hydraulic parameters simultaneously. Lu et al. (2014) investigated effect of rice husk biochar on physical properties of clayey soil. They found that with presence of biochar, the plasticity index and tensile strength was reduced. The extent of cracking was also reduced. However, their studies were mainly focused in loosely compacted soil without any simultaneous measurement of soil water retention characteristics. Further, any details regarding measurement of soil suction in their study were not reported. However, all these studies lack investigation about influence of biochar on cracking potential of soil. Cracking potential in previous studies (Gadi et al. 2017) is quantified using crack intensity factor (CIF). Desiccation cracks are a matter of prominent concern in geotechnical engineering. Cracks formed because of desiccation can greatly affect the permeability (Li et al. 2009) and hence, stability of the slopes. Under the equivalent continuum assumption, Li et al. (2009) derived the permeability function for cracked soil (k_s) by overlapping those for crack network (k_c) and the soil matrix (k_m). Mathematically, the permeability function is shown in equation 1.

$$k_s(\psi) = k_c(\psi) + (1 - CIF)k_m(\psi) \tag{1}$$

Desiccation cracks are important as they can lead to sequential failure of an existing structure. According to Peron et al. (2009), desiccation cracks lead to preferential paths for water infiltration and can cause increase in pore water pressure and leaks which would result in the failure of the structure. Pore-water pressure is inversely proportional to the shear strength of soil (Li et al. 2011). In addition, cracks can develop to become a part of a slip surface that has no shear strength inducing slope failures (Li et al. 2017). The net amount of water left in the soil substrate after considering evapotranspiration and drainage in green infrastructure is referred to as water balance. The amount of water balance in green infrastructure will depend on the water retention capacity as well as the permeability of soil substrate. Thus, if the water retention capacity increases for a soil stratum, it largely helps in water conservation for vegetation and reduces the demand for irrigating green infrastructure and in agriculture. The amount of cracking has been further found to influence infiltration into soil surface and water balance (Nova´k et al. 2000, Gopal et al. 2018). Based on equation proposed by Li et al. (2009, 2011) in equation 1, permeability of soil can be estimated for cracked soil. It has been found from literature (Li et al. 2009) that cracks are usually dependent on soil suction and water content (Li et al. 2009). The role of suction and water content could be important to understand the mechanism of crack in soils amended with BC. This is because with presence of BC, there is a tendency of higher water retention that can affect the development of cracks. The relative significance of suction and water content in crack development (i.e., CIF) is not clear. Soil water retention characteristic of a porous medium is represented by the change in moisture/water content with increasing suction. Water content is defined as the volumetric ratio of water to soil and suction is defined as the negative pressure developed in the pore spaces of soil (Fredlund and Rahardjo 1993). Soil water retention of a soil directly affects the water retaining capacity, soil strength, hydraulic conductivity, etc. which is imperative to the functioning of agricultural fields and green infrastructures.

2.5 Scope and objectives of the thesis

The critical appraisal of the reviewed literature show that physico-biochemical and mechanical properties of lignocellulose bio-material has not been investigated for application in soil reinforcement. Specifically, the influence of inherent bio-polymers of natural fibers on these properties was not investigated. Water hyacinth (WH), being one of the world's most invasive weed and having suitable bio-chemical composition showcased potential as a limited life natural fiber/geotextile/biochar. The conversion of WH plant to suitable biomaterial for use in green infrastructure and agriculture represents a more sustainable strategy for management of this recalcitrant weed. With this is view, the main objective of the current study is to investigate the efficacy of WH based biomaterial in geo-environment applications by measuring certain hydro-mechanical parameters. Following are the different scope of this study to achieve the objective:

(i) Characterize the bio-chemical, mechanical and physical properties of WH.

(ii) Investigate the mechanical and hydraulic behavior of soil amended with WH biomaterial.

(iii) Assess the use of WH fibers and biochar in soil reinforcement as compared to conventionally used natural fibers (jute, coir, etc.) and peanut shell biochar respectively.

(iv) Evaluate the degradation rate of treated and untreated WH fibers to predict its performance period in sub soil conditions.

(v) Treat the natural fibers to increase its mechanical performance in RDFS and reduce moisture absorption.

Chapter 3

Materials and experimental methodology

3.1 General

The materials used and salient experimental methodologies related to the thesis is presented in this chapter. It includes evaluation of the geotechnical properties of the soils, morphological characteristics and chemical properties. A section is also included to determine optimum column dimension to conduct infiltration test using a disk infiltrometer.

3.2 Material properties

3.2.1 Fiber

Percentages of cellulose, lignin, hemicellulose and ash of each type of natural fiber (coir, jute and WH) were determined as per the procedures given by Jenkins (1930), TAPPI Test Methods (1996), Goering and Van Soest (1970) and ASTM E1755-01 (2007), respectively. Moisture content of the fibers was determined using oven-drying method (at 50˚C for 12 h) as per Methacanon et al. (2010) to avoid any biomass loss. Mean tensile strength at breakage, Young's modulus and specific gravity of tested fibers were determined according to IS-1670-(1991) and IS-2720-Part 3-(1980), respectively. The specific gravity for coir, jute and WH was found to be 1.24 ± 0.10, 1.12 ± 0.05 and 0.7 ± 0.03 (Mean ± standard error of mean) respectively. The average diameter of the fibers used was 0.4 ± 0.1 mm for jute and coir, while WH has a diameter of 2 ± 0.8 mm for maintaining the same fiber aspect ratio.

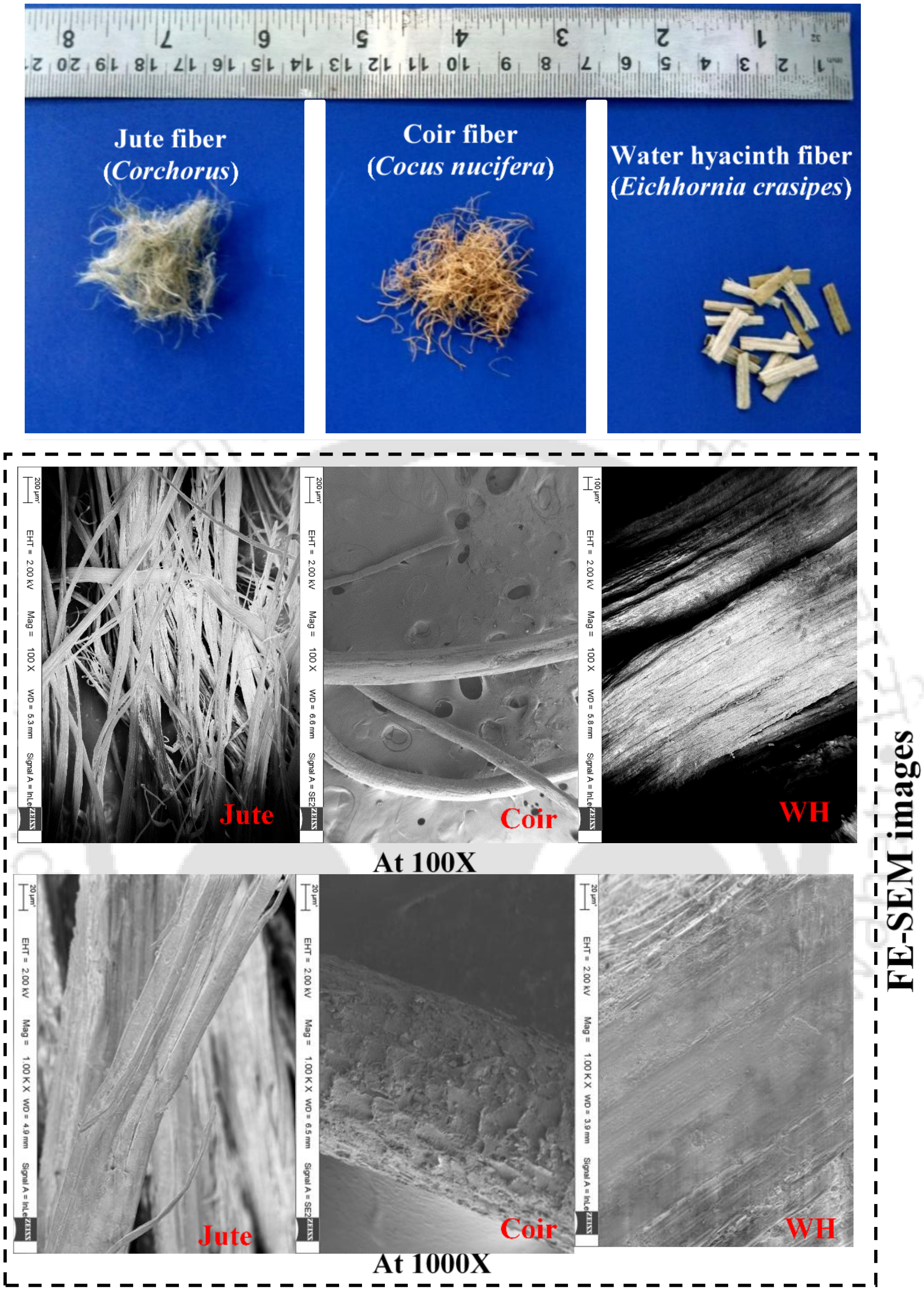

Fig. 3.1. Surface morphology of jute, coir and water hyacinth fibers at different magnifications

Table 3.1 summarizes some physical and biochemical properties of each fiber type expressed in mean and standard error of mean. Jute has the highest cellulose content and thus show highest tensile strength among tested fibers. On the other hand, coir has the highest percentage of lignin and it is the most ductile fiber (i.e., the highest elongation at break). Jute and WH, which have the highest hemicellulose content, showcases higher moisture absorbing ability. Figure 3.1 shows the Field Emission Scanning Electron Microscope (FE-SEM) images of jute, coir and WH, highlighting the surface morphology of the tested fibers at two magnification levels. WH is a monofilament fiber and each individual fiber is constituted by fibrils that would not be dissociated during mixing with soil. On the contrary, jute and coir have multifilament fibers segregate into finer fibers upon mixing with soil. The individual coir fiber shows a rougher surface at 1000X as compared to the other fibers.

Table 3.1. Properties of fibers used in this study

Physical properties					**Bio-chemical composition**			
Natural moisture content (%)	Elastic Young's modulus	Breaking tensile strength (MPa)	Moisture Absorption Capacity (%)	Elongation at break (%)	Cellulose (%)	Hemicellulose (%)	Lignin (%)	Ash (%)
Coir								
7 ± 1.2	7.2 ± 2.2	150 ± 3	12.6 ± 1.5	26 ± 2.2	43 ± 2.3	15 ± 1.1	38 ± 2.2	2 ± 0.8
Jute								
14 ± 1.3	17 ± 3	500 ± 11	40 ± 1.4	10 ± 1.8	60 ± 3.4	22 ± 1.9	16 ± 1.6	1 ± 0.9
Water hyacinth								
12 ± 2.1	12 ± 1.8	313 ± 8	95 ± 3.4	14 ± 1	46 ± 2.6	21 ± 2	11 ± 0.9	11 ± 1.5

3.2.2 Soil

Two soils were used in this study, sourced from north-east India and another from Shantou, China. The soil from India (Soil 1) was mostly used in all of the investigation. The soil from China (Soil 2) was used only in those sections where biochar was investigated. The soil index properties of soils used in this study are tabulated in Table 3.2.

Table 3.2. Soil index properties

Soil Property	Standard	Soil 1	Soil 2
Specific Gravity	ASTM D 854	2.63	2.65
Particle size distribution (%)	ASTM D 422		
Coarse Sand (4.75mm-2mm)		0	0
Medium Sand (2mm-0.425mm)		7	37
Fine Sand (0.425mm-0.075mm)		28	21
Silt (0.075mm-0.002mm)		40	37
Clay (<0.002mm)		25	5
Atterberg Limits (%)	ASTM D 4318		
Liquid Limit		42	43
Plastic Limit		24	26
Shrinkage Limit		19	16
Compaction properties	ASTM D 698		
Optimum Moisture Content (%)		17	16.5
Maximum Dry Density (kN/m^3)		16.5	15.8

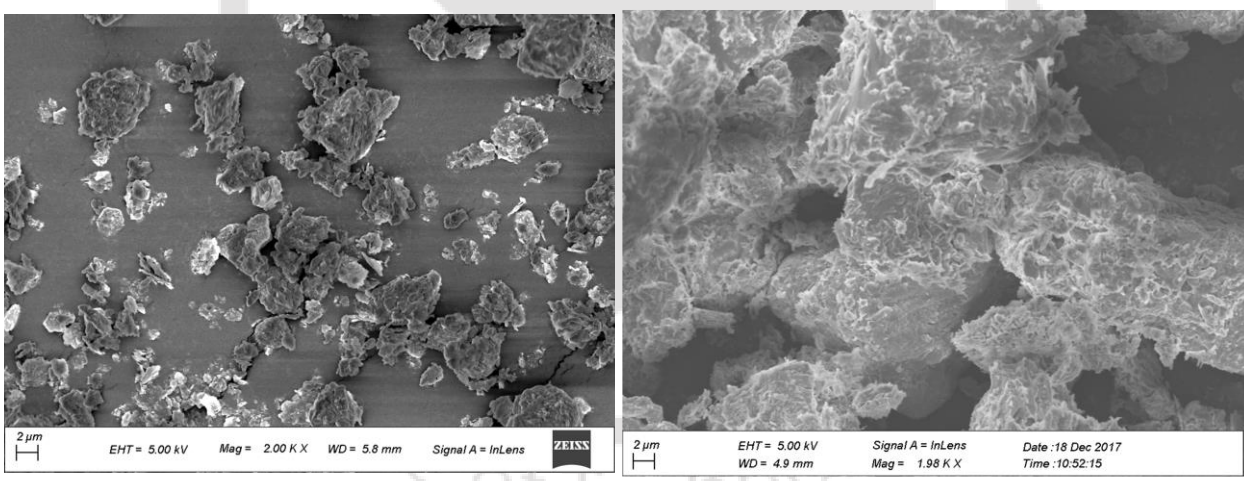

Soil 1 Soil 2

Fig.3.2 Surface morphology of the two soils studied at 2K X magnification by FE-SEM

The surface morphology of the two soils has been presented at 2K X magnifications. It is seen that soil 1 has more fine particles as compared to soil 2 which is in accordance with the particle gradation listed in Table 3.2.

3.2.3 Biochar

The biochar feedstock was WH stems sourced from Deepor Lake in North-east India to avoid any genetic variability. The stems were chopped evenly and fed in a pyrolysis chamber at 350-400 ℃ based on thermo-gravimetric analysis (TGA; Fig. 3.3) of the sample. An automatic crusher was adopted to crush the coarse BC acquired from pyrolysis which was then sieved through 2mm sieves. The basic and engineering properties of the BC are tabulated in Table 3.3 and Table 3.4. The Atterberg limits and compaction characteristics of pure WH BC could not be determined as it is cohesionless when not mixed with soil. The elemental analyzer (Bird et al. 2017) was used to measure the carbon, hydrogen, nitrogen and oxygen content in the biochar produced. The ash content and cation exchange capacity is measured by ASTM E1755-01 (2007) and the ammonium acetate method (Thomas 1982). The surface morphology of BC particles is compared with that of the soil and soil-WH BC using FE-SEM images as shown in Fig. 3.4(a-b). The FE-SEM was performed using ZEISS SIGMA microscope analysis setup. It can be evidently viewed that a majority of the BC particles are smaller in size as compared to soil particles and consists mostly silt sized particles (<75 micron). The change in the pore structure of soil-BC composite occurs means resulting from its mixture with soil (Fig. 3.4c). Also, the BC appears to have inherent intra-pores with its matrix (Fig. 3.4d) which makes it susceptible to absorb additional water as compared to only bare soil. These intra-pores are developed due to WH being a lingo-cellulose material and upon pyrolysis leads to pores due to hemicellulose and cellulose degrading first followed by lignin (Lehmann and Joseph 2015, Pardo et al. 2018). The relevance of intra-pores of biochar in retaining additional water will be discussed chapter 5. The Fourier-transform infrared spectroscopy (FTIR) analysis was done by LT-4100 device (LABTRONICS instruments ltd) to analyze the surface functional groups. The functional groups are majorly hydrophilic with OH- hydroxyl group as well as COOH- carboxyl group and is also presented in Fig. 3.5.

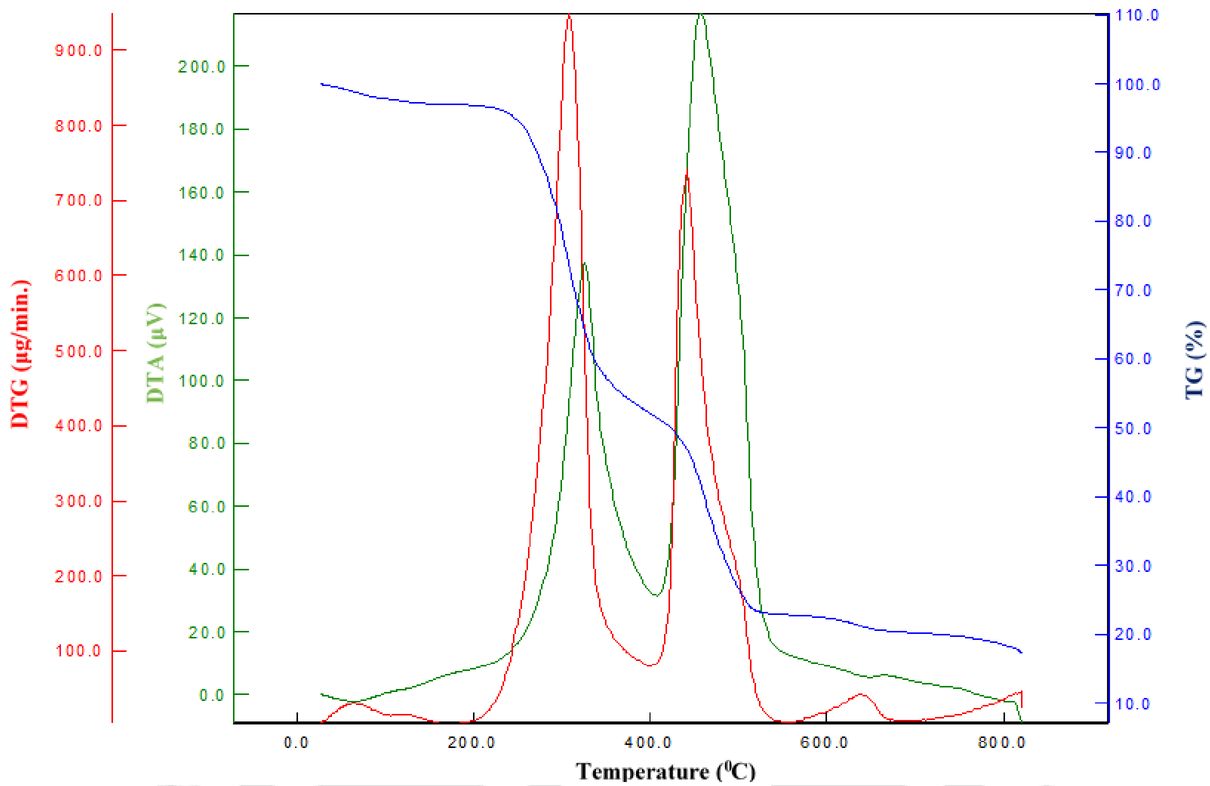

Fig. 3.3. Thermo-gravimetric analysis (TGA) of water hyacinth used in the current study

Table. 3.3 Basic properties of WH BC

Soil properties	Standard	WH BC
Particle size distribution	ASTM D 422	
Coarse Sand (2 – 4.75 mm)		0.00
Medium Sand (0.425 - 2 mm)		000
Fine Sand (0.075 – 0.425 mm)		30.48
Silt (<0.075 mm)		68.52
Clay (<0.002 mm		1
Atterberg limits	ASTM D 4318	
Liquid limit (LL)		ND
Plastic limit (PL)		ND
Plastic Index (PI)		ND
Max. Dry Density (kN/m^3)	ASTM D 698	ND

OMC (%)	ASTM D 698	ND
Specific gravity	ASTM D 854	0.8
pH	ASTM D 4972	7.69

ND-Cannot be determined

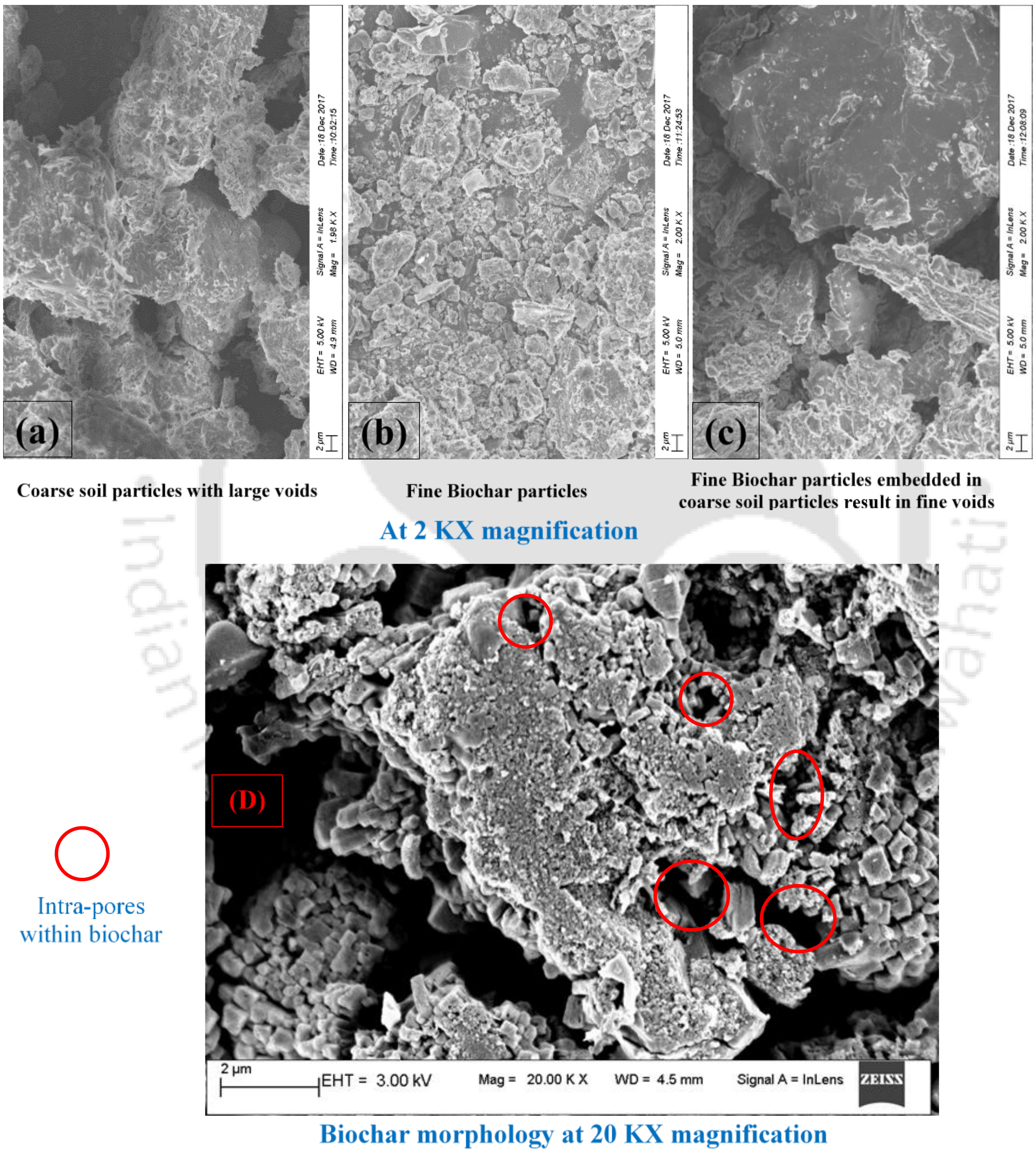

Fig. 3.4 FE-SEM images of (a) Soil, (b) WH-BC, (c) Soil-WH BC composite (5% BC) at 2K X magnification and BC intra-pore morphology

Table 3.4 Basic properties of water hyacinth biochar

Feedstock	Pyrolysis process	Pyrolysis temperature (℃)	Elemental analysis				Ash content (%)	CEC (cmol kg^{-1})
			C (%)	H (%)	O (%)	N (%)		
WH stem sourced from Deepor lake,India	Slow pyrolysis	350-400	53.39	42.80	1.99	1.82	39	21.95

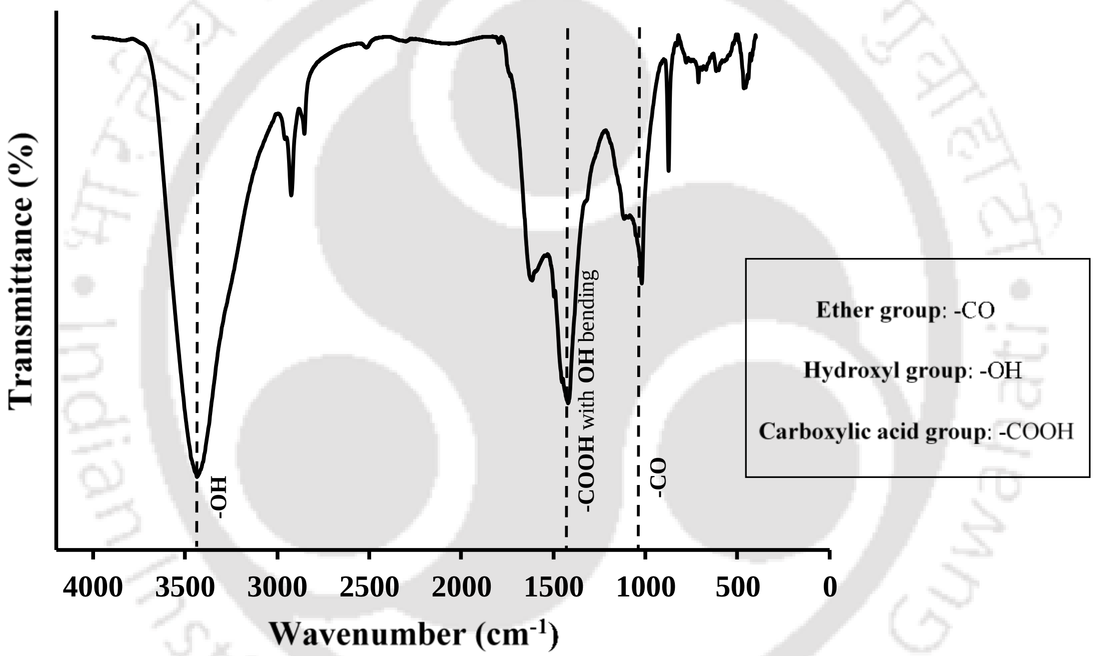

Fig. 3.5 FTIR response of water hyacinth biochar used in the study

3.3 Experimental methodology

3.3.1 Measurement of soil suction and water content

MPS-6 sensors (currently TEROS21 of METER devices) and EC-5 sensors (range from 0-100%; with an error of ±1%; Decagon devices 2016a) were used to measure matric suction and volumetric water content, respectively. The EC-5 determines volumetric water content (θ) by measuring the dielectric constant of the soil (or other porous media) using capacitance/frequency domain technology. The zone of influence of the probe is 4 cm around the edge of the prongs and 1 cm from the bottom end of the prong. The performance of MPS-6 sensors has been previously evaluated and validated by various existing studies (Tripathy et al. 2016, Bianchi et al. 2017, López-Vicente and Álvarez 2018). TEROS21 is able to measure suction range from 10 to 100,000 kPa as per the data provided by the manufacturer. However, in this thesis, the maximum suction measured was 3500 kPa. TEROS21 sensors consist of a porous ceramic disk with a known moisture release curve. After the porous material has equilibrated with the surrounding soil, the sensor measures the water content of the porous material, and the sensor uses the moisture release curve to translate moisture content into negative water potential.

MPS6 sensor for suction measurement **EC-5 sensor for water content measurement**

Fig. 3.6 MPS6 (currently TEROS21) and EC5 sensors used in the current study

Soil water retention curve (SWRC) was obtained using the aforementioned sensors for the soils and composites used in this current study. The measured SWRC data points can be used to fit a continuous SWRC using van Genuchten (vG) Eq 3.1 (Carsel and Parrish 1988).

$$\theta(\psi) = \theta_r + \frac{(\theta_s - \theta_r)}{\left[1 + (\alpha|\psi|)^n\right]^m} \tag{3.1}$$

where:

m = 1 – (1/n)

ϴ(ψ) = volumetric water content at suction ψ

ϴs = volumetric water content at saturation

ϴr = residual volumetric water content

α = fitting parameter primarily dependent on the air entry value

n = fitting parameter depending on the rate of extraction of water from the soil

3.3.2 Infiltration measurement using Mini-disk infiltrometer

3.3.2.1 Background of mini-disk infiltrometer

Mini disk infiltrometer (MDI) (Fig. 3.7; Decagon devices 2013), is a recent development for establishing infiltration characteristics of the soil. The existing infiltrometers are not suitable to be used in the laboratory due to their larger size and cumbersome procedure, there by prohibiting controlled experimental studies for defining infiltration with adequate repeatability (Angulo-Jaramillo et al. 2000). It primarily determines the unconfined axisymmetric water flow beneath a circular surface under a constant, negative pressure head (Angulo-Jaramillo et al. 2016). The hydraulic conductivity obtained from both these instruments are based on flow that is initially transient followed by achieving steady-state flow. MDI is a miniaturized tension disc infiltrometer allowing simple and rapid determination of soil hydraulic parameters. Apart from the basic working principle, MDI is different from other infiltrometer as it has a compact size and water needed for operation is very small. These features make it conducive for point measurements in both field as well as laboratory that are sometimes limited by complicated experimental configuration, difficult manual transportation of equipment, limited access to water and highly irregular surface (Madsen and Chandler 2007). In the recent past, several laboratory column studies (Bhave and Sreeja 2013, Meshesha et al. 2016) were conducted to assess infiltration using MDI.

3.3.2.2 Determination of column dimension for infiltration test

Necessity for accurate column dimension

The onset of laboratory applications of MDI needs further exploration in terms of choosing laboratory apparatus so that the wetting front of MDI does not interact with the apparatus during the test duration. Since the measurement methodology of MDI is based on three dimensional propagation of wetting front, it is essential to know the zone of influence and boundary effects in laboratory measurements. Water flux movement in the soil beneath MDI disc is due to gravity (vertical direction) and capillarity (horizontal direction). However, as compared with one-dimensional infiltration (as observed in other infiltrometers), the importance of capillarity relative to gravity is greater in case of MDI (Angulo-Jaramillo et al. 2016). Steady-state infiltration rate as well as time required to achieve it is greater for three-dimensional axisymmetric flow than for the corresponding one-dimensional infiltration (Clothier and Scotter 2002). Although in field condition, there is no restriction in confinement, the influence zone in horizontal direction would help in deciding appropriate laboratory setup for conducting column infiltration test. There are no recommendations available in the literature related to this and use of different column dimensions may lead to erroneous estimation of infiltration rate. Hence, the variability in infiltration rate (k_{h0}) due to column dimensions needs to be studied to avoid erroneous estimations.

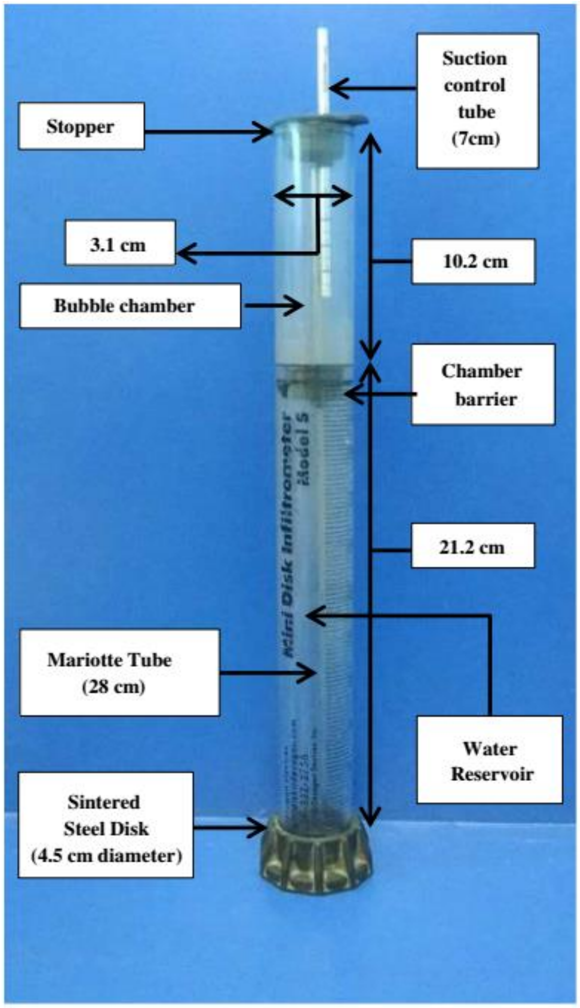

Fig. 3.7 Overview of the MDI

Calibration of infiltration column dimensions

The soils particularly used in this sub-study are different from the soils used in the main study. The soils required were obtained from different locations in the north-eastern part of India and designated in Table 3.5. These soils were subjected to basic characterization according to the procedure outlined in the literature (ASTM D4318-93, ASTM D854-06, ASTM D698-07, ASTM

D2487-10) and the details are listed in Table 3.5. The soils represent wide variation in grain size distribution (Fig.3.8), difference in percentage composition and coefficient of uniformity (C_u) (Table 3.5). The specific gravity of the soils ranges from 2.25 to 2.79, liquid limit from 33% to 60%; and plastic limit from 19% to 30%. The total silt and clay content (grain size less than 75 micron), which is the parameter considered in this study ranges from nearly 1% to 80%. The maximum dry density of the soils varied between 14 kN/m^3 to 18.6 kN/m^3. The natural soil was sieved as per ASTM- D2487-10 to consider particles finer than 4.75 mm in this study. However, the majority of the grain size in the selected soils falls below 2 mm as can be seen in Fig. 3.8.

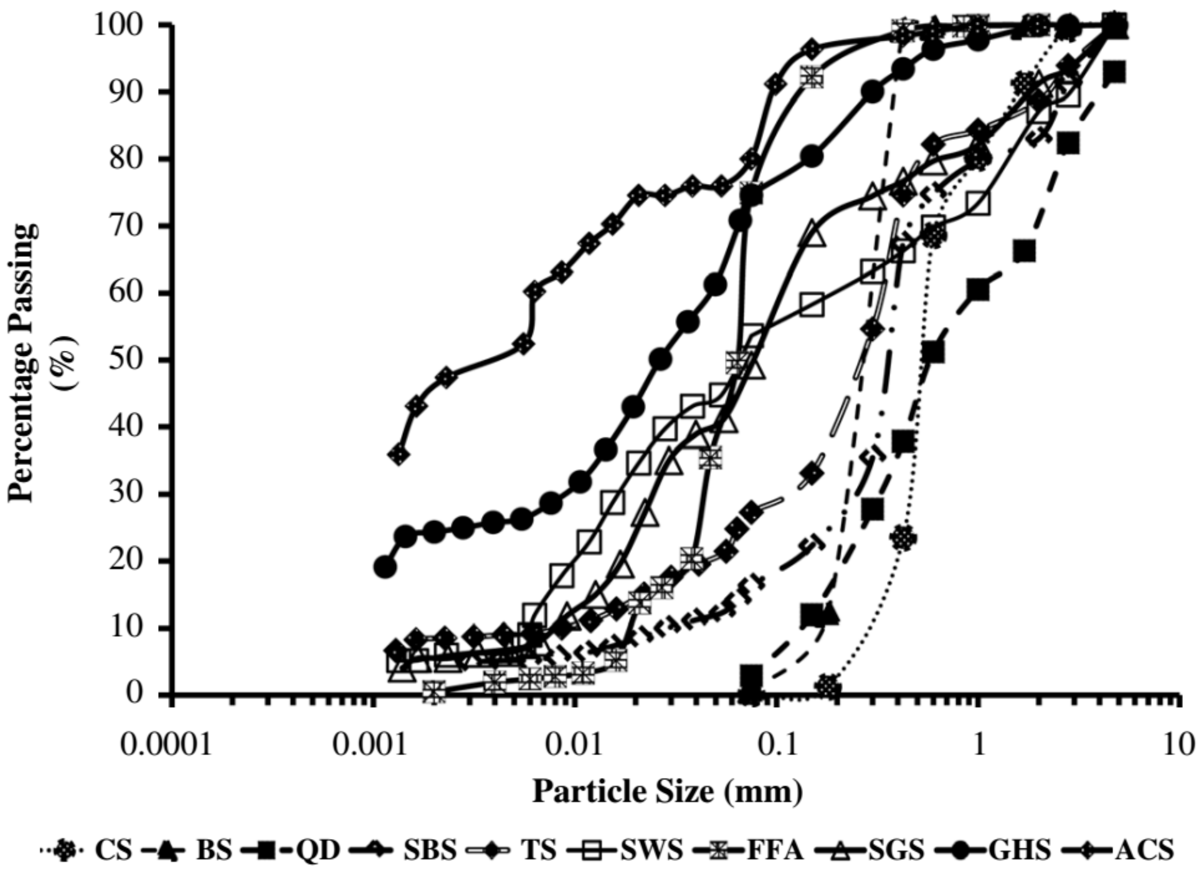

Fig. 3.8 Grain size distribution of selected soils

Table 3.5 Basic property of ten soils for investigation of infiltration rate

Soil Type	Constr-uction Sand	Brahm-aputra Sand	Quarry Dust	Shillong Brown Soil	Tezpur Soil	Sikkim Grey Soil	Farakka Fly Ash	Sikkim White Soil	Guwahati Hill Soil	Arunac-hal Clay Soil
Soil Designation	CS	BS	QS	SBS	TS	SGS	FFA	SWS	GHS	ACS
Percentage Composition (%): Coarse sand (4.75-2)mm	9	0	34	17	11	33	0	35	0	0
Medium Sand (2 mm - 425 micron)	67	1	28	15	14	11	1	15	6	2
Fine Sand (425-75) micron	24	98	35	51	48	20	24	10	19	18
Silt (75 -2) micron	0	1	3	12	18	32	74	35	50	33
Clay (<2 micron)				5	9	4	1	5	25	47
Coefficient of Uniformity (Cu)	2.9	1.3	6.8	21.1	8.90	11.1	3.40	40.0	___	___
Specific Gravity	2.67	2.70	2.59	2.64	2.62	2.71	2.16	2.79	2.69	2.25
Maximum Dry Density (kN/m^3)	17.8	17.2	16	17.1	16.9	17.8	13.8	18.6	17.1	14
Liquid Limit (%)	N/A	N/A	N/A	35	33	41	N/A	38	40	60.23
Plastic Limit (%)	N/A	N/A	N/A	19.78	21.32	19.69	N/A	20	20	29.67
USCS Classification	SP	SP	SW	SM	SM	ML	ML	ML	ML	OH
Classification Description	Poorly Graded Sand	Poorly Graded Sand	Well Graded Sand	Silty Sand	Silty Sand	Inorganic Silt and fine sands with low plasticity	Inorganic Silt	Inorganic Silt and fine sands with low plasticity	Inorganic Silt and clay with low plasticity	Organic clay
Total Silt & Clay content (%)	0	1	3	17	27	36	75	40	75	80

<u>Methodology to determine adequate column dimension</u>

The MDI (Decagon devices 2013) primarily incorporates Zhang's method (Zhang 1997a, b) to estimate k_{h0}. This semi empirical approach adopts an empirical parameter "A" which is based on van Genuchten parameters (vG) as tabulated in Carsel and Parrish (1988). A series of tests were performed to determine the k_{h0} of ten soils using MDI and with varying mold dimension. PVC cylindrical molds of diameter 4.5 cm, 8 cm, 10 cm, 15 cm and 25 cm were fabricated in-house. To study the effect of the mold dimension, a parameter - mold ratio (MR) has been adopted, which is defined by Eq. 3.2.

$$MR = \frac{M_{dia}}{MDI_{dia}} \quad \textbf{(3.2)}$$

where:

M_{dia} = diameter of the mold in which MDI is tested,

MDI_{dia} = diameter of the MDI (4.5 cm).

The mold dimensions mentioned above represents mold ratio of 1, 1.8, 2.2, 3.3 and 5.5 as shown in Fig. 3.9. The depth of all the molds was 15 cm except for 4.5 cm mold where the depth was 20 cm. A higher depth was provided for 4.5 cm mold to ensure that the wetting front does not reach the bottom of the mold for the soils considered in this study. This aspect was verified by visual observation while dismantling the set up after the end of every test. Air dried soil was compacted into the mold at 0.9 times maximum dry densities (MDD). The compaction state of each soil was maintained initially at 0.9 MDD for air dried state. The same compaction state was chosen for all type of soils to have a common comparison for all the ten tested soils. The MDI was placed centrally over the mold as shown in Fig. 3.9 for maintaining axisymmetric flow condition. For each test, three repetitions were performed and presented to appraise the variability in the measured results. Soils obtained for testing were previously air-dried until there was no considerable moisture variation. The soil mass for each individual test was calculated corresponding to a desired density and volume of mold. The soil inside the mold was compacted in three equal layers to achieve the desired density.

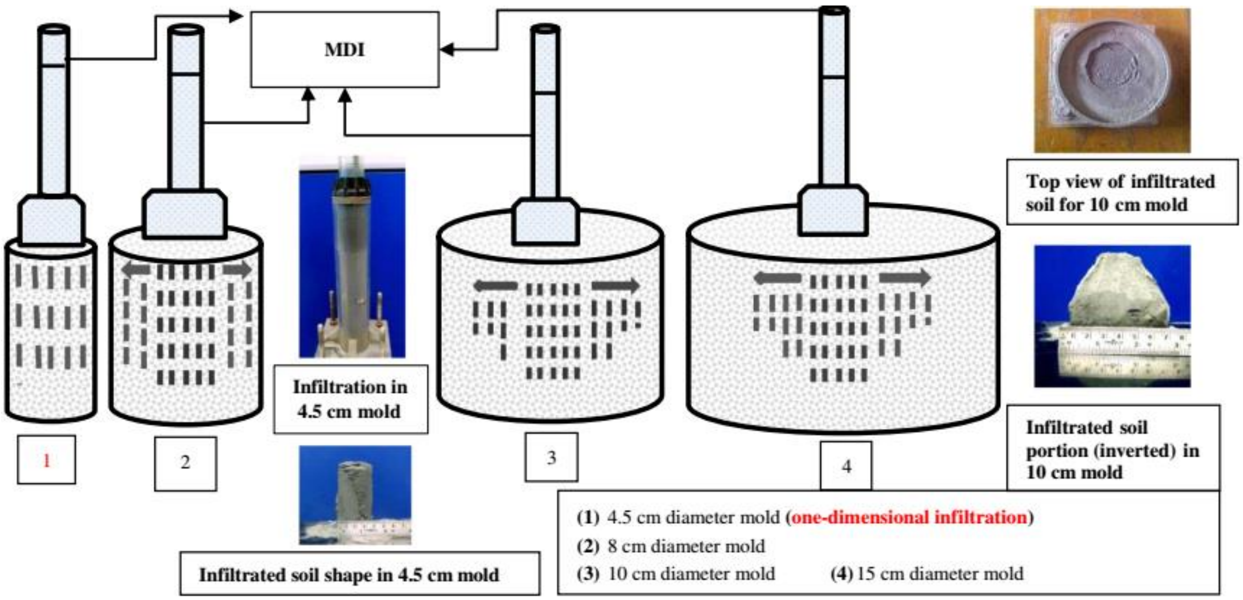

Fig. 3.9 Schematic effect of sample diameter (mold ratio) on infiltration through MDI

Table 3.6 Summary of infiltration rates (mean, standard deviation, variance) of ten soils based on Carsel and Parrish (1988) using MDI

Soil Type	Constru-ction Sand	Brahma-putra Sand	Quarry Dust	Shillong Brown Soil	Tezpur Soil	Sikkim Grey Soil	Farakka Fly Ash	Sikkim White Soil	Guwaha-ti Hill Soil	Arunac-hal Clay Soil
Silt and Clay content, PF_{75} (%)	0	1	3	17	27	36	75	40	75	80
Tension on infiltration surface (cm)	6	6	3	3	2	3	3	2	2	0.5
Mean Hydraulic Conductivity (m/s)	9.45E-04	4.40E-04	1.01E-04	1.22E-05	6.11E-06	2.65E-05	1.18E-05	3.16E-06	5.07E-06	1.23E-07
Standard Deviation	2.81E-05	1.63E-05	6.24E-06	2.46E-07	1.31E-07	4.59E-07	4.62E-07	9.43E-08	1.66E-07	4.17E-09
Variance	7.92E-10	2.67E-10	3.89E-11	6.04E-14	1.69E-14	2.10E-13	2.13E-13	8.89E-15	2.76E-14	1.74E-17
Threshold mould ratio (cm)	3.3	2.2	2.2	2.2	2.2	2.2	2.2	2.2	2.2	2.2

To measure infiltration, the MDI was placed on the soil surface and water was allowed to infiltrate at the set tension. The applied suction head was same for all the three replicates for a particular soil. However, different suction head was applied for different types of soil based on their gradation ranging from coarse grained soils to fine grained clay soil. The relevance of suction is to regulate the flow through macro pores present at the soil surface (Decagon devices 2013). The probability of macropores expected in coarse grained soil will be relatively more than that for fine-grained soil and consequently the pressure head is adjusted accordingly. It is to be noted that the negative pressure head range applied on the soil surface during experiment is at a minimal range of 0 to 0.07 kPa which can only minimize water flow through macropores. Additionally, the Zhang's approach of measuring kh_0 requires a well-defined cumulative infiltration Vs time curve. In case of coarse grained soil, if no negative pressure head is applied, the flow is very rapid and a well-defined cumulative infiltration Vs time curve is not achieved. Thus, a higher suction head of 6 cm was applied on the MDI for coarse grained soil and a minimum suction head of 0.5 cm was applied for clay soil. The tension set was varied for different soil types as reported in Table 3.6 by following the recommendation in the manufacturer's manual. It is to be noted that the hydraulic conductivity measured using MDI is primarily unsaturated because it is an unconfined three dimensional flow in unsaturated soil. However, the hydraulic conductivity obtained from MDI is assumed to be near saturated hydraulic conductivity (k_{h0}) as the soil directly beneath the MDI ceramic disk is considered to be nearly saturated (due to unavoidable entrapped air). Flow under MDI is an axisymmetric three dimensional flow and is governed by Darcy's Law for unsaturated soil (Richard's equation; Ross 1990). The flow is however maintained under constant negative pressure head which is maintained by a Mariotte tube (Zhang 1997a, b). From the initial condition of time equal to zero, the volume of water that infiltrate into the soil was measured as a function of time. The area of the disk being previously known, the cumulative depth of water infiltrating (I) into the soil was obtained and was plotted as a function of square root of time as shown in Fig 3.10. Transient infiltration for a disk infiltrometer (representing three-dimensional infiltration process) can be approximated using Eq. 3.3 [8-9].

$$I = C_1 t + C_2 \sqrt{t} \tag{3.3}$$

where:

C_1, C_2 = fitting constants obtained by the linear fitting technique of differentiated Linearization as suggested by Vandervaere et al. (2000a, b),

t = time.

The near saturated hydraulic conductivity (k_{h0} corresponding to applied disk tension (h_0)) defined by Zhang (1997) is given by Eq. (3.4)

$$k_{h0} = \frac{C_1}{A} \tag{3.4}$$

where:

"A" = parameter dependent on vG SWCC parameters, tension applied on disk and radius of disk as represented by Eq. (3.5.1 and 3.5.2).

$$A = \frac{11.65(n^{0.1}-1)\exp[2.92(n-1.9)\propto h_0]}{(\propto r_0)^{0.91}} \quad ; \qquad \text{For } n > 1.9 \tag{3.5.1}$$

$$A = \frac{11.65(n^{0.1}-1)\exp[7.5(n-1.9)\propto h_0]}{(\propto r_0)^{0.91}} \quad ; \qquad \text{For } n < 1.9 \tag{3.5.2}$$

where:

n, α = the vG parameters for the soil,

r_0 = the disk radius,

h_0 = the suction applied on the disk.

The parameters “n” and “α” for different soil texture is listed in Carsel and Parrish [25]. For MDI the value of r_0 is 2.25 cm.

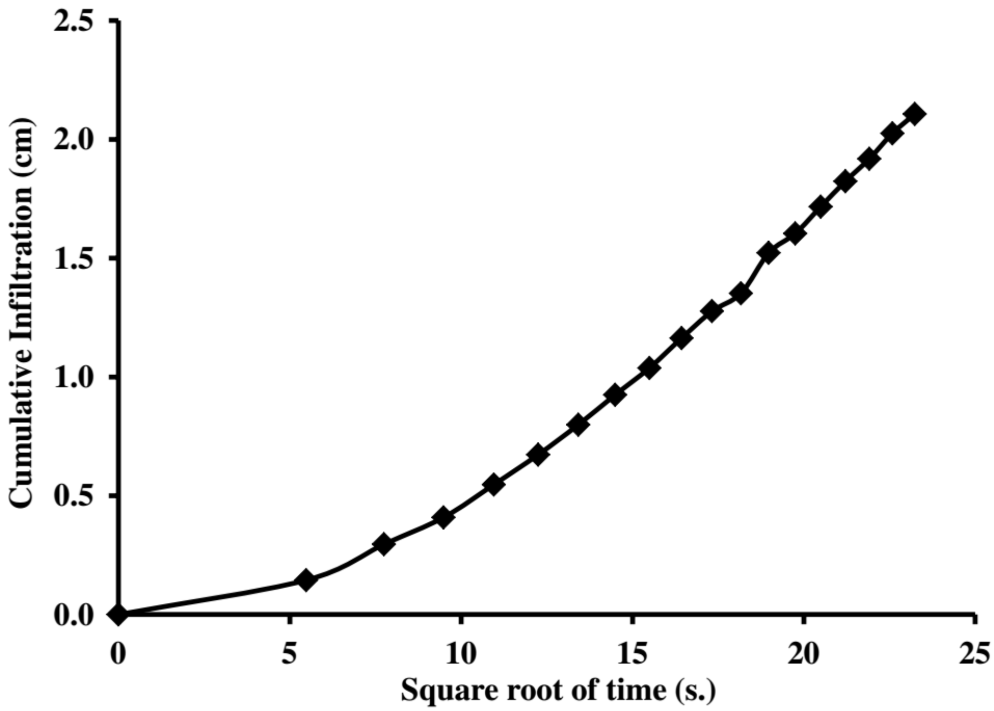

Fig. 3.10 Measured cumulative Infiltration variation with square root of time for FFA soil

Effect of mold dimension on hydraulic conductivity

Figure 3.11 presents the results of “k_{h0}” variation with mold ratio for all the ten soils considered in this study. Mold ratio corresponding to 1 represents one dimensional infiltration; where lateral flow is not allowed (refer Fig.3.9). It was noted that “k_{h0}” increased with mold ratio and approached a constant value corresponding to a threshold mold ratio for all the soils. The variation in “k_{h0}” with mold ratio indicates the mold boundary effect restricting lateral expansion of three dimensional axisymmetric bulb of infiltrating water. This would reduce the amount of water infiltrated due to the quick saturation of soil beneath the infiltrometer. When the mold ratio is greater than or equal to threshold diameter, the "k_{h0}" value approaches a constant value indicating negligible influence of boundary effect of the mold. The discussed threshold mold ratio obtained represents a condition where the lateral wetting front does not interact with the mold. This would cause increased infiltration for a given time as compared to the case where lateral spreading of water is restricted. Based on the above discussion, it can be summarized that for any two successive mold ratios, if there is no considerable variation in the "k_{h0}" value (refer values in red ellipse for Figs. 3.11) then there is no effect of mold boundary on the infiltrated soil. Except construction sand (Fig. 3.11a), all other soils considered in this study achieved constant "k_{h0}" for mold ratio ≥ 2.2. For construction sand, "k_{h0}" value remained constant for mold ratio ≥ 3.3. This may be due to the higher infiltration and re-distribution of water in sand as compared to other soils. The relatively less capillary forces in sand result in higher hydraulic conductivity and lateral spreading as compared to other soils. This aspect was visually examined while dismantling the set up. The equilibrium or threshold mold ratio for any soil type was considered as the least mold ratio beyond which there was no appreciable variation in "k_{h0}" and is tabulated in Table 3.6. As a general guideline, this study recommends a mold ratio ≥ 3.5 corresponding to axisymmetric flow condition while determining "k_{h0}" using MDI in the laboratory. The variation of k_{h0} value from one-dimensional restricted flow to three-dimensional undisturbed flow was observed to be of the order of one for most of the soil (7 out of 10). All pure sands (CS and BS) showed variation of k_{h0} less than the order of one as the effect of capillary lateral flow is less in case of sand.

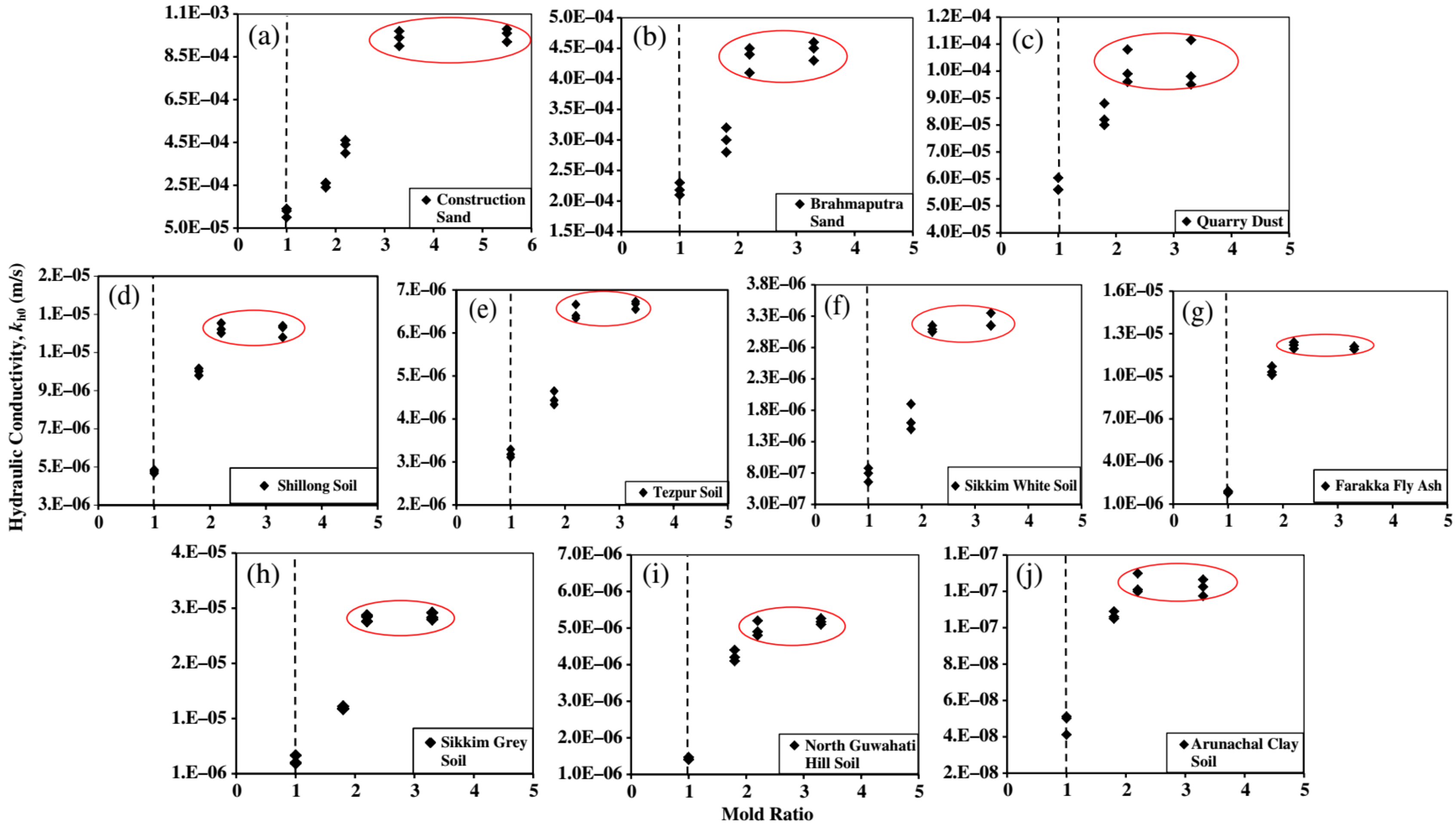

Fig. 3.11 Variation of hydraulic conductivity with change in mold ratio for ten different soils

3.3.4 Microbial activity measurement by fluorescein diacetate analysis

Background of fluorescein diacetate analysis

Soil microbial activity indirectly reflects the microbial processes of soil microorganisms and is basically described as enzymatic activities in soil that are primarily the expression of bacteria, fungi and plant roots (Schnürer 1982). So, measuring the enzymatic catalysis characterizes soil fertility and quality as well as guide to the suitability of the soil for microbial growth. There are various methods for studying this enzymatic activity or soil microbial activity such as Dehydrogenase, Protease, Histidase, Acid phosphatase, Arylsulphatase etc (Burns 1982). But these methods are specific to an enzyme. One of the most rapid and easiest method is FDA hydrolysis or Fluorescein Diacetate hydrolysis (Meriles et al. 2009) which gives an overall estimation of this enzymatic activity of microbial population.

Fluorescein diacetae assay (FDA) hydrolysis measures the enzymatic activity of microbial populations and can provide an estimate of overall microbial activity in an environmental sample. The assay is considered non-specific because it is sensitive to activity of several enzyme classes including lipases, esterases and proteases. Fluorescein diacetate (FDA) is a relatively non-polar compound. As a result of this it is assumed that it diffuses easily through cell membrane, where it is hydrolyzed by non-specific enzymes to the fluorescent compound. In addition, FDA can also be hydrolyzed by extracellular enzymes produced by the soil microflora.

Fluorescein diacetate (3´6´-diacetyl-fluorescein) is a fluorescein conjugated to two acetate radicals. This colorless compound is hydrolyzed by both free (exo-enzymes) and membrane bound enzymes releasing a colored end product-fluorescein, and absorbs strongly in the visible wavelength (490 nm) and can be measured by spectrophotometry. Non-specific esterase, proteases and lipases, which have been shown to hydrolyze FDA, are involved in the decomposition of many types of lignocellulose tissue. The ability to hydrolyze FDA thus seems widespread, especially among the major decomposers- bacteria and fungi.

Reagents and procedure for FDA analysis

The following five reagents were prepared for conducting the FDA analysis as per instruction given by Adam and Duncan (2001).

1) **Potassium phosphate buffer (60 mM), pH 7.6:** Amounts of 8.7 g K_2HPO_4 and 1.3 g KH_2PO_4 were dissolved in approximately 800 ml deionized water. The contents were made up to 1 L with deionized water. The buffer was stored in the fridge (48ºC) and pH checked on day of use.
2) **Chloroform/methanol (2:1):** Chloroform (666 ml) was added to a 1L volumetric flask. The flask was made up to 1L with methanol and the contents mixed thoroughly.
3) **FDA stock solution (1000 mg):** Fluorescein diacetate (0.1 g) (3´6´-diacetyl-fluorescein was dissolved in approximately 80 ml of acetone and the contents of the flask made up to 100 ml with acetone. The solution was stored at -20ºC.
4) **Fluorescein stock solution (2000μg):** Fluorescein sodium salt (0.2265 g) was dissolved in approximately 80 ml of 60 mM potassium phosphate buffer pH 7.6 and the contents made up to 100 ml with buffer.
5) **Fluorescein standard solution (20μg):** Stock solution (1ml of 2000 μg fluorescein ml^{-1}) was added to a 100 ml of volumetric flask and the contents made up to the mark with 60mM

potassium phosphate buffer pH 7.6. 1-5μg ml^{-1} standards were prepared from this standard solution by appropriate dilution in 60 mM potassium phosphate buffer pH 7.6.

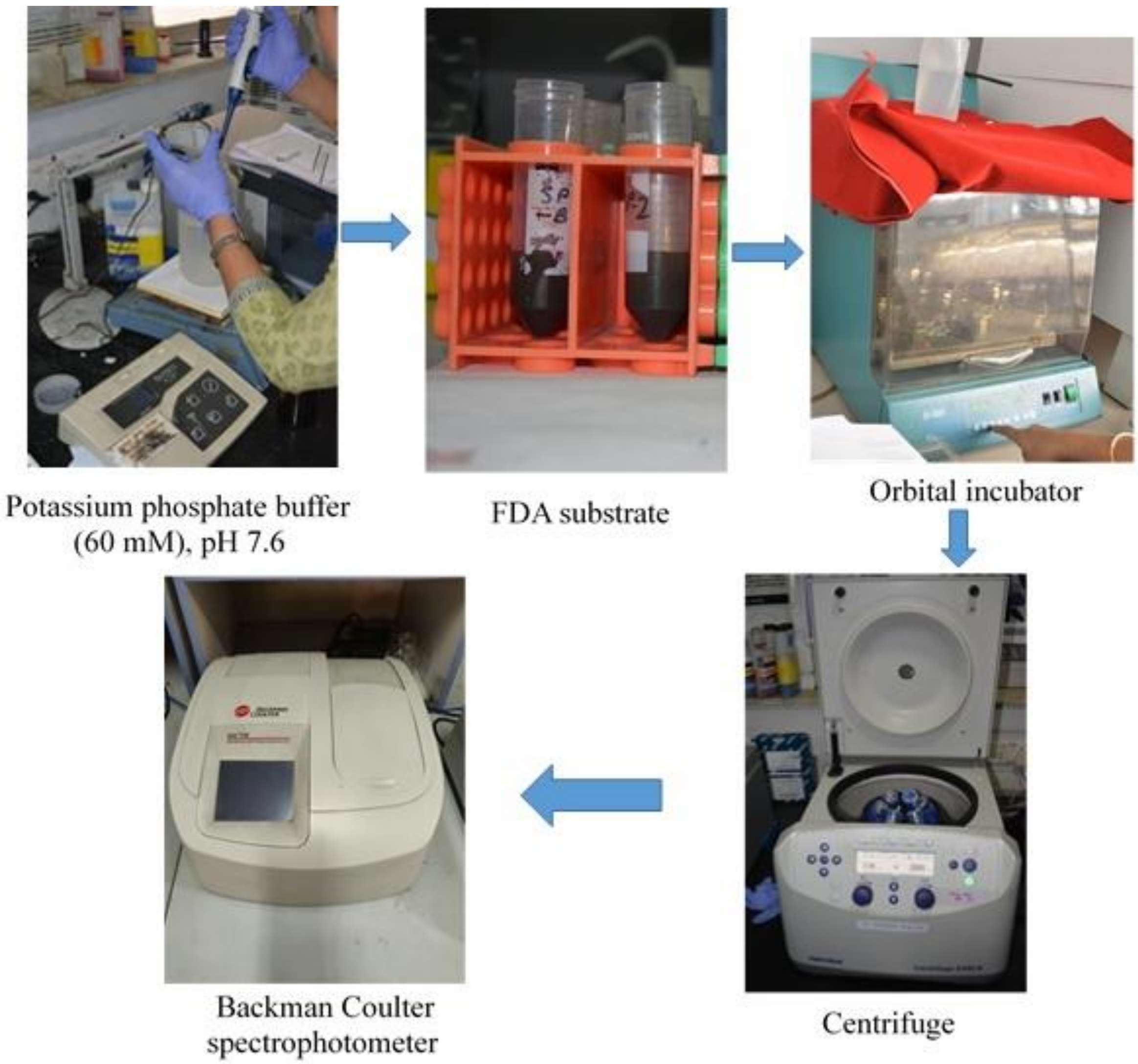

Fig.3.12 Microbial activity determination stages by FDA analysis

Two grams of soil (2 mm sieved) was collected from soil location, placed in a 50 ml conical flask and 15 ml of 60 mM potassium phosphate buffer pH 7.6 was added to it (Fig.3.12). Stock solution (0.2 ml 1000 mg FDA ml^{-1}) was added to start the reaction. Blanks were prepared without the addition of FDA substrate along with a 5 number of sample replicates. The flasks were stoppered and the contents shaken by hand. The flasks were then placed in an orbital incubator

(Jiotech Orbital Incubator, 100 rev min^{-1}) at 30ºC for 20 min (Fig.3.12). The following steps involving chloroform/methanol were carried out in a fume hood. Once removed from the incubator, 15 ml of chloroform/methanol (2:1 v/v) was added immediately to terminate the reaction. Stoppers were replaced on the flasks and the contents shaken thoroughly by hand. The contents of the conical flasks were then transferred to 50 ml centrifuge tubes and centrifuged at 2000 rev min^{-1} for approximately 3 min (Eppendorf, centrifuge 5430R). The supernatant from each sample was then filtered (Whatman-No 2) into 50 ml conical flasks and the filtrates measured at 490 nm on a spectrophotometer (Backman Coulter spectrophotometer; Fig.3.12). The concentration of fluorescein released during the assay was calculated using the calibration graph produced from 0 to 5 mg Fluorescein ml^{-1} standards which were prepared from a 20 mg fluorescein ml^{-1} standard solution. The 0 mg ml^{-1} fluorescein standard was used to zero the spectrophotometer before each set of blanks and samples were read.

Chapter 4

Mechanical characteristics of soil-WH biomaterial composite

4.1 General

The mechanical strength of water hyacinth (WH) biomaterial for cover material and subgrade reinforcement was investigated in this chapter and strength characteristics were juxtaposed with that of the conventionally used biomaterial. A series of unconfined compression strength (UCS) tests was conducted on soil reinforced with randomly distributed bio-fibers of WH, coir and jute fibers. The influence of different fiber percentages, soil-fiber composite density and moisture content on the strength parameters of the soil-fiber composite was assessed. Further, geotextiles made from WH were assessed for their tensile strength corresponding to different filament type. The geotextiles, thus developed, were tested using CBR apparatus to have an initial assessment in subgrade layer. In-house developed WH-biochar was juxtaposed against peanut shell (PE) biochar as a soil-biochar composite in terms of mechanical strength by conducting UCS test.

4.2 Strength characteristics of soil-WH fiber composite

UCS tests were conducted on both unreinforced and reinforced soil-fiber composites (WH, jute and coir) at nine different compaction states corresponding to three moisture contents (OMC, OMC −5% and OMC +5%) and three soil densities (0.95 MDD, MDD and 1.05 MDD). The philosophy of selecting nine compaction states in the current study is twofold: (i) to understand the variability in properties associated with the variability in compaction states with unforeseen factors inclusive of the changes in compaction energy; (ii) to study the variation in properties when the density changes for a given moisture content and when the moisture content changes for a given density. The influence of variation in percentage fiber content (at 0.50%, 0.75% and 1% by dry weight of soil) on UCS was also investigated for each type of fiber (WH, jute and coir). The fiber addition was restricted to 1%, as the fibers tend to form pockets of low density (weak zone) within the soil sample. Tests were repeated thrice for each compaction states (total 108 tests for one fiber type) to check any variability in observed UCS. In total, 270 tests were carried out for unreinforced or bare (27) and reinforced soil (243). All UCS tests were conducted at a constant strain rate of 1.25 mm/min as suggested by IS-2720 part-10 (1991).

In this study, it was ensured that there is minimal variability in the fiber used for soil reinforcement. The WH plants used in the study were selected from the same water body, thus avoiding uncertainties related to genetic variation. The jute and coir fibers used in this study were also derived from common sources. All selected plants were air dried for three days, until there was no significant change in moisture content (Prabakar and Sridhar 2002). The stem of dried WH plants were separated from their roots and cut into fibers of required dimension (length 28 mm and mean diameter of 0.4 mm). Aspect ratio (Length/Diameter) of 70 was targeted for all types of fibers used. Thus jute and coir fibers with same dimensions (length 14 mm and mean diameter of 0.2 mm) were cut for mixing. It is to be mentioned that coir and jute being multifilament fibers (refer Fig. 4.1), upon mixing, further segregates into even finer fibers and ultimately forms the soil fiber matrix. WH, being a monofilament fiber (refer Fig. 4.1) did not exhibit such further separation on mixing. Amount of fibers to be added were initially weighed and dry mixed uniformly in an oven dried soil sample. Following this mixing process, the required amount of water (according to test program) was added to the soil–fiber mixture. These mixtures were sealed inside plastic bags and kept inside a desiccator for 24 hours for uniform distribution of water. After that, the UCS samples were prepared by static compaction in a specially prepared mold, which facilitates uniform compaction from both ends.

4.2.1 Stress-strain response of fiber reinforced sample as compared to bare soil

Fig. 4.2 portrays the stress–strain response of bare and fiber reinforced soil (compacted at 0.95 MDD and OMC -5%). The stress-strain response of bare soil is highlighted by an increase in stress up to peak strength, followed by a sharp reduction in stress on further straining. The sharp reduction in stress is corresponding to failure along the shear plane, as represented by the sample in Fig. 4.2. The fiber reinforced soil (coir fiber) attains higher peak strength at strains greater than that of bare soil. The post peak reduction is found to be considerably less for fiber reinforced soil as compared to bare soil. This behavior is attributed to rearrangement of soil particles and its interaction with adjoining fiber, along the plane of failure. After attaining peak stress, the rearrangement or rotation of particles mobilizes the tensile strength of the interlocked fibers gradually. This mobilization of tensile strength throughout the individual fibers, in turn can resist the applied shear forces along the failure plane (Li et al. 2005). Furthermore, as shown by Tang et al. (2007), the "bridge effect" of fibers in the soil-fiber matrix, resist the sliding of soil mass along the shear plane. The fibers develop tensile stresses in it in the process of resisting the sliding of the soil, as shown by the coir reinforced sample in Fig. 4.2. The difference between peak strength and post peak strength is quite less for reinforced soil as compared to unreinforced soil, indicating that the post peak ductility of the soil has increased with fiber inclusion. Similar behavior of fiber reinforced soil in the case of sand reinforced with polypropylene fibers has been reported (Yetimoglu and Salbas 2003). For the sake of brevity, the results of other fibers are not presented as they exhibited similar behavior.

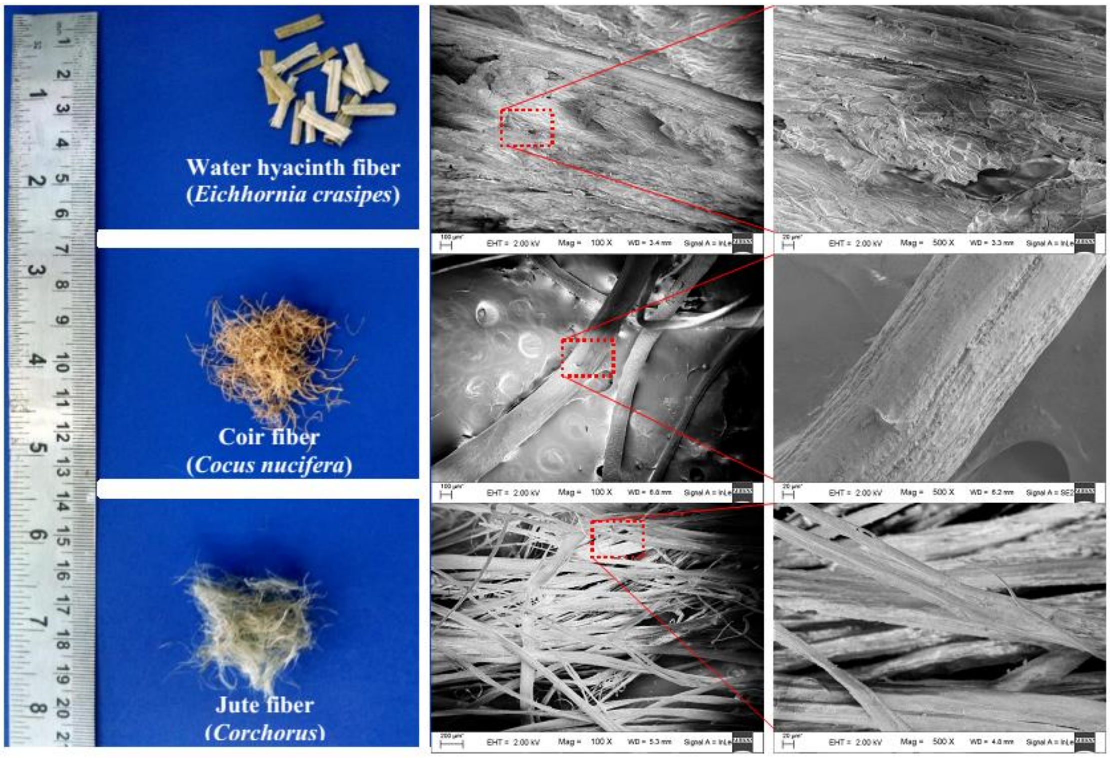

Fig. 4.1 Pictorial description and FESEM image (at 100X and 500X) of natural fibers used for soil reinforcement

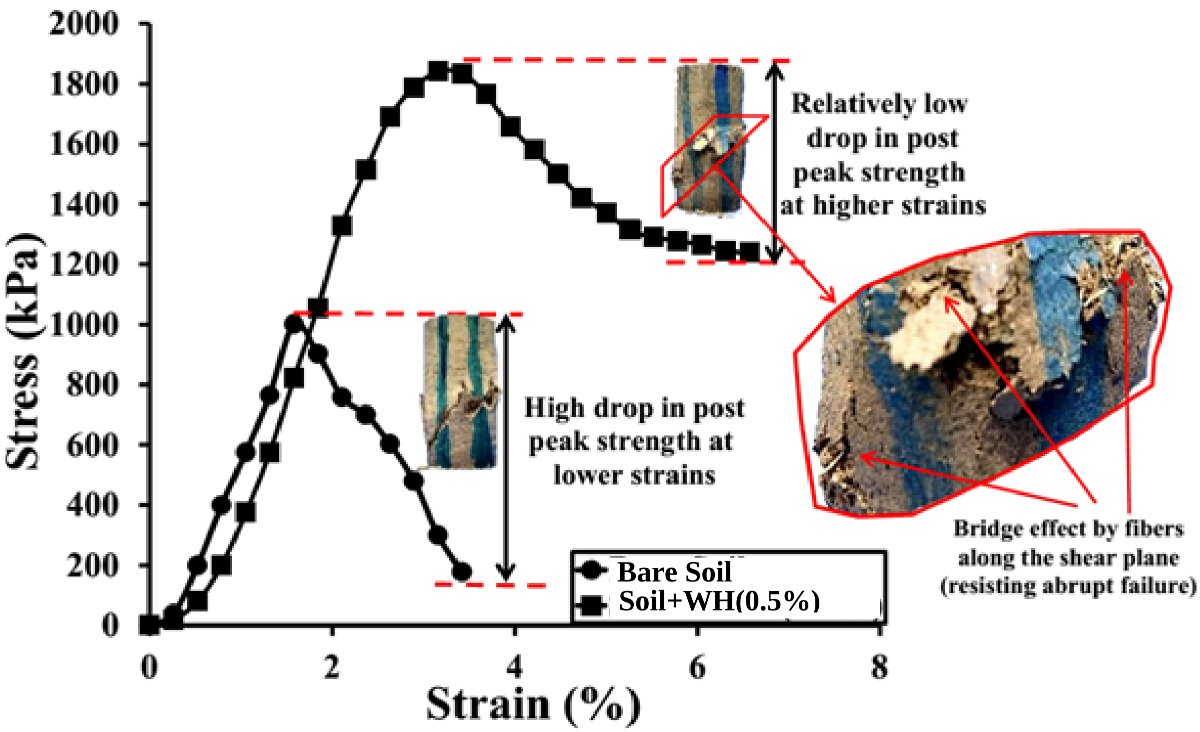

Fig. 4.2 Stress-strain response of WH fiber reinforced sample as compared to bare soil (at 0.95 MDD and OMC -5%)

4.2.2 Effect of density and moisture content on the UCS of fiber reinforced soil

Figure 4.3 shows the UCS variation with the change in density of soil samples at the selected compaction states for 1% coir fiber content. Both unreinforced and reinforced strength (mean along with the error bar from the three test trials) are presented in the figure. The results portray an increase in UCS with a corresponding increase in density for both soil-fiber composite as well as for unreinforced soil. This increase in soil strength is due to higher interlocking between soil-soil and soil-fiber at a denser state. As observed in the figure; with decrease in moisture content at a particular density, both bare and reinforced soil exhibited higher strength. This increase in unconfined compressive strength can be attributed to increase in soil suction corresponding to lower moisture content (Chae et al. 2010; Khan et al. 2014).

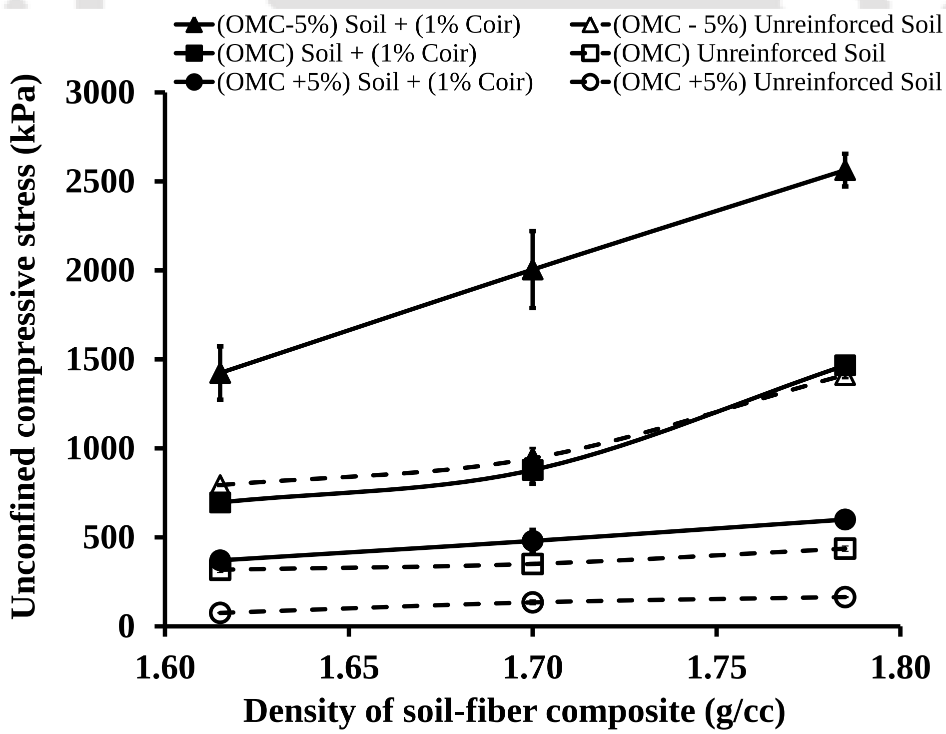

Fig. 4.3 UCS variation with the change in density of soil samples at different moisture contents (for 1% coir fiber content)

Fiber reinforced soil exhibited higher UCS for all the nine compaction state considered in this study with respect to bare soil. Significant UCS increase (1070 kPa at OMC -5% for 17 kN/m^3) on the inclusion of fibers is observed at lower moisture content. With increase in moisture, UCS decreases (580 kPa at OMC and 360 kPa at OMC +5% for 17 kN/m3) due to decrease in soil suction and frictional resistance attributed to higher lubrication along the soil-fiber interface. During loading, this lubrication effect of water can cause less load transfer between the soil particles and fibers as reported in the case of polypropylene fiber (Maher and Ho 1994). This trend as seen in Fig.4.3 was observed for all three fiber type and fiber percentage.

4.2.3 Effect of fiber inclusion on the strength and ductility of the soil-fiber composite

Figure 4.4 shows a typical stress-strain response of bare and fiber reinforced soil and the important parameters used in this study which include peak stress, peak strain and ultimate stress. For comparison, the ultimate stress here is considered at 1.5% after peak strain. The inclusion of fiber in soil resulted in the increase in soil strength and affected the ductility of the soil-fiber composite. There are various parameters used to measure and quantify; the strength and ductility of fiber reinforced soil (Maher and Ho 1994; Kaniraj and Havanagi 2001; Kaniraj and Gayathri 2003; Anagnostopoulos et al. 2013). The peak strength improvement factor (PSF) has been used to indicate relative gain in UCS for fiber reinforced soil (Anagnostopoulos et al. 2013) as given by Eq. 4.1.

$$\text{PSF}\ (\%) = \left[\frac{(\sigma_{pr} - \sigma_{pb})}{(\sigma_{pb})} * 100\right] \qquad (4.1)$$

Where, σ_{pr}, σ_{pb} are peak stress for reinforced and bare soil, respectively as shown in Fig. 4.4.

Another approach to indicate the actual improvement in strength is expressed by the ratio of peak strength of fiber reinforced soil to the peak strength of bare soil (Maher and Ho 1994). This ratio is termed as strength improvement factor (SIF) for a reinforced soil, with values higher than 1 indicating an improvement in soil compressive strength with that of bare soil. In this work, the SIF parameter (Eq. 4.2) is adopted for measuring the strength improvement due to fiber inclusion.

$$\mathrm{SIF} = \frac{\sigma_{pr}}{\sigma_{pb}} \tag{4.2}$$

The ductility of a soil is improved by the inclusion of fiber, as it can take higher load stress corresponding to larger strains as compared to bare soil (refer Fig. 4.4). The consideration of strain corresponding to peak stress also gives an understanding of its relative ductility as compared to bare soil. Thus, a factor termed as mobilized peak strain ratio (MPSF) for soil-fiber composite is defined to understand the change in mobilized ductility at peak strengths (refer Fig. 4.4) as compared to that of bare soil. MPSF is defined as the ratio of peak strain of reinforced soil to that of the peak strain of bare soil for the same compaction state. MPSF values greater than 1 indicate an improvement in ductility and higher the value, more ductility is observed for the soil-fiber composite. MPSF is defined mathematically as in Eq. 4.3.

$$\mathrm{MPSF} = \frac{\varepsilon_{pr}}{\varepsilon_{pb}} \tag{4.3}$$

Where, ε_{pr}, ε_{pb} are peak strain corresponding to peak stress for reinforced and bare soil (refer Fig. 4.4).

For shearing stage after peak strength is achieved, the ductility of the soil is also measured by the brittleness index, I_b (Consoli et al. 1998; Hamidi and Hooresfand 2013). I_b (Eq. 4.4) is defined as the ratio of fall in post peak strength to that of the ultimate stress for a certain strain rate. The fall in post peak strength is the difference between peak stress and ultimate stress. As the index value decreases towards zero, the stress-strain response becomes increasingly ductile.

$$I_b = \frac{(\sigma_{pr} - \sigma_{ultr})}{(\sigma_{ultr})} \text{ or } I_b = \frac{(\sigma_{pb} - \sigma_{ultb})}{(\sigma_{ultb})} \quad (4.4)$$

σ_{ultr}, σ_{ultb} – Ultimate stress for reinforced and bare soil respectively (refer Fig. 4.4).

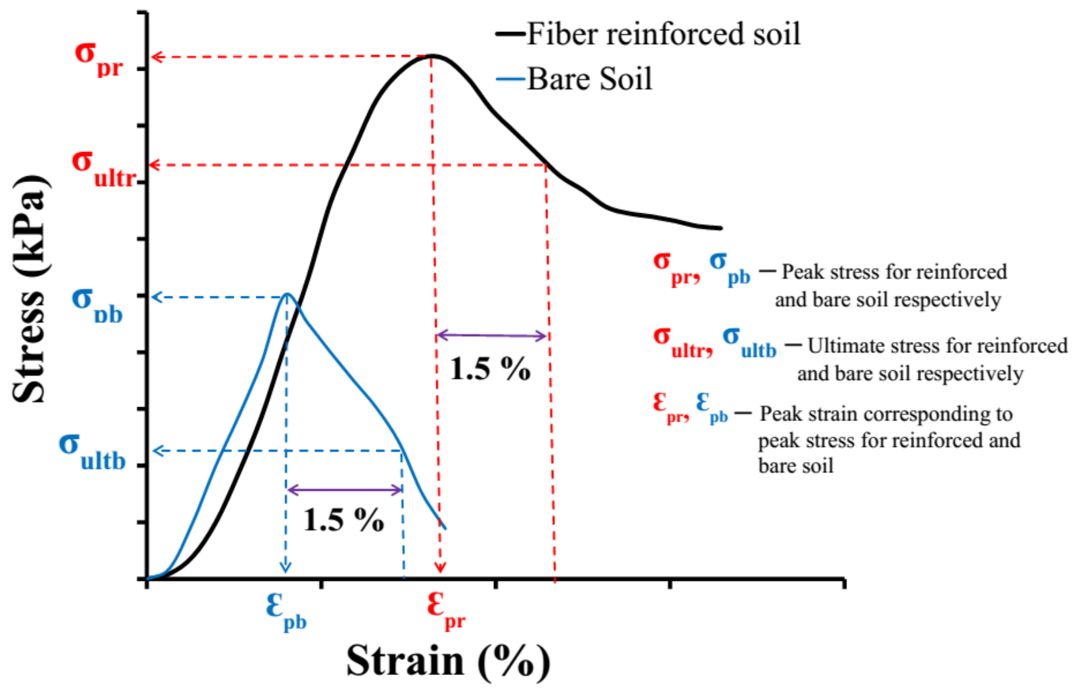

Fig. 4.4 Description of parameters in stress strain response of bare and fiber reinforced soil for calculating SIF, PSF and NDI

However, this parameter does not represent the absolute brittleness of the material. Thus, a new normalized ductility index (NDI) is proposed to represent soil ductility during shearing. NDI in Eq. 4.5 is defined as the ratio of fall in post peak strength to that of the peak stress. Thus, 1 is the limiting value of this index which indicates complete brittle failure (where σ_{ultr} or σ_{ultb} is taken as 0 at same strain). NDI equal to 0 represents purely ductile behavior with no change in stress on further straining (peak and ultimate values are same). In this study, the ultimate stress is considered at 1.5% strain greater than peak strength for the sake of uniformity. This value of 1.5 % is taken corresponding to the minimum post peak strain possible for the bare soil that can facilitate comparison of UCS for reinforced and bare soil.

$$\mathrm{NDI} = \frac{(\sigma_{pr} - \sigma_{ultr})}{(\sigma_{pr})} \text{ or } \frac{(\sigma_{pb} - \sigma_{ultb})}{(\sigma_{pb})} \tag{4.5}$$

4.2.4 Strength improvement factor (SIF)

Figure 4.5 indicates the SIF variation for the natural fibers at various compaction states. For a particular density, SIF is significant with increase in moisture content. The inclusion of fiber at higher moisture content increases the strength of the soil-fiber composite in comparison to bare soil by increasing the adhesive forces along the soil-fiber interface. This is due to higher surface roughness and adhesive bonds developed between free hydroxyl groups of cellulose and hemicellulose, Methacanon et al. 2010). Although, the stress increment at higher moisture content is relatively less than that of drier state (refer Fig. 4.3), the fiber inclusion significantly improves the ratio of stress resisted as compared to bare soil. No significant trend in SIF change with increase in density is observed, for a particular moisture content. With increment in coir and jute fiber content, SIF is found to increase for all compaction states. With higher fiber content, imposed load is transferred more to the fibers rather than only being resisted by soil particles, thus increasing the UCS of the soil-fiber composite. However, for WH fibers the highest SIF values were observed at 0.75% fiber content after which it remains relatively constant. Among the three fibers tested, jute showcased the highest soil-fiber composite strength in majority of the tested conditions (19 out of 27 for all possible combinations of fiber content, density and moisture content), due to its inherent tensile strength corresponding to its highest cellulose content. However, coir and WH inclusion also improved the compressive strength of the soil by at least 50%.

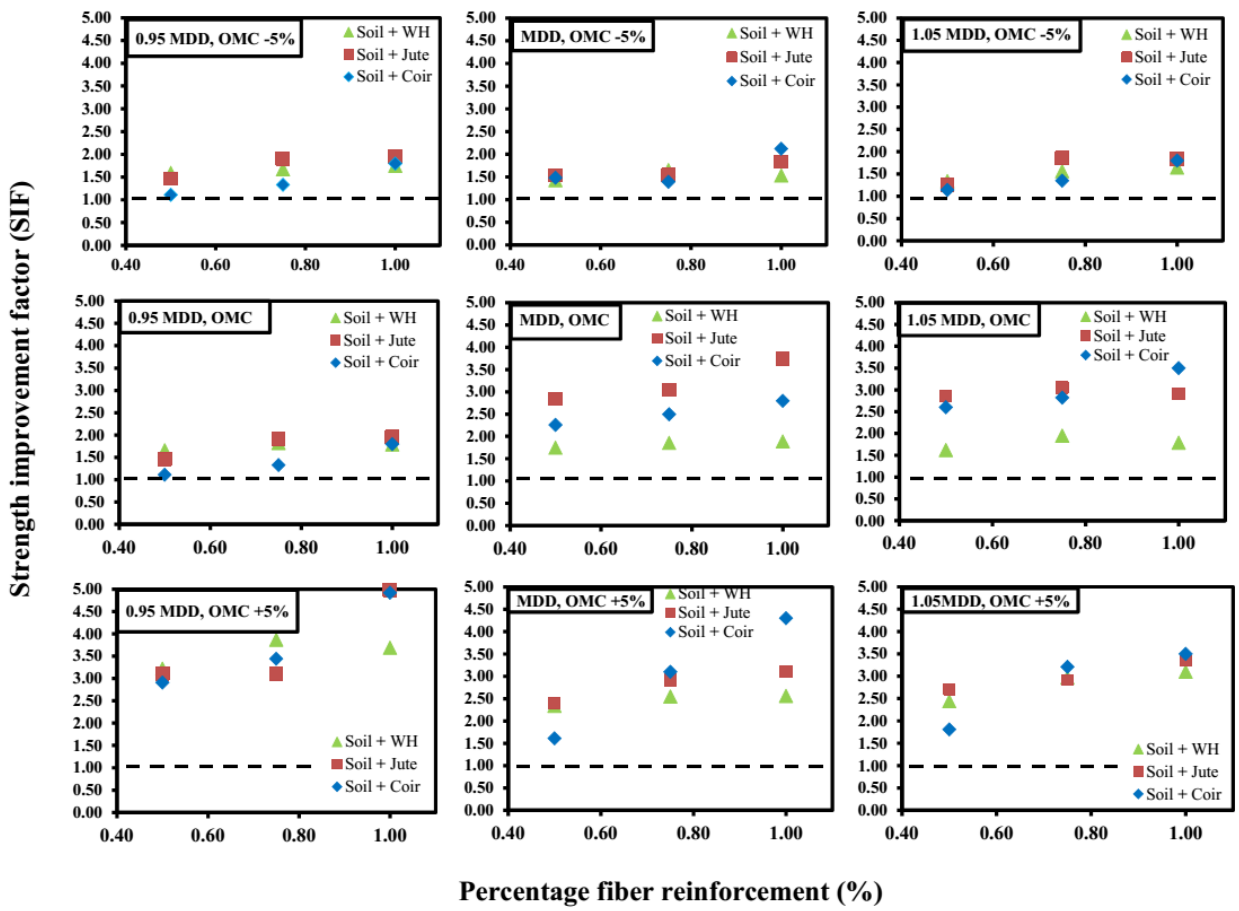

Fig. 4.5 Strength improvement factor for different compaction states and types of fiber reinforcement

4.2.5 Mobilized peak strain factor (MPSF)

Figure 4.6 represents the variation of MPSF parameter at the selected compaction states. For all types of fibers constituting 0.5%, there is no significant improvement in ductility for all the compaction states. The amount of fibers in the composite is probably not enough to resist the deformation before reaching peak strength, as compared to bare soil. However, with further increase in fiber content there is a gradual increase in the MPSF, thus indicating improvement in the ductility of the composite during loading. At lower moisture contents (OMC, OMC -5%) the effect of fiber inclusion on MPSF is relatively higher than that at relatively wet condition (OMC

+5%). At higher water content, the MPSF values are comparatively less as compared to dry condition. This is due to bare soil undergoing high strains at that state, and consequently the MPSF ratio is less, even though there is an increase in strain for reinforced soil. Coir showed relatively higher values for MPSF among all the fibers, at the tested combinations. This is probably due to the highest value of elongation at break for coir fibers, among the tested fibers. Coir, being a more extensible filament among the tested fibers, can undergo high amount of deformation under loading, thus resulting in higher values of MPSF for the soil-fiber composite. The effect of density for particular moisture content did not have a pronounced effect on MPSF.

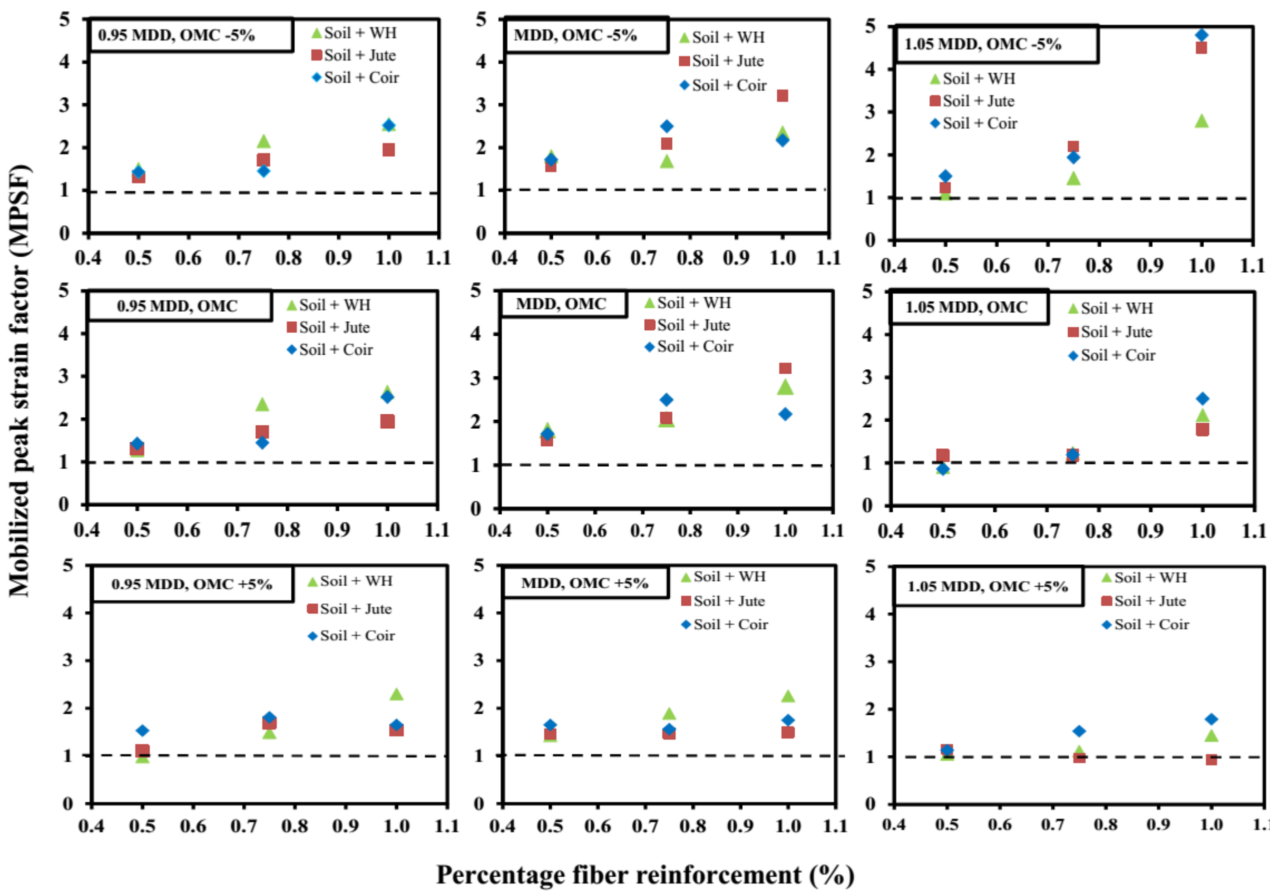

Fig. 4.6 MPSF variation for different compaction states and types of fiber reinforcement

4.2.6 Normalized ductility index (NDI)

Figure 4.7 depicts the normalized ductility of the soil-fiber composite at different compaction states. It can be noted that bare soil ductility is improved with increase in density for particular water content as indicated by decreasing value of NDI. This is due to higher amount of soil particles resisting the developed shear band at higher density, as compared to loose soil.

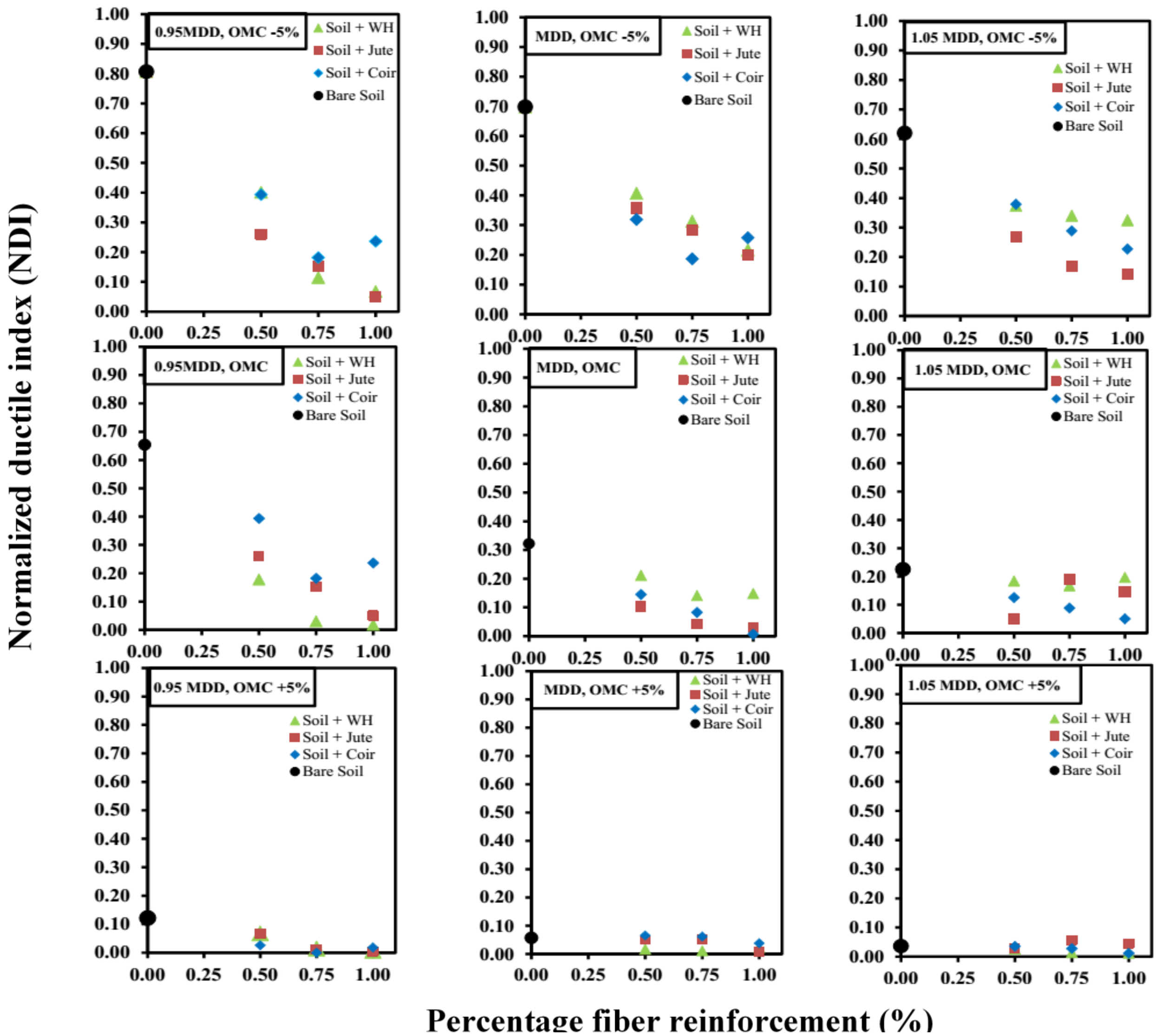

Fig. 4.7 Normalized ductile index variation at different compaction states for different types of fiber reinforcement

At a particular density, increment in moisture content results in increased ductility due to increase in adhesive and cohesive forces between particle interfaces (soil-soil, soil-water, fiber-water and soil-fiber). At higher moisture content, it is seen that the inclusion of fiber does not significantly increase the ductility of the soil. On the other hand, for lower moisture content, the ductility is significantly improved by the inclusion of fibers.

This improvement at relatively lower moisture content is due to the formation of active fiber bridges along the shear plane (refer Fig. 4.2). As the moisture content increases, the inclusion of fiber does not significantly improve the ductility of the soil-fiber composite, owing to lubrication along the soil-fiber interface, which probably increases the chance of slippage along the shear plane. Regardless of fiber type and compaction state, the NDI value decreases with increase in fiber content, thus making the soil-fiber composite more ductile. With increase in fiber content, the amount of fibers along the shear plane increases, thus amplifying the “bridging” effect. The incremental bridge effect decreases the drop in post peak strength as the fiber content increases.

4.3 Strength characteristics of soil-WH geotextile composite

A series of tensile strength tests were conducted on WH filament and woven geotextiles. This was followed by California bearing ratio (CBR) test to demonstrate the soil strength improvement attributed to the inclusion of WH limited life geotextile (LLG). CBR tests are widely adopted to investigate the feasibility of natural as well as synthetic geotextile as soil reinforcement especially for road pavement (Holtz and Sivakugan 1987, Bergado et al. 2001, Yetimoglu et al. 2005). Increase in CBR value indicates improvement in soil subgrade strength and decrease in design pavement thickness, thus economizing road construction (IRC, 37- 2012). Test results from this study were compared with those reported in the literature for other natural filaments.

4.3.1 Water hyacinth filament and geotextile

WH plants of similar length (45 ± 3.4 cm) and girth were selected from the same location for making filament and geotextiles, so as to avoid any genetic variation. All the selected WH stems were initially sun dried until there was no change in the weight due to moisture variation. The dried stem was further used for making filament and geotextiles. The designation of the filaments is given as in Table 4.1 where the first two alphabets represent the type of manufacture (WP= Woven pattern, FP= Flattened pattern), the number represent the mean breadth of the filament and the last two alphabets represent plant type. The FP13 filament is obtained by flattening the WH plant stem. The woven filaments were fabricated from FP13 WH filament. WP2.5 filaments was obtained by slitting the FP13 filament into four parts along its longitudinal axis. Two such slitted parts was woven to obtain WP2.5 filaments. The WP6 filament was obtained by weaving two parts of the FP13 filament, where each part was obtained by axially splitting the FP13 filament. The WP11 filament was obtained by weaving two intact FP13 WH filaments together. All the filaments as shown in Fig. 4.8 were tested to obtain its tensile strength and elongation at break, the results of which are discussed later. One particular filament was used to weave geotextiles of two different patterns as shown in Fig. 4.9. The warp and weft pattern (WW-GT; Fig. 4.9 (a)) was chosen to weave one such geotextile. A circular pattern of weaving which is quite common among the handicraft industry in North East region of India was also adopted to weave the other geotextile (C-GT; Fig. 4.9 (b)).

Table 4.1 Specification of WH filaments

Type of manufacture	Flattened	Woven	Woven	Woven
Filament Designation	FP13 WH	WP2.5 WH	WP6 WH	WP11 WH
Mean Breadth (mm)	13 ± 0.34	2 ± 0.45	6 ± 0.49	11 ± 0.42
Mean Thickness (mm)	1.5 ± 0.13	2 ± 0.08	2.2 ± 0.21	2.3 ± 0.12
Breaking tensile stress (MPa)	17 ± 1.23	18 ± 1.65	20.65 ± 1.8	32.50 ± 2.03
Elongation at break (mm)	60 ± 2.31	39.5 ± 3.06	44.50 ± 1.36	61 ± 1.49

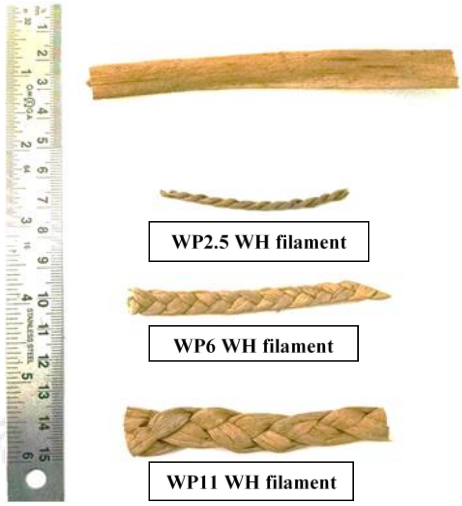

Fig. 4.8 Overview of 4 types of WH filaments (with reference to **table 4.1**).

(a)

(b)

Fig. 4.9 Overview of woven geotextiles (a) WW-GT (b) C-GT

4.3.2 Test program and specimen preparation

The experimental study included a series of tensile strength test on filaments and geotextiles. The tensile test for the WH filaments was done according to the procedure given in IS-1670- (1991) (IS-1670-1991) where the gauge length was maintained at 200 mm and strain rate equal to 300 mm/min. The procedure given in ASTM D4595-11 was adopted to obtain the tensile strength and elongation at break of the geotextiles. The gauge length and the strain rate adopted for the geotextile testing was 100 mm and 300 mm/min, respectively.

This study adopted laboratory CBR test for the initial assessment of reinforcing capability of WH geotextile. The soil sample was mixed with water content corresponding to OMC, packed in a polythene cover and kept in a desiccator for 24 hours to achieve uniform distribution of water throughout the soil. The mold used for CBR testing was a rigid metal cylinder with an inside diameter of 150 mm and a height of 175 mm as shown in Fig.4.10. The matured soil was statically compacted into the CBR mold at MDD using a circular spacer disc as per the specification given in IS-9669 - (1980) for both unreinforced and reinforced soil.

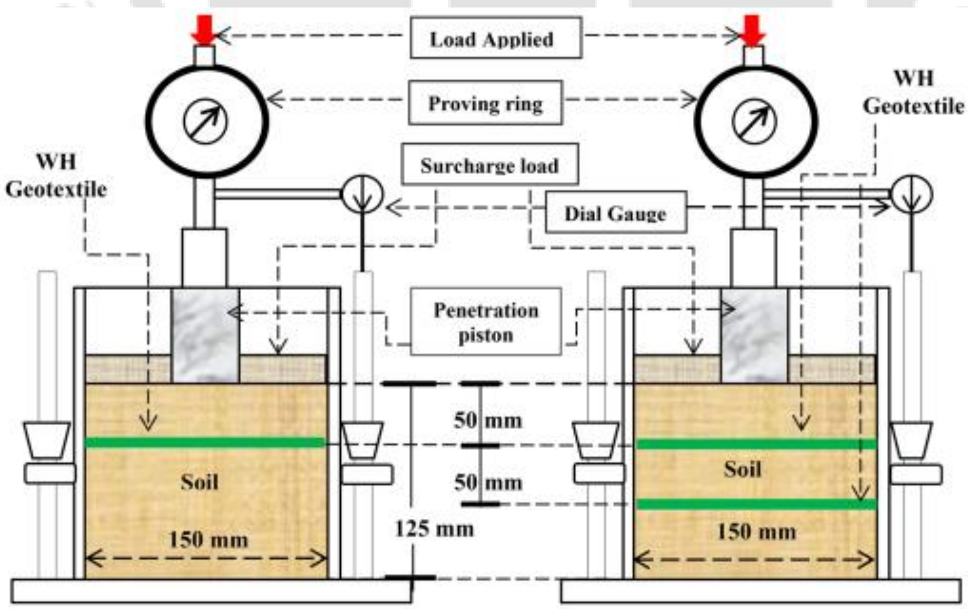

Fig. 4.10 Schematic illustration of soil-WH geotextile arrangement in the CBR setup

The tests for measuring CBR were carried out as per provisions of IS-2720-Part 16, (1987). An automatic loading machine equipped with a movable base at a rate of 1.25 mm per minute vertically was used for static compaction. A calibrated device with load measurement was used to penetrate the piston of diameter 50 mm into the soil. The loads were calculated for a penetration up to 20 mm, to observe its peak and post peak failure. The WH geotextiles were placed in one and two layers as shown in Fig. 4.10 in the CBR mold. The position of single geotextile was placed at a depth of 50 mm below the soil surface (Yetimoglu et al. 2005). The second geotextile was placed 50 mm below the initial geotextile layer. Each experiment was repeated at least three times for ensuring repeatability of trends. Those test results with variation more than 5% variability was discarded and additional tests were conducted.

4.3.3 Mechanical property of water hyacinth filaments and geotextiles

Figure 4.11 shows the comparison of tensile stress variation with elongation for WH filament stems of different diameter. For 11 mm diameter (WP11 WH filament), elongation at break was found to be 60 mm, which is around 30% and 38% higher than filament with 6 mm and 2.5 mm diameter. For the woven filament, it was observed that with increase in the breadth there was a gradual increase in the breaking tensile stress. This is probably due to increase in contact area between individual units of the filament with increasing breadth. The tensile strength of WH filaments is comparable with the maximum strength of coir filaments (Subaida et al. 2008), reed filament (Methacanon et al. 2010) and sisal filament (Vadivambal et al. 2015) as shown in Fig. 4.11 with colored reference lines. The FP13 filament showed comparatively low tensile stress at failure with respect to the woven filaments. The elongation at break for all type of filaments increased with increasing breadth of the specimen. The results are summarized in Table 4.1.

Among all the fibers compared in Fig. 4.11, WP11 WH filament exhibited maximum tensile strength. This clearly proves the potential of WH filament as LLG.

Based on the measured tensile strength and elongation at break, the WP11 WH filament was chosen as the weaving material for the geotextiles. The tensile strength results for the geotextiles are presented in Fig. 4.12. The mean tensile strength of WW-GT and C-GT was found to be 26.5 kN/m and 22 kN/m, respectively. The possible increase in tensile strength of WW-GT over C-GT can be attributed to the difference in yarn tenacity, which is specific to the weaving pattern. Yarn tenacity is defined as the ultimate (breaking) force of the fiber (in gram-force units) divided by the linear density. The weaving pattern is found to be an important variable affecting yarn tenacity of geotextiles (Subaida et al. 2008). The tensile strength of the WH geotextiles is attributed to the presence of higher percentage of cellulose in the plant stem (Methacanon et al. 2010).

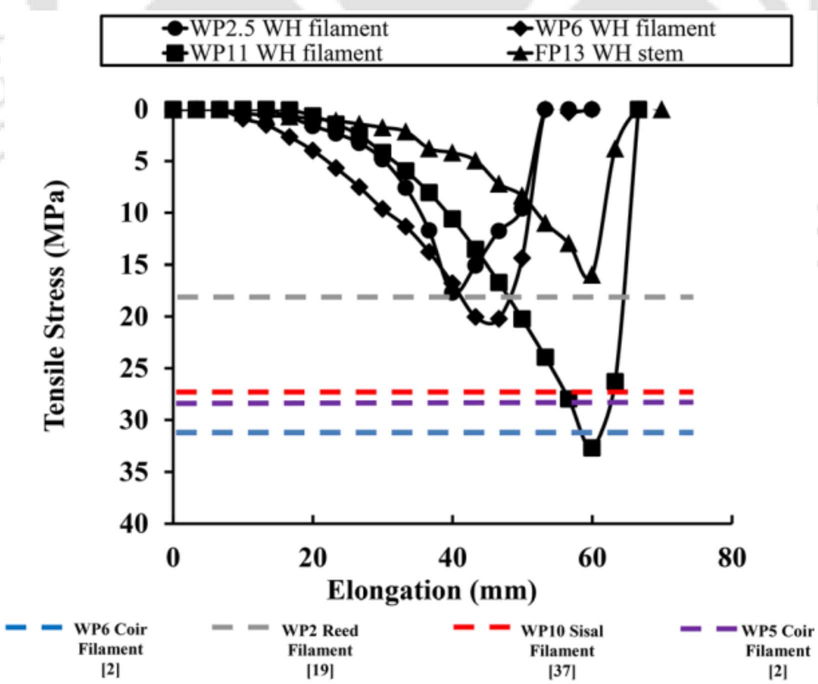

Fig. 4.11 Tensile stress variation with elongation for four types of WH filaments

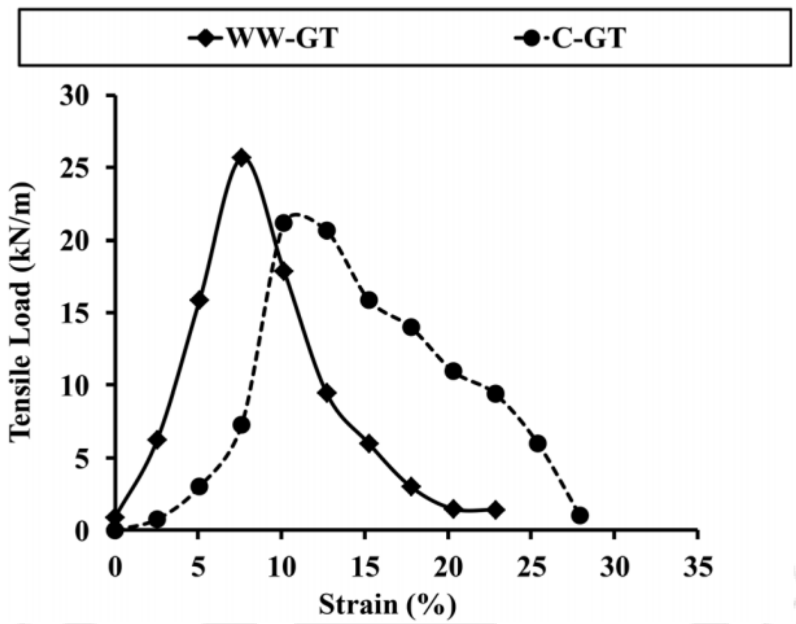

Fig. 4.12 Tensile load variation with strain for WH geotextiles

The tensile strength results of WH geotextiles are higher by approximately 176.67% to 331.25% compared to some of the conventionally used coir geotextiles (Subaida et al. 2008). However, for fair comparison, it requires an in depth understanding of the bio-chemical composition of the coir geotextiles, which is not reported in the above referred study. In addition, the aperture size needs to be uniform with referred coir geotextiles, which is not known.

4.3.4 Effect of water hyacinth geotextile reinforcement on CBR

Figure 4.13 shows the comparison of load versus piston penetration for both unreinforced and reinforced soil specimens. From the results, it is evident that the two layered geotextile-soil exhibited peak piston load marginally higher than single layered geotextile-soil. Accordingly, the CBR values were computed from the load-penetration results and summarized in Fig. 4.14. The mean CBR value of unreinforced soil was found to be 6.13 (±0.07) %. For a single layered geotextile-soil arrangement (Fig. 4.10), the CBR values increased to 8.43 (±0.2) % for WW-GT and 7.20 (±0.1) % for C-GT. With inclusion of two layered geotextile-soil arrangement (Fig. 4.10), the CBR values further increased to 8.48 (±0.17) % and 7.68 (±0.1) % for WW-GT and C-GT, respectively. However, the increase in CBR value for two layered geotextile compared to one layered geotextile is not significant. Figure 4.14 also indicates that the weaving pattern influences the CBR value of reinforced soil. The WW-GT single layer reinforcement was found to exhibit higher CBR than C-GT two layered reinforcement. The increase in reinforced CBR values with respect to unreinforced soil, indicate an improvement in the subgrade soil strength, which in turn helps decreasing the pavement thickness as suggested in road design provisions for specific design traffic (IRC 37-2012).

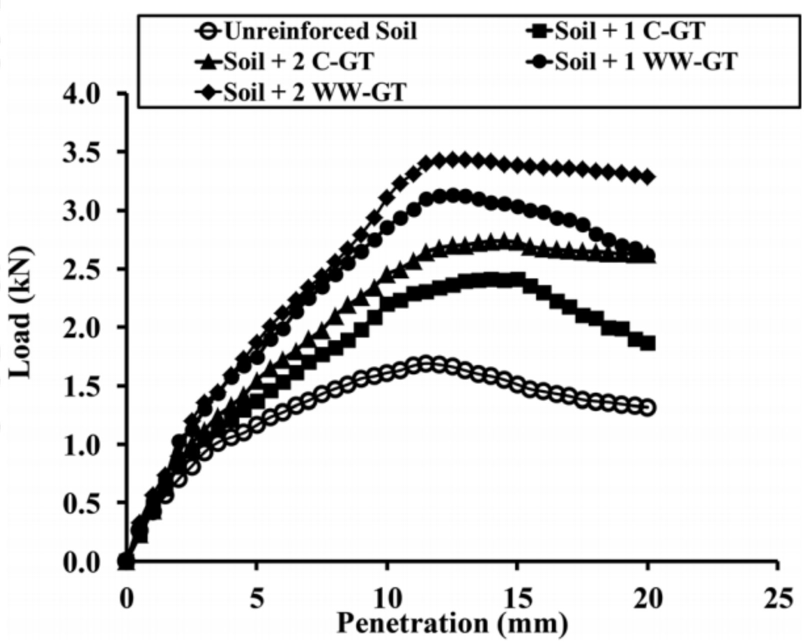

Fig. 4.13 Load variation with penetration of CBR plunger for the tested conditions

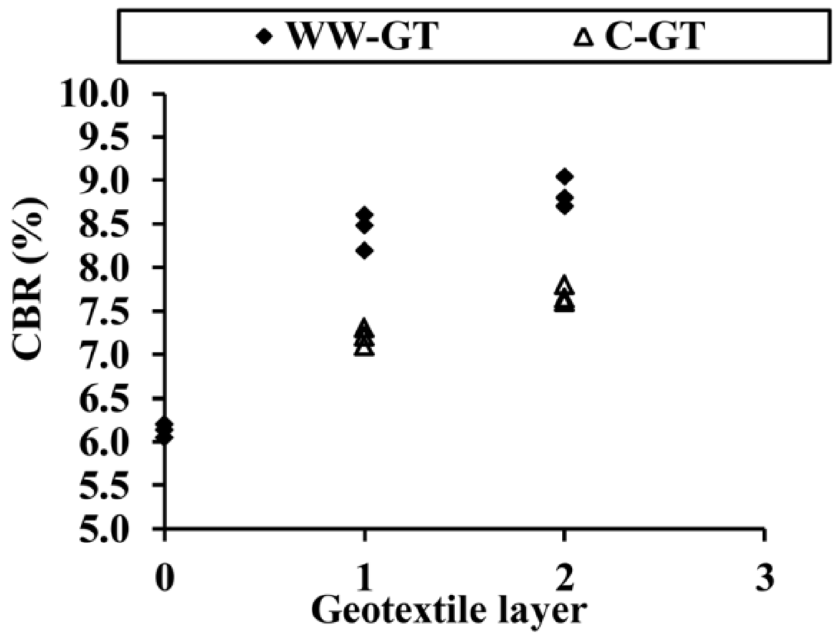

Fig. 4.14 Increase of CBR values with addition of WH geotextiles

A CBR value is an index property and an established parameter for pavement design. However, to represent the peak load property of the soil-geotextile systems tested, the peak load ratio (PLR) as adopted in the previous literature (Bergado et al. 2001) was used. The PLR is defined as

$$PLR = \frac{Lr}{Lu} \qquad \text{------------- (4.6)}$$

Where, Lr is the peak load for geotextile reinforced soil and Lu is the peak load for unreinforced soil. The PLR values for the tested conditions are presented in Fig. 4.15. The mean peak load ratio for WW-GT and C-GT is found to be 1.86 and 1.42 for one layered geotextile system, respectively. In case of two layered geotextile system, the mean PLR further improved to 2.04 and 1.62 for WW-GT and C-GT, respectively. This increase in PLR value directly indicates the efficacy of using WH geotextile in resisting compressive load.

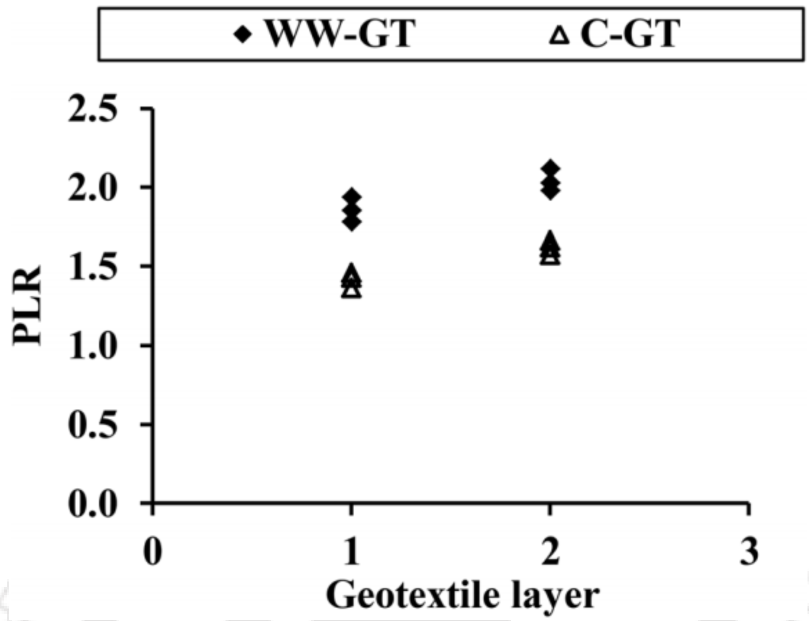

Fig. 4.15 Increase of PLR values with addition of WH geotextiles

4.4 Strength characteristics of soil-WH biochar composite

The unconfined compressive strength of biochar produced from WH was compared with that of peanut shell (PE) biochar. Soil-PE biochar composite has been advocated as a cover material for landfill systems due to its efficacy in methane gas oxidation, vegetation growth and in increasing the water holding capacity of surface layer (Wong et al. 2016, 2017, 2018, Ni et al. 2018). The UCS was obtained for both WH and PE biochar at same compaction energy along the compaction curve corresponding to OMC, OMC-5% and OMC+5% conditions. The OMC and MDD shift with the addition of biochar was significant for soil-biochar composites at 5% and 10% as shown in Fig 4.16. Hence, all the tests were conducted at same compaction energy for comparing their UCS.

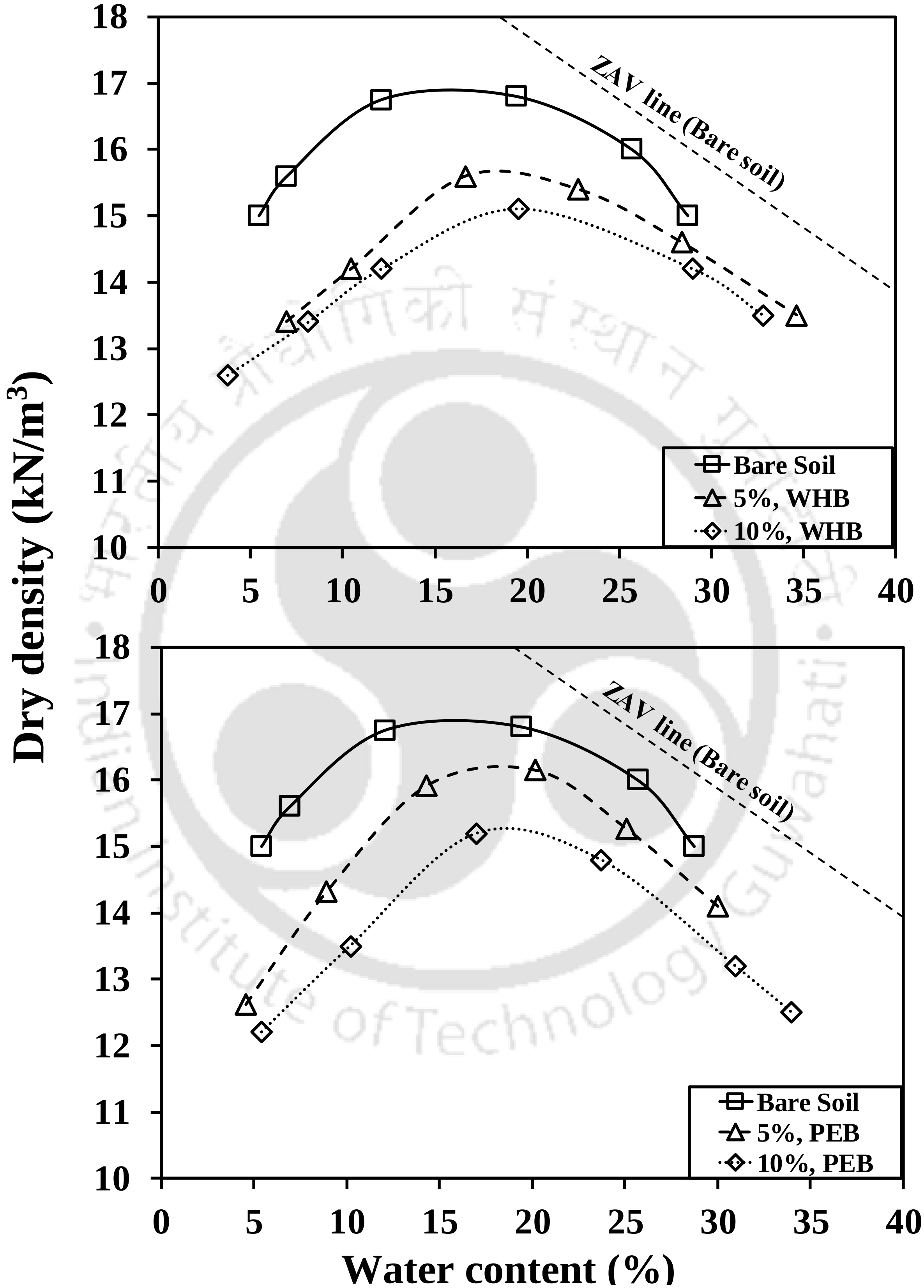

Fig. 4.16 Compaction curve for soil-biochar composites at 5% and 10%

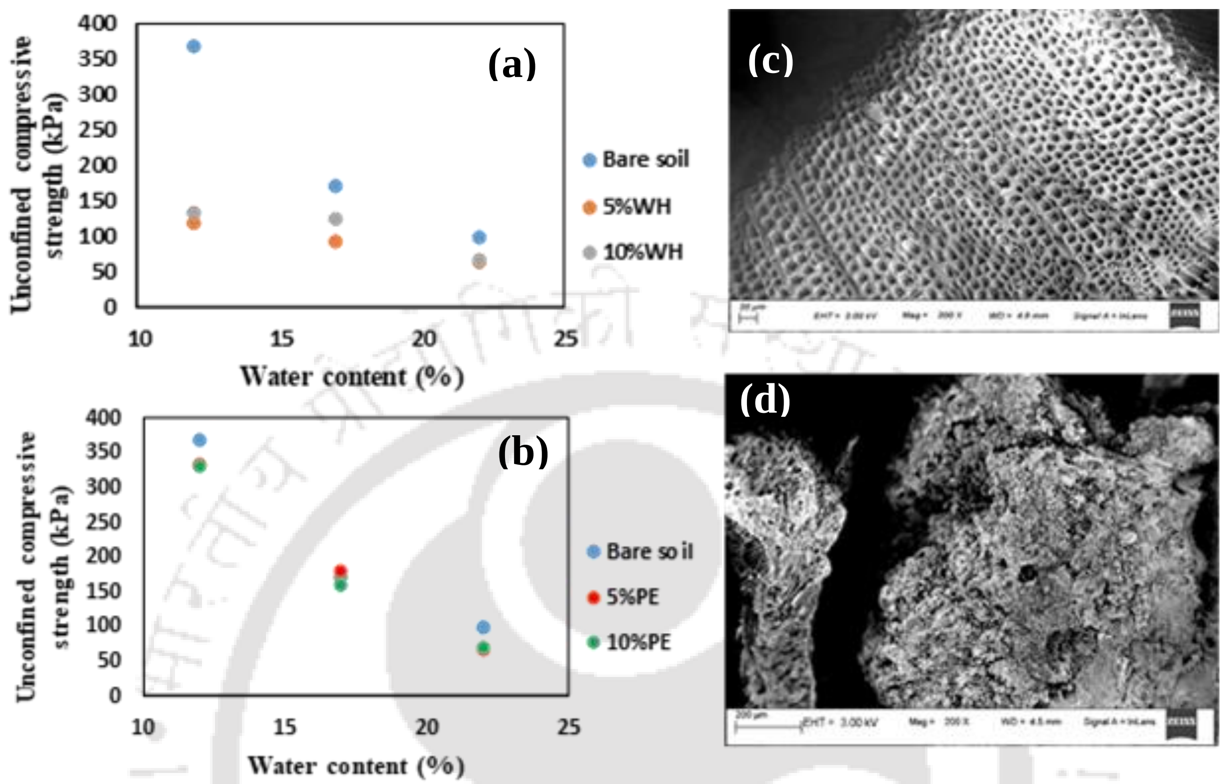

Fig. 4.17 UCS of soil-biochar composite (WH, PE) and bare soil (a, b) along with biochar morphology (c,d)

It was seen that with respect to bare soil, the UCS decreased for WH-biochar and can be attributed to the porous structure of individual biochar material (Fig. 4.17). Furthermore, WH biochar is a cohesion less material and thus the undrained cohesion will definitely decrease. The, peanut shell biochar did not show a rapid decrease of strength as compared to bare soil. However, peanut shell is relatively dense and has a coarser surface (Fig. 4.17) which can increase the interface friction. The surface roughness was investigated by Occhio 500nanoXY particle shape and size analyzer (Cabanettes et al., 2018) which is used for precision measurement of powdered materials (refer Fig. 4.18a). The instrument consists of an integrated computer with an in-built imaging software and a particle dispersion device that facilitates capturing of powdered material (Fig.4.18 a-b). The software can measure particle and its morphology ranging from 0.2µm to 2000µm. The instrument and the in-built software have been certified by ISO 13322-1 and ISO 9276-6 respectively. The shape parameters obtained and their definition have been reported in Table 4.2. However, three major parameters i.e. roundness (waddel's concept in Fig. 4.18c), circularity and Occhio roughness has been discussed majorly to explain the mechanical parameters tested in results section. PE biochar has a rougher surface and low roundness which can facilitate greater soil-biochar and biochar-biochar interface friction as compared to WH biochar. This observation on particle roughness of PE biochar can also be observed in the FE-SEM images in Fig. 4.17.

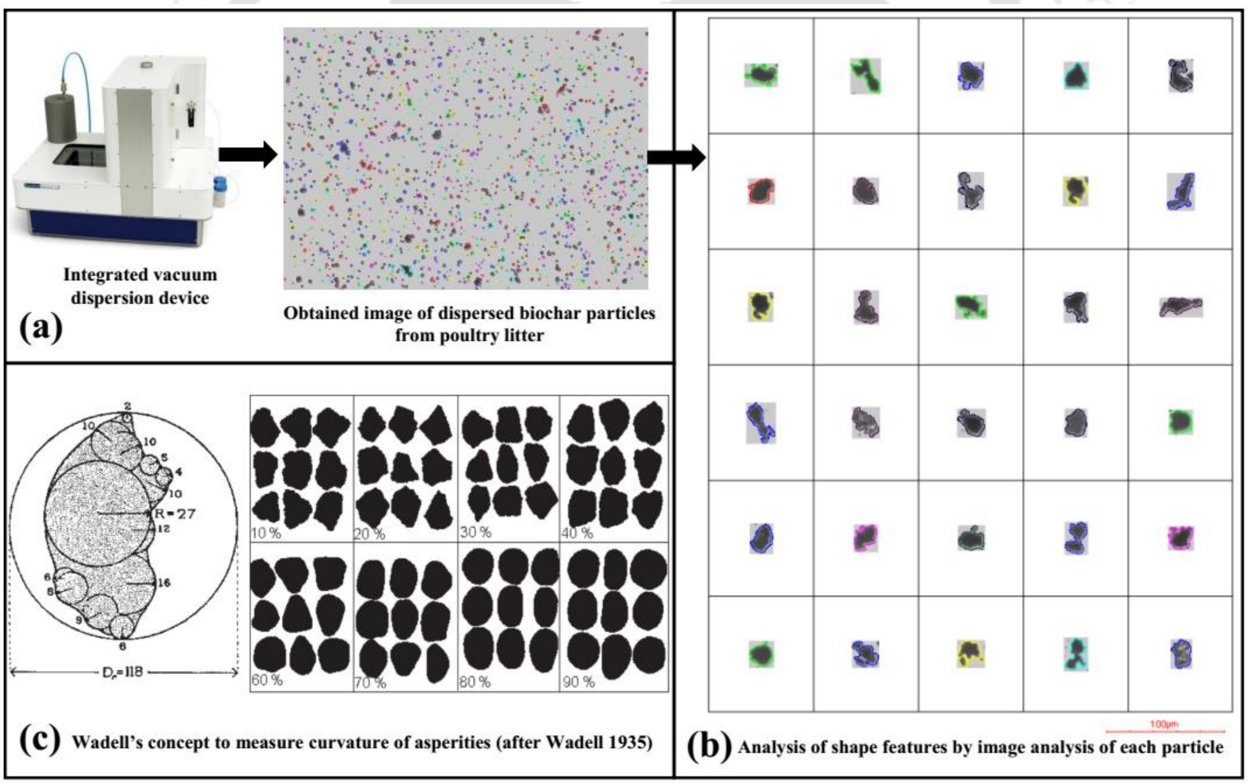

Fig. 4.18 Description of a) 500nano XY particle shape analyzer, b) resultant image obtained for a biochar type and c) concept of particle roundness (after **Wadell 1935**)

Table 4.2 Mean shape parameters measured from Particle characteristic analyzer

Parameter	Definition	Mean value	
		PE	WHB
Volume-equivalent diameter	The diameter of a sphere having the same volume as the particle	8.8.0 (µm)	3.8 (µm)
Area-equivalent diameter	The diameter of a sphere having the same projection area as particle	12.6 (µm)	8.6 (µm)
Inner diameter	The biggest circle inscribed into the projection area of the particle.	8.4 (µm)	7.1 (µm)
Thickness	Approximation of the particle width for very long and concave particle	4.3 (µm)	4.3 (µm)
Roundness	The degree to which the projection area of the particle is similar to a circle. The ration of the area-equivalent diameter to Feret diameter maximum	52.4 (%)	76.4 (%)
Circularity	The degree to which the projection area of the particle is similar to a circle, considering the smoothness of the perimeter.	73.7 (%)	83.6 (%)
Occhio roughness 80%	The ratio of smooth reference to the particle projection area. The smooth reference is defined by inscribed circles tangent to each point of the particle projection outline with a radius greater than 80% of the maximum inscribed circle	25.5 (%)	14.8 (%)

4.5 Summary

The summary from this chapter can be discussed for the three soil-WH biomaterial tested as follows

1) *Soil-WH fiber composite*

To explain the soil-fiber composite ductility, two new physical parameters has been identified. Among the three fibers tested (WH, coir and jute), jute showcased the highest strength in majority of the tested conditions. However, coir and WH fibers are equally competent for increasing SIF at least by 50%. Among the tested soil-fiber composite, coir reinforced soil showcased highest ductility at the tested conditions, which is attributed to its high elongation at break. The post peak ductility of soil-fiber composite is dependent mainly on the fiber percentage and the compaction state. This is mainly governed by the development of fiber bridges in the shear band and also due to "lubrication" effect.

2) *Soil-WH geotextile composite*

The tensile strength properties of both filaments and geotextiles manufactured from WH demonstrates that it is a potential material for manufacturing LLGs. The weaving pattern of WH geotextile was found to influence its tensile strength with WW-GT geotextile exhibiting higher tensile strength as compared to C-GT. The observed biochemical characteristics (significant amount of cellulose present in the WH stem) of WH filament clearly justify its high tensile strength.

The CBR of unreinforced soil increased significantly with the inclusion of WH geotextile. This clearly indicates its efficacy as subgrade reinforcement for short term strength of pavements. The use of two layered geotextile-soil system resulted in higher peak load ratio compared to that of single layered geotextile- soil system. However, the increase in CBR value for two layered geotextiles with respect to one layered geotextile is not significant.

3) *Soil-WH biochar composite*

The compressive strength of soil-WH biochar composite is less than bare soil at all moisture contents. In contrast to soil-PE biochar composite, the UCS for soil-WH biochar composite was lower and can be attributed to high intra pores seen in individual WH biochar particle. Furthermore, the surface roughness of PE biochar is higher than WH biochar as seen from shape parameters measured from Particle characteristic analyzer.

Chapter 5

Hydraulic characteristics of soil-WH composite

5.1 General

The major objective of this chapter is to investigate the hydraulic characteristics of soil-WH biomaterial. This is done by assessing three major hydraulic properties- infiltration rate, soil water retention and desiccation potential. For soil-WH fiber, all three properties have been measured using reduced scale column experiments and juxtaposed against conventional fibers (jute and coir). For soil-WH biochar, the desiccation and retention characteristics have been measured. The effect of drying-wetting phenomenon on retention and desiccation potential have been explored in the chapter.

5.2 Soil-water retention and desiccation characteristics of soil-WH fiber composite

The objective of this work is to investigate the effects of three different natural lignocellulose fibers (Fig. 3.1) on the water retention and desiccation potential of compacted clayey silt soil. Water retention and desiccation are important parameters in surface layers as they determine the amount of water that can be stored in the medium and the possibility of preferential flow through cracks. Compacted soil-lignocellulose fiber composite samples were exposed to uncontrolled ambient environmental conditions and subjected to 15 controlled wetting/drying cycles for 105 days. In each cycle, any surface crack formation, matric suction induced and moisture content near the soil surface of each sample were monitored.

5.2.1 Test Setup and Procedures

Schematic test setup used in the current study is depicted in Fig. 5.1. All soil types (bare and soil-fiber composite) were compacted in a Poly Vinyl Chloride (PVC) mold, which has an inner diameter of 290 mm and height of 250 mm. The diameter was chosen to meet the requirement of preparing a representative elementary volume (137.5 mm in diameter) sample for studying crack development pattern (Li and Zhang 2010). The mold was placed on a perforated base plate, where a filter paper was placed to prevent loss of soil particle. All soil samples were statically compacted to 0.9 MDD by applying a vertical compaction force of 60 kN in the mold (Reddy and Jagadish 1993). The maximum dry density (MDD) of bare soil, coir fiber reinforced soil, jute fiber reinforced soil and WH fiber reinforced soil are 16.5kN/m3, 15.8 kN/m3, 15.7kN/m3 and 15.6 kN/m3, respectively. The OMC varied by less than 1.2% for all fiber reinforced soil. It was noted that the difference in standard Proctor compaction states of fiber-reinforced soil and bare soil was negligible. Hence, the compaction parameters of bare was used for fiber reinforced soils. The compaction level of 0.9 MDD is commonly used in embankment soil (Li et al. 2016). Before compaction, a thin layer of lubricant was applied on the inner surface of the mold to reduce soil-PVC interface friction. To achieve uniform soil density, the compaction procedure was divided into three layers with equal thickness. Initially, the soil was oven dried and fibers of 0.75% (by mass; typically used in soil-fiber composite applications) were dry-mixed to create a soil-fiber mixture. Initial water content of 17% (w/w) was sprayed on the soil-fiber mixture and the mix was placed in the mold for compaction. Despite of thorough mixing between the soil and the fibers, it is acknowledged that compacting the specimen vertically in the confined mold would make the fibers in the composite orientated predominantly sub-horizontally (Ibraim et al. 2012). The final height of each sample was 170 mm. For each soil type (unreinforced; reinforced by coir, jute and WH), three replicates (in three separate molds) were prepared (i.e., 12 molds in total).

After soil compaction, the specimens were kept outdoor (exposed to natural environment), inside an open steel frame with a transparent roof for the entire monitoring period. This arrangement allows free air circulation over the specimen and the environment. The purpose of transparent roof was to eliminate direct precipitation while allowing sunlight to pass through it. A sprinkler system was attached on top of the soil column for applying controlled wetting. The system was connected to a Mariotte's bottle so that a constant water head can be maintained during testing for producing controlled intensity and duration of wetting. Wetting events are not intended to relate with natural precipitation events but rather to stimulate crack closure and surface wetting of the soil types. A digital camera (model: Canon EOS 700d) with an adjustable frame was also mounted on top of the soil column to obtain periodic time-lapse images (method described in next section) of the soil surface for studying the crack development patterns during drying cycles. All suction and moisture sensors were installed diametrically at opposite ends at 40 mm soil depth, where cracks were expected to be developed. Although the exact crack propagation path and cracking depth were unknown prior to testing, the choice of sensors' depth was based on laboratory observation from previous desiccation research on compacted silt (Cui et al. 2014, Song et al. 2016). It is recognized that it is not easy to use discrete sensors, like TEROS21 sensors in this study or tensiometers, for measuring suction at the air-soil surface due to stringent boundary conditions required. However, for better understanding of the behavior of crack evolution in relation to soil moisture regime, it is not uncommon to assume the soil suction and water content in the crack zone to be uniform during data interpretation (Trabelsi et al. 2012; Cui et al. 2014). To prevent water leakage during each wetting event, a layer of anabond adhesive was applied to gaps around the sensor installation holes. Both TEROS 21 (formerly known as MPS6) and EC-5 sensors were connected to an EM-50 data logger system (Decagon Devices 2016a) for data logging. The SWRC of each soil specimen was obtained by relating the suction and moisture content measured during the monitoring period.

After compaction, all the soil columns were wetted immediately. A total water volume of 1500 ml was applied, and it is equivalent to a rate of 6 mm/min and a return period of 100 years of rainfall in India (Guhathakurta et al. 2011) and Hong Kong (Lam and Leung, 1995). After wetting, suction ranges between 9 and 12 kPa in all specimens. During this wetting process, negligible soil volume change (less than 2% reduction of plane specimen area) was observed. Subsequently, the columns were subjected to a continuous drying period of 7 days, when suction reached the range of wilting point (i.e. around 1500-3000 kPa; Feddes 1982, Cassel and Nielsen 1986, Lazarovitch et al. 2018) beyond which the natural fibers would have lost their mechanical strength against crack formation (Mesbah et al. 2004). After the drying event, all columns were wetted again, following the identical procedures described above. This wetting/drying cycle was repeated by 15 times for all soil columns. During the entire monitoring period, minimal soil volume change (both radially and vertically in the mold) was observed. The meteorological data, including solar radiation, air temperature and air relative humidity were monitored by a microclimate monitoring station (Decagon Devices 2016a). The climate monitoring station was placed next to the specimens at a distance of only 1.5 m. Since the steel frame where the specimens were tested was open to the natural environment, the climate data measured is thus representative of the conditions experienced by the specimen. Fig. 5.2 shows the variation of weather parameter during the 105-day monitoring period. The average relative humidity and temperature along with the error in mean were 82.6 ± 11% and 27.8 ± 6.8^{0}C, respectively, while the solar radiation varied from 10 to 20 MJ/m^2/day. Camera images of the soil surface were captured daily to analyze the desiccation crack formed during all drying cycles.

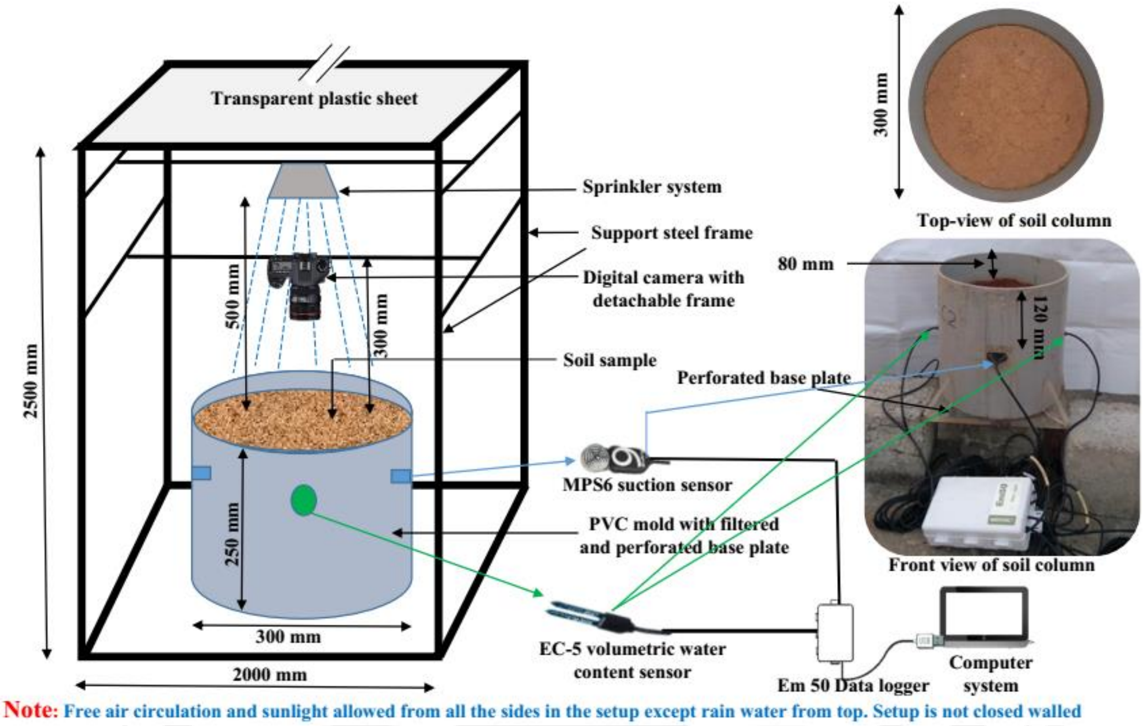

Fig. 5.1. Schematic representation of soil column setup

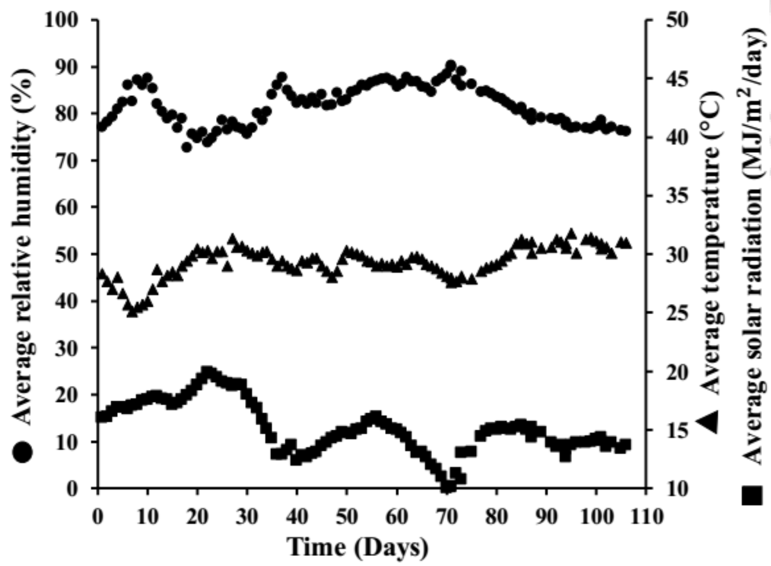

Fig. 5.2. Weather conditions under which the soil columns are exposed

5.2.2 Measurement of crack intensity factor (CIF)

Non-intrusive imaging approach was used to quantify crack development pattern in this study. A non-dimensional parameter, CIF, is defined as the ratio of crack area (A_c) to the total soil surface area considered (A_t). This parameter has been used extensively in many studies to quantify soil cracking pattern (Miller et al. 1998; Li et al. 2016; Jayanthi et al. 2017; Chaduvula et al. 2017, Gadi et al. 2017). After taking the soil surface images using the camera, an image processing algorithm was developed in Python language (Van der et al. 2014) to analyze the images for determining CIF. The Python code is given in the appendix. During desiccation, cracks display a darker color than the surrounding intact soil in an image (Yesiller et al. 2000). This contradistinction in color between cracks and intact soil in the same image helps to quantify CIF.

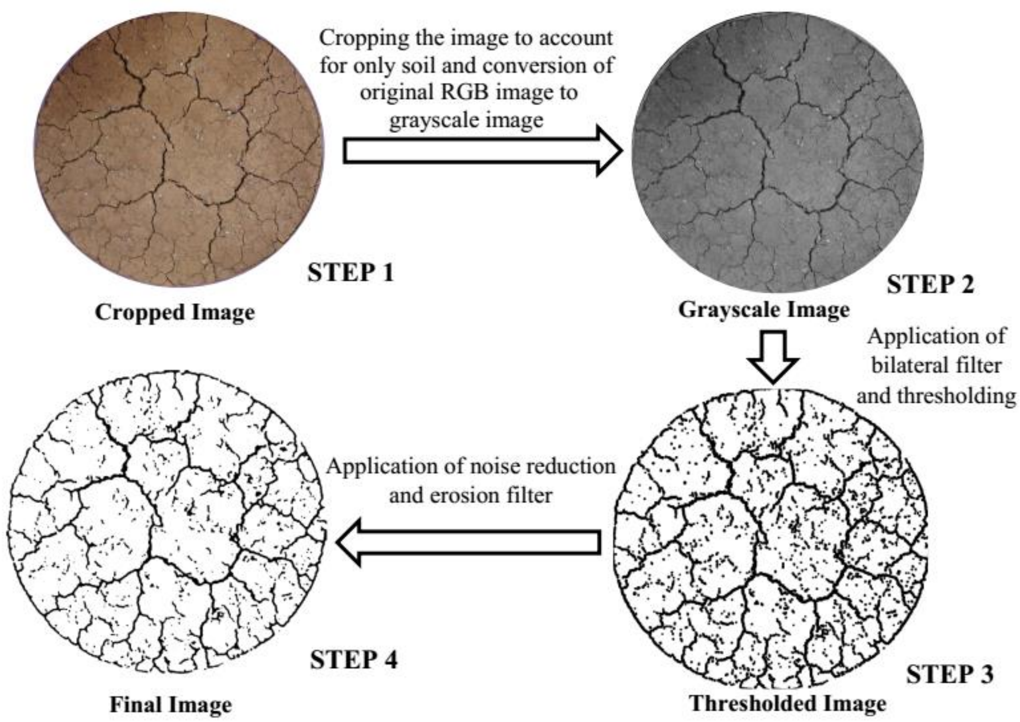

Fig. 5.3. Procedure for measuring pixels of soil and cracks to estimate CIF

Fig. 5.3 depicts the step-by-step procedures for measuring area (pixels) of soil and cracks to estimate CIF. Initially, the captured image is cropped to remove any boundary shrinkage (sample area shrinks by at max 2% which is quite negligible) and account for only soil surface. Thereafter, the original colored image is converted to grayscale to easily distinguish between cracks and soil due to the color distinction. Thereafter the image is analyzed based on different threshold levels which clearly delineate the cracks from the soil. Finally, erosion and noise reduction filters are applied to only account for cracks developed whose pixels are calculated. The ratio of area (pixels) of the cracks (black portion; A_c) to the total soil surface (both white and black; A_t) were determined as CIF for each soil type.

5.2.3 Soil water retention of soil-WH Fiber composite

Fig. 5.4 shows the drying soil water retention curve of the bare soil and the three soil-fiber composites. The measured SWRC was fitted with equation proposed by van Genuchten (1980), and the fitting parameters are summarized in Table 5.1. It can be observed from the figure that the addition of nature fibers increases the water retention capacity of the parent soil, approximately from 34.5% to 36% - 38%, depending on the fiber type (see the parameter θ_s in Table 5.1). The marginal increase in water holding capacity is because the bio-polymer in each type of fiber has free hydroxyl groups, and the water molecules could be adsorbed into the fiber by hydrogen bonds (Pejic et al. 2008). The highest water retention is displayed by jute and WH, both of which have relatively high hemicellulose biopolymer content and hence free hydroxyl groups (Methacanon et al. 2010). However, the presence of lignocellulose does not seem to significantly alter the rate of desaturation (as quantified by the parameter n in Table 5.1). Hence, the inclusion of lignocellulose fibers alters the SWRC of the soil by only moderately increasing the saturated water content.

Table 5.1. Fitting parameters for SWRC and CIF vs suction curves for soil-fiber composites and bare soil

	∝	n	θ_s	θ_r
		SWRC		
Bare Soil	0.0040	1.3	0.345	0.04
Coir + Soil	0.0063	1.35	0.365	0.065
Jute + Soil	0.0070	1.47	0.37	0.070
WH + Soil	0.0070	1.45	0.38	0.070
		CIF vs Suction		
	∝	**n**	**CIF_b**	**CIF_p**
Bare Soil	0.0020	1.30	0	6.7
Coir + Soil	0.0026	1.24	0	1.2
Jute + Soil	0.0012	1.60	0	3
WH + Soil	0.0021	1.53	0	3.3

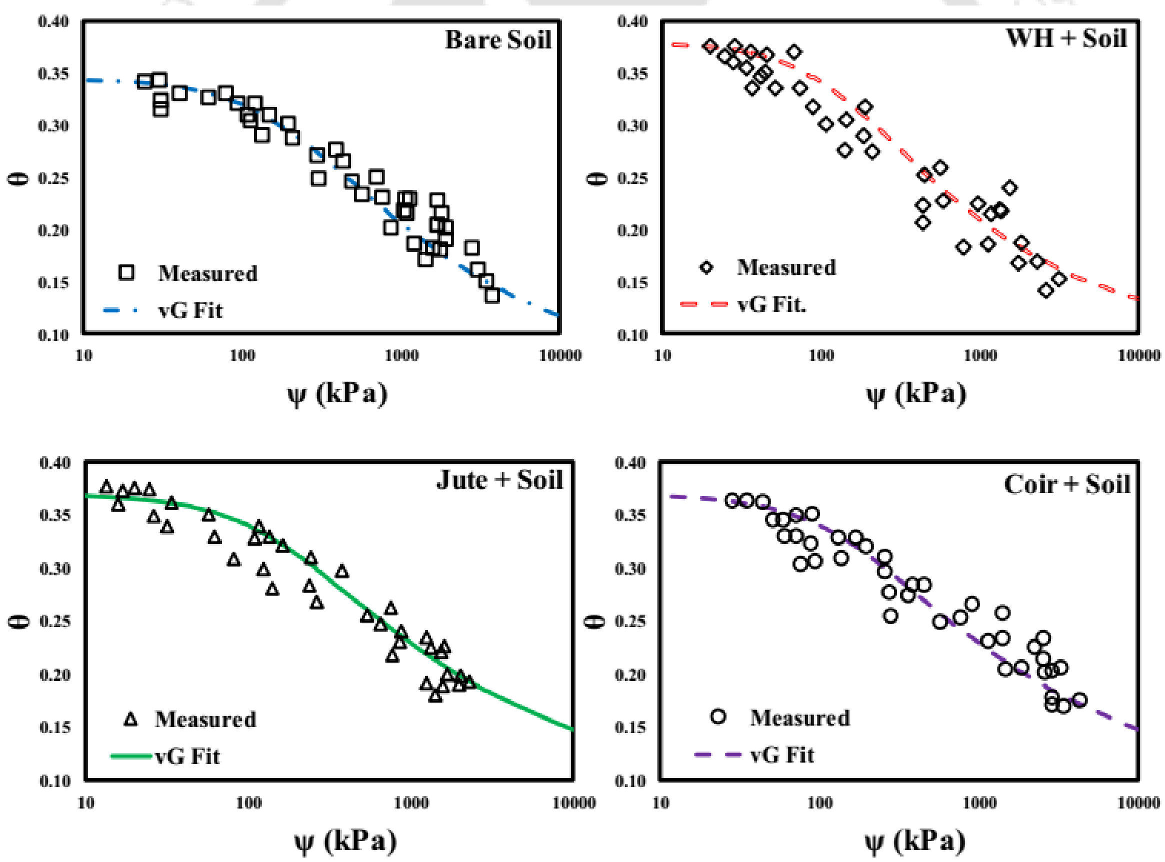

Fig. 5.4. Measured and fitted (vG) drying SWRC for all selected soil types

5.2.4 CIF variation with time and drying cycles

Progressive crack propagation of the four different soil types with time (at 2, 5, 7 and 35 days) is shown in Fig. 5.5. Careful visual inspection of the images suggests that the unreinforced or bare soil (denoted as B) exhibited the greatest intensity of desiccation, whereas coir-reinforced soil (C) was subjected to the least for the same monitoring period. Jute (J) and WH-reinforced soil have intermediate intensity of desiccation. Apparently, the natural fibers, regardless of the types, were in tensile action (i.e., “bridge effect”; Tang et al. 2010, 2016) to reduce crack widening (Fig. 5.5). In general, the CIF increased with time for all soil types for a particular drying cycle.

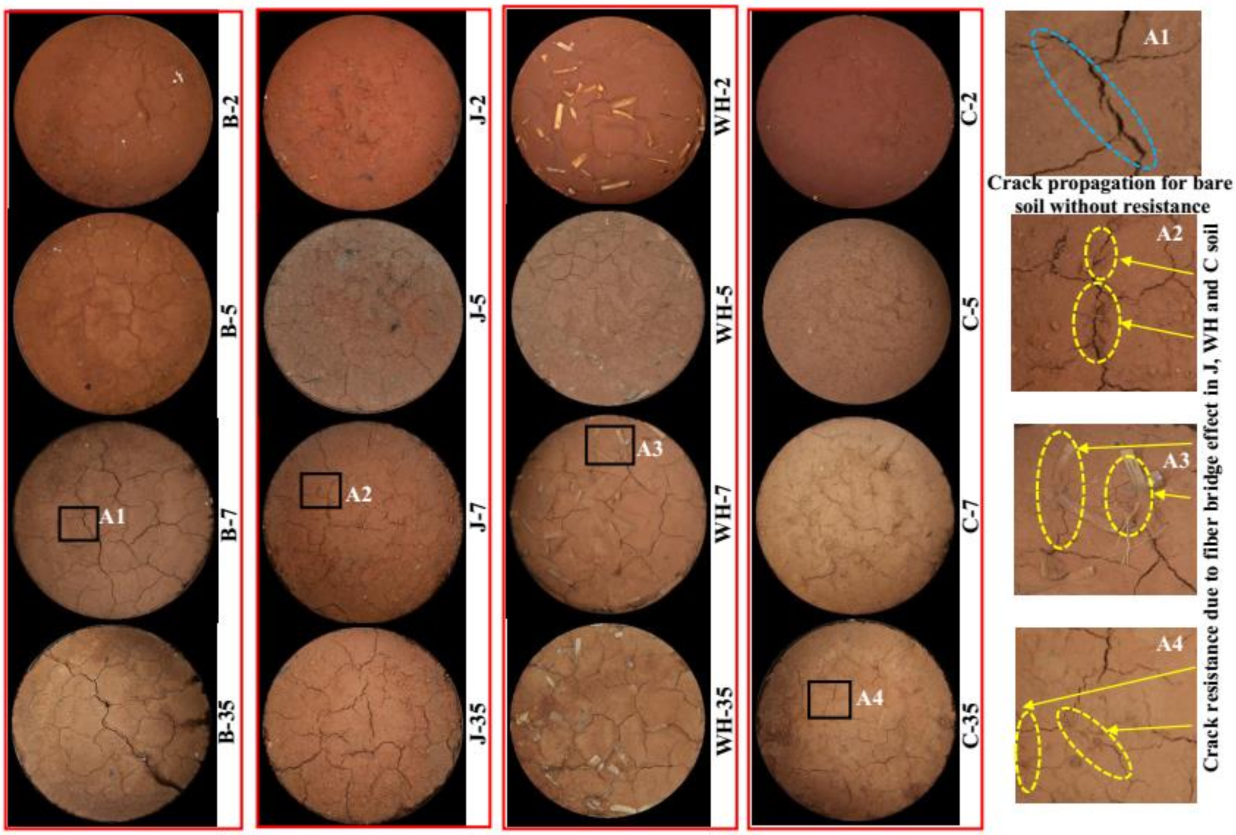

Fig. 5.5. Progressive crack propagation with time (at 2,5,7 and 35 days) for the selected soils and bridge effect of fibers

Fig. 5.6 depicts the variation of mean CIF with standard error (taking into consideration of all three replicates) of all soil types during the entire 105 days of monitoring. For simplicity the first 5 DCs (35 days) are discussed in detail at first. For the bare soil, the mean CIF increased almost exponentially during all five cycles, meaning that cracks were always formed as the soil continued drying. This was associated with the development of soil matric suction upon evaporation (Fig. 5.7), which induced tensile stress (disequilibrium) within the soil matrix and initiated crack formation from the weakest point of the soil. During wetting, the mean CIF dropped abruptly implying closure of cracks. Crack closure occurs in low or moderate plastic soils due to soil swelling or possibly because of clogging of cracks by particles eroded from the crack fracture surfaces during permeation (Li et al. 2011). Interestingly, although similar drying and crack formation patterns are found in the subsequent cycles, apparently there is a progressive increase in the mean peak CIF. Based on the weather data obtained during the monitoring period, soil evaporation rate E_p can be estimated by the Penman's equation (Penman 1948).

$$E_p = \frac{\Delta R_n + \rho_a c_p (e_s - e_a)/r_a}{(\Delta + \gamma)\lambda} \tag{5.1}$$

where E_p (mm/day) is evaporation rate, Δ (kPa K^{-1}) is slope of the saturation vapor pressure curve, Rn (MJ m^{-2} day^{-1}) is net irradiance, γ ($\approx$ 66 Pa K^{-1}) is psychometric constant, ρa = Air density (kg m^{-3}), cp = Specific heat capacity of air ($\approx$ 0.00101 MJ kg^{-1} K^{-1}), U_2 (m/s) is wind speed, e_s-e_a = δe =Vapour pressure deficit (kPa), λ ($\approx$ 2.26 MJ kg^{-1}) is the latent heat of vaporization, T_a is temperature in Kelvin, e_s (kPa) is saturated vapor pressure of air, P is air pressure (Pa) ($\approx$ 101.3 kPa). These parameters were obtained from the measured meteorological data by the following equations (Allen et al. (1998) and Shuttleworth (2007))

$$\rho_a = \frac{P}{RT_a}\,; \tag{5.2}$$

$$\Delta = 0.133 * [\frac{5336}{{T_a}^2} * e^{\left(21.07 - \frac{5336}{T_a}\right)}]; \tag{5.3}$$

$$\delta e = (1 - RH) * e_s; \tag{5.4}$$

$$e_s = 0.133 * [e^{\left(21.07 - \frac{5336}{T_a}\right)}] \tag{5.5}$$

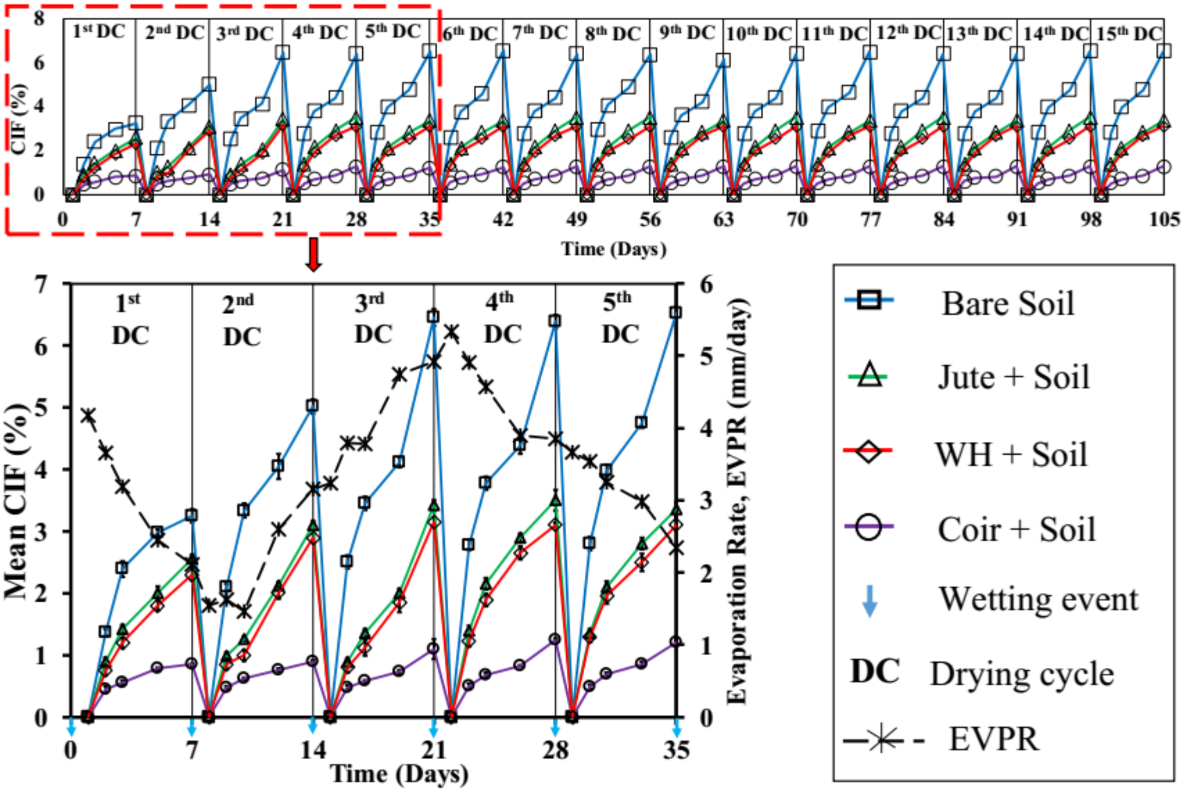

Fig. 5.6. CIF variation for the selected soils for the monitoring period of 105 days

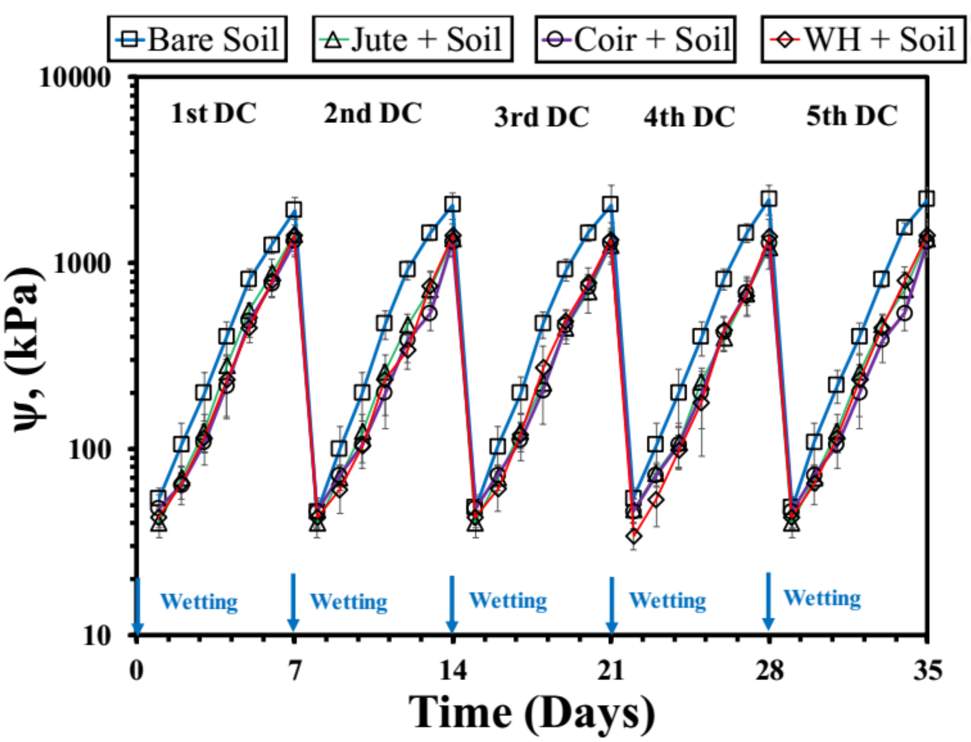

Fig. 5.7. Suction variation for the selected soils for the initial 35 days of monitoring

The calculated evaporation rate during the 35-day monitoring period is in Fig. 5.6. It is clear that the change of CIF during the five drying cycles did not correspond to that of evaporation rate, especially in the 1st, 4th and 5th cycles. Song et al. (2016) studied the evolution of desiccation cracks of highly expansive clay (CH) soil under controlled environmental conditions in the laboratory. They found that as cracks propagated, the evaporation rate changes in three stages where evaporation rate gradually decrease for a particular drying cycle. The current evaluation in Fig 5.6 implies that CIF change is not only sensitive to the evaporation rate due to the uncontrolled environment adopted in the current work. The observed trend of CIF might be explained from the soil microscopic point of view. Soils subjected to the first drying cycle after compaction should shrink and this process might cause irreversible fabric changes (Yong and Warkentin 1975). Delage et al. (1995) who tested desiccation of compacted silt also observed this kind of soil microstructural change due to soil moisture changes. Apparently, the increase in peak CIF ceases beyond the third drying cycle for the rest of the monitoring period. The mean maximum CIF and their standard deviation are reported in Table 5.1 for the entire monitoring period. Al Wahab and El-Kedrah (1995) who tested the desiccation behavior of compacted clays of medium plasticity also showed that their dimensionless crack index became constant after three drying cycles.

Fig 5.6 also shows that the CIF of soil-lignocellulose fiber composite is always less (at least by half, except the initial two drying cycles) than that of bare soil. Coir-fiber reinforced soil has the lowest CIF, followed by WH- and Jute-reinforced soils which have similar CIF. This is consistent with the measurements of suction shown in Fig 5.7, where the magnitude of suction induced in all lignocellulose fiber-reinforced soil was always smaller than that in the bare soil. This is because the presence of hemicellulose biopolymer in the natural fibers enhance water holding capacity of the soil. Apparently, there is no difference of induced suction among the three types. The fiber inclusion reduces cracking potential of soil via two mechanisms – by mobilizing the tensile strength of the interlocked fiber during drying and by increasing soil-fiber interface friction; which in turn resists the soil tensile stresses induced during drying (Tang et al. 2012, Chaduvula et al. 2017). Coir has the greatest ability to reduce crack formation because it is a multifilament fiber, meaning that more number of fibers could mobilize their tensile strength simultaneously across a crack plane. Although the coir fiber has smaller tensile strength than jute and WH, the coir monofilament fiber has higher lignin content and hence a coarser surface, providing higher soil-fiber interface friction. A study reported by Hathaway and Penny (1975) show that the effects of lignin content on tensile strength of natural fiber become more significant when the fiber moisture content is higher. This might be another mechanism that the coir fiber (which has the highest lignin content among the other two), provides further tensile strength in resisting soil cracking after wetting.

5.2.5 Effect of fiber inclusion on resisting cracks at varying suction

Fig. 5.8 relates CIF with suction induced in all three soil-fiber composites and bare soil, assuming that soil suction in all specimens is uniform in the top 40 mm for assisting the interpretation of soil-fiber interaction on crack evolution. The corresponding fitted SWRC of the soils are also depicted in the figure for reference. Firstly, when suction is less than the air-entry value (~60 kPa), CIFs in all soil types are zero and no crack was formed. Thereafter in the second stage, the CIF of all cases increased as soil moisture content reduced. Apparently, the rate of increase reduced significantly when fiber was added and is depends on the fiber type. In the final stage, the CIF in all cases, regardless of the presence of fiber or fiber type, stopped increasing after a certain moisture content and it seems to attain a maximum peak value. In general, the three-stage soil response was consistent with the findings reported by an unreinforced silty clay soil reported by Li et al. (2011). Both the present study and that presented by Li et al. (2011) show that it is reasonable to use air-entry value to be a threshold suction, where cracks start to form. While Li et al. (2011) suggested to use residual water content to demarcate the minimum suction required to reach the peak CIF, the present study finds suction beyond (~3000) kPa is a more suitable choice for the soil type studied. Moreover, the shape of the CIF-suction relation in the intermediate second stage appears to be more closely follow an exponential function for the soil and natural fiber tested in this study, rather than a linear relation proposed by Li et al. (2011). Exponential relation is similarly reported by Cui et al. (2014, 2016) who tested desiccation of compacted high swelling clay (CH). More importantly, it is revealed from Fig. 5.8 that the two threshold suctions associated with zero and peak CIFs are independent with the presence of fiber and the fiber type used for soil reinforcement.

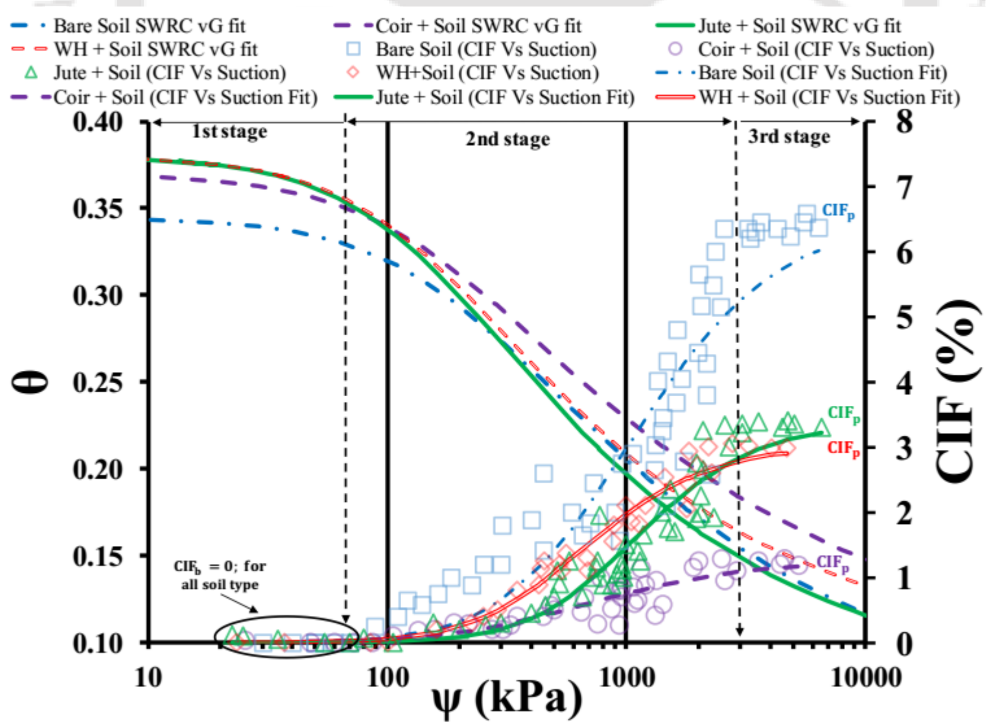

Fig. 5.8. CIF Vs Suction plot and corresponding SWRC fit for the selected soil types and maximum crack reduction index (CRI) for soil-natural fiber composites

Visual inspection suggests that the CIF-ψ relation mirrors the SWRC. Hence, the following empirical equation that follows the form of the equation proposed by van Genuchten (1980) may be used to describe the CIF-suction curve:

$$\mathrm{CIF}(\psi) = \mathrm{CIF_p} - \frac{\mathrm{CIF_p}}{[1+(\propto|\psi|)^{-n}]^{m}} \tag{5.6}$$

$$m = 1 + 1/n \tag{5.7}$$

where ψ_b is suction at air-entry value (AEV) before which CIF_b is zero regardless of fiber type; ψ_s is suction corresponding to residual moisture content; n is a fitting coefficient associated with the curvature at the intermediate stage; and CIF_p is the peak CIF at suctions beyond ψ_s, which is fiber type-dependent. All fitted parameters are listed in Table 5.2 for different soil-fiber composites. Moreover, there are evident decreases of CIF_p when the fiber is present, further highlighting the effectiveness of using lignocellulose fibers to resist desiccation cracks. This effectiveness is represented by a dimensionless index called crack reduction index, CRI which is defined by the ration of maximum CIF of bare soil with respect to that of fiber reinforced soil type. As seen in Fig. 5.8, an almost six-fold decrease in crack is shown by coir (CRI = 5.93). By comparing the values of CIF_p in Table 5.2 with the fiber biochemical properties, it is apparent that decrease in CIF_p is better explained by the lignin content (contributing to elongation at breakage), while cellulose content (influencing tensile strength at breakage) does not seem to have a sound correlation.

Indeed, as soil dries and shrinks, it is unlikely that the tensile stress mobilized in the fibers within the soil matrix would exceed the peak tensile strength of lignocellulose fiber. This study shows that it may be mainly the fiber ductility (which is governed by the lignin content), not its tensile strength, that governs the CIF_p. Nonetheless, it should be mentioned that Eqs. (5.6) and (5.7) are empirical and should be treated with cautions. These equations were derived based on the assumption that the transient measurements of matric suction synchronize the dynamic process of crack propagation, which requires careful examination, if not impossible.

Table 5.2. Maximum CIF variation for the monitoring period (Mean ± standard error of mean)

	Day	**Bare**	**Coir + Soil**	**Jute + Soil**	**WH + Soil**
		CIF (%)	CIF (%)	CIF (%)	CIF (%)
Maximum CIF at the end of each cycle	7	3.25 ± 0.10	0.85 ± 0.02	2.56 ± 0.06	2.32 ± 0.10
	14	5.02 ± 0.11	0.90 ± 0.02	3.11 ± 0.07	2.89 ± 0.07
	21	6.45 ± 0.13	1.11 ± 0.16	3.42 ± 0.09	3.15 ± 0.08
	28	6.39 ± 0.11	1.25 ± 0.02	3.51 ± 0.17	3.11 ± 0.05
	35	6.52 ± 0.10	1.20 ± 0.04	3.35 ± 0.11	3.12 ± 0.08
	42	6.30 ± 0.12	1.15 ± 0.07	3.30 ± 0.15	3.10 ± 0.08
	49	6.65 ± 0.08	1.15 ± 0.16	3.26 ± 0.12	3.05 ± 0.18
	56	6.69 ± 0.14	1.20 ± 0.05	3.34 ± 0.06	3.12 ± 0.12
	63	6.82 ± 0.20	1.21 ± 0.06	3.40 ± 0.16	3.02 ± 0.15
	70	6.91 ± 0.11	1.25 ± 0.07	3.26 ± 0.20	2.98 ± 0.15
	77	7.06 ± 0.19	1.25 ± 0.14	3.35 ± 0.12	2.95 ± 0.13
	84	6.91 ± 0.18	1.25 ± 0.12	3.41 ± 0.22	3.08 ± 0.28
	91	7.10 ± 0.29	1.27 ± 0.06	3.28 ± 0.16	3.10 ± 0.12
	98	7.21 ± 0.19	1.25 ± 0.12	3.33 ± 0.13	3.15 ± 0.08
	105	7.27 ± 0.28	1.27 ± 0.16	3.31 ± 0.17	3.18 ± 0.16

5.3 Infiltration characteristics of soil-WH fiber composite

Randomly distributed fiber reinforced soil (RDFS) using natural fibers has been extensively studied with respect to their mechanical properties. However, these soil-fiber composites are exposed to cycles of precipitation in the field when employed for erosion protection and embankment stabilization. Infiltration rate of a soil-fiber composite consequently becomes an important parameter to design geotechnical infrastructures (such as road embankments, rural subgrade, etc.) and predict run-off along with soil erosion behavior. The infiltration process in soil-fiber composites has rarely been investigated through a controlled laboratory study. This study investigates the infiltration rate in compacted natural fiber reinforced soil composite. Laboratory investigation using mini disk infiltrometer (MDI) was conducted to compare the infiltration rate in soil-fiber composite reinforced with three natural fibers. Jute, coir and water hyacinth fibers of same aspect ratio were used to reinforce soil at three different fiber percentages at varying densities. A series of laboratory infiltration tests were conducted using mini disk tension infiltrometer (MDI) on three different fibers (jute, coir and WH) at varying soil densities and fiber compositions. The effect of density on the infiltration rate was analyzed for both bare and fiber reinforced soil. The individual effect of fiber type has also been discussed with respect to its surface morphology and filament arrangement. Additionally, image analysis was performed to inspect probable preferential flow through the fiber reinforced soil.

5.3.1 Measurement of infiltration rate

Tension disk infiltrometers are popularly used for estimation of infiltration rate in soils (Smettem and Clothier 1989, Reynolds and Elrick 1991, Angulo-Jaramillo et al. 2000). The results obtained from the tension infiltrometer is useful for determining the soil hydraulic properties such as near saturated and near surface hydraulic conductivity, sorptivity and soil water repellency (Zhang et al. 1997, Lewis et al. 2006). Tension disk infiltrometers are designed to maintain negative (less than atmospheric) water pressure head under which water would infiltrate at the soil-atmosphere boundary (Dohnal et al. 2010, Wooding 1968). A major advantage of using such infiltrometers is that it eliminates flow in macro pores (basically hollow cavities that might be found in soil) due to induced suction (Wooding 1968). Mini disk infiltrometer (MDI) (Fig. 5.9; Decagon Devices 2013), is a recent development among the tension disk infiltrometers for establishing infiltration characteristics of the soil. The use of MDI is suitable to conduct the experimental studies with adequate repeatability, as the existing infiltrometers being large in size are not fit to be used in the laboratory (Moody et al. 2009, Homolák et al. 2009, Beal et al. 2016, Rezaei et al. 2015, Appels et al. 2016). However, only limited range of pressure heads can be established on the infiltration surface (Angulo-Jaramillo et al. 2016). In the recent past, several laboratory column studies (Bhave and Sreeja 2013, Meshesha et al. 2016, Ibrahim et al. 2017) were conducted to assess infiltration using MDI. Thus, the MDI was chosen to conduct infiltration experiments as it is easy to use in laboratory and there is no need of auguring which might disturb the soil-fiber orientation. The infiltration below the MDI is a three dimensional due to capillarity and gravity (Angulo-Jaramillo et al. 2016); and does not need the soil to be saturated initially for conducting the experiment. The suction head can be maintained by adjusting the movable suction control tube affixed to the upper chamber.

Sintered steel disk (4.5 cm diameter) attached at the bottom of lower chamber helps in transferring suction head to soil surface. Using this approach, the water infiltration is induced at soil surface and hence there is a development of three dimensional wetting front within subsurface. The proposed method by Decagon devices (2013) to obtain near-surface hydraulic conductivity (k_{h0}) has not been followed in this study. This is primarily due to k_{h0} value being calculated from empirically determined van Genuchten parameters for bare soil. However, in this case for fiber reinforced soil, the van Genuchten parameters are unknown as the water retention characteristic of composite soil will be different due to the moisture absorption capacity of natural fibers. Hence, a simplified approach of obtaining infiltration rate or flow rate was adopted. Here, infiltration rate (I) at any time interval (dt), can be determined by equation 5.8 as follows:

$$I(t) = \frac{1}{A}\left(\frac{dV}{dt}\right) \tag{5.8}$$

Where, (dV) is change of volume of water infiltrated within a given time (dt), and A is cross sectional area of infiltrometer. The cumulative volume of water infiltrated (V) with time (t) is obtained for soil-fiber composite as shown in Fig. 5.10. A second degree polynomial equation was fitted to V-t response and the relevant fitting parameters were obtained. The polynomial equation was further differentiated with respect to time (t) to obtain (dV/dt) for calculating I(t) as shown in equation 5.8.

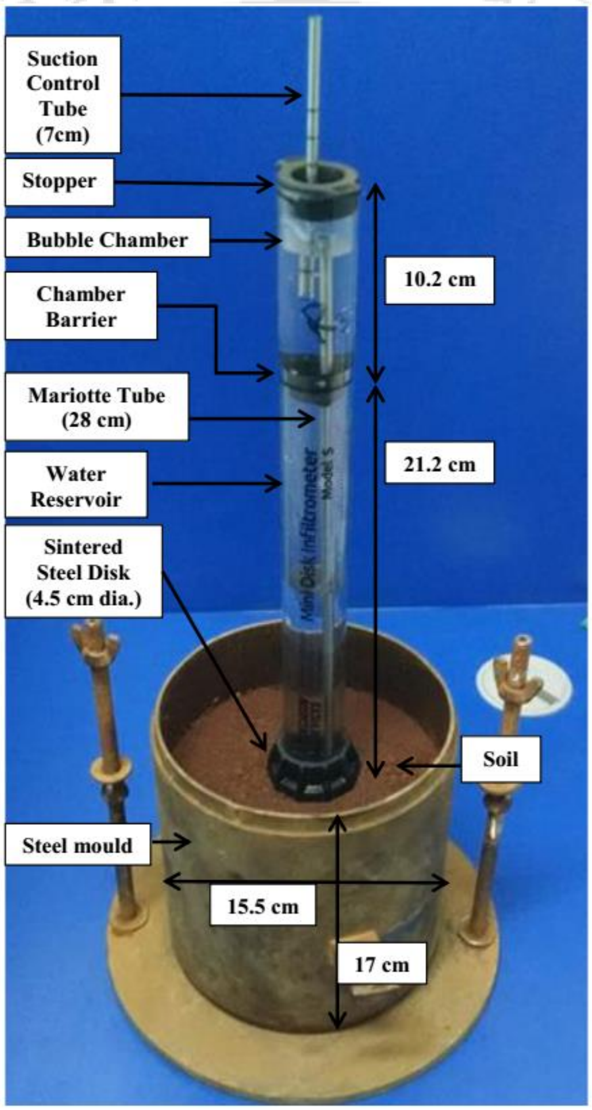

Fig. 5.9 Overview of mini disc infiltrometer and test setup

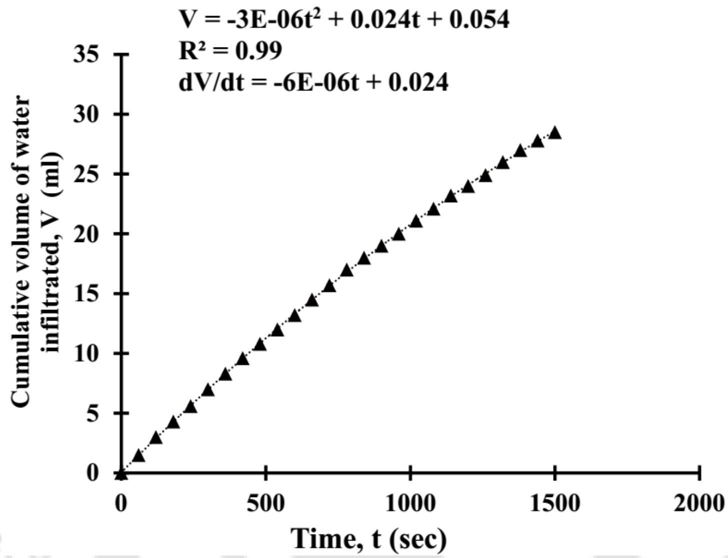

Fig. 5.10 Measured cumulative infiltration variation with time for that of WH fiber reinforced soil

5.3.2 Test setup and procedure

The test setup for conducting infiltration experiments is shown in Fig. 5.9. A steel mold was chosen for enabling compaction at higher densities (0.9 MDD and 1.05MDD). Static compaction was used to compact the soil at targeted densities. The soil was compacted in three equal layers (volume). The orientation of fibers is generally along the direction orthogonal to the axis of compaction in each layer (Diambra et al. 2007, Ibraim et al. 2012). However, the fiber distribution is assumed to be uniform due to random mixing in all the layers. The samples are compacted at moisture content (OMC-5%) and three corresponding densities (0.7 MDD, 0.9 MDD and 1.05 MDD). This moisture content is chosen as initial condition as this corresponds to peak strength (compressive) of the soil-fiber composite as stated in Chapter 4. The dimensions of the mold were chosen to mitigate any interaction between the three dimensional wetting front formed below the infiltrometer disk and the mold boundary, thus preventing preferential flow along the boundary. The wetting front is checked after completion of MDI test by auguring the soil and then observing the wetting front. Furthermore, the surface wetting front due to water saturation (which has a sharp dark contrast with that of the unsaturated soil) also gives an indication that there is no disturbance with the test mold. Three fiber percentages (0.5%, 0.75% and 1% by dry weight of soil) were selected for each fiber type. Fiber percentage was restricted to 1% to avoid formation of pockets having low densities. The soil densities chosen were 0.7 MDD, 0.9 MDD and 1.05 MDD. The densities were selected as per their use in agricultural soil (0.7 MDD) and in case of compacted soil for subgrade (0.9 MDD and 1.05 MDD) (Dexter et al. 2004). Equal volume of water was infiltrated into the soil for all the tested conditions and the suction head of MDI was kept at 2 cm for all the tests. Such small value of head was applied to minimize any flow of water through macro-pores. It should be noted that in this study, not many macropores are expected due to relatively higher degree of compaction. Studies in literature were found to adopt similar suction head value (around 1-2 cm) for measuring infiltration rates using MDI (Lichner et al. 2007, Fodor et al. 2011). For each test condition, three trials were done to check the repeatability of results. A total of 90 tests were performed in this study to account for bare soil (9 tests) and fiber reinforced soil (81 tests).

Image-processing software ImageJ was used in this study for analyzing the spread of dye when colored solution was infiltrated (Schneider et al. 2012). The purpose of the experiment was to delineate the spread of water in the soil-fiber composite during infiltration from MDI. To assess the spread of infiltrating water in soil-fiber composite, Brilliant Blue FCF dye was added to the infiltration water at a concentration of 4 grams per liter. This dye is most commonly used dye tracers for hydrological sub-surface studies (Flury et al. 1994, Cey et al. 2009). Canon EOS 600D with lens range (18-55 mm), horizontal/vertical resolution of 72 dpi was used to record images by maintaining the focal length, exposure time and ISO speed as 23 mm, 1/30 sec and ISO-640, respectively. Photographs were captured from a fixed position. For the analysis, the captured image is imported into ImageJ and the digitized image is cropped to only account for the soil surface. The dyed portion of soil is obtained using color threshold technique using ImageJ, where the concentration of dye is accounted by selecting individual pixels with dye color.

5.3.3 Effect of fiber reinforcement on the infiltration rate of the soil-fiber composite

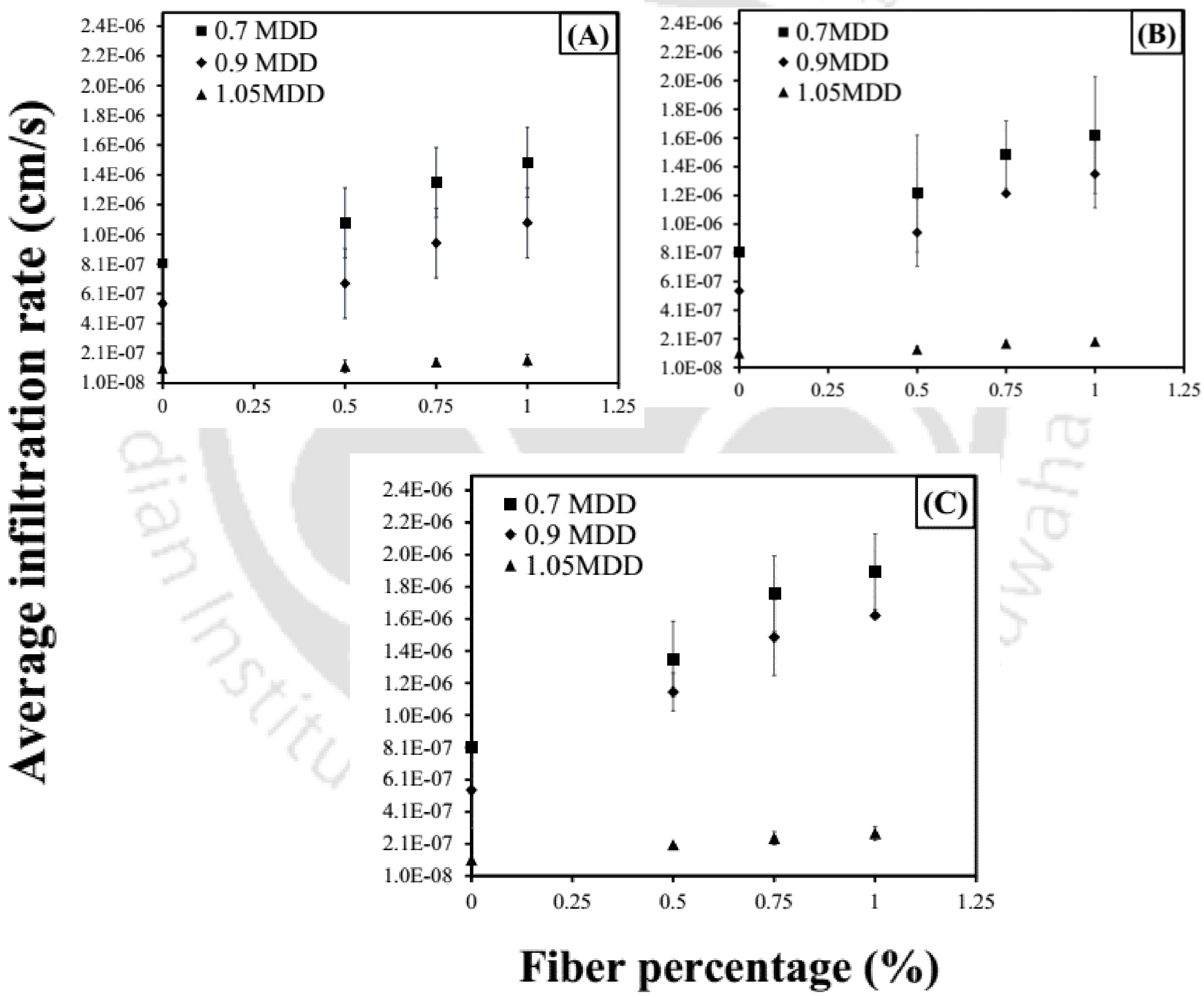

Fig. 5.11 Measured average infiltration rate for (a) Coir fiber (b) Jute fiber and (c) WH fiber

Figure 5.11 depicts the measure of average infiltration rate of the soil-fiber composite for all the selected fiber type. There is a gradual rise in the infiltration rate observed with increase in fiber percentage. This increase is more pronounced at lower densities due to relatively low packing at 0.7 MDD and 0.9 MDD. At lower densities, the space between particles (soil-soil, soil-fiber) is relatively loosely packed, and it is easier for water to flow within the composite. At 1.05 MDD, the increase in infiltration is not significant as the void spaces between individual particles are very less for water flow. The increase in infiltration due to the inclusion of fibers is probably due to the formation of preferential flow path along the soil-fiber interface. This preferential flow of water is similar to that of flow in rooted soil (Zhan et al. 2007, Bartens et al. 2008).

5.3.4 Dye tracer experiment to investigate preferential flow path in soil-fiber composite

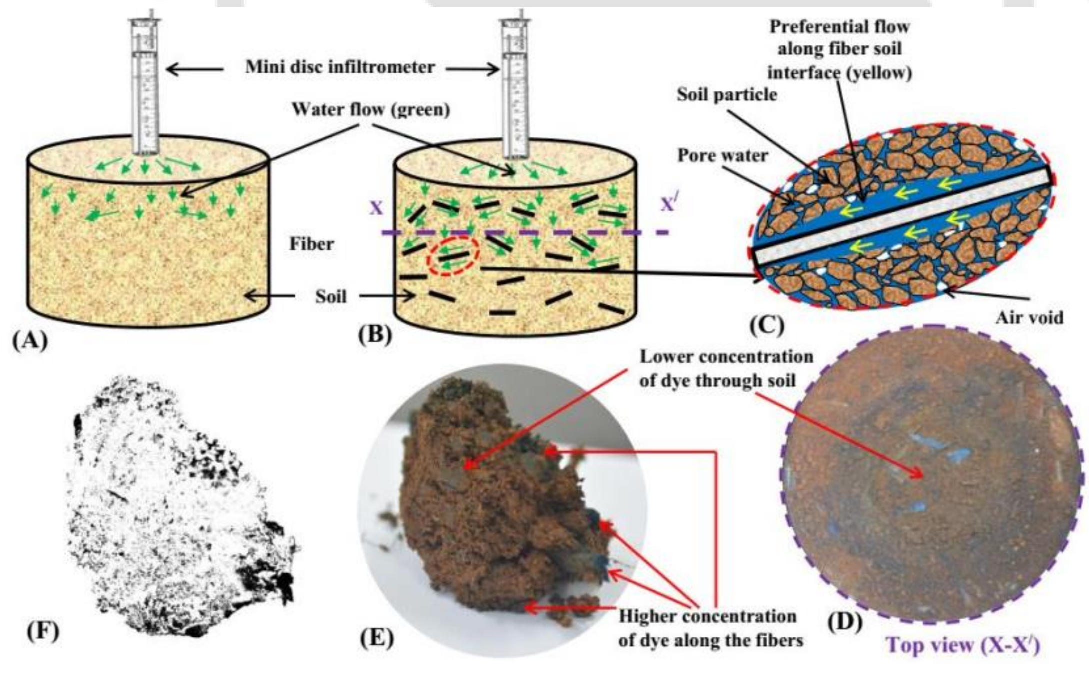

Fig. 5.12 Representation of (a-b) infiltration in bare and reinforced soil (c) preferential flow along soil-fiber interface; (d) sectional view of dye tracer experiment mold; (e) original sample and (f)

analyzed sample of soil-fiber composite (WH reinforced) after dye tracer experiment at 4 cm depth from surface

To test the hypothesis of water flow along the soil-fiber interface (Fig. 5.12 (a-c)), dye tracer experiment on the soil-fiber composites were carried out. The size of the sample was 200 mm (diameter) and 250 mm (length). Samples were uniformly compacted and mixed (Fig. 5.12 (d)). The dye solution of equal volume was allowed to infiltrate in the sample. After infiltration tests, each sample was carefully cut to investigate its section. On visual inspection of sample, it is observed that high concentration of dye accumulated along the fiber surface. Fig. 5.12 (d) represents a random sample extracted from 4cm depth of the soil-WH fiber composite after dye tracer test. On analyzing the sample using image analysis, it is seen that highest blue color concentration is observed along the fiber surface (refer black color representing dye color in Fig. 5.12 (e)). This is due to dye solution additionally flowing along the soil-fiber interface in case of the composite as against the movement of water along soil pores for bare soil.

5.3.5 Effect of fiber type on infiltration rate

To discuss the effect of fiber type on the infiltration rate, an infiltration improvement factor (IIF) is defined in this study as the ratio (dimensionless) of average infiltration of fiber reinforced soil to that of average infiltration of bare soil. Infiltration increase is showcased if the IIF value is greater than 1. Figure 5.13 depicts the change in IIF at the selected densities for all the three fiber type. Among the three fibers, WH fiber reinforced composite showcased the highest IIF values for all densities. Coir and jute exhibited relatively less IIF as compared to WH. This may be attributed to the surface roughness of the fiber type and also due to induced tortuosity by the fibers. The surface roughness of WH is comparably higher than that of coir and jute. Due to this rough surface morphology observed in WH, water can flow with relative ease along the soil-fiber interface voids, as that compared to the other two fibers. Moreover, WH is a monofilament fiber, whereas coir and jute are highly multifilament fibers. Coir and jute fibers, being multifilament in nature, these fibers have a higher tendency to intermingle in the composite as compared to monofilament WH. Due to this intermingling for jute and coir fibers, there is a high probability of water flow being excessively tortuous along the soil-fiber interface. This tortuosity of water flow in coir and jute might further decrease infiltration rate within the soil-fiber composite.

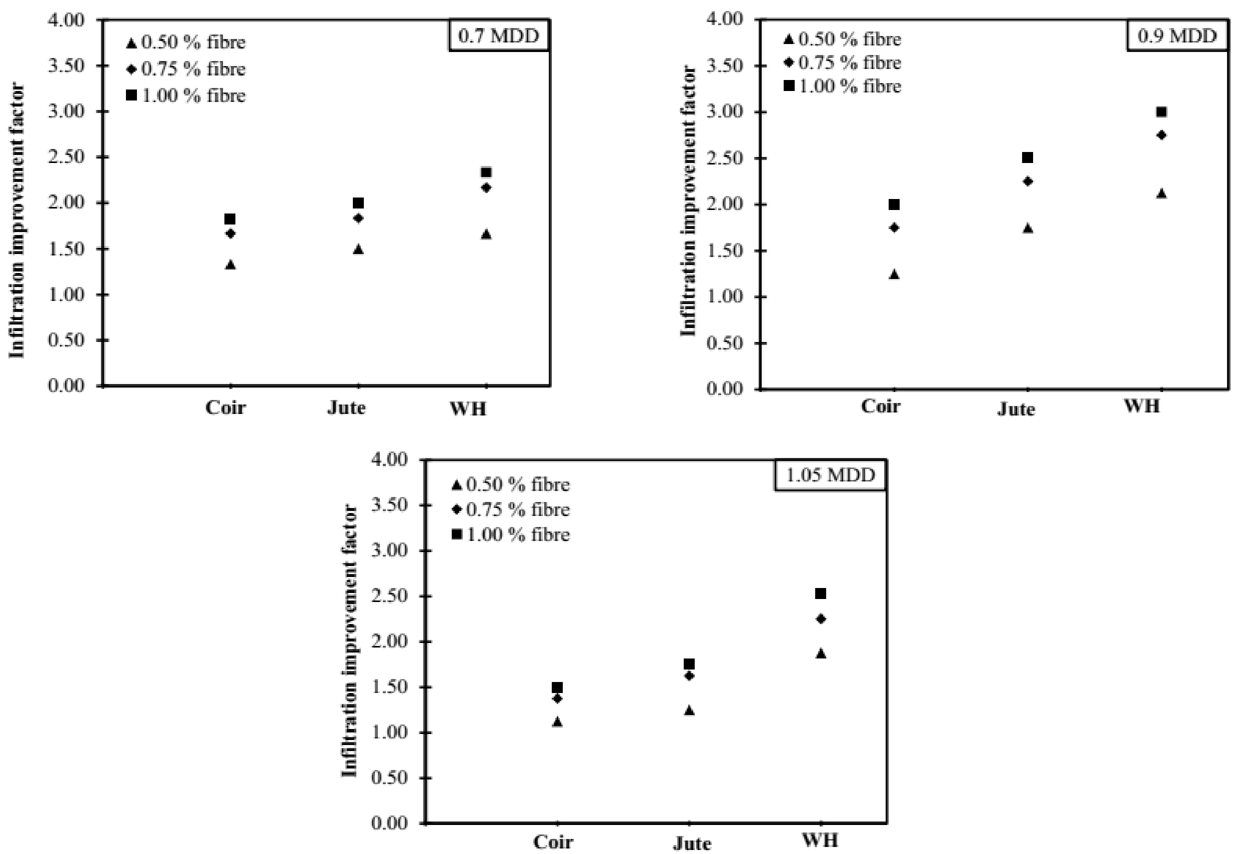

Fig. 5.13 Infiltration improvement factor of selected fibers at (a) 0.7 MDD (b) 0.9 MDD and (c) 1.05 MDD

5.4 Soil water retention and desiccation characteristics of soil-WH biochar composite

Recent studies explored the efficacy lignocellulose species as a biochar (BC) in improving soil fertility and metal adsorption. However, the soil water retention (SWR) property and crack potential of soil-WH biochar composite was not studied. The major objective of this work is to investigate the SWR property and corresponding crack intensity factor (CIF) for compacted soil-WH BC composites. Soil-WH BC composites at five percentages (0, 2, 5, 10 and 15) was compacted and soil parameters such as suction (ψ), water content (θ) and CIF were simultaneously monitored for 63 days (including 9 drying-wetting cycles).

5.4.1 Test plan and preparation of soil column tests

The schematic test arrangement used in the study is shown in Fig. 5.14. All the tests were done in a transparent enclosure with openings on opposite ends. The test series were divided into five sets- one bare soil (BS) and four soil-WH BC composites. In the current study, the four composites are designated as SXBC where X represents the BC weight percentage (at 2, 5, 10 and 15) with respect to dry soil. The motive of investigating the biochar percentage from 2% to 15% is to quantitatively gauge its effect on water retention and desiccation cracking of soil-biochar composite. The range was explored based on previous work (Reddy et al. 2015, Wong et al. 2017) on geo-environmental application. Both BS and SXBC soil was compacted in a cylindrical column made of Poly Vinyl Chloride (PVC) with a diameter of 300 mm and height of 250 mm. The column dimensions are selected as per the requisite representative elementary diameter (137.5 mm) for studying crack development pattern (Li and Zhang 2010). The column was provided with a perforated base plate, where a filter paper was placed to prevent soil particle loss but allowing free any drainage of water. Three replicates were provided for each series and thus a total 15 columns were monitored in the study. All test series were statically compacted in three layers up to 170 mm at 0.9 MDD and OMC, as per compaction conditions in engineering projects (Li.et al. 2016). A thin layer of grease was applied on the inner surface of the cylinder to minimize soil-PVC friction before the compaction process. Initially, the soil was oven dried and biochar percentage (by mass) were dry-mixed to create a soil-biochar mixture. It is important to note that biochar added was air dried before mixing. The soil-BC mixture is sprayed with requisite distilled water to minimize lumps during mixing. Distilled water was used throughout the experimentation tenure to minimize the effect of any salts on suction measurements.

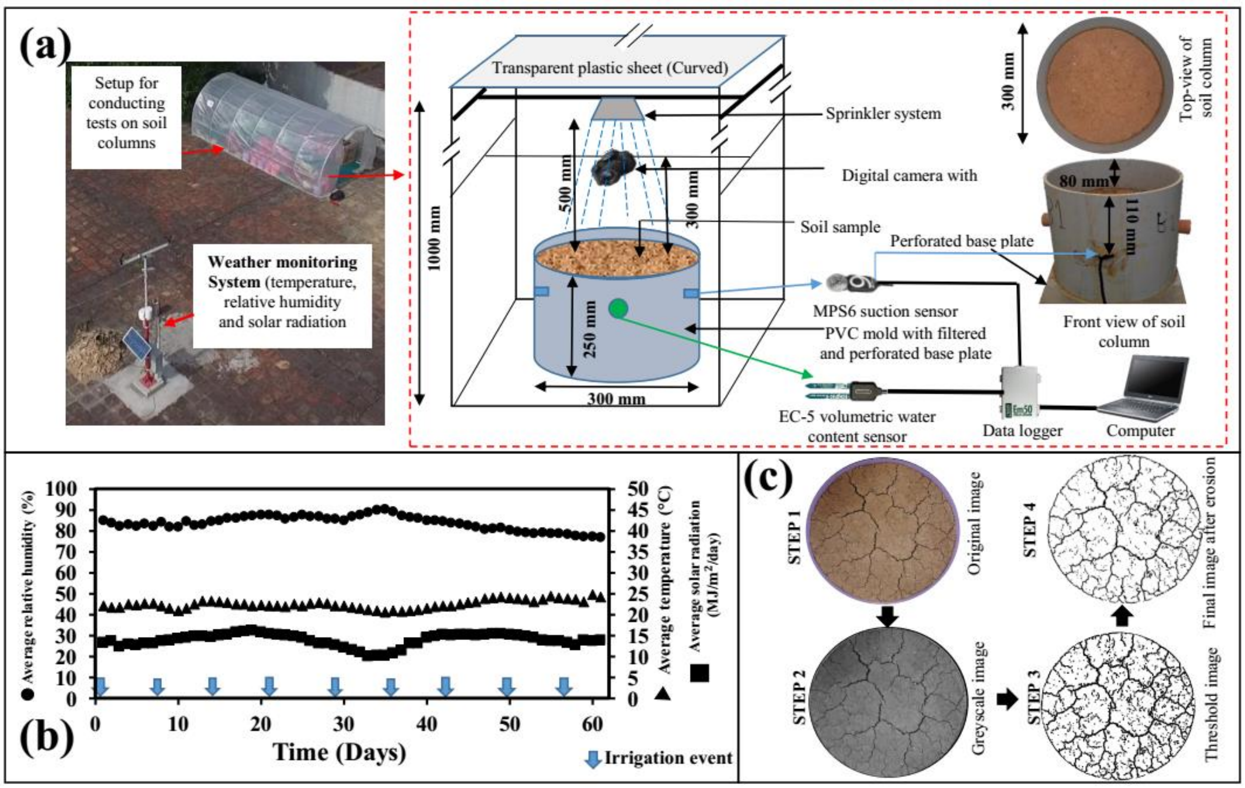

Fig. 5.14 Schematic representation of (a) setup for conducting tests on soil columns; (b) Local daily environmental conditions of test for 62 days; and (c) Procedure for measuring cracks from original image as per developed algorithm to calculate CIF

Each column was kept in the transparent enclosure, after preparing the compacted sample, where the specimen was exposed to natural environment and controlled irrigation applied during monitoring period. A sprinkler system was attached on top of the soil columns for applying controlled irrigation (1000 ml) at an interval of 7 days from start of the experiment as shown in Fig. 5.14 (a-b). This results in 9 drying-wetting cycles which encapsulates crack opening due to repeated wetting events. A digital camera (model: Canon SX 60HS) at the same height was used to obtain periodic time-lapse images of the soil surface during drying cycles. Two suction sensors (TEROS21 formerly known as MPS-6) and two volumetric water content sensors ((EC-5) were installed at diametrically opposite ends during compaction at 30 mm soil depth as referred in Fig. 5.14 (a-b). All sensors were connected to an EM-50 data logger system for monitoring continuous change in these parameters (Decagon Devices 2016).

The monitoring period for all the 15 columns were done for 63 days. The meteorological parameters subjected on the columns, such as solar radiation, temperature and relative humidity were measured by a weather monitoring system as shown in Fig. 5.14a. The daily weather condition and irrigation patterns during the monitoring period is consequently shown in Fig. 5.14b. The irrigation pattern resulted in 9 drying cycles for the monitoring period. The average relative humidity and temperature during the monitoring period was 83.7 ± 9% and 22.48 ± 6.80, respectively. Average solar radiation during this period varied from 10.12 to 16.10 MJ/m^2/day.

5.4.2 Effect of WH biochar on soil water retention curve

It is seen in Fig.5.15 that the saturated water content or the water retention capacity of soil increases with addition of WH BC. The water retention capacity of BS is (29.5± 0.89) %, and with addition of 15%WH BC to soil it increases to (48.45± 0.59) %. This increase of water retention capacity is proportional to the WH BC percentage added to the soil (Fig.5.16). Evaporation of water from soil results in the water content decrease with increasing suction and this phase represents the unsaturated phase of soil. The tension in the air-water menisci induces tensile stresses on the soil particles which is represented by the suction forces (Li et al. 2011). The soil ultimately reaches a residual water content for very high suction beyond which there is no change in water content due to drying (Leong and Rahardjo 1997). In the current study, the soil cannot be said to have reached that stage as the drying period (7 day) may not be enough to evaporate all the water for all series. Hence, the minimum available water content (Fig. 5.15) is used to indicate and compare the water available at the current drought conditions for all test series. The minimum available water content increases from 9.97% to 21.48% for BS and S15BC respectively. For WH BC inclusion from 2% to 10%, the minimum available water content ranges from 16.5% to 18%. This increases in minimum available water content (by at least 6.53%) is particularly crucial during critical drought period expected for agricultural fields (de Melo Carvalho et al. 2014). The increase in water retention by SXBC as compared to BS at both saturated and drought range can be discussed in three aspects. The particle size distribution of soil and FESEM images (Chapter 3) clearly show that WH BC is fine grained as compared to the coarse grained particles of BS. The inclusion of WH BC particles decreases the inter-particle void spaces. The decrease in inter-particle spaces by fine grained BC increases the capillary action as compared to BS (Ng and Menzies 2007). Another aspect that is widely known for biochar's ability to retain water is because of its porous structure (de Melo Carvalho et al. 2014, Ulyett et al. 2014, Ajayi, and Rainer 2017). The WH BC also showcased this highly porous structure which makes the material conducive to store and retain water. FTIR analysis (Chapter 3) further indicate that WH biochar has hydrophilic surface functional groups which attract water molecules increasing the retention capacity of the composite.

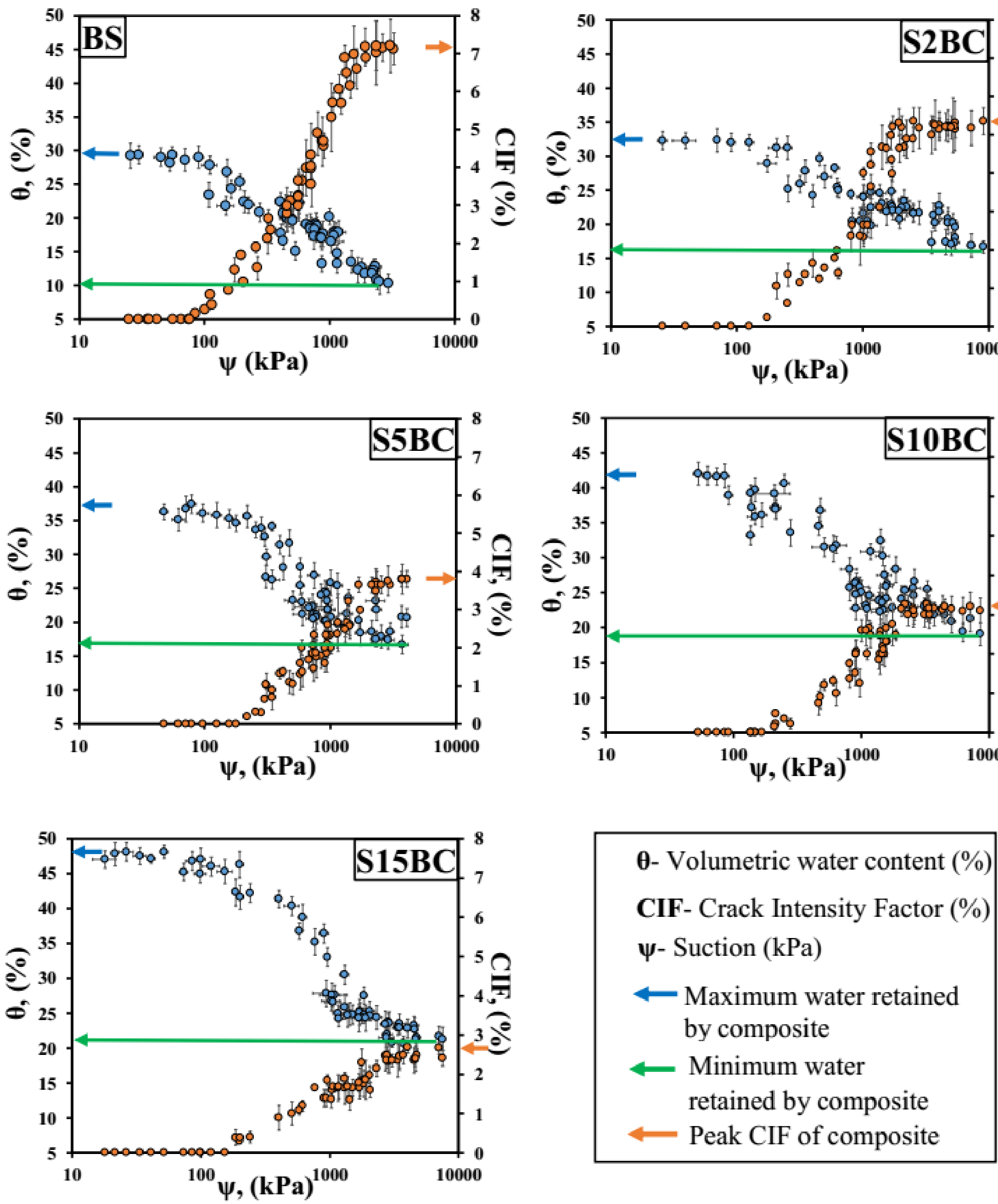

Fig. 5.15 Measured soil water retention (SWR) and soil desiccation characteristics (SDCC) for bare soil and soil-BC composites

5.4.3 Effect of WH biochar on crack intensity factor

The CIF variation with corresponding suction and water content along with mean and standard error from three replicates are presented in Fig. 5. 15. Cracks form on the surface when the tensile forces generated by air-water menisci increases than the soil tensile strength (Shin and Santamarina 2011). The CIF variation with the SWR property of soil is generally divided in to three stages (Li and Zhang 2010). Firstly, the soil surface does not showcase any cracks when it is saturated at the surface. This behavior is shown in all test series tested in the current study (refer Fig. 5.15). In the second stage, cracks start to appear on the surface due to evaporation of water and increases in size when the air-water interface develops in the unsaturated phase during drying. This increase in crack aperture is accompanied by soil contraction which is inherent to the cohesive nature of the soil (Cordero et al. 2017). Cracks ultimately increases and becomes constant in the third stage at very high suctions as the tensile forces cannot induce further contraction of particles due to drying (Yesiller et al. 2000). This is the maximum crack potential of the soil and shown by the peak CIF in the current study (Fig. 5.15). The inclusion of WH BC, the peak CIF decreases from 7% to 2.8% for BS and S15BC respectively as seen in Fig. 5.16a. The WH BC inclusions even at 5% reduces the peak CIF by half as compared to BS. This decreases in surface cracks can be explained by two reasons. First, as the SXBC composites retain more water than BS, thereby decreasing cracking. Secondly, even though inclusion of BC increases the finer content in soil, but these particles possess less cohesion than BS particles as reported in previous literature (Zong et al. 2014). Hence, the SXBC composites shrink less than BS resulting in reduced CIF values.

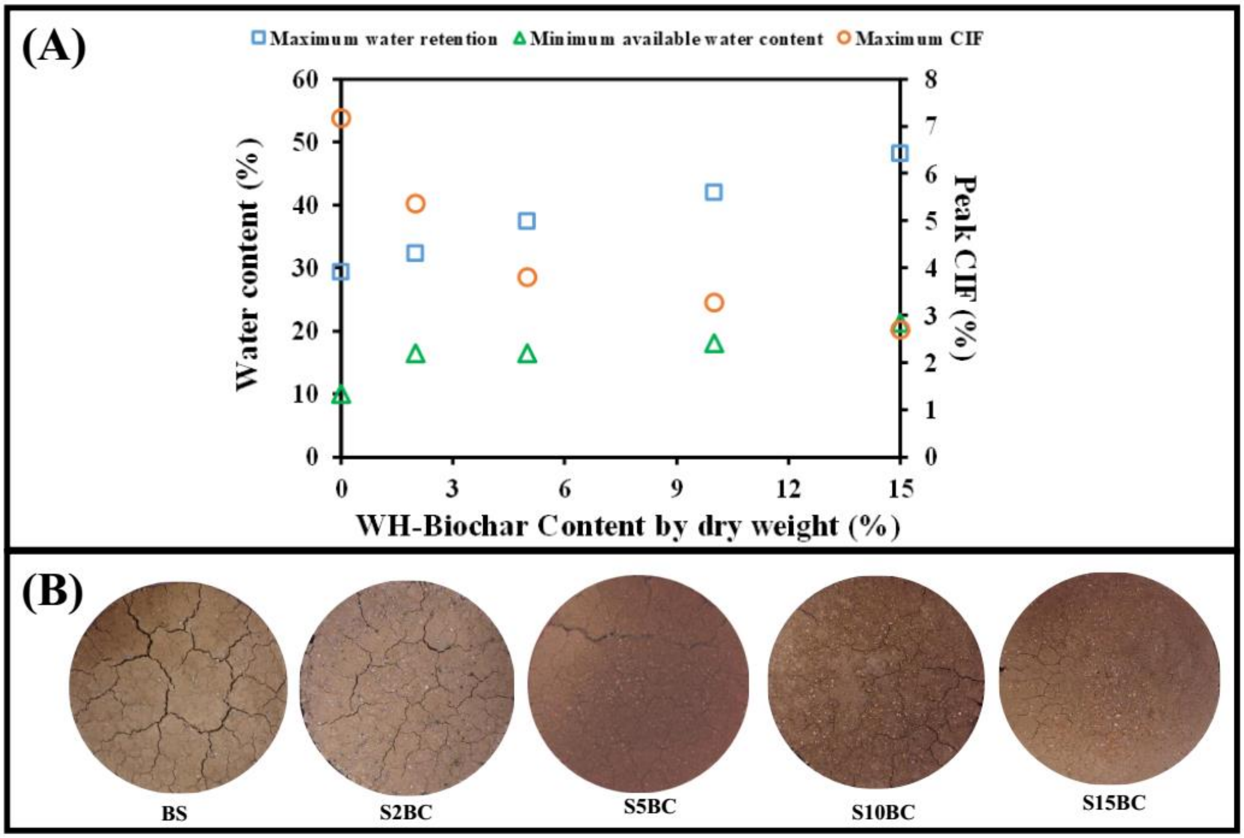

Fig. 5.16 Variation of (a) maximum, minimum water retention and (a-b) peak CIF with percentage weight inclusion of WH Biochar.

5.6 Summary

The summary from the chapter can be discussed with regard to infiltration, soil water retention characteristics and desiccation cracking potential as follows.

1) Soil-water retention and desiccation characteristics of soil-WH fiber composite

Among the three fibers tested, jute and WH showcased the highest water retention ability because they have the highest hemicellulose biopolymer content. However, the inclusion of lignocellulose does not significantly alter the rate of desaturation of the soil. It is shown that the nonlinear relation between peak CIF and induced suction for all fiber-reinforced soils mirrors the shape of the corresponding SWRC.

Cracks formed when suction is higher than the air-entry value of the soil. Compared to the unreinforced soil, the crack development due to the increase in suction for all fibre-reinforced soils (regardless the type considered) and the peak CIF were both smaller. Among the fibers tested, coir has the lowest CIF, hence greatest ability in resisting crack formation (six-fold reduction of soil cracking potential). This is attributed to the fact that coir is multifilament nature and has higher lignin content than other two fibers. These features make the coir fiber coarser (hence higher interface friction with soil) on its surface and makes the fiber more ductile when tensile stress is mobilized upon soil drying and shrinkage.

2) Infiltration characteristics of soil-WH fiber composite

Inclusion of fibers in soil resulted in an increase in infiltration rate for all the cases. This is due to water flowing along the soil-fiber interface along with flow through the soil pores. This increase in infiltration is more pronounced at lower densities as compared to higher densities. This is due to less inter particle void present in high density conditions as compared to low density.

Dye tracer experiment on soil-fiber composite was conducted to affirm the hypothesis of higher water flow along the soil-fiber interface in case of soil-fiber composite. Among the natural fibers, WH showcased the highest increase in infiltration as compared to jute and coir. This is due to WH having higher surface roughness as compared to jute and coir, which facilitates higher inter particle void along the soil-fiber interface. Additionally, higher tortuosity in case of jute and coir can result in obstruction in the water flow thus decreasing infiltration rate as compared to that in the case of WH.

3) Soil water retention and desiccation characteristics of soil-WH biochar composite

The results show that water retention capacity increases from 29.5± 0.89 % to 48.45± 0.59 % for BS and S15BC respectively and the increase is proportional with WH BC percentage. Minimum available water content increases from 9.97% to 21.48% for BS and S15BC respectively. This hydrophilic nature of WH BC amended soils can be attributed to the fine grained nature of WH BC, surface functional groups and also due to its porous structure as seen from the particle size distribution and FE-SEM images. Inclusion of WH BC results in a gradual decrease of CIF from 7% to 2.8%.

Chapter 6

Hydraulic characteristics of Vegetated soil-WH composite

6.1 General

This chapter investigates the vegetation potential of compacted soil-WH biomaterial in the form of natural fibers. Vegetation cover is not favored in compacted soil due to unfavorable conditions for root growth. The early plant establishment period is essential for mitigating progressive failures triggered by erosion and desiccation cracks. During this period, the soil is highly susceptible to progressive erosion failure due to formation of desiccation cracks. In tropical regions, green infrastructures have to undergo multiple drought cycles which induces desiccation cracks and also lead to water stressed condition of plants. The use of organic materials is thus advocated in green infrastructure for increasing water retention and favoring vegetation growth. The water retention curve, vegetation growth and other allied shoot parameters were measured. Vegetation growth was monitored under natural conditions with controlled precipitation for bare soil juxtaposed with soil-WH fiber composite.

6.2 Hydraulic characteristics of Vegetated soil-WH composite

The main objective of this study is to explore the influence of inclusion of natural fibers from waste weed (WH) on hydraulic characteristics (water retention and cracking) of vegetated soil. This will provide an insight on the feasibility of such waste for use as addition in cover materials of green infrastructure. Three series considered in this study include control bare soil (BS), (soil + grass (SG)) and (soil + grass + WH (SGWH)). Grass parameters (Stomatal conductance-SC, Evapotranspiration-Etr, grass density-GD, shoot length-SL) and soil parameters (suction- ψ, volumetric moisture content-θ, crack intensity factor-CIF, Evaporation-Er) were monitored for all series. A monitoring period of 73 days starting from rhizome transplantation was conducted to mimic early plant establishment (critical period in soil bio-engineering applications against erosion resistance; Schmidt et al. 2001). All three series of experiment undergo eight drying cycles in compacted soil under natural environmental conditions and controlled irrigation scheduling.

6.2.1 Test plan, setup and instrumentation

Three test series (BS, SG, SGWH) were conducted in compacted soil where plant characteristics (E_{tr}, SC, GD and SL) and soil properties (ψ, θ, CIF) were measured. Two grass species (*Axonopus Compressus* and *Cynaodon Dactylon*) were selected based on their easy availability, drought tolerance and use in green infrastructure application (Ng et al. 2014, Garg et al. 2015a, Avilés-Nova et al. 2008). Figure 6.1 shows the vegetated soil column and bare column. A total of 51 columns (24 each for SG and SGWH, 3 for BS) with diameter 300 mm adhering to minimum representative elementary volume requirement (REV) (Li and Zhang 2010) for surface-cracks and height 250 mm were constructed in-house for installing (ψ; MPS-6) and (θ; EC-5) sensors. Li and Zhang (2010) determined minimum REV by analysing the crack features from small to larger area of a cracked sample and found a minimum diameter (137.5 mm) above which the variation in crack intensity factor in relation to domain size was negligible. The slender WH stems were separated from the plant and fragmented in to uniform fiber pieces (length 28 mm and mean diameter of 0.4 mm). Initially, the soil was oven dried and fibers of 0.75% (by mass) were dry-mixed to create a uniform soil-fiber mixture. Requisite amount of water (15% by mass) is sprayed on the soil-fiber mixture to prevent any formation of lumps during mixing. The soil-fiber composite was compacted up-to 170 mm height in 3 layers corresponding to 0.9MDD as practiced for grass species (Ng et al. 2014, Li et al. 2016). Three rhizomes for both species were transplanted into the middle of soil column at 20 mm depth for enabling equal distribution of growth. Thereafter, all columns were exposed to atmospheric conditions by keeping it inside a transparent roof (on steel frame), which allows natural daily sunlight and wind but restricts precipitation. The steel frame is provided with a sprinkler system for controlled irrigation and digital camera. The captured time-lapse images were used to evaluate the CIF and GD. The CIF and GD represents the area of cracks and grass seen respectively from top to the total area of soil. SC was measured using leaf Porometer (Decagon Devices 2006). A micro-climate monitoring system (Decagon-Devices) was placed just next to the columns for measuring meteorological parameters. Based on the weather data obtained during the monitoring period, soil evaporation rate Ep and potential evapotranspiration (Etr) of vegetated soil was estimated by the Penman equation (Penman 1948) and Penman- Monteith equation (Monteith 1965, Allen 1998) respectively as shown below in Eq.6.1 and Eq.6.2. The overall parameters tested are summarized in Table 6.1.

$$E_p = \frac{\Delta R_n + \rho_a c_p (e_s - e_a)/r_a}{(\Delta + \gamma)\lambda} \qquad (6.1)$$

$$Etr = \frac{\Delta (R_n - G) + \rho_a c_p (e_s - e_a)/r_a}{\{\Delta + \gamma (1 + \frac{r_s}{r_a})\}\lambda} \qquad (6.2)$$

Where,

Δ = Slope of saturation vapor pressure curve (kPa k^{-1}); R_n = Radiant energy (MJ $m^{-2}d^{-1}$); G = Soil heat flux (MJ $m^{-2}d^{-1}$) (assumed negligible as the amount is minimal as compared to R_n); ρ_a = Air density (kg m^{-3}); c_p = Specific heat capacity of air (1.013×10^{-3} MJ kg^{-1} K^{-1}); e_s-e_a = Vapor pressure deficit (kPa); e_s = Saturated vapor pressure (kPa); e_a = Actual vapor pressure (kPa); r_a =

Aerodynamic resistance (sm^{-1}); r_s = Surface/canopy resistance (sm^{-1}); γ = Psychometric constant, ($\gamma \approx 66$ Pa K^{-1}); λ = Latent heat of vaporization (2.257 MJ kg^{-1})

The parameter r_a and r_s were estimated based on the correlation provided in Allen (1998). While calculating r_a and r_s, the average height of the grass and stomatal conductance from grass leafs were measured using measuring scale and leaf Porometer (Decagon devices)

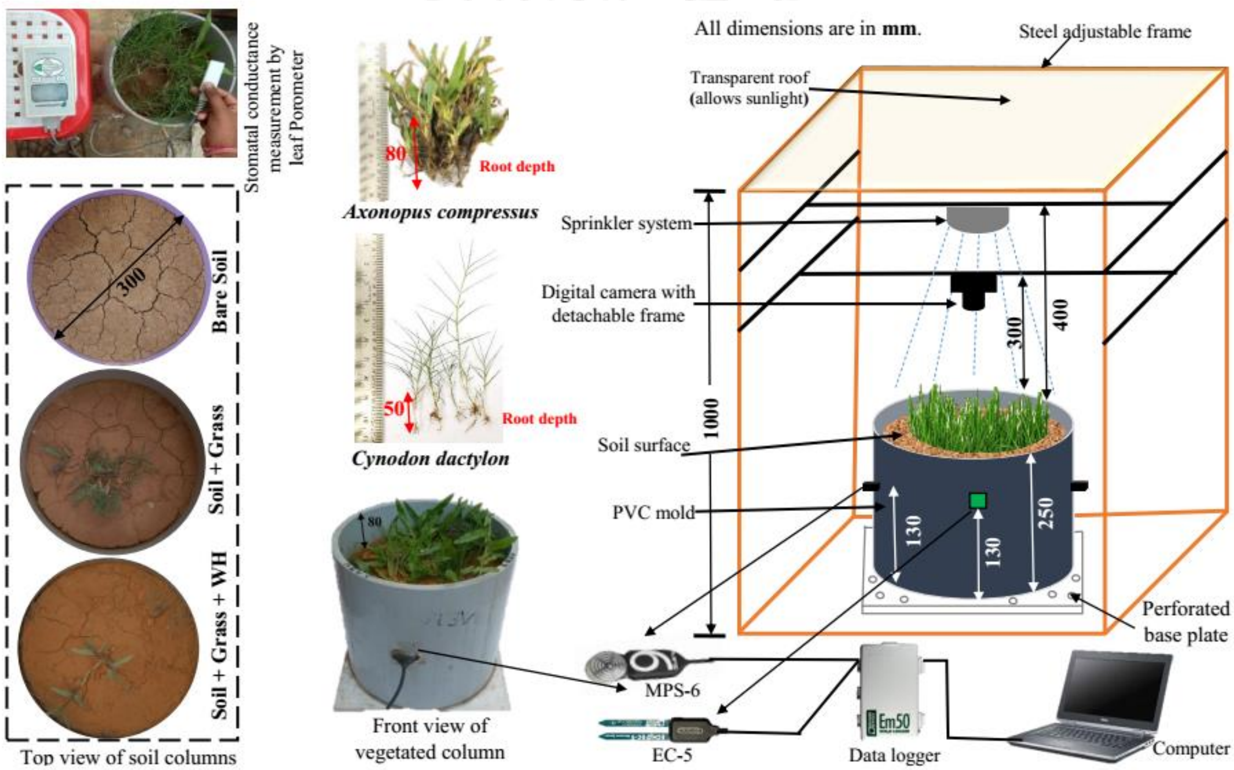

Fig. 6.1 Schematic representation of experimental setup used to measure CIF, VD, suction and stomatal conductance.

Table 6.1 Number of columns taken in consideration during the experimental period to measure various parameters

Time Period (days)		17-25	25-32	32-39	39-46	46-53	53-60	60-67	67-73
Drying cycle		1	2	3	4	5	6	7	8
(Bare Soil) **BS**	Number of columns	3	3	3	3	3	3	3	3
Parameters Investigated	CIF, ψ, θ, E_r	✓	✓	✓	✓	✓	✓	✓	✓
(Soil + Grass) **SG**	Number of columns	24	21	18	15	12	9	6	3
Parameters Investigated	CIF, ψ, θ GD, SL, E_{tr},	✓	✓	✓	✓	✓	✓	✓	✓
(Soil + Grass + WH fiber) **SGWH**	Number of columns	24	21	18	15	12	9	6	3
Parameters Investigated	CIF, ψ, θ, GD, SL, E_{tr},	✓	✓	✓	✓	✓	✓	✓	✓

6.2.2 Test procedure

The parameters (Table 6.1) were monitored for a period of 73 days after transplantation. An initial period of 18 days was taken by the rhizomes to grow into grass leaves (3-4 in number for each species) under daily irrigation (500 ml). Thereafter, the plants were water stressed for a period of 7 days and then irrigated on the 7th day consecutively. The irrigation period was kept at 7-day interval based on the observed suction near wilting point (around 1500 kPa; Feddes et al. 1982) generated in the root zone. This is also to ensure survival of grass species during the testing period. The depth of the suction sensors from soil surface is 40 mm (Fig. 6.1) which is well within the root zone (Ng et al. 2014) of the grass species (*Cynadon dactylon* (50 mm), *Axonopus compressus* (80 mm)). The maximum crack generated in each drying cycle and corresponding grass growth was quantified by CIF and GD respectively by developing an image analysis algorithm in Python Programming Language (Fig. 6.2).

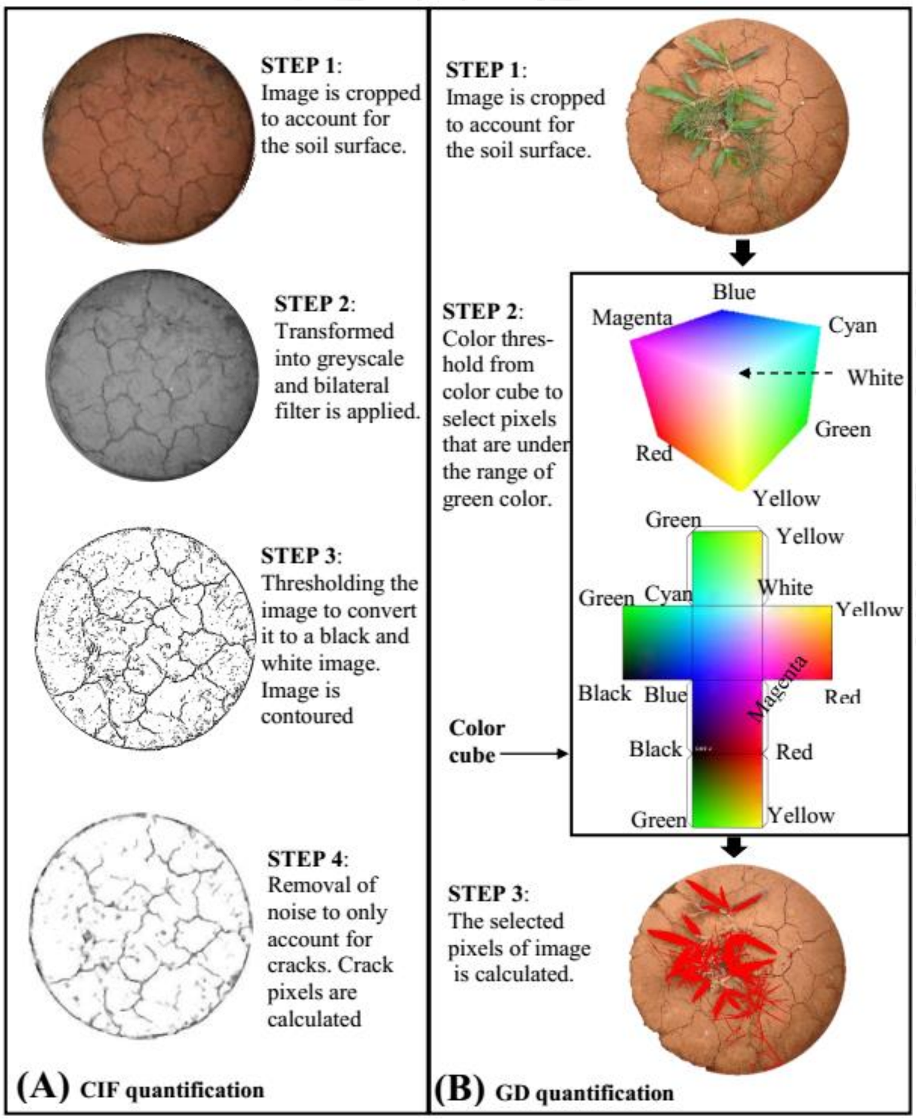

Fig. 6.2 Steps to measure cracks and vegetation to ultimately quantify CIF and GD respectively

To obtain CIF data of vegetated soil column, images were captured by cutting off the vegetation shoot entirely from 3 vegetated columns for each series at the end of each drying cycle (refer Table 6.1). In all vegetated test columns, two grass species (*Cynadon dactylon, Axonopus compressus*) were grown combined and hence the GD incorporates both grass type. The CIF in vegetated soil was obtained by cutting off both the grass species at the measurement time. Evapotranspiration (E_{tr}) and evaporation (E_r) rate was measured by change in weight of vegetated and bare column over a drying cycle (Leung et al. 2015).

6.2.3 Interpretation of monitoring results

Figure 6.3 shows the evolution of desiccation cracks at the end of each drying cycles in the form of average CIF for both bare (BS) and vegetated soil (SG, SGWH). The corresponding GD for SG and SGWH are also reported. In the current study, all parameters except SC and SL are measured at the end of each drying cycle-DC. Based on the comparison of CIF for both BS and SG, it can be seen that both exhibit similar cracking for the first two DCs corresponding to initial GD (10%). Beyond this, CIF for bare soil increases up to 2.65% ± 0.56% at the end of the 6th cycle and becomes constant thereafter. Peak CIF for the same soil compacted at 0.8 MDD and similar irrigation patterns previously reports a CIF of 3.15 (Gadi et al. 2017). SG showcases barely any increase in CIF after GD of 40% and 6th DC. The CIF was found to actually decrease in last two cycles for SG. This is noteworthy, as even though initial grass growth (40%) induces CIF up to 2.1 ±0.26 (not as much as BS) but thereafter, it reduces crack formation. This behaviour of CIF in SG for last 5 cycles may be attributed to two factors; (i) the root bridge effect which restricts crack growth (Zhou et al. 2009); and (ii) intercepted radiant energy due to growing grass cover reduces suction on the surface (Garg et al. 2015b). On the contrary to both BS and SG, WH fiber inclusions in SGWH resulted in lower CIF throughout the monitoring period. As compared to maximum CIF in BS and SG, WH-fiber inclusion lowers the desiccation potential by 55.5% and 25% respectively. This reduction in CIF for SGWH throughout monitoring period can be attributed to "bridge effect" of WH-fibers.

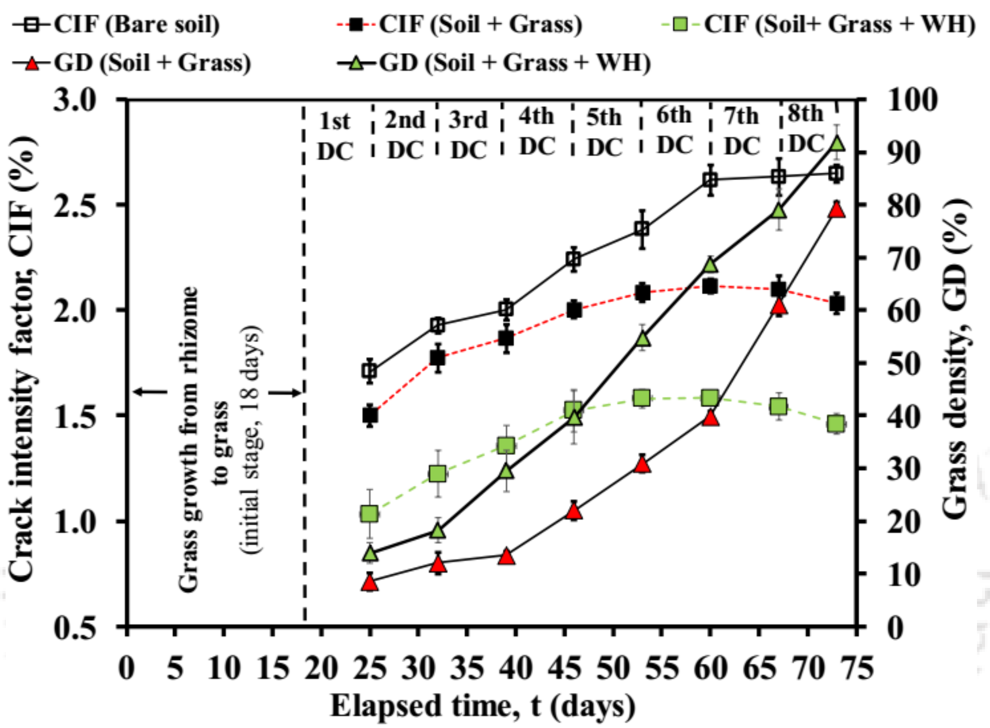

Fig. 6.3 Variation of CIF (bare and vegetated) and GD measured during the monitoring period

The vegetation growth for SG and SGWH is discussed by GD observed in the monitoring period. It is clearly seen that SGWH showcases a higher GD, especially after the 3rd cycle. The possible reasoning is discussed with the water retention behaviour discussed later. GD only gives lateral vegetation growth and thus the average SL was also measured manually (Fig. 6.4a) to take into account for longitudinal growth. It can be observed from figure that SGWH showcases higher SL than SG which indicates that WH-fiber inclusions aids in the initial establishment of vegetative layer.

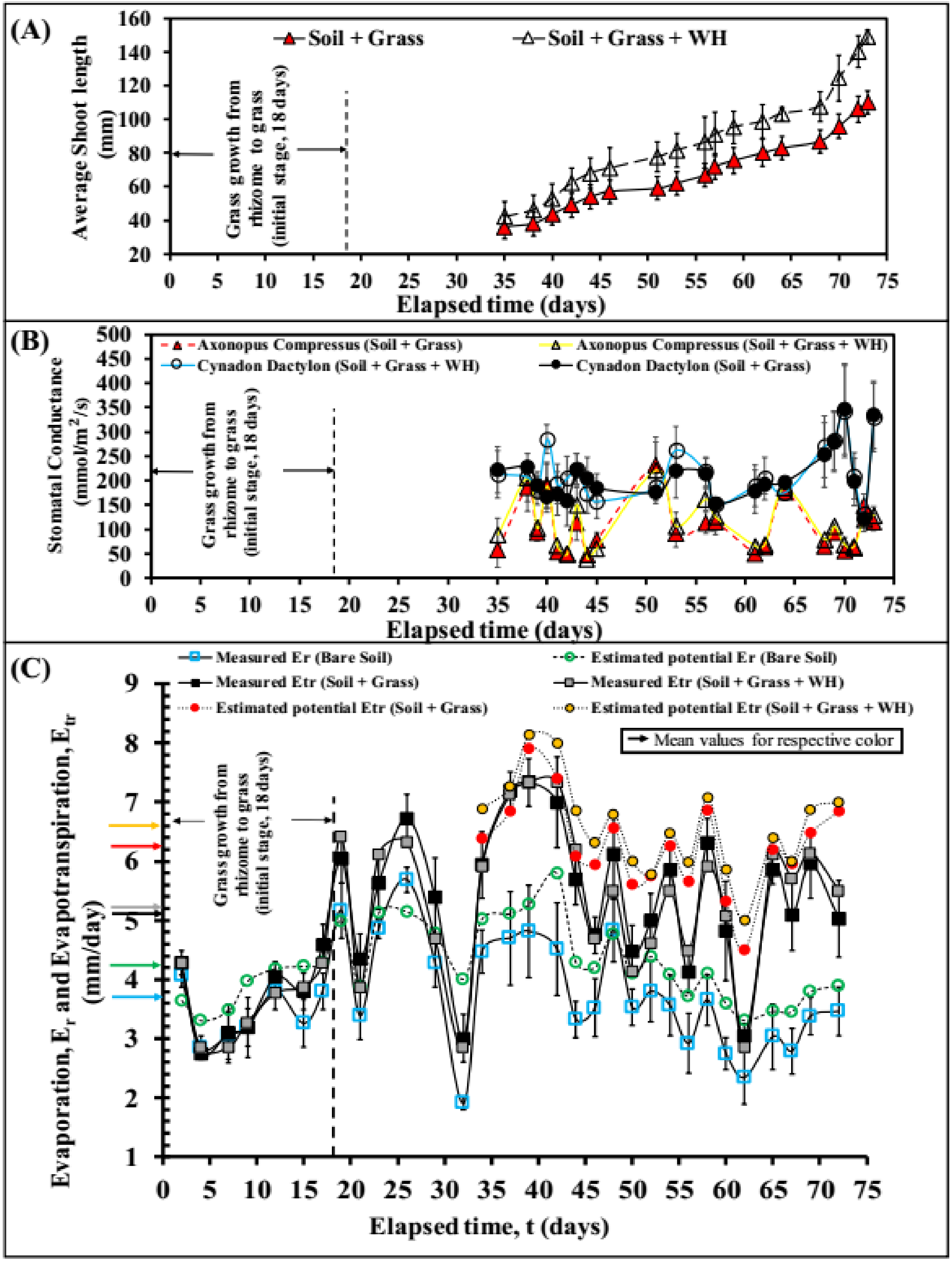

Fig. 6.4 Variation of measured parameters (a) Stomatal Conductance; (b) Evaporation and evapotranspiration; and (c) Shoot length during the monitoring period

Stomatal conductance-SC of both species was further monitored after 35 days of transplantation in all vegetated columns to the effect on plant growth (i.e., photosynthesis) due to inclusion of WH-fibers. Fig. 6.4b shows that *Cynadon Dactylon* has higher SC as compared to *Axonopus Compressus* for all test series. However, there is no significant variation observed in SC values for either species with WH-fiber inclusions. Based on measured SC and atmospheric conditions, the potential E_{tr} was estimated for both series (SG and SGWH). The measured E_{tr} was noted to be same for both SG and SGWH. However, the potential E_{tr} of SGWH is seen to be relatively higher than that of SG.

The measured ψ-θ data points for all three series are shown in Fig. 6.5 and is representative of the variation observed after 43rd day of monitoring when vegetation growth was adequate. It is clearly seen that SG showcases higher water retention for most of the suction range (25-1000 kPa) as compared to BS. Increase in water retention for SG can be related to the change in soil pore size and distribution which influence water retention (Ng and Leung 2011). The increase in maximum water retention for SG (35.7%) as compared to BS (32.1%) is attributed to three possible reasons. They are (i) water retention in roots (Taleisnik et al. 1999); (ii) root reduces overall pore size (Scanlan and Hinz 2010, Scholl et al. 2014); and (iii) root exudation which secretes enzymes in the root zone (Traoré et al. 2000). Pore size decrease can thus increase retention capacity.

The highest water retention among the three series is shown by SGWH. Addition of WH-fibers increase the composites' water retention capacity throughout the suction range. This hydrophilic nature of the composite can be addressed from the surface morphology of WH-fibers and its inherent bio-chemical composition. FE-SEM images shows the surface morphology of the fiber and it is stacked with fine pores that is conducive to absorb moisture (Methacanon et al., 2010). Furthermore, WH has a very high hemicellulose content which is a bio-polymer with available hydroxyl groups that attracts water molecules (Rowell and Stout 2002). WH-fibers being highly hydrophilic, naturally improves the soil's ability to retain more water and is conducive for the roots even at drought conditions. This can be a probable reason for high grass growth (GD and SL) in case of SGWH as compared to SG.

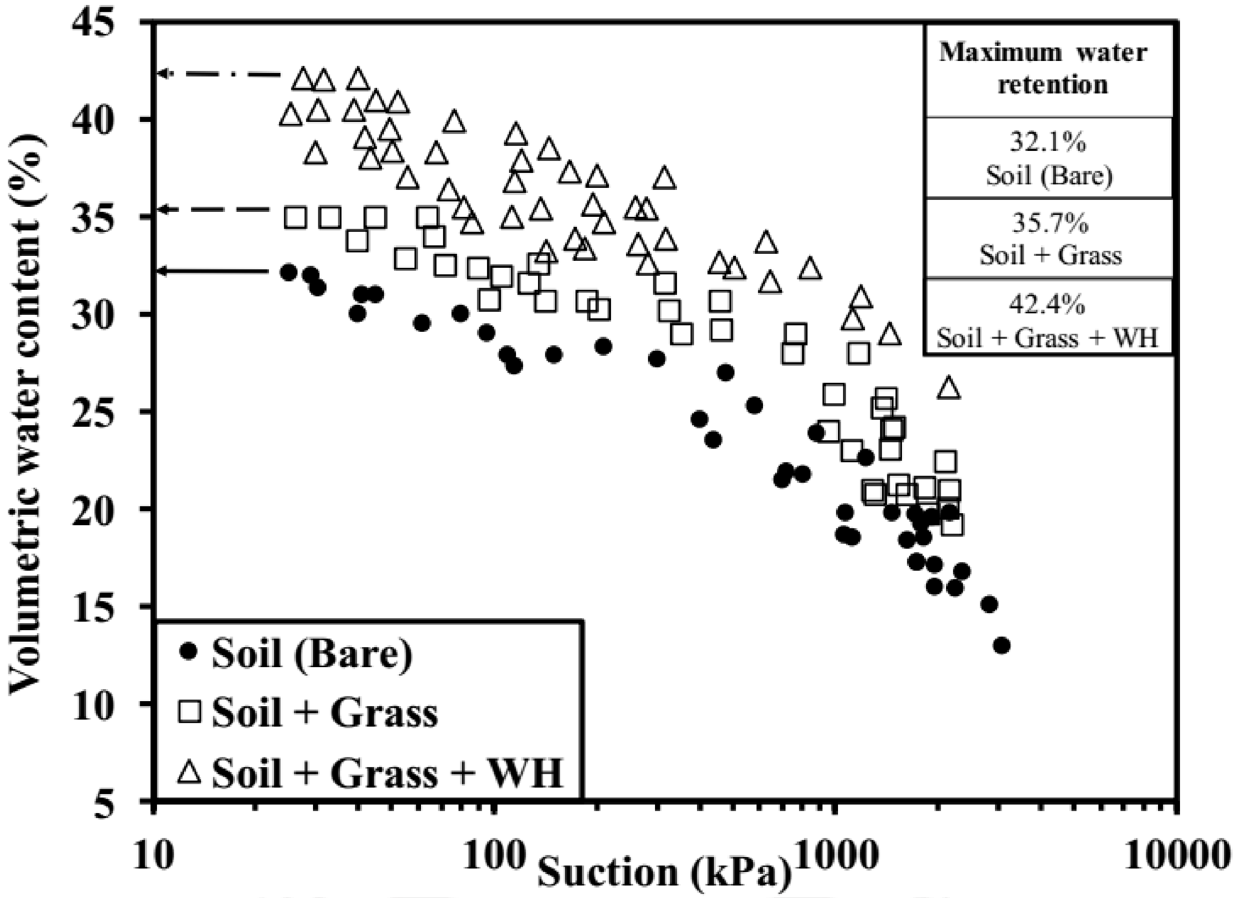

Fig. 6.5 Measured suction and water content relationship of the three series of soil

6.3 Summary

This chapter explores the potential of fiber from waste weed *Eichhornia Crassipes* for enhancing the water retention and reducing the crack in vegetated soil through a set of simple tests in drought condition. Grass parameters (Stomatal conductance (SC), Evapotranspiration rate (E_{tr}), Grass density (GD), Shoot length (SL) and soil parameters (matric suction (ψ), volumetric water content (θ), Crack intensity factor (CIF), Evaporation rate (E_r) were monitored in all soil series for 73 days. Image analysis was done to measure the CIF and GD of soil. It is seen that SGWH decreases the crack potential of soil by 55.5% and 25% as compared to BS and SG respectively. Inclusion of WH-fibers increases the GD and SL as compared to SG. However, there is no significant variation in SC values for either species with WH-fiber inclusions. SG showcases higher water retention for most of the suction range (25-1000 kPa) as compared to BS. The highest water retention among the three soil series is shown by SGWH. WH-fiber inclusion increases the composites' water retention capacity throughout the suction range due to its hydrophilic nature. The porous surface morphology and high hemicellulose content of WH fiber makes the composite conducive to retain higher moisture for vegetation growth in drought conditions. This is reflected in the high grass growth seen in the study. However, there is need to study the long-term effect of fiber degradation and its effect on vegetation growth. The knowledge from the current study can be applicable in urban green infrastructure such as green roofs where irrigation scheduling is generally practiced (Blonquist et al. 2006, Davis and Dukes 2010, Poë et al. 2015). The research impacts the bio-engineering of slopes. Due to the turf grass species increase in slopes is used for minimizing surface soil erosion due to raindrop impact, soil reinforcement by roots and increasing transpiration induced suction that can add to the strength (Vannoppen et al. 2015).

Chapter 7

Bio-degradation and treatment of WH fiber

7.1 General

Natural fibers are inherently prone to biodegradation. There is no study that reports the bio-degradation of natural fibers embedded in highly compacted soil for geo-technical application. The chapter attempts to explore the effect of fiber bio-degradation on the compressive strength and microbial activity of soil-fiber composite. The change in fiber bio-chemical composition as a function of embedded time in soil was also measured. Field monitoring was done for one year on three natural fibers embedded in compacted soil. A basic understanding of bio-degradation and its relationship with bio-chemical composition and consequent bio-activity is presented. A nano-coating by chemical precipitation technique was further explored for surface treatment of WH fibers. This is done to explore the efficacy of the treatment against moisture absorption and enhancement in strength. Furthermore, the soil-treated WH fiber composite was tested for its mechanical strength by conducting Unconfined compressive strength (UCS) test, direct shear and CBR tests.

7.2 Bio-degradation assessment of natural fibers in compacted soil

This section explores the effect of bio-degradation on the compressive strength and microbial activity of soil-fiber composite. Fiber bio-chemical composition change along with embedded time was measured and discussed in tandem with the UCS and microbial activity. This assessment gives an initial understanding of the mechanical performance of natural fibers with degradation. The experiment was conducted in field wherein compacted soil-fiber composite was buried within the soil and exposed to natural environmental conditions.

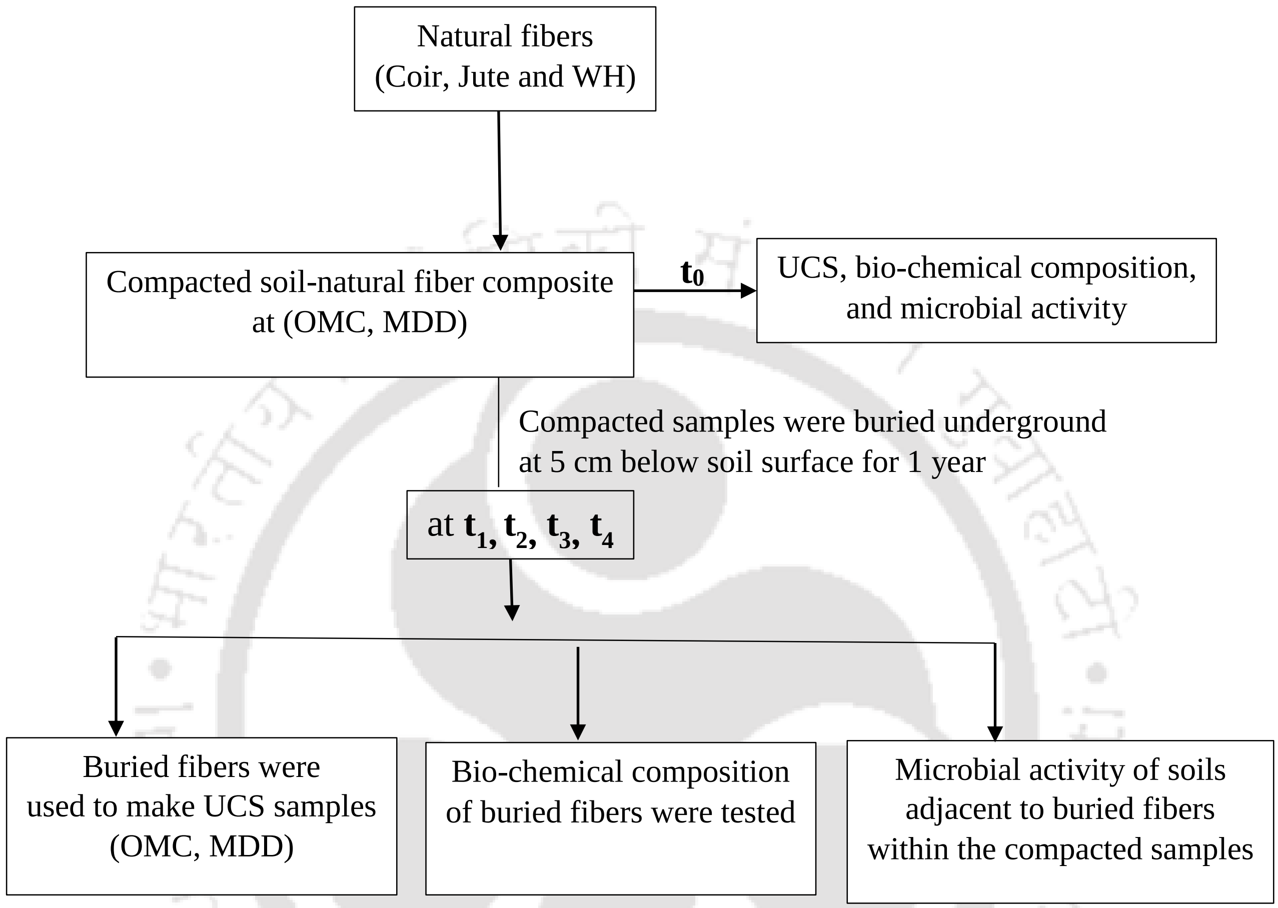

t_0 correspond to time just after compacted samples were made.
t_1, t_2, t_3 and **t_4** corresponds to 3, 6,9 and 12 months, respectively.

Fig.7.1 Flowchart depicting experimental approach for measuring effects of fiber bio-degradation on UCS, microbial activity and fiber bio-chemical composition

7.2.1 Test plan and setup

The soil used and the fiber dimensions for WH, jute and coir were kept same as discussed in section 4.2. Fig.7.1 provides the flowchart depicting experimental steps for measuring effects of fiber bio-degradation on UCS, microbial activity and fiber bio-chemical composition.

Cylindrical samples (50 mm X 100 mm) of soil-fiber composite were prepared at compaction condition of OMC and MDD. Thereafter, the UCS of the composite was measured along with the sample bio-activity by Fluorescence Di-acetate (FDA) analysis. The sample preparation procedure for making UCS samples as discussed in section 4.2 was adopted and only the sample compacter mould of bigger dimensions was used. The experimental matrix undertaken is tabulated in Table 7.1. In total, 36 (12 X 3) cylindrical samples were prepared and buried in soil. After the samples were buried and at different time intervals (as shown in Fig.7.1), the fiber biochemical properties were measured by taking 3 fibers from top, bottom and middle of each soil-fiber composite (coir, jute and WH). Thereafter, the soil was tested for bio-activity by FDA analysis (Green et al. 2006, Adam and Duncan 2001) while the rest of the degraded fibers was used to make samples of requisite dimension for UCS testing. The details of FDA analysis are given in Chapter 3. The new UCS samples were compacted at OMC and MDD with the degraded fibers for proper comparison of UCS regardless of field moisture status. The environmental parameters were measured by installing a micro-climate monitoring system near the burial site and the data is shown in Fig. 7.2. Parameters such as daily average solar radiation, rainfall depth, temperature and relative humidity were measured for the embedded time.

Table 7.1 Experimental matrix for the field bio-degradation test

Time interval	Soil-degraded fiber composite			Fiber properties		
	Samples tested	UCS	FDA analysis	Cellulose	Hemi-cellulose	Lignin
1	3	✓	✓	✓	✓	✓
90	3	✓	✓	✓	✓	✓
180	3	✓	✓	✓	✓	✓
270	3	✓	✓	✓	✓	✓
360	3	✓	✓	✓	✓	✓

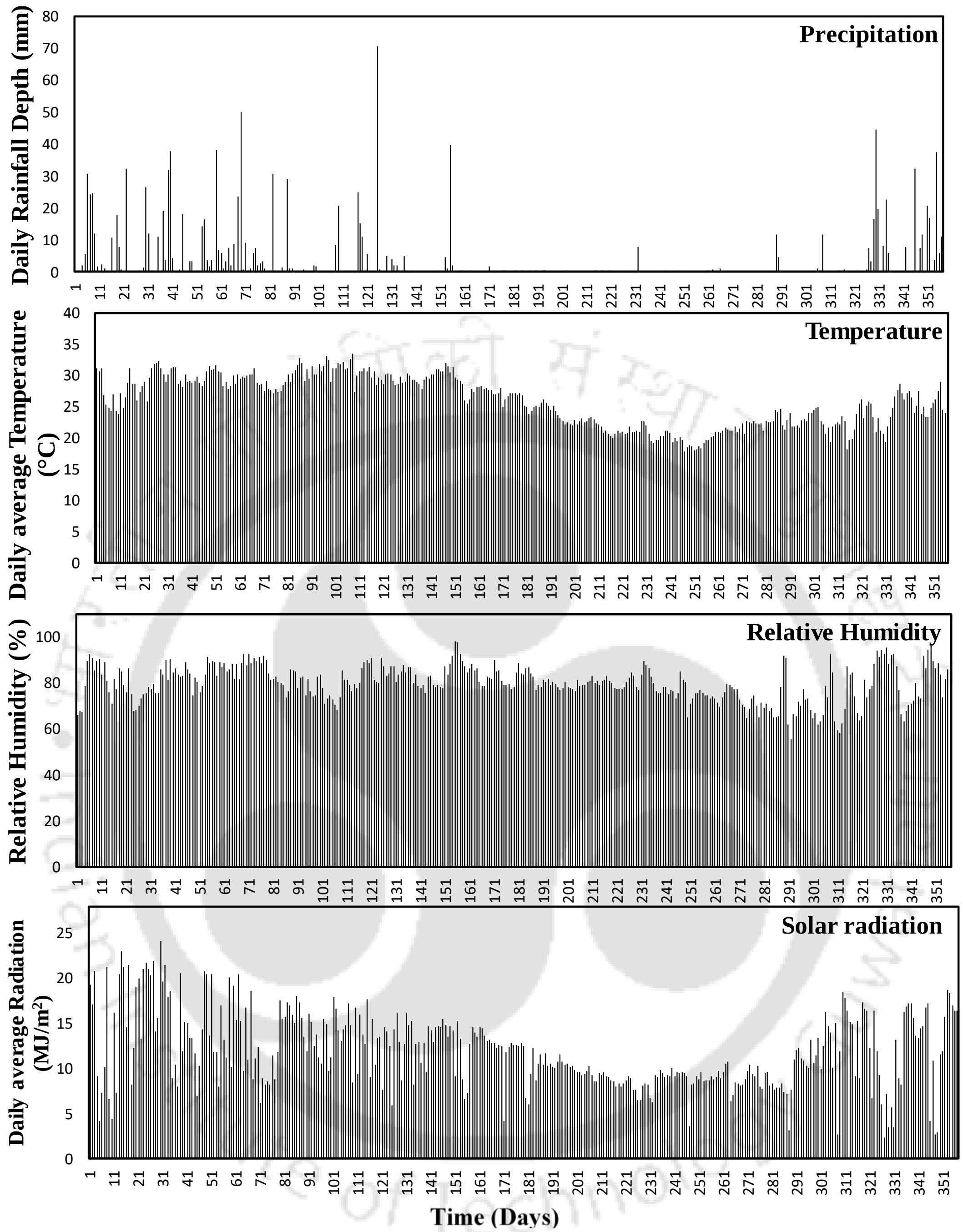

Fig. 7.2 Weather data from micro-climate monitoring system

7.2.2 Bio-chemical composition change with bio-degradation

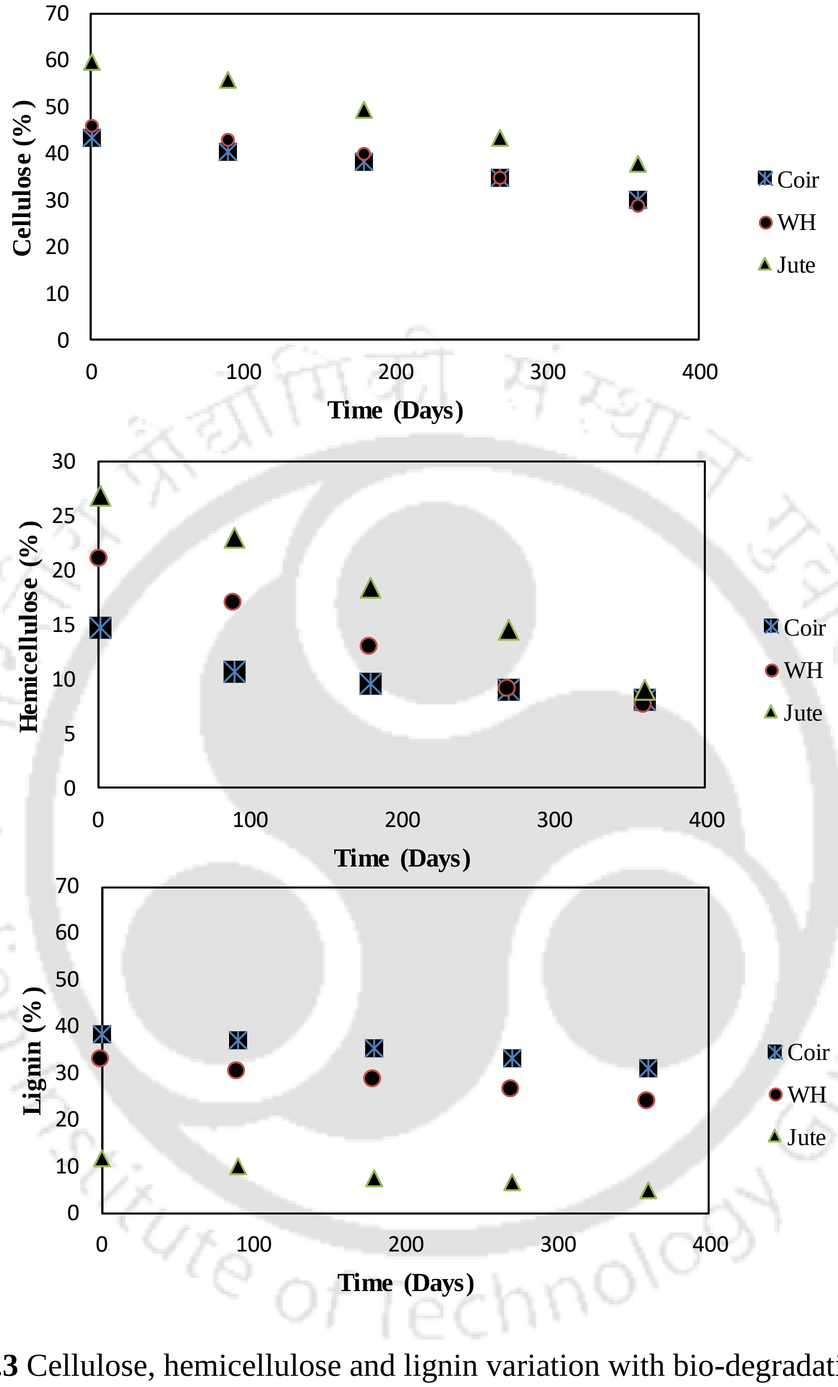

Fig.7.3 Cellulose, hemicellulose and lignin variation with bio-degradation time

Fig.7.3 showcases the change in cellulose, hemi-cellulose and lignin content of fiber with buried time. It was seen that hemicellulose decreased the most followed by cellulose and lignin. The decrease in hemicellulose is due to its highest affinity for moisture absorption which is conducive for micro-organisms to act on it (Rowell and Stout 2007). The insolubility and complexity of the lignin polymer allow it to resist degradation by microorganisms as reported in the literature (Campbell and Sederoff 1996, Methacanon et al. 2010). Therefore, lignin is considered to be important for geotechnical purpose as soil reinforcement, as it majorly indicates resistance to microbial degradation in soils.

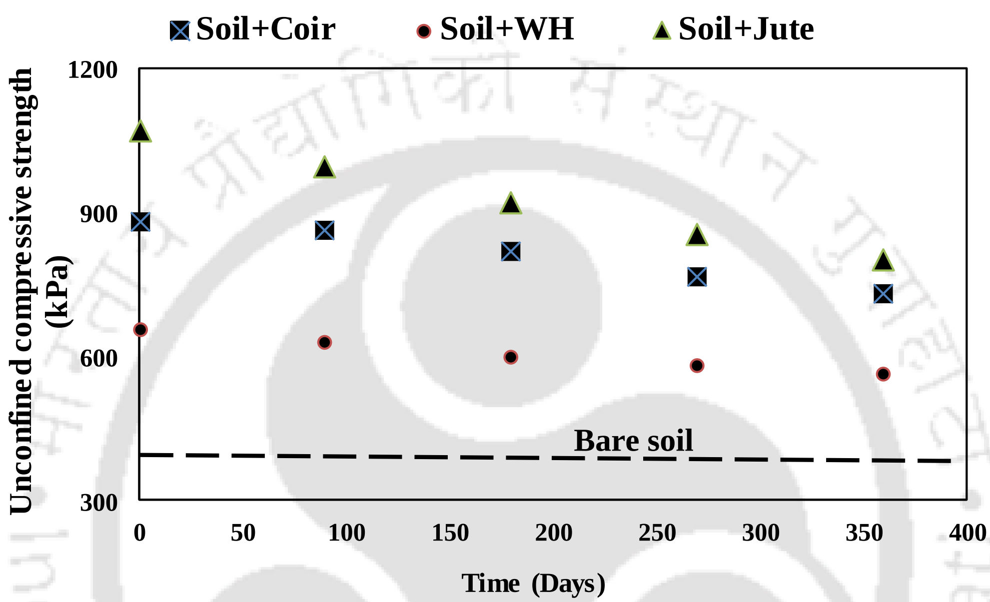

Fig. 7.4 UCS variation with time for soil-degraded fiber composite

7.2.3 Effect of bio-degradation on UCS of soil-fiber composite

Fig. 7.4 presents the UCS for soil-natural fiber composites with the degraded fibers. All soil-fiber composite showed a decrease in UCS with respect to initial state (non- degraded). It can be clearly seen that for the one-year period of embedded time, all soil-natural fiber composite exhibit UCS greater than at least 1.68 times for bare soil. Thus, its feasibility for short term reinforcement is not substantially affected by bio-degradation. Among all the soil-fiber composites, jute reinforced soil showcased the highest drop from its initial state (22.72%). This can be explained with respect to moisture absorption capacity of the fiber due to its high hemicellulose content facilitating higher microbial growth. The FDA analysis result (Fig. 7.5) of all composites and bare soil with time give further evidence that microbial activity was highest in jute reinforced soil. WH and coir showcased similar drop in UCS from its initial state by 14.75% and 16.08% respectively. It was also seen that inclusion of natural fibers regardless of fiber type greatly increased the microbial activity in comparison to bare soil. This is due to the fact that the fibers provide additional food source to various micro-organisms in the soil.

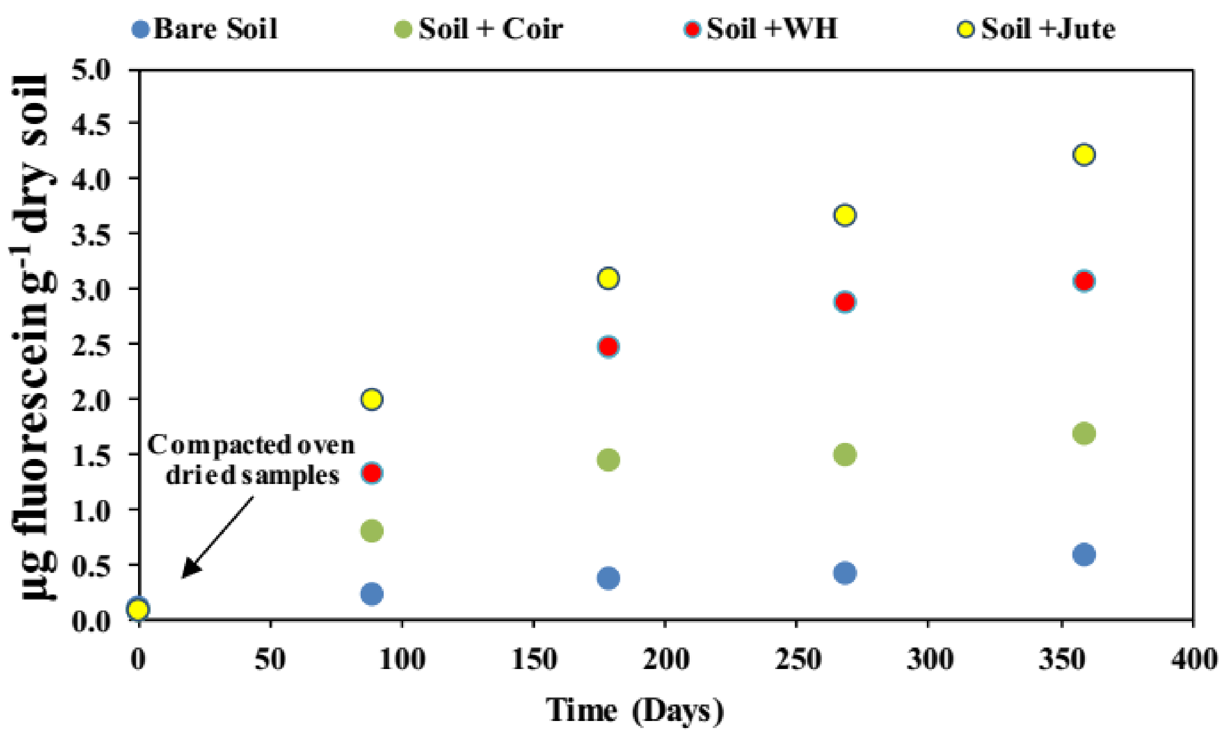

Fig. 7.5 Bio-activity variation with time in terms of fluorescein for the monitored time

7.3 Nano-coating of water hyacinth fiber

This study explores the possibility of using treated WH natural fibers for reinforcing and improving the subgrade strength of pavements. It is well known that the natural fibers have limited life when used in soils due to its degradation with time. For improving the longevity of the fiber and enhance the mechanical performance of the soil-fiber composite, effort was made in this study to chemically coat the natural fiber surface with nanoparticles of ferric hydroxide. The chemical coating can alter the short term as well as long term mechanical and chemical characteristics of WH fiber impregnated soil, which is not well understood. This study focuses on the short term behavior of ferric hydroxide coated WH fiber amended soil. The efficacy of coating on WH fiber was initially analyzed by field emission scanning electron microscopy (FE-SEM) and energy dispersive X-ray (EDX) analysis. The tensile strength and moisture absorption test was done for both untreated and treated WH fiber to understand the influence of coating. Unconfined compressive strength test and direct shear tests were performed to evaluate the improvement in mechanical characteristics of chemically altered randomly distributed fiber reinforced soil.

7.3.1 Treatment process of WH fibers

Nano modification method proposed by Anggraini et al. (2015) was adopted in this study to impregnate nanoparticles of ferric hydroxide on the WH fiber surface. Schematic procedure of fiber treatment using quick precipitation method of impregnating nanoparticles is shown in Fig.7.6 Stems of WH plants of similar length (45 ± 3.4 cm) and girth (4.5 ± 0.5 cm) were selected for treatment. All the selected WH plants were sun dried until there was no considerable weight change due to moisture variation. Fiber dimensions of length 20 mm and mean diameter of 0.4 mm was obtained from the dried plants (Fig.7.7). For nano treatment, 50 g of WH fibers were soaked in 500 mL aqueous solution of 0.5 M $FeCl_3$ in a beaker for a period of 24 hours to ensure absorption of the solution on the fiber surface and pores. The beaker was left undisturbed under room temperature (24^0 C). The soaked WH fibers were separated from the $FeCl_3$ aqueous solution and were kept in a perforated plate to drain excess $FeCl_3$ solution. 500 mL of 0.5 M Sodium Hydroxide (NaOH) was then added to it and kept for 24 hours in room temperature. During this treatment,

$Fe(OH)_3$ quickly precipitates as nanoparticles on the fiber surfaces and in the pores of WH fibers. The WH fibers were separated from the NaOH solution and washed with distilled water to remove the unwanted products (NaCl and NaOH) of the reaction. Fibers were then dried at ambient room temperature. Equation 7.1 shows the reaction of the treatment to impregnate $Fe(OH)_3$ nanoparticle.

$$FeCl_3 + 3NaOH \rightarrow Fe(OH)_3 + 3NaCl \qquad \textbf{(7.1)}$$

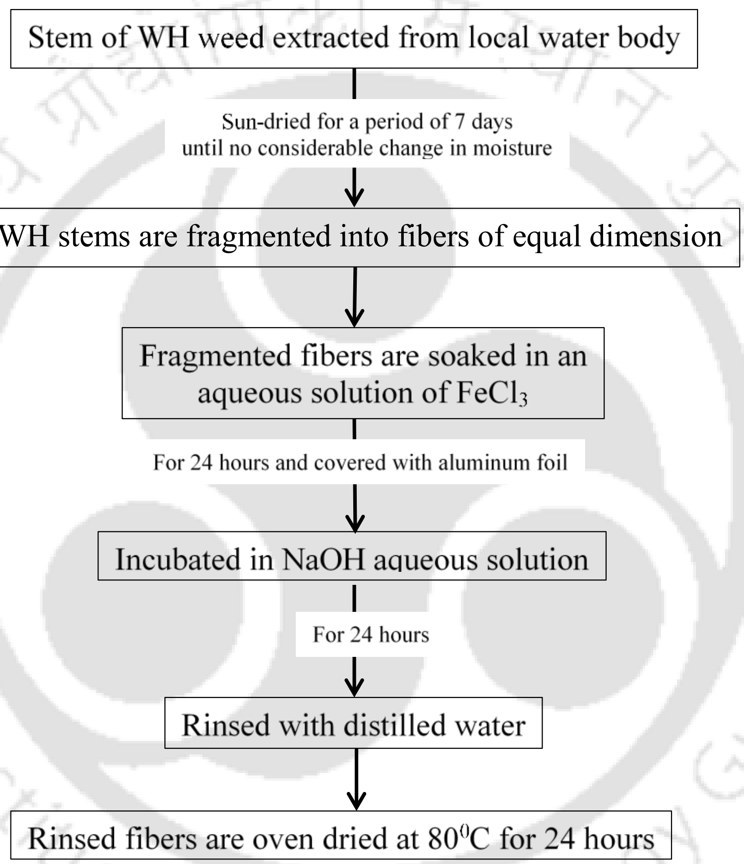

Fig.7.6 Schematic procedure of fiber treatment using quick precipitation method

7.3.2 Morphology and physical properties of untreated and treated fiber

The effectiveness of chemical treatment on the fiber surface is investigated by observing the surface morphology of both untreated (UF) and treated fiber (TF) using FE-SEM images shown in Figs.7.7 (a) and (b), respectively. As seen in the figure, FE-SEM images at magnification of 10

KX and 50 KX depict the fiber surface at micro and nano scale. In both magnifications, there is visible coating of panicle-like nanoparticles on the TF surface as compared to that of UF. This indicates that the deposition of nanoparticles on the WH surface has taken place due to the treatment. To confirm Fe^{3+} bonding with the hydroxyl group of fibers, further investigation was done using the results of EDX tests conducted on both UF and TF as shown in Figs. 7.8 (a) and 7.8 (b), respectively.

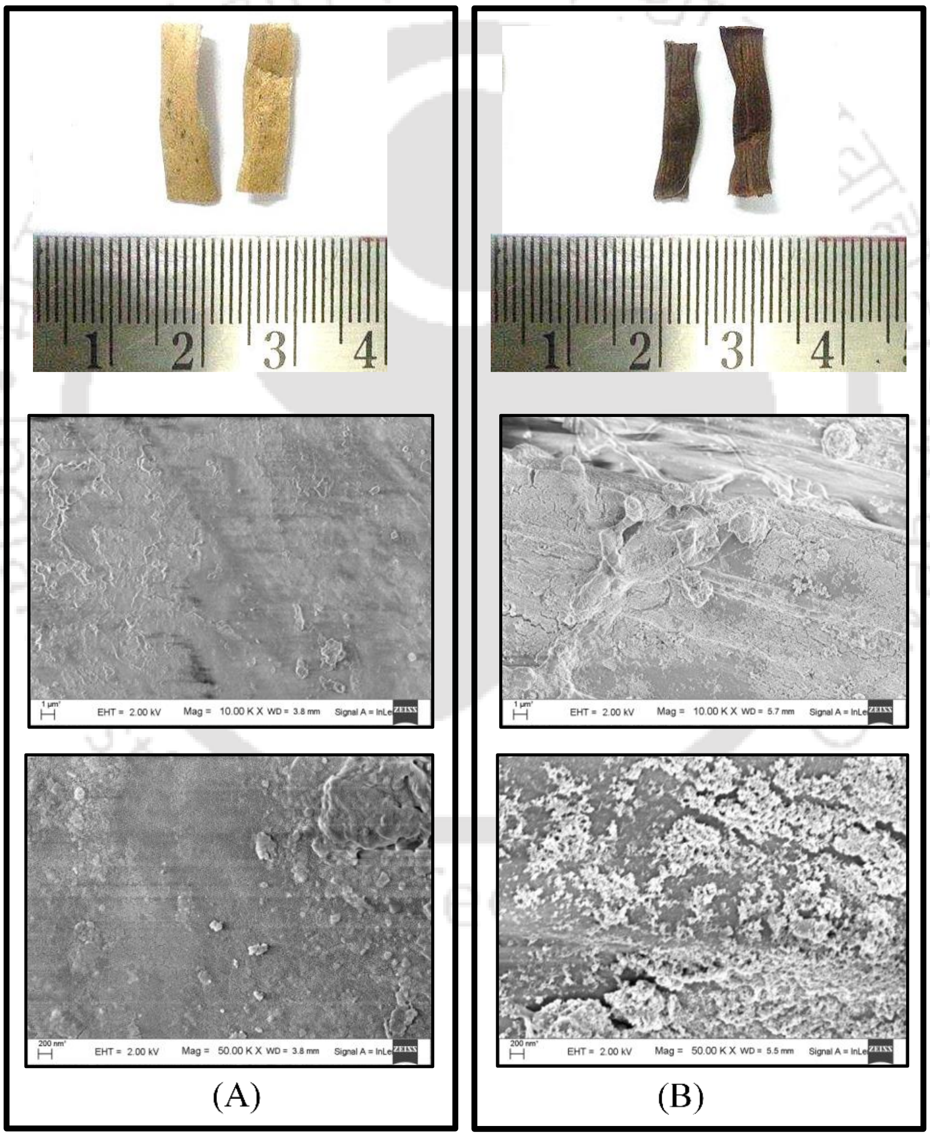

Fig. 7.7 Magnified images showing surface morphology of (A) UF and (B) TF using FE-SEM image analysis (at 10 KX and 50 KX magnifications).

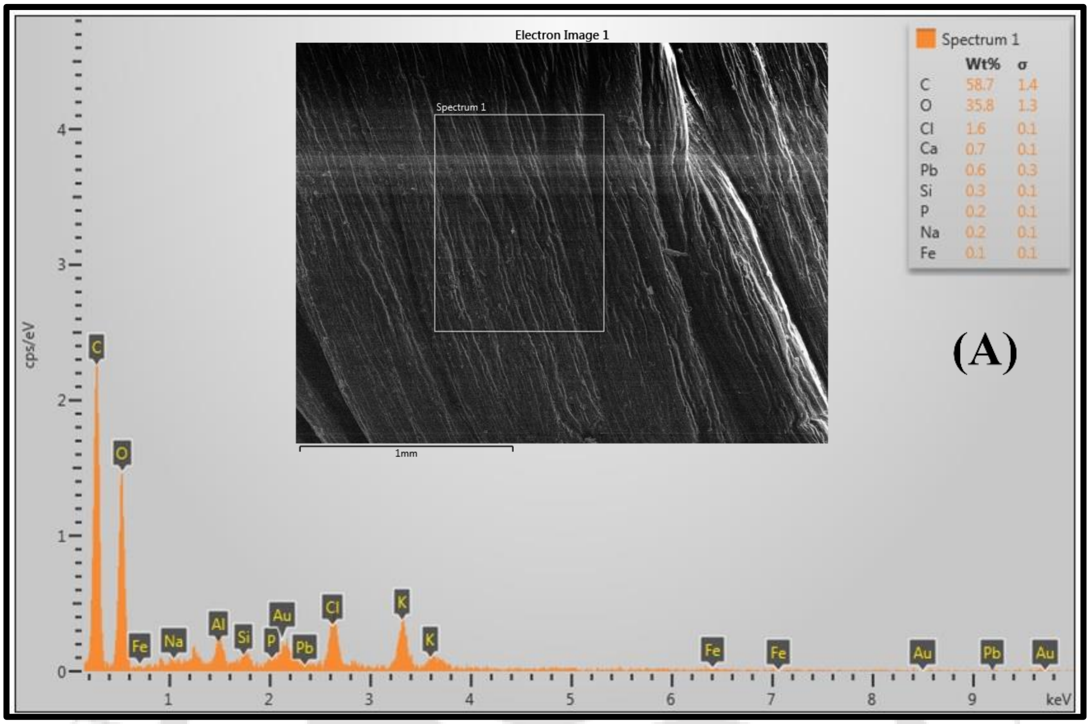

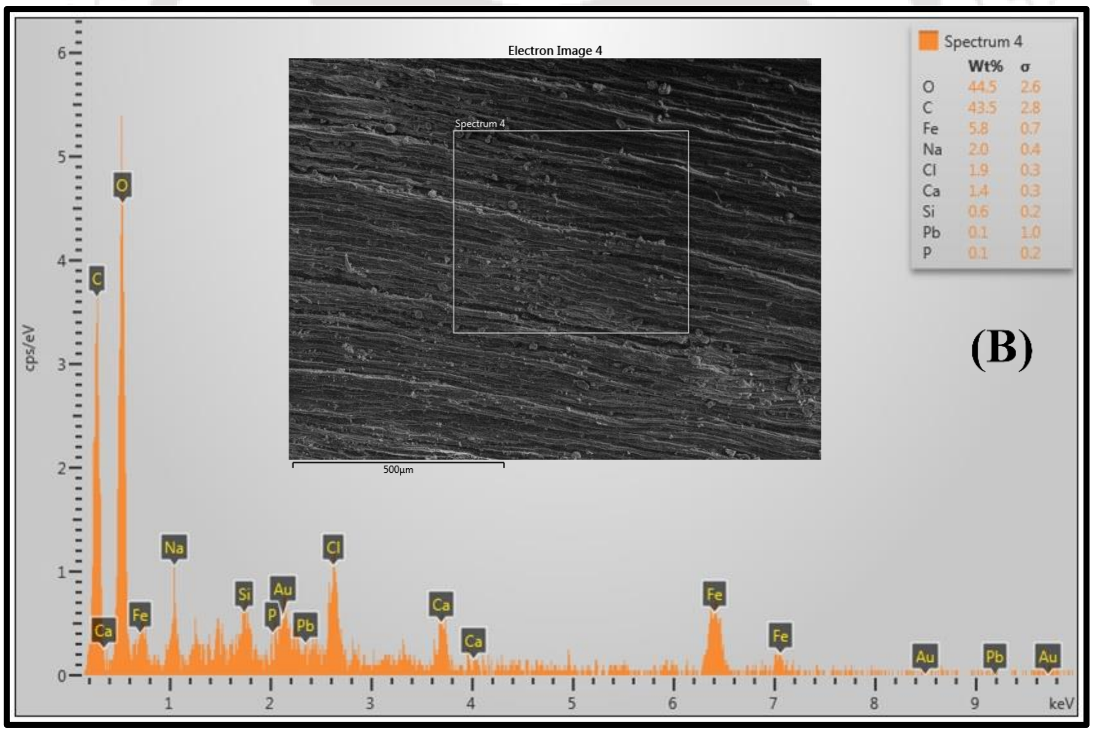

Fig. 7.8 EDX results for (a) UF and (b) TF showcasing increase in Fe weight percentage (increased from 0.1 ±0.1 to 5.8 ±0.7)

The elemental spectrum obtained from the EDX images tested for both UF and TF is indicative that there is an increase in the (Fe) elemental composition from (0.1 ± 0.1) for UF to (5.8 ± 0.7) for TF. The moisture absorption of TF decreased significantly from 580 ± 48% for UF to 255 ± 26%, indicating that the nano treatment fiber resulted in becoming more hydrophobic. This decrease in moisture absorption can be explained by less area of fiber surface exposed for water molecules (refer Fig.7.7 (b)) and also due to alkali treatment (NaOH) which replaces the hydroxyl group on the fiber surface. Less moisture absorption contributes to lower rate of biodegradation. The tensile strength of the material was determined according to (IS-1670-1991) and was found to increase from 312 ± 15 MPa to 370 ± 26 MPa. This increase in tensile strength is attributed to the crystallization of Fe nanoparticles into the pores of cellulosic cells and available capillaries in the fiber structure **(Anggraini et al. 2016)**. The filling and cross linkage effects of crystalized $Fe(OH)_3$ contribute to the load sharing phenomenon during tensile loading. The effect of this treatment increases the tensile strength of fiber by 1.25 times which is comparable with similar treatment on coir fibers (1.3 times) (Anggraini et al. 2016). However, the mean elongation at break decreased marginally from 15% for UF to 13% for TF, respectively.

7.3.3 Unconfined compressive strength, direct shear and CBR test of soil-treated fiber composite

A series of UCS tests were done on both UF and TF soil-WH fiber composites at nine different compaction states. The selected compaction corresponds to three soil densities (0.95 MDD, MDD and 1.05 MDD) and three moisture contents (OMC, OMC −5% and OMC +5%). The fiber percentage added to the soil was kept constant at 0.75% of dry mass of soil which is the optimum percentage required for maximum strength (section 4.2.4). Three replicate samples were tested for each compaction state to check repeatability in UCS results for bare soil (BS); untreated fiber reinforced soil (UF + S) and treated fiber reinforced soil (TF + S). A total of 108 UCS tests were conducted for the selected compaction states for all three different soil combinations (BS, UF + S, TF + S). Additionally, moisture content in the soil-fiber composites was cross-checked by oven-drying after the completion of UCS test. Fibers were initially weighed and dry mixed uniformly with an oven dried soil sample, following which the required amount of water was added to the soil–fiber mixture. These mixtures were sealed inside plastic bags and stored inside a desiccator for 24 h to attain moisture equilibrium within the soil. Finally, the UCS samples were prepared in a specially prepared UCS mold, which facilitates uniform static compaction from both ends. A constant strain rate of 1.25 mm/min was adopted to conduct the UCS tests as recommended by ASTM-D2166 (2000).

The shear strength parameters cohesion (c in kPa) and angle of internal friction (Φ^0) was determined by direct shear (DS) tests conducted on as compacted states of BS, (UF + S) and (TF + S). The samples for DS tests were compacted in the similar manner as done for UCS tests by static compaction. The strain rate was maintained at 1.25 mm/min as recommended by ASTM-D3080-2012. Three replicates were tested for each compaction state to ensure repeatability. It may be noted that the soil samples were not saturated before conducting the DS test, which is the general practice followed in ASTM- D3080-2012. The shear strength parameters obtained in this study can be used only for comparing the improvement in mechanical characteristics of different soil-fiber combinations stated above and not for design purpose. The moisture content of the samples was determined by using oven drying after DS test and it was found that the moisture content was within ±1% of targeted moisture content.

This study adopted laboratory CBR test for understanding the subgrade performance of BS, (UF + S) and (TF + S). Both soaked and un-soaked CBR tests were conducted on all the three soil combinations according to ASTM-D1883-2005 for OMC, MDD compaction state. The soil after mixing was kept in a desiccator for 24 hours to achieve uniform distribution of water throughout the soil. The compacted sample was subjected to a penetration of 15 mm to obtain load versus deformation response.

7.3.3 Effect of nano-coating fiber inclusions in strength characteristics of soil

Figure 7.9 shows the UCS of all the three soil-fiber combinations (BS, UF + S and TF + S) at nine compaction states. The UCS variation in terms of compaction states were discussed with respect to moisture content i.e. dry of OMC (OMC – 5%), OMC and wet of OMC (OMC + 5%). From Fig.7.9, it is evident that random inclusions of fiber in soil results in increase in UCS values. This phenomenon is due to fiber tensile strength being mobilized upon loading and subsequent increase in the soil-fiber composite strength (Tang et al. 2007, Tang et al. 2010). Among the soil-fiber composites, (TF + S) showcased higher UCS values for all the compaction states. The higher tensile strength of TF due to impregnation of nanoparticles results in enhanced mobilization of strength as compared to UF, thus resulting in increase in UCS for TF + S. Additionally, this behavior in TF + S is attributed to higher interfacial adherence and frictional interaction between TF and the soil particles (Anggraini et al. 2016). It is can be seen in Fig. 7.7 that the treated WH fibers have a comparatively rougher surface compared to untreated WH fiber. The UCS values of UF + S in the current study are comparable to UCS test conducted in literature for coir fibers (Anggraini et al. 2015). The UCS values at (MDD, OMC) for UF + S is lower by around 70 kPa as compared to treated coir fiber reinforced soil. However, this variation is expected as the soil used in the aforementioned literature is a clay soil with higher cohesion property than the soil used in the current study (silty sand).

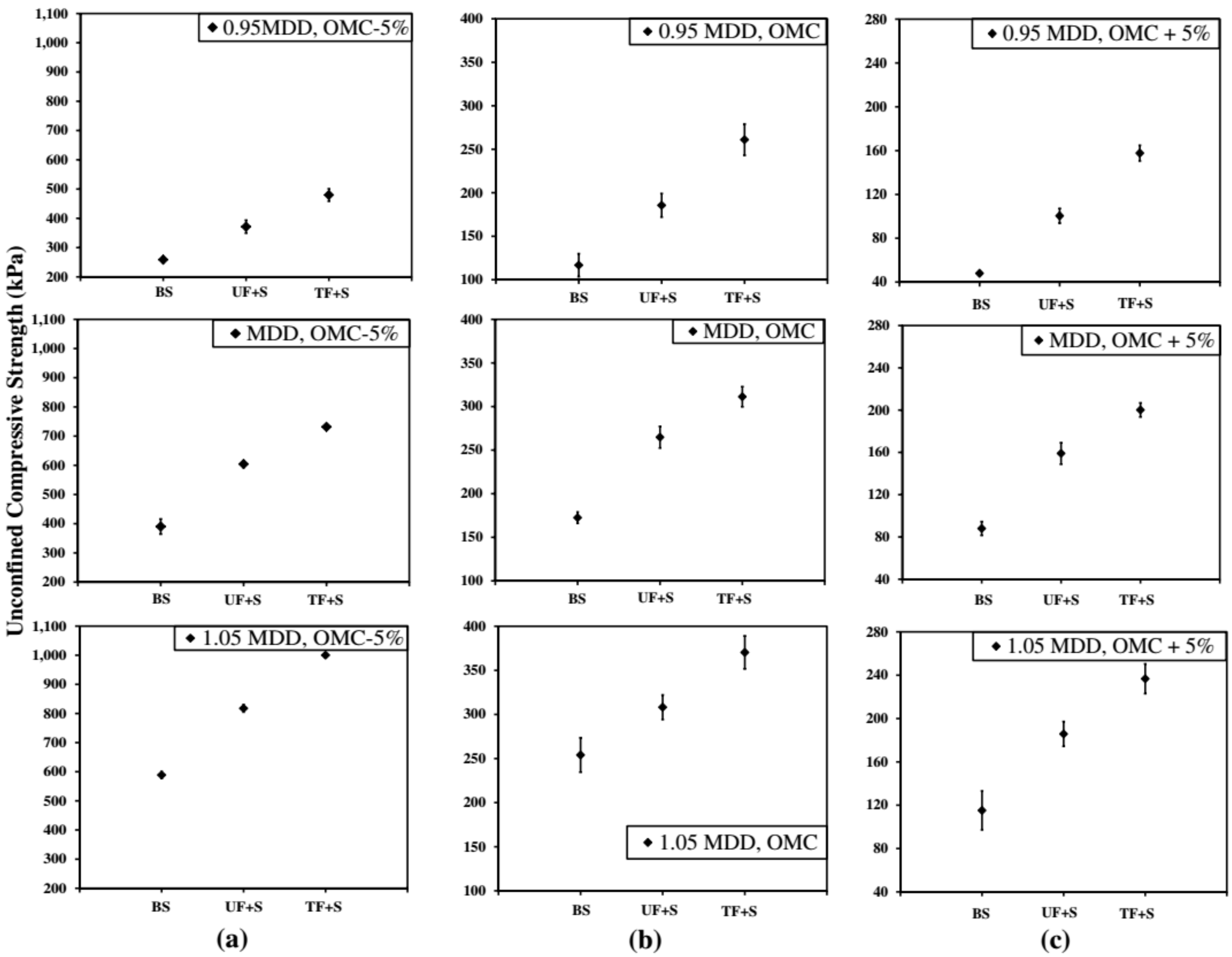

Fig. 7.9 UCS values for BS, (UF + S) and (TF + S) at selected compaction states (a) dry of OMC (b) OMC and (c) wet of OMC.

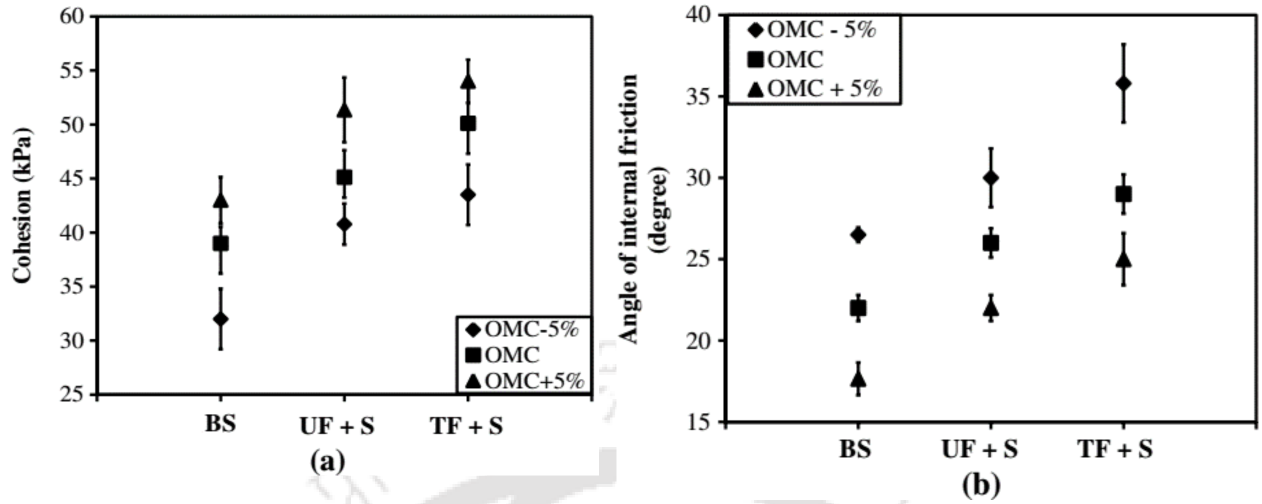

Fig. 7.10 Shear strength parameters (a) Cohesion and (b) Angle of internal friction] for BS, (UF + S) and (TF + S)

The shear strength parameters (cohesion, (c) and angle of internal friction, (ϕ)) of as compacted sample are shown in Fig. 7.10. Cohesion was seen to increase with rise in initial moisture content for all the soil types. This is due to corresponding increase in plasticity with a rise in initial moisture content. With inclusion of fibers there is a considerable increase in "c" as compared to BS at any moisture content. However, the "c" value does not increase significantly with inclusion of treated fibers as compared to untreated fibers. The "ϕ" value increase with impregnation of fibers into the soil due to fiber interlocking with the soil particles and mobilizing tensile strength on loading. This increase in strength is also due to the rough fiber surface that allow for further friction among the soil-fiber interface. (TF +S) showcased the highest "ϕ" as its surface roughness is significantly more than that of untreated fibers (refer Fig. 7.7). Moisture content induces "lubrication" effect in the fiber interface, which results in lower "ϕ" as the water content gradually increases. Thus, for any soil type, with increase in moisture there is a gradual decrease in "ϕ".

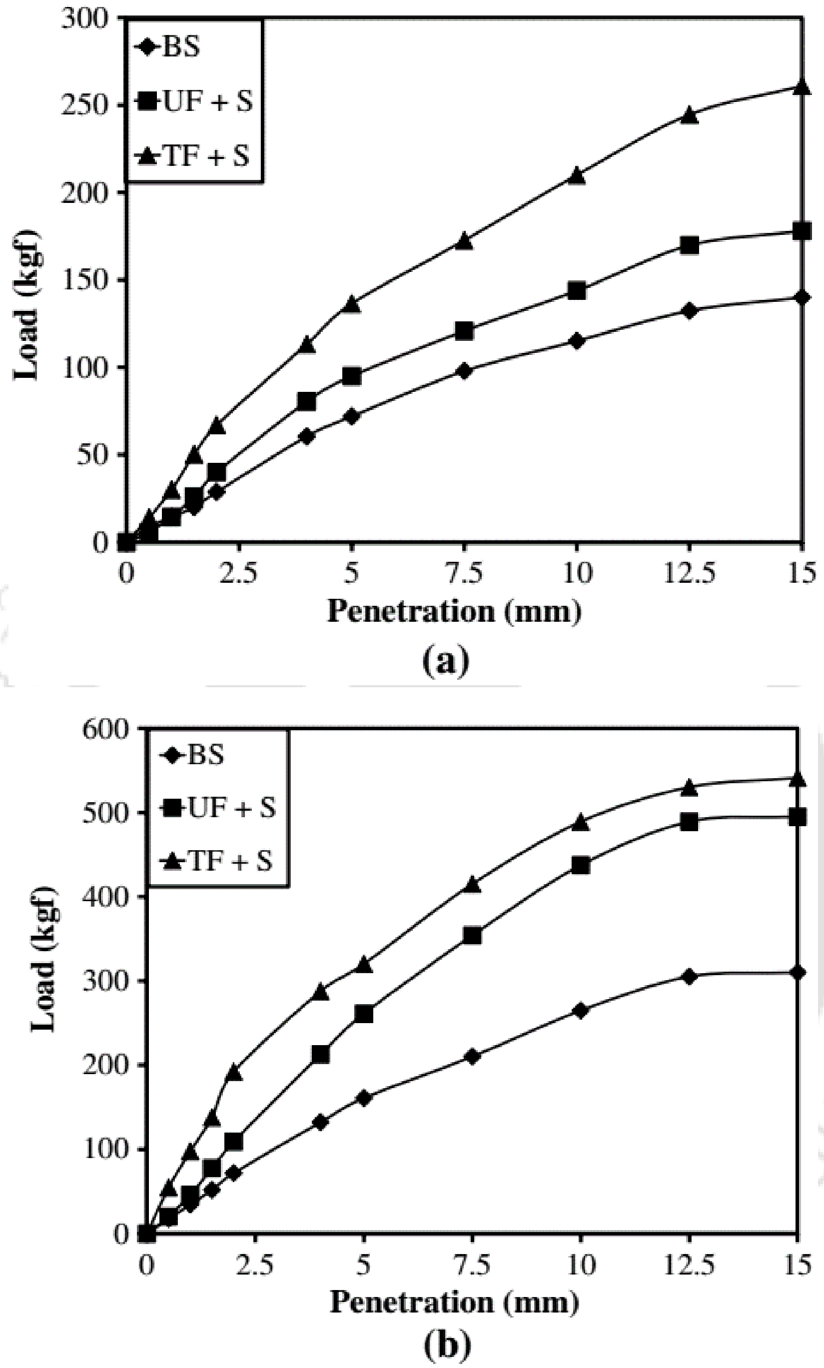

Fig. 7.11 Load Vs penetration graph for BS, (UF + S) and (TF + S) in (a) soaked and (b) unsoaked state

Figure 7.11 represents the load vs penetration graph for all the selected soil combinations (BS, (UF + S), (TF + S)) in (a) soaked and (b) unsoaked states. It is evident that the inclusion of fibers increases the load bearing capacity of the soil for both soaked and unsoaked conditions. The

(TF + S) showcased the highest load bearing capacity among all the soils. This increase for (TF + S) is due to enhanced tensile strength and surface roughness of TF which in turn increases the composite strength (Anggraini et al. 2016). It is evident that soaked load bearing capacity is relatively less than that of unsoaked state due to less strength and low suction in soaked state (Vanapalli et al. 1996, Vanapalli et al. 1998). Based on the load vs penetration graph, the CBR values for both soaked and unsoaked state have been calculated and the results are shown in Fig.7.12.

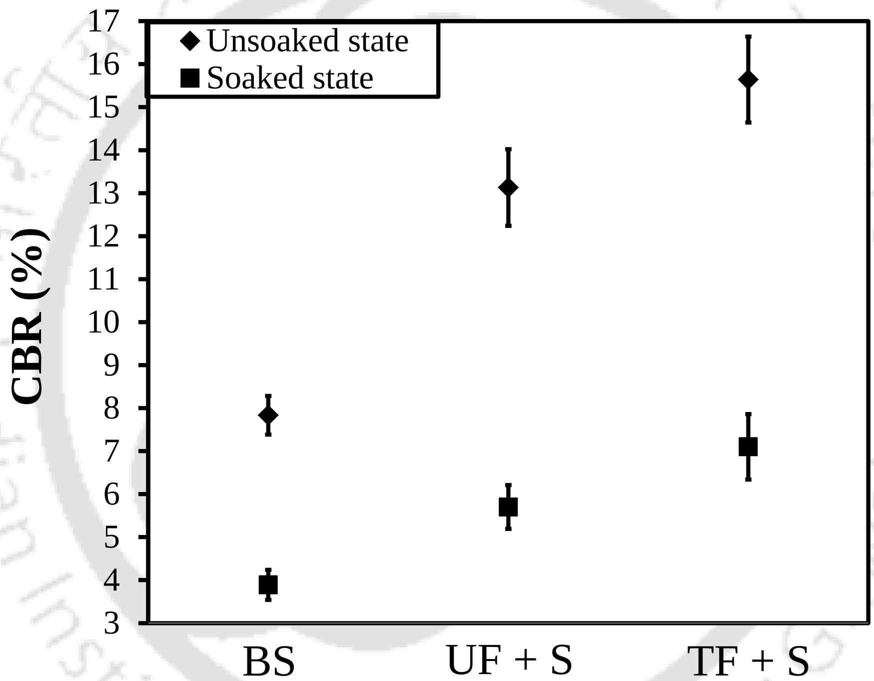

Fig. 7.12 CBR values for BS, (UF + S) and (TF + S) in soaked and unsoaked state

It can be noted that TF + S showcased the highest CBR for both soaked and unsoaked state. The increase in CBR for both the states represents TF + S as the most suitable subgrade material among the selected combinations. Consequently, the pavement thickness of such subgrade will be less as compared to BS and (UF + S). As per IRC: 37 -2012 design code (IRC-37-2012) and the obtained soaked CBR result in this study, the pavement thickness of BS for 100 million standard axles (msa) traffic, is 335 mm. Under the same traffic conditions, the pavement thickness for (UF + S) and (TF + S) decreases to 272 mm and 227 mm, respectively. The study clearly demonstrates the efficacy of chemically treated natural fiber impregnated soil for subgrade pavement and its cost effectiveness (in terms of reduction in thickness). However, further studies are required to understand the long term performance of treated fiber considering the effect of biodegradation.

7.4 Summary

The summary of findings from this chapter can be discussed for the three soil-WH biomaterial tested as follows.

1) *Bio-degradation assessment of natural fibers in compacted soil*

- Among the bio-polymers, hemicellulose showcased the highest percentage decrease due to bio-degradation in soil. Jute reinforced soil exhibited the highest decrease in compressive strength and is attributed to degradation of high hemicellulose bio-polymer in jute.
- During the one-year embedded time, all soil-natural fiber composite exhibit UCS greater than at least 1.68 times for bare soil. Thus, the feasibility for short term reinforcement was not affected substantially by the bio-degradation.
- High hemicellulose content in jute also facilitated the most microbial activity as seen from the FDA analysis.

2) *Nano-coating of WH fiber by ferric hydroxide treatment*

- The analysis of FE-SEM and EDX results clearly shows the chemical coating of Fe nanoparticles on WH fiber. The chemical treatment was found to decrease the hydrophilic nature of WH fiber. The fiber tensile strength of treated fiber (TF) increased by 1.25 times as compared to untreated fiber (UF).

- The (TF + S) composite showcased the highest UCS values for all the compaction states due to the enhanced mobilization of tensile strength of TF as compared to UF.
- Due to the interlocking of particles and mobilization of tensile strength during shearing. (TF + S) composite showcased a significant increase in “c” and “ϕ” as compared to BS.
- The load versus penetration graph obtained from CBR tests indicate that TF + S has superior load bearing capacity among the tested soil combinations. Based on the increase in CBR values for both soaked and unsoaked conditions, it is evident that use of such composite in subgrade can decrease the pavement thickness. According to IRC: 37 -2012, the TF +S composite decrease the pavement thickness by 108 mm for 100 msa traffic in Indian conditions.

Chapter 8

Conclusions

The following conclusions were drawn from the study conducted on soil-biomaterial in the form of natural fibers, geotextiles and biochar made from water hyacinth (WH). They are discussed with respect to four section.

Mechanical performance

- For WH fiber, the optimum fiber content with respect to compressive strength was obtained as 0.75% and for other natural fibers considered in this study are at 1%. The UCS was directly proportional to the amount of cellulose and hemicellulose bio-polymer.
- The warp and weft pattern WH geotextile facilitated a higher tensile strength along with higher CBR value.
- The compressive strength of soil-WH biochar composite is less than bare soil at all compaction states.

Hydraulic characteristics

- A mold ratio that is greater than or equal to 3.5 was recommended to be used for determining infiltration rate using the mini-disk infiltrometer in column experiments.
- Among the three fibers tested, jute and WH showcased the highest water retention capability because they have the highest hemicellulose biopolymer content. Among the fibers tested, coir showcased greatest ability in resisting crack formation due to its multifilament nature and high lignin content.

- Among the natural fibers, WH showcased the highest increase in infiltration characteristics as compared to jute and coir.
- Water retention capacity increases from 29.5± 0.89 % to 48.45± 0.59 % for bare soil to WH biochar amended soil respectively and the increase is proportional with WH BC percentage (2-15%). Furthermore, inclusion of WH BC results in a gradual decrease of Crack intensity factor from 7% to 2.8%.

Vegetation potential

- Vegetated soil on compacted soil-WH fiber composite showcased a decrease in desiccation potential by 55.5% and 25% as compared to bare soil and vegetated soil without fiber inclusion respectively.

Degradation and nano-coating studies

- During the one-year buried time in soil, the UCS of all natural fiber amended soil decreased almost linearly. However, after a year of burial time showcased strength which was at least 1.68 times greater to that of unreinforced soil.
- According to IRC:37-2012, the soil-treated WH fiber composite decreases the pavement thickness by 108 mm for 100 msa traffic in Indian conditions. The nano-coating treatment resulted in low moisture absorption and high tensile strength for the WH fibers.

Major contributions from the study

1. Explored the significance of bio-chemical composition of lignocellulose fibers with geotechnical properties such as composite compressive strength and water retention characteristics.

2. Developed an in-house produced WH fibers and geotextiles showcased efficacy in surface soil reinforcement.
3. Demonstrated the potential of WH biochar amended soil in increasing the retention capacity and decreasing the desiccation potential (by at least half).
4. Investigated the infiltration characteristics for soil-natural fiber composites for the first time and provided evidence for preferential flow in such composites.
5. Influence of WH fibers on water retention and cracking of compacted vegetated soils was investigated.
6. Presented the short term performance of WH fibers incorporating bio-degradation in field conditions including biochemical change and change in microbial activity.
7. The usefulness of nano-coating of natural WH fibers in reducing bio-degradation and improvement in strength was shown in this study.

Chapter 9

Limitations of the study and future scope

1. The effect of different aspect ratio on the mechanical and hydraulic performance of the soil-WH fiber has not been assessed. This can be done to find the optimum fiber aspect ratio.
2. The effect of biochar production conditions on the mechanical and hydraulic response of soil-WH biochar composite was not investigated in the current study. The effect of pyrolysis can directly affect the amount of intra pores and surface functional groups deeming it either hydrophobic or hydrophilic.
3. The vegetation potential of compacted soil-WH biochar composite along with that of coir and jute needs to be assessed.
4. A long term bio-degradation assessment of natural geotextiles needs to be explored for evolving bio-degradation kinetics of natural fibers. Incorporation of ferric hydroxide coated fibers in the degradation experiment would provide a better idea about the time dependent degradation of the WH-fiber-reinforced soil after applying the nano-coating.
5. Desiccation reported in the current study is two-dimensional. A three dimensional measure of desiccation using tomography would give a better understanding of soil cracking in soil-biomaterial composites.

References

Abbott, L.K., Macdonald, L.M., Wong, M.T.F., Webb, M.J., Jenkins, S.N. and Farrell, M., 2018. Potential roles of biological amendments for profitable grain production–a review. Agriculture, Ecosystems & Environment, 256, pp.34-50.

Abel, S., Peters, A., Trinks, S., Schonsky, H., Facklam, M., Wessolek, G., 2013. Impact of biochar and hydrochar addition on water retention and water repellency of sandy soil. Geoderma 202, 183e191

Abtahi, M., Allaie, H. and Hejazi, M., 2009. An investigative study on chemical soil stabilization. 8th Int cong civ eng, Shiraz, Iran.

Adam, G. and Duncan, H., 2001. Development of a sensitive and rapid method for the measurement of total microbial activity using fluorescein diacetate (FDA) in a range of soils. Soil Biology and Biochemistry, 33(7-8), pp.943-951.

Aggarwal, P. and Sharma, B., 2010, September. Application of jute fiber in the improvement of subgrade characteristics. In Proc of int conf on adva in civ eng, Trabzon, Turkey (pp. 27-30).

Ahmad, F., Bateni, F. and Azmi, M., 2010. Performance evaluation of silty sand reinforced with fibres. Geotextiles and Geomembranes, 28(1), pp.93-99.

Ahmed, M.J., Hameed, B.H., 10 September 2018. Adsorption behavior of salicylic acid on biochar as derived from the thermal pyrolysis of barley straws. J. Clean. Prod. 195, 1162e1169.

Ajayi, A.E. and Rainer, H.O.R.N., 2017. Biochar-induced changes in soil resilience: Effects of soil texture and biochar dosage. Pedosphere, 27(2), pp.236-247.Allen, R.G., Pereira, L.S., Raes, D.

and Smith, M., 1998. Crop Evapotranspiration-Guidelines for computing crop water requirements-FAO Irrigation and drainage paper 56. Fao, Rome, 300(9), p. D05109.

Akil, H., Omar, M.F., Mazuki, A.A.M., Safiee, S.Z.A.M., Ishak, Z.M. and Bakar, A.A., 2011. Kenaf fiber reinforced composites: A review. Materials & Design, 32(8-9), pp.4107-4121.

Al Wahab, R.M. and El-Kedrah, M.A., 1995, February. "Using fibers to reduce tension cracks and shrink/swell in a compacted clay." In Geo-environment 2000: Characterization, Containment, Remediation, and Performance in Environmental Geotechnics, ASCE, 791-805.

Albrecht, B.A. and Benson, C.H., 2001. "Effect of desiccation on compacted natural clays." J. Geotech. Geoenviron. 127(1): 67-75. https://doi.org/10.1061/(asce)1090-0241(2001)127:1(67)

Allen, R.G., Pereira, L.S., Raes, D. and Smith, M., 1998. Crop Evapotranspiration-Guidelines for computing crop water requirements-FAO Irrigation and drainage paper 56. Fao, Rome, 300(9), p. D05109.

Alvarado, S., Guédez, M., Lué-Merú, M.P., Nelson, G., Alvaro, A., Jesús, A.C. and Gyula, Z., 2008. Arsenic removal from waters by bioremediation with the aquatic plants Water Hyacinth (Eichhornia crassipes) and Lesser Duckweed (Lemna minor). Bioresource Technology, 99(17), pp.8436-8440.

Álvarez-Mozos, J., Abad, E., Giménez, R., Campo, M.A., Goñi, M., Arive, M., Casalí, J., Díez, J. and Diego, I., 2014. Evaluation of erosion control geotextiles on steep slopes. Part 1: Effects on runoff and soil loss. Catena, 118, pp.168-178.

Álvarez-Mozos, J., Abad, E., Goñi, M., Giménez, R., Campo, M.A., Díez, J., Casalí, J., Arive, M. and Diego, I., 2014. Evaluation of erosion control geotextiles on steep slopes. Part 2: Influence on the establishment and growth of vegetation. Catena, 121, pp.195-203.

AlWahab, R.M. and Alqedra, M., 1995. Using Fibres to Reduce Tension Cracks and Shrink/Swell Cycles in a Compacted Clay. Using Fibres to Reduce Tension Cracks and Shrink/Swell Cycles in a Compacted Clay, 1(2).

Anagnostopoulos, C.A., Tzetzis, D. and Berketis, K., 2014. Shear strength behavior of polypropylene fiber reinforced cohesive soils. Geomechanics and Geoengineering, 9(3), pp.241-251.

Anand, S., 2008. Designer natural fibre geotextiles—a new concept.

Anggraini, V., Asadi, A., Farzadnia, N., Jahangirian, H. and Huat, B.B., 2016. Reinforcement benefits of nanomodified coir fiber in lime-treated marine clay. Journal of Material Civil Engineering 28(6): 06016005. https://doi.org/10.1061/(asce)mt.1943-5533.0001516

Anggraini, V., Asadi, A., Huat, B.B. and Nahazanan, H., 2015a. Effects of coir fibers on tensile and compressive strength of lime treated soft soil. Measurement. 59, pp.372-381. https://doi.org/10.1016/j.measurement.2014.09.059

Anggraini, V., Huat, B.B., Asadi, A. and Nahazanan, H., 2015b. Effect of coir fibers on the tensile and flexural strength of soft marine clay. Journal of Natural Fibers, 12(2), pp.185-200.

Angulo-Jaramillo, R., Bagarello, V., Iovino, M. and Lassabatere, L., 2016. Infiltration measurements for soil hydraulic characterization. Berlin, Germany: Springer.

Angulo-Jaramillo, R., Vandervaere, J.P., Roulier, S., Thony, J.L., Gaudet, J.P. and Vauclin, M., 2000. Field measurement of soil surface hydraulic properties by disc and ring infiltrometers: A review and recent developments. Soil and Tillage Research, 55(1-2), pp.1-29.

Anon. "The Value of Sisal Hemp for the Manufacture of Marine Cordage, Reports of Recent Investigations at the Imperial Institute," Bull. Imperial Inst., Vol. 25, 1927, pp. 359–368.

Appels, W.M., Bogaart, P.W. and van der Zee, S.E., 2016. Surface runoff in flat terrain: How field topography and runoff generating processes control hydrological connectivity. Journal of hydrology, 534, pp.493-504.

Artidteang, S., Bergado, D.T., Tanchaisawat, T. and Saowapakpiboon, J., 2012. Investigation of tensile and soil-geotextile interface strength of kenaf woven limited life geotextiles (LLGs). Lowland Technology International, 14(2), pp.1-8.

ASTM (2007) D422–63. "Standard test method for particle-size analysis of soils." ASTM International, West Conshohocken. doi, 10, p.1520. https://doi.org/10.1520/d0422-63r07.

ASTM (2007) E1755-01. "Standard method for the determination of ash in biomass." Annual Book of ASTM Standards 11(5), ASTM International, Philadelphia, PA. https://doi.org/10.1520/e1755-01.

ASTM (2010) D4318. "Standard Test Methods for Liquid Limit, Plastic Limit, and Plasticity Index of Soils." ASTM International, West Conshohocken, PA. https://doi.org/10.1520/d4318-10.

ASTM (2011) D2487-11. "Standard Practice for Classification of Soils for Engineering Purpose (Unified Soil Classification System)." ASTM International, West Conshohocken, PA. https://doi.org/10.1520/d2487-11

ASTM D 1557-2012, "Standard Test Method for Laboratory Compaction Characteristics of Soil Using Modified Effort." ASTM International, West Conshohocken, Pennsylvania, USA. 2012

ASTM D 2487-11, Standard Practice for Classification of Soils for Engineering Purpose (Unified Soil Classification System), ASTM International, West Conshohocken, PA, 2011, www.astm.org

ASTM D-2166 (2000) Standard test method for unconfined compressive strength of cohesive soil. Annual book of ASTM Standards, American Society for Testing and Materials, Philadelphia vol 04:08

ASTM D422, 63-07. "Standard Test Method for Particle-Size Analysis of Soils." ASTM International, West Conshohocken, PA, 2007, DOI: 10.1520/D0422-63R07.

ASTM D422–63 Standard test method for particle-size analysis of soils. ASTM International, West Conshohocken. doi, 10, p. 1520; 2007.

ASTM D4318-00, "Standard Test Methods for Liquid Limit, Plastic Limit, and Plasticity Index of Soils," Annual Book of ASTM Standards, ASTM International, West Conshohocken, PA. 2000.

ASTM E1755-01(2015), Standard Method for the Determination of Ash in Biomass, ASTM International, West Conshohocken, PA, 2015, www.astm.org

ASTM, D1883. 2005."Standard test method for CBR (California Bearing Ratio) of laboratory-compacted soils." Annual Book of ASTM Standards 4.

ASTM, D2166 (2000) Standard test method for unconfined compressive strength of cohesive soil. Annual book of ASTM Standards, American Society for Testing and Materials, Philadelphia 4 (2003): 08.

ASTM, D3080. 3080-12: Standard test method for direct shear test of soils under consolidated drained conditions. Annual Book of ASTM Standards 4 (2012): 290-5.

ASTM, D3080-06. 2006. Standard Test Method for Direct Shear Test of Soils Under Consolidated Drained Conditions

ASTM, D4972. (2007). “Standard test method for pH of soils”. ASTM International, West Conshohocken/PA.

ASTM, D698-00a, (2002). Standard test methods for laboratory compaction characteristics of soil using standard effort. Annual book of ASTM standards, 4, pp.78-88.

ASTM, D854 92. 1994. Standard test method for specific gravity of soils. Annual Book of ASTM Standards, 4, pp.80-3.

Avilés-Nova, F., Espinoza-Ortega, A., Castelán-Ortega, O.A. and Arriaga-Jordán, C.M., 2008. Sheep performance under intensive continuous grazing of native grasslands of Paspalum notatum and Axonopus compressus in the subtropical region of the Highlands of Central Mexico. Tropical animal health and production, 40(7), pp.509-515.

Ayuba, K., Olorunnaiye, E.S. and Rickson, J., 2014. Application of geotextile materials in soil erosion control. Journal of Research in National Development, 12(2), pp.265-271.

Azadegan, O., Kaffash, A.E., Yaghoubi, M.J. and Pourebrahim, G.R., 2012. Laboratory study on the swelling, cracking and mechanical characteristics of the palm fiber reinforced clay. Electronic Journal of Geotechnical Engineering, 17, pp.47-54.

Azwa, Z.N., Yousif, B.F., Manalo, A.C. and Karunasena, W., 2013. A review on the degradability of polymeric composites based on natural fibres. Materials & Design, 47, pp.424-442.

Babu, G.S., Vasudevan, A.K. and Haldar, S., 2008. Numerical simulation of fiber-reinforced sand behavior. Geotextiles and Geomembranes, 26(2), pp.181-188.

Bartens, J., Day, S.D., Harris, J.R., Dove, J.E. and Wynn, T.M., 2008. Can urban tree roots improve infiltration through compacted subsoils for stormwater management? Journal of Environmental Quality, 37(6), pp.2048-2057.

Bashir, Saqib, Hussain, Qaiser, Akmal, Muhammad, Riaz, Muhammad, Hu, Hongqing, Ijaz, Shahzada Sohail, Iqbal, Muhammad, Abro, Shaukat, Mehmood, Sajid, Ahmad, Munir, 2018. Sugarcane bagasse-derived biochar reduces the cadmium and chromium bioavailability to mash bean and enhances the microbial activity in contaminated soil. J. Soils Sediments 18 (3), 874e886.

Basu, D., Misra, A. and Puppala, A.J., 2014. “Sustainability and geotechnical engineering: perspectives and review.” Canadian Geotechnical Journal, 52(1), pp.96-113. https://doi.org/10.1139/cgj-2013-0120

Basu, G., Roy, A.N., Bhattacharyya, S.K. and Ghosh, S.K., 2009. Construction of unpaved rural road using jute–synthetic blended woven geotextile–A case study. Geotextiles and Geomembranes, 27(6), pp.506-512.

Beal, L.K., Huber, D.P., Godsey, S.E., Nawotniak, S.K. and Lohse, K.A., 2016. Controls on ecohydrologic properties in desert ecosystems: Differences in soil age and volcanic morphology. Geoderma, 271, pp.32-41.

Beg, M.D.H. and Pickering, K.L., 2008. Accelerated weathering of unbleached and bleached Kraft wood fibre reinforced polypropylene composites. Polymer Degradation and Stability, 93(10), pp.1939-1946.

Belmonte, B.A., Benjamin, M.F.D., Tan, R.R., 2018. Bi-objective optimization of biochar-based carbon management networks. J. Clean. Prod. 188, 911e920.

Bera, A.K., Chandra, S.N., Ghosh, A. and Ghosh, A., 2009. Unconfined compressive strength of fly ash reinforced with jute geotextiles. Geotextiles and Geomembranes, 27(5), pp.391-398.

Bergado, D.T., Youwai, S., Hai, C.N. and Voottipruex, P., 2001. Interaction of nonwoven needle-punched geotextiles under axisymmetric loading conditions. Geotextiles and Geomembranes, 19(5), pp.299-328.

Bhattacharyya, R., Fullen, M.A., Booth, C.A., Kertesz, A., Toth, A., Szalai, Z., Jakab, G., Kozma, K., Jankauskas, B., Jankauskiene, G. and Bühmann, C., 2011. Effectiveness of biological geotextiles for soil and water conservation in different agro-environments. Land Degradation & Development, 22(5), pp.495-504.

Bhattacharyya, R., Fullen, M.A., Davies, K. and Booth, C.A., 2009. Utilizing palm-leaf geotextile mats to conserve loamy sand soil in the United Kingdom. Agriculture, ecosystems & environment, 130(1-2), pp.50-58.

Bhave, S. and Sreeja, P., 2013. Influence of initial soil condition on infiltration characteristics determined using a disk infiltrometer. ISH Journal of Hydraulic Engineering, 19(3), pp.291-296.

Bianchi, A., Masseroni, D., Thalheimer, M., de Medici, L.O. and Facchi, A., 2017. Field irrigation management through soil water potential measurements: a review. Ital. J. Agrometeorol, 2, pp.25-38.

Bianchini, F. and Hewage, K., 2012. Probabilistic social cost-benefit analysis for green roofs: a lifecycle approach. Building and Environment, 58, pp.152-162.

Bird, M., Keitel, C. and Meredith, W., 2017. Analysis of biochars for C, H, N, O and S by elemental analyzer. Biochar: A Guide to Analytical Methods, p.39.

Bishop, A.W. and Blight, G.E., 1963. "Some aspects of effective stress in saturated and partly saturated soils." Geotechnique. 13(3): 177-197. https://doi.org/10.1680/geot.1963.13.3.177

Bjerre, A.B. and Skammelsen, S., 1997. Development of chemical and biological processes for production of bioethanol. Optimization of the wet oxidation process and characterization of products (No. RISO-R--967 (EN)). Risoe National Lab..

Bledzki, A.K. and Gassan, J., 1999. Composites reinforced with cellulose based fibres. Progress in polymer science, 24(2), pp.221-274.

Blight, G.E. and Leong, E.C. eds., 2012. "Mechanics of residual soils." CRC Press. https://doi.org/10.1201/b12014-2

Blonquist Jr, J.M., Jones, S.B. and Robinson, D.A., 2006. Precise irrigation scheduling for turfgrass using a subsurface electromagnetic soil moisture sensor. Agricultural water management, 84(1-2), pp.153-165.

Boldrin, D., Leung, A.K. and Bengough, A.G., 2017. Root biomechanical properties during establishment of woody perennials. Ecological Engineering, 109, pp.196-206.

Bos, H.L., 2004. The potential of flax fibres as reinforcement for composite materials. Eindhoven: Technische Universiteit Eindhoven.

Bottinelli, N., Zhou, H., Boivin, P., Zhang, Z.B., Jouquet, P., Hartmann, C. and Peng, X., 2016. Macropores generated during shrinkage in two paddy soils using X-ray micro-computed tomography. Geoderma, 265, pp.78-86.

Boutron, O., Gouy, V., Touze-Foltz, N., Benoit, P., Chovelon, J.M. and Margoum, C., 2009. Geotextile fibres retention properties to prevent surface water nonpoint contamination by pesticides in agricultural areas. Geotextiles and Geomembranes, 27(4), pp.254-261.

Bramley, H., Hutson, J. and Tyerman, S.D., 2003. Floodwater infiltration through root channels on a sodic clay floodplain and the influence on a local tree species Eucalyptus largiflorens. Plant and Soil, 253(1), pp.275-286.

Bruce, D.A. and Jewell, R.A., 1986. Soil nailing: application and practice-part 1. Ground Engineering, 19(8), pp.10-15.

Burns, R.G., 1982. Enzyme activity in soil: location and a possible role in microbial ecology. Soil Biology and Biochemistry, 14(5), pp.423-427.

Cabanettes, F., Joubert, A., Chardon, G., Dumas, V., Rech, J., Grosjean, C. and Dimkovski, Z., 2018. Topography of as built surfaces generated in metal additive manufacturing: A multi scale analysis from form to roughness. Precision Engineering, 52, pp.249-265

Campbell, M.M. and Sederoff, R.R., 1996. Variation in Lignin Content and Composition (Mechanisms of Control and Implications for the Genetic Improvement of Plants). Plant physiology, 110(1), p.3.

Cantoni, R., Collotta, T., Ghionna, V.N. and Moretti, P.C., 1989. A design method for reticulated micropile structures in sliding slopes. Ground engineering, 22(4).

Carsel, R.F. and Parrish, R.S., 1988. Developing joint probability distributions of soil water retention characteristics. Water resources research, 24(5), pp.755-769.

Cassel, D.K. and Nielsen, D.R., 1986. Field capacity and available water capacity. Methods of Soil Analysis: Part 1—Physical and Mineralogical Methods, (methodsofsoilan1), 901-926. https://doi.org/10.2136/sssabookser5.1.2ed.c36

Center, T. D., Hill, M. P., Cordo, H., and Julien, M. H., "Water Hyacinth. Biological Control of Invasive Plants in the Eastern United States," Report No. FHTET-2002-04, US Forest Service, Morgantown, WV, 2002.

Cey, E.E. and Rudolph, D.L., 2009. Field study of macropore flow processes using tension infiltration of a dye tracer in partially saturated soils. Hydrological Processes: An International Journal, 23(12), pp.1768-1779.

Chaduvula, U., Viswanadham, B.V.S. and Kodikara, J., 2017. A study on desiccation cracking behavior of polyester fiber-reinforced expansive clay. Applied Clay Science, 142, pp.163-172.

Chae, J., Kim, B., Park, S.W. and Kato, S., 2010. Effect of suction on unconfined compressive strength in partly saturated soils. KSCE Journal of Civil Engineering, 14(3), pp.281-290.

Chaiyaput, S., Bergado, D.T. and Artidteang, S., 2014. Measured and simulated results of a Kenaf Limited Life Geosynthetics (LLGs) reinforced test embankment on soft clay. Geotextiles and geomembranes, 42(1), pp.39-47.

Chan, E. and Elevitch, C.R., 2006. Cocos nucifera (coconut). Species profiles for Pacific Island agroforestry, 2, pp.1-27.

Chang, S.K., Lee, D.H., Wu, J.H. and Juang, C.H., 2011. Rainfall-based criteria for assessing slump rate of mountainous highway slopes: a case study of slopes along Highway 18 in Alishan, Taiwan. Engineering geology, 118(3-4), pp.63-74.

Chauhan, M.S., Mittal, S. and Mohanty, B., 2008. Performance evaluation of silty sand subgrade reinforced with fly ash and fibre. Geotextiles and geomembranes, 26(5), pp.429-435.

Cheah, J. and Morgan, T.K., 2009. UKU: concept to construction using flax-fibre reinforced stabilised rammed earth. In Proceedings of the 11th International Conference on Non¬-conventional Materials and Technologies (NOCMAT 2009).

Chen, H.X. and Zhang, L.M., 2014. A physically-based distributed cell model for predicting regional rainfall-induced shallow slope failures. Engineering geology, 176, pp.79-92.

Chen, X.W., Wong, J.T.F., Ng, C.W.W. and Wong, M.H., 2016. "Feasibility of biochar application on a landfill final cover—a review on balancing ecology and shallow slope stability." Environ. Sci. Pollut. R. 23(8): 7111-7125. https://doi.org/10.1007/s11356-015-5520-5

Chewonarin, T., Kinouchi, T., Kataoka, K., Arimochi, H., Kuwahara, T., Vinitketkumnuen, U. and Ohnishi, Y., 1999. Effects of roselle (Hibiscus sabdariffa Linn.), a Thai medicinal plant, on the mutagenicity of various known mutagens in Salmonella typhimurium and on formation of aberrant crypt foci induced by the colon carcinogens azoxymethane and 2-amino-1-methyl-6-

phenylimidazo [4, 5-b] pyridine in F344 rats. Food and Chemical Toxicology, 37(6), pp.591-601.

Chunkao, K., Nimpee, C. and Duangmal, K., 2012. The King's initiatives using water hyacinth to remove heavy metals and plant nutrients from wastewater through Bueng Makkasan in Bangkok, Thailand. Ecological Engineering, 39, pp.40-52.

Clothier, B. and Scotter, D., 2002. 3.5 Unsaturated water transmission parameters obtained from infiltration. Methods of Soil Analysis: Part 4 Physical Methods, (methodsofsoilan4), pp.879-898.

Congress IR.:37-2012. Guidelines for the design of flexible pavements. Second Revision, IRC. 2001.

Consoli, N.C., Prietto, P.D. and Ulbrich, L.A., 1998. Influence of fiber and cement addition on behavior of sandy soil. Journal of Geotechnical and Geoenvironmental Engineering, 124(12), pp.1211-1214.

Cordero, J.A., Useche, G., Prat, P.C., Ledesma, A. and Santamarina, C., 2017. Soil desiccation cracks as a suction–contraction process. Géotechnique Letters.

Correia, A.G., Winter, M.G. and Puppala, A.J., 2016. A review of sustainable approaches in transport infrastructure geotechnics. Transportation Geotechnics. 7: 21-28. https://doi.org/10.1016/j.trgeo.2016.03.003

Costa, S., Kodikara, J. and Shannon, B., 2013. Salient factors controlling desiccation cracking of clay in laboratory experiments. Géotechnique. 63(1):18. https://doi.org/10.1680/geot.9.p.105

Costa, S., Kodikara, J., Barbour, S.L. and Fredlund, D.G., 2017. Theoretical analysis of desiccation crack spacing of a thin, long soil layer. Acta Geotechnica. 1-11. https://doi.org/10.1007/s11440-017-0602-9

Cousins, W.J., 1978. Young's modulus of hemicellulose as related to moisture content. Wood science and technology, 12(3), pp.161-167.

Crafter, S. A., Njuguna, S. G., and Howard, G. W., “Wetlands of Kenya,” presented at the KWWG Seminar on Wetlands of Kenya, National Museums of Kenya, Nairobi, Kenya, July 3–5 1992, ICUN, Gland, Switzerland, -unpublished.

Cucci, G., Lacolla, G. and Caranfa, G., 2018. Spatial distribution of roots and cracks in soils cultivated with sunflower. Archives of Agronomy and Soil Science, 64(1), pp.13-24.

Cui, Y.J., Tang, C.S., Tang, A.M. and Ta, A.N., 2014. Investigation of soil desiccation cracking using an environmental chamber. Italian Geotechnical Journal. 1: 9-20.

Czepiel, P.M., Mosher, B., Crill, P.M. and Harriss, R.C., 1996. Quantifying the effect of oxidation on landfill methane emissions. Journal of geophysical research: Atmospheres, 101(D11), pp.16721-16729.

Danso, H., Martinson, B., Ali, M. and Mant, C., 2015. Performance characteristics of enhanced soil blocks: a quantitative review. Building Research & Information, 43(2), pp.253-262.

Danso, H., Martinson, D.B., Ali, M. and Williams, J.B., 2015, June. Effects of sugarcane bagasse fibre on the strength properties of soil blocks. In First International Conference on Bio-Based Building Materials.

Das, G.K., Hazra, B., Garg, A. and Ng, C.W.W., 2018. "Stochastic hydro-mechanical stability of vegetated slopes: An integrated copula based framework." Catena. 160: 124-133. https://doi.org/10.1016/j.catena.2017.09.009

Dasaka, S.M. and Sumesh, K.S., 2011. Effect of coir fiber on the stress–strain behavior of a reconstituted fine-grained soil. Journal of natural fibers, 8(3), pp.189-204.

Dasog, G.S. and Shashidhara, G.B., 1993. Dimension and volume of cracks in a Vertisol under different crop covers. Soil science, 156(6), pp.424-428.

Dasog, G.S., Acton, D.F., Mermut, A.R. and Jong, E.D., 1988. Shrink-swell potential and cracking in clay soils of Saskatchewan. Canadian Journal of Soil Science, 68(2), pp.251-260.

Davies, K., Fullen, M.A. and Booth, C.A., 2006. A pilot project on the potential contribution of palm-mat geotextiles to soil conservation. Earth Surface Processes and Landforms: The Journal of the British Geomorphological Research Group, 31(5), pp.561-569.

Davis, S.L. and Dukes, M.D., 2010. Irrigation scheduling performance by evapotranspiration-based controllers. Agricultural water management, 98(1), pp.19-28.

De Bhowmick, Goldy, Ajit K. Sarmah, and Ramkrishna Sen. "Production and characterization of a value added biochar mix using seaweed, rice husk and pine sawdust: A parametric study." Journal of Cleaner Production 200 (2018): 641-656.

de Melo Carvalho, M.T., de Holanda Nunes Maia, A., Madari, B.E., Bastiaans, L., Van Oort, P.A.J., Heinemann, A.B., Soler da Silva, M.A., Petter, F.A., Marimon Jr, B.H. and Meinke, H., 2014. Biochar increases plant-available water in a sandy loam soil under an aerobic rice crop system. Solid Earth, 5(2), pp.939-952.

Decagon Devices, 2016a. “Operator’s manual version 2. EC-5 Soil Moisture Sensor.” Decagon Devices, Inc.950 NE Nelson Court, Pullman, WA99163.

Decagon Devices, 2016b. “Operator’s manual version 2. MPS-2 & MPS-6 Dielectric Water Potential Sensors.” Decagon Devices, Inc.950 NE Nelson Court, Pullman, WA99163.

Decagon Devices, D. (2006). Leaf porometer. Operator’s manual. Version 1.0. Decagon Devices. Inc., Pullman, WA.

Decagon devices. Minidisk Infiltrometer User’s Manual Version 10. Decagon Devices, Pullman, WA. 2013.

Delage, P., Audiguier, M., Cui, Y.J. and Howat, M.D., 1996. Microstructure of a compacted silt. Canadian Geotechnical Journal, 33(1), pp.150-158.

Delmer, D. P. and Amor, Y., “Cellulose Biosynthesis,” Plant Cell, Vol. 7, No. 7, 1995, pp. 987–1000.

Dexter, A.R., 2004. Soil physical quality: Part I. Theory, effects of soil texture, density, and organic matter, and effects on root growth. Geoderma, 120(3-4), pp.201-214.

Diambra, A., Russell, A.R., Ibraim, E. and Muir Wood, D., 2007. Determination of fibre orientation distribution in reinforced sands. Géotechnique, 57(7), pp.623-628.

Dileep, A., Balan, K., and Vincent, S., “Effect of Water Hyacinth on Engineering Properties of Clayey Soil,” presented at the Proceedings of Indian Geotechnical Conference, Roorkee, India, December 22–24, 2013.

Dittenber, D.B. and GangaRao, H.V., 2012. Critical review of recent publications on use of natural composites in infrastructure. Composites Part A: Applied Science and Manufacturing, 43(8), pp.1419-1429.

Divya, P.V., Viswanadham, B.V.S. and Gourc, J.P., 2018. Hydraulic conductivity behaviour of soil blended with geofiber inclusions. Geotextile and Geomembranes. 46(2): 121-130. https://doi.org/10.1016/j.geotexmem.2017.10.008

Dohnal, M., Dusek, J. and Vogel, T., 2010. Improving hydraulic conductivity estimates from minidisk infiltrometer measurements for soils with wide pore-size distributions. Soil Science Society of America Journal, 74(3), pp.804-811.

Dungani, R., Karina, M., Sulaeman, A., Hermawan, D. and Hadiyane, A., 2016. Agricultural waste fibers towards sustainability and advanced utilization: a review. Asian Journal of Plant Sciences, 15(1/2): 42-55. https://doi.org/10.3923/ajps.2016.42.55

Dutta, R.K., Khatri, V.N. and Gayathri, V., 2012. Effect of addition of treated coir fibres on the compression behaviour of clay. Jordan journal of civil engineering, 159(700), pp.1-13.

Dykhuizen, R.C., 1987. Transport of solutes through unsaturated fractured media. Water Research, 21(12), pp.1531-1539.

El-Shekeil, Y.A., Sapuan, S.M., Jawaid, M. and Al-Shuja'a, O.M., 2014. Influence of fiber content on mechanical, morphological and thermal properties of kenaf fibers reinforced poly (vinyl chloride)/thermoplastic polyurethane poly-blend composites. Materials & Design, 58, pp.130-135.

English, B., 1995. Geotextiles–a specific application of biofibers. Proc a Semin Res Ind Appl Non Food Crop, pp.79-86.

Faruk, O., Bledzki, A.K., Fink, H.P. and Sain, M., 2012. Biocomposites reinforced with natural fibers: 2000–2010. Progress in polymer science, 37(11), pp.1552-1596.

Feddes, R., Kowalik, P., Zaradny, H., 1982. Simulation of Field Water Use and Crop Yield. Centre for Agricultural Publishing and Documentation, Wageningen, the Netherlands

Flury, M. and Flühler, H., 1994. Brilliant Blue FCF as a dye tracer for solute transport studies—a toxicological overview. Journal of Environmental Quality, 23(5), pp.1108-1112.

Fodor, N., Sándor, R., Orfanus, T., Lichner, L. and Rajkai, K., 2011. Evaluation method dependency of measured saturated hydraulic conductivity. Geoderma, 165(1), pp.60-68.

Fox, W.E., 1964. A study of bulk density and water in a swelling soil. Soil Science, 98(5), pp.307 316.

Frederick, T.W. and Norman, W., 2004. Natural fibers plastics and composites. EUA: Kluwer Academic Publishers.

Fredlund, D.G., Rahardjo, H. and Rahardjo, H., 1993. Soil mechanics for unsaturated soils. John Wiley & Sons.

Frost, J.D. and Han, J., 1999. Behavior of interfaces between fiber-reinforced polymers and sands. Journal of geotechnical and geoenvironmental engineering, 125(8), pp.633-640.

Gadi, V.K., Bordoloi, S., Garg, A., Kobayashi, Y. and Sahoo, L., 2016. Improving and correcting unsaturated soil hydraulic properties with plant parameters for agriculture and bioengineered slopes. Rhizosphere, 1, pp.58-78.

Gadi, V.K., Bordoloi, S., Garg, A., Sahoo, L., Berretta, C. and Sekharan, S., 2018. Effect of shoot parameters on cracking in vegetated soil. Environmental Geotechnics, 5(2), pp.123-130.

Gadi, V.K., Garg, A., Prakash, S., Wei, L. and Andriyas, S., 2018. A non-intrusive image analysis technique for measurement of heterogeneity in grass species around tree vicinity in a green infrastructure. Measurement, 114: 132-143.

Garg, A. and Ng, C.W.W., 2015. Investigation of soil density effect on suction induced due to root water uptake by Schefflera heptaphylla. Journal of Plant Nutrition and Soil Science, 178(4), pp.586-591.

Garg, A., Coo, J.L. and Ng, C.W.W., 2015. Field study on influence of root characteristics on soil suction distribution in slopes vegetated with Cynodon dactylon and Schefflera heptaphylla. Earth Surface Processes and Landforms, 40(12), pp.1631-1643.

Garg, A., Leung, A.K. and Ng, C.W.W., 2015. Comparisons of soil suction induced by evapotranspiration and transpiration of S. heptaphylla. Canadian Geotechnical Journal, 52(12), pp.2149-2155.

Gassan, J., Chate, A., and Bledzki, A. K., “Calculation of Elastic Properties of Natural Fibers,” J. Mater. Sci., Vol. 36, No. 15, 2001, pp. 3715–3720.

Genet, M., Stokes, A., Salin, F., Mickovski, S.B., Fourcaud, T., Dumail, J.F. and Van Beek, R., 2005. The influence of cellulose content on tensile strength in tree roots. Plant and Soil. 278(1-2): 1-9. https://doi.org/10.1007/978-1-4020-5593-5_1

Ghavami, K., Toledo Filho, R.D. and Barbosa, N.P., 1999. Behaviour of composite soil reinforced with natural fibres. Cement and Concrete Composites, 21(1), pp.39-48.

Ghestem, M., Sidle, R.C. and Stokes, A., 2011. The influence of plant root systems on subsurface flow: implications for slope stability. Bioscience, 61(11), pp.869-879.

Giridhar, J., Kishore and Rao, R.M.V.G.K., 1986. Moisture absorption characteristics of natural fibre composites. Journal of reinforced plastics and composites, 5(2), pp.141-150.

Goering, H.K., Van soest PJ 1970. Forage fiber analyses (apparatus, reagents, procedures and some applications). Agriculture handbook, 379, p.20.

Gopal, P., Ratnam, R., Farooq, M., Garg, A. and Gogoi, N., 2018, October. Influence of Biochar Obtained from Invasive Weed on Infiltration Rate and Cracking of Soils: An Integrated Experimental and Artificial Intelligence Approach. In The International Congress on Environmental Geotechnics (pp. 351-358). Springer, Singapore.

Gray, D.H. and Al-Refeai, T., 1986. Behavior of fabric-versus fiber-reinforced sand. Journal of Geotechnical Engineering, 112(8), pp.804-820.

Gray, D.H. and Ohashi, H., 1983. Mechanics of fiber reinforcement in sand. Journal of Geotechnical Engineering, 109(3), pp.335-353.

Green, V.S., Stott, D.E. and Diack, M., 2006. Assay for fluorescein diacetate hydrolytic activity: optimization for soil samples. Soil Biology and Biochemistry, 38(4), pp.693-701.

Greenwood, J.R., Norris, J.E. and Wint, J., 2004. Assessing the contribution of vegetation to slope stability. Proceedings of the ICE-Geotechnical Engineering, 157(4), pp.199-207.

Gruda, N., 2008. The effect of wood fiber mulch on water retention, soil temperature and growth of vegetable plants. Journal of sustainable agriculture, 32(4), pp.629-643.

Gu, H., 2009. Tensile behaviours of the coir fibre and related composites after NaOH treatment. Materials & Design, 30(9), pp.3931-3934.

Guhathakurta, P., Sreejith, O.P. and Menon, P.A., 2011. Impact of climate change on extreme rainfall events and flood risk in India. Journal of earth system science, 120(3), p.359.

Güllü, H. and Khudir, A., 2014. Effect of freeze–thaw cycles on unconfined compressive strength of fine-grained soil treated with jute fiber, steel fiber and lime. Cold Regions Science and Technology, 106, pp.55-65.

Guo, Y., Han, C. and Yu, X., 2017. "Laboratory characterization and discrete element modeling of shrinkage and cracking in clay layer." Can. Geotech. J. 999: 1-9. https://doi.org/10.1139/cgj-2016-0674

Hamidi, A. and Hooresfand, M., 2013. Effect of fiber reinforcement on triaxial shear behavior of cement treated sand. Geotextiles and Geomembranes, 36, pp.1-9.

Hathaway, R.L. and Penny, D., 1975. Root strength in some Populus and Salix clones. New Zealand Journal of Botany, 13(3), pp.333-344.

Hawkins, T.R., Beyersdorff, L.E. and Vitale, R.W., Midwest Industrial Supply Inc, 2006. Method of chemical soil stabilization and dust control. U.S. Patent 7,081,270.

Hazra, B., Gadi, V., Garg, A., Ng, C.W.W. and Das, G.K., 2017. Probabilistic analysis of suction in homogeneously vegetated soils. Catena, 149, pp.394-401.

Hearle, J.W. and Morton, W.E., 2008. Physical properties of textile fibres. Elsevier.

Hejazi, S.M., Sheikhzadeh, M., Abtahi, S.M. and Zadhoush, A., 2012. A simple review of soil reinforcement by using natural and synthetic fibers. Construction and building materials, 30, pp.100-116.

Hejazi, S.M., Sheikhzadeh, M., Abtahi, S.M. and Zadhoush, A., 2012. A simple review of soil reinforcement by using natural and synthetic fibers. Construction and building materials, 30, pp.100-116.

Hill, C.A., Khalil, H.A. and Hale, M.D., 1998. A study of the potential of acetylation to improve the properties of plant fibres. Industrial Crops and Products, 8(1), pp.53-63.

Holliger, C. and Zehnder, A. J., “Anaerobic Biodegradation of Hydrocarbons,” Curr. Opin. Biotechnol., Vol. 7, No. 3, 1996, pp. 326–330.

Holtz, R.D. and Sivakugan, N., 1987. Design charts for roads with geotextiles. Geotextiles and Geomembranes, 5(3), pp.191-199

Homolák, M., Capuliak, J., Pichler, V. and Lichner, Ľ., 2009. Estimating hydraulic conductivity of a sandy soil under different plant covers using minidisk infiltrometer and a dye tracer experiment. Biologia, 64(3), pp.600-604.

Hughes, J.M.O., Withers, N.J. and Greenwood, D.A., 1975. A field trial of the reinforcing effect of a stone column in soil. Geotechnique, 25(1), pp.31-44.

Ibrahim, A., Usman, A.R.A., Al-Wabel, M.I., Nadeem, M., Ok, Y.S. and Al-Omran, A., 2017. Effects of conocarpus biochar on hydraulic properties of calcareous sandy soil: influence of particle size and application depth. Archives of Agronomy and Soil Science, 63(2), pp.185-197.

Ibraim, E., Diambra, A., Russell, A.R. and Wood, D.M., 2012. Assessment of laboratory sample preparation for fibre reinforced sands. Geotextiles and Geomembranes, 34, pp.69-79.

Indraratna, B., Muttuvel, T., Khabbaz, H. and Armstrong, R., 2008. Predicting the erosion rate of chemically treated soil using a process simulation apparatus for internal crack erosion. Journal of Geotechnical and Geoenvironmental Engineering, 134(6), pp.837-844.

IRC, 37. 2012. Guidelines for the design of flexible pavements (Third revision). Indian code of practice.

IS (1991) 1670-1991. "Determination of Breaking Load and Elongation at Break of Single Strand Textiles and Yarns." Bureau of Indian Standards Publications, New Delhi.

IS (1991) 2720-Part 3-1980 "Methods of Test for Soils. Determination of Specific Gravity." Bureau of Indian Standards Publications, New Delhi.

IS-2720 (Part 10). "Determination of Unconfined Compressive Strength". Bureau of Indian Standards Publications, New Delhi. (1991).

IS-2720-Part 16, Methods of Test for Soils. Laboratory Determination of CBR, Bureau of Indian Standards Publications, New Delhi, India, 1987.

IS-2720-Part 3, 1980. Methods of Test for Soils. Determination of Specific Gravity, Bureau of Indian Standards Publications, New Delhi, India,

IS-9669, Specifications for CBR moulds and its Accessories, Bureau of Indian Standards Publications, New Delhi, India, 1980.

Islam, M.S. and Iwashita, K., 2010. Earthquake resistance of adobe reinforced by low cost traditional materials. Journal of Natural Disaster Science, 32(1), pp.1-21.

Islam, S., 2013. Use of vegetation and geo-jute for slope protection.

Ismail, S. and Yaacob, Z., 2011. Properties of laterite brick reinforced with oil palm empty fruit bunch fibres. Pertanika Journal of Science and Technology, 19(1), pp.33-43.

ISO, D., 13322-1. Particle Size Analyis-Image Analysis Methods, Part, 1.

ISO, I., 9276-6 Representation of Results of Particle Size Analysis–Part 6: Descriptive and Quantitative Representation of Particle Shape and Morphology. 2008.

Jähn, A., Schröder, M.W., Füting, M., Schenzel, K. and Diepenbrock, W., 2002. Characterization of alkali treated flax fibres by means of FT Raman spectroscopy and environmental scanning electron microscopy. Spectrochimica Acta Part A: Molecular and Biomolecular Spectroscopy, 58(10), pp.2271-2279.

Jairaj, C., Kumar, M.P. and Raghunandan, M.E., 2018. "Compaction characteristics and strength of BC soil reinforced with untreated and treated coir fibers." Innovative Infrastructure Solutions. 3(1): 21. https://doi.org/10.1007/s41062-017-0123-2

Jamellodin, Z., Talib, Z., Kolop, R. and Noor, N., 2010, August. The effect of oil palm fibre on strength behaviour of soil. In Proceedings of the 3rd Southeast Asian Natural Resources and Environmental Management (SANREM) Conference, Kota Kinabalu, Sabah, Malaysia (pp. 3-5).

Jayanthi, P.N.V., Kuntikana, G. and Singh, D.N., 2017. Stabilization of Fine-Grained Soils against Desiccation Cracking Using Sustainable Materials. Advances in Civil Engineering Materials, 6(1), pp.36-67.

Jayawardhana, Y., Kumarathilaka, P., Herath, I., & Vithanage, M., 2016. Municipal solid waste biochar for prevention of pollution from landfill leachate. In Environ mater waste. 117-148.

Jenkins, S.H., 1930. The determination of cellulose in straws. Biochemical Journal, 24(5), p.1428.

Ji, C., Cheng, K., Nayak, D., Pan, G., 2018. Environmental and economic assessment of crop residue competitive utilization for biochar, briquette fuel and combined heat and power generation. Journal of Cleaner Production. 192, 916e923

Jiang, C., Zhao, G.F. and Khalili, N., 2017. On crack propagation in brittle material using the distinct lattice spring model. International Journal of Solids and Structures, 118, pp.41-57.

John, M.J. and Thomas, S., 2008. Biofibres and biocomposites. Carbohydrate polymers, 71(3), pp.343-364.

Johnson, J.R. and Hill, H.O., 1944. A study of shrinkage and swelling properties of Rendzina soils. In Soil Sci. Soc. Am. Proc. 9 (pp. 24-29).

Johnson, M.S. and Lehmann, J., 2006. Double-funneling of trees: Stemflow and root-induced preferential flow. Ecoscience, 13(3), pp.324-333.

Johnson, W.C., 1962. Controlled Soil Cracking as a Possible Means of Moisture Conservation on Wheatlands of the Southwestern Great Plains 1. Agronomy Journal, 54(4), pp.323-325.

Joseph, K., Mattoso, L.H.C., Toledo, R.D., Thomas, S., Carvalho, B.J., Pothen, L. and Kala, S., 2000. Natural Fiber Reinforced Thermoplastic Composites. Nat. Polymer Agro Fiber Based Composites, pp.159-200.

Juang, C.H., Jhi, Y.Y. and Lee, D.H., 1998. Stability analysis of existing slopes considering uncertainty. Engineering Geology, 49(2), pp.111-122.

Kaniraj, S.R. and Gayathri, V., 2003. Geotechnical behavior of fly ash mixed with randomly oriented fiber inclusions. Geotextiles and Geomembranes, 21(3), pp.123-149.

Kaniraj, S.R. and Havanagi, V.G., 2001. Behavior of cement-stabilized fiber-reinforced fly ash-soil mixtures. Journal of geotechnical and geoenvironmental engineering, 127(7), pp.574-584.

Kersavage, P.C., 1973. system for automatically recording the load-elongation characteristics of single wood fibers under controlled relative humidity conditions.

Khalil, H.A., Hossain, M.S., Rosamah, E., Azli, N.A., Saddon, N., Davoudpoura, Y., Islam, M.N. and Dungani, R., 2015. The role of soil properties and its interaction towards quality plant fiber: A review. Renewable and Sustainable Energy Reviews, 43, pp.1006-1015.

Khan, F.S., Azam, S., Raghunandan, M.E. and Clark, R., 2014. Compressive strength of compacted clay-sand mixes. Advances in Materials Science and Engineering, 2014.

Khedari, J., Charoenvai, S. and Hirunlabh, J., 2003. New insulating particleboards from durian peel and coconut coir. Building and environment, 38(3), pp.435-441.

Khedari, J., Watsanasathaporn, P. and Hirunlabh, J., 2005. Development of fibre-based soil–cement block with low thermal conductivity. Cement and concrete composites, 27(1), pp.111-116.

Krisnanto, S., Rahardjo, H., Fredlund, D.G. and Leong, E.C., 2014. Mapping of cracked soils and lateral water flow characteristics through a network of cracks. Engineering Geology 172, pp.12-25. https://doi.org/10.1016/j.enggeo.2014.01.002

Krisnanto, S., Rahardjo, H., Fredlund, D.G. and Leong, E.C., 2016. Water content of soil matrix during lateral water flow through cracked soil. Engineering Geology 210, pp.168-179. https://doi.org/10.1016/j.enggeo.2016.06.012

Kumar, D., Nigam, S., Nangia, A. and Tiwari, S., 2015. Improvement in CBR values of soil reinforced with jute fibre. Int. J. Engrg. Tech. Res, 3(5), pp.290-293.

Lam, C.C. and Leung, Y.K., 1994. Extreme rainfall statistics and design rainstorm profiles at selected locations in Hong Kong. Royal Observatory.

Lazarovitch, N., Vanderborght, J., Jin, Y. and van Genuchten, M.T., 2018. The Root Zone: Soil Physics and Beyond. Vadose Zone Journal, 17(1).

Leao, A.L., Rowell, R. and Tavares, N., 1998. Applications of natural fibers in automotive industry in Brazil—thermoforming process. In Science and technology of polymers and advanced materials (pp. 755-761). Springer, Boston, MA.

Lee, F.H., Lo, K.W. and Lee, S.L., 1988. "Tension crack development in soils." J. Geotech. Eng-Asce. 114(8):915-929. https://doi.org/10.1061/(asce)0733-9410(1988)114:8(915)

Lehmann, J., Joseph, S. (Eds.), 2015. Biochar for Environmental Management: Science, Technology and Implementation. Routledge

Lekha, K.R., 2004. Field instrumentation and monitoring of soil erosion in coir geotextile stabilised slopes—a case study. Geotextiles and Geomembranes, 22(5), pp.399-413.

Leong, E.C. and Rahardjo, H., 1997. Review of soil-water characteristic curve equations. Journal of geotechnical and geoenvironmental engineering, 123(12), pp.1106-1117.

Leung, A.K., Garg, A. and Ng, C.W.W., 2015. Effects of plant roots on soil-water retention and induced suction in vegetated soil. Engineering Geology, 193, pp.183-197.

Lewis, S.A., Wu, J.Q. and Robichaud, P.R., 2006. Assessing burn severity and comparing soil water repellency, Hayman Fire, Colorado. Hydrological Processes: An International Journal, 20(1), pp.1-16.

Li, C., 2005. Mechanical response of fiber-reinforced soil (Doctoral dissertation).

Li, D.Q., Jiang, S.H., Cao, Z.J., Zhou, W., Zhou, C.B. and Zhang, L.M., 2015. A multiple response-surface method for slope reliability analysis considering spatial variability of soil properties. Engineering Geology, 187, pp.60-72.

Li, F., Shen, K., Long, X., Wen, J., Xie, X., Zeng, X., Liang, Y., Wei, Y., Lin, Z., Huang, W. and Zhong, R., 2016. Preparation and characterization of biochars from Eichornia crassipes for cadmium removal in aqueous solutions. PloS one, 11(2), p.e0148132.

Li, J. and Zhang, L., 2009, October. Formation and repeatability of crack network in soil. In Proceedings of the 17th International Conference on Soil Mechanics and Geotechnical Engineering, Alexandria, Egypt (pp. 5-9).

Li, J.H. and Zhang, L.M., 2010. Geometric parameters and REV of a crack network in soil. Computers and Geotechnics, 37(4), pp.466-475.

Li, J.H. and Zhang, L.M., 2011. Study of desiccation crack initiation and development at ground surface. Engineering Geology, 123(4), pp.347-358.

Li, J.H., Li, L., Chen, R. and Li, D.Q., 2016. Cracking and vertical preferential flow through landfill clay liners. Engineering Geology, 206, pp.33-41.

Li, J.H., Lu, Z., Guo, L.B. and Zhang, L.M., 2017. Experimental study on soil-water characteristic curve for silty clay with desiccation cracks. Engineering Geology 218,70-76.

Li, J.H., Zhang, L.M. and Li, X., 2011. Soil-water characteristic curve and permeability function for unsaturated cracked soil. Canadian Geotechnical Journal, 48(7), pp.1010-1031.

Li, X., Tabil, L.G. and Panigrahi, S., 2007. Chemical treatments of natural fiber for use in natural fiber-reinforced composites: a review. Journal of Polymers and the Environment, 15(1), pp.25-33.

Li, Y., Mai, Y.W. and Ye, L., 2000. Sisal fibre and its composites: a review of recent developments. Composites science and technology, 60(11), pp.2037-2055.

Lichner, L., Orfánus, T.O.M.Á.Š., Nováková, K.A.T.A.R.Í.N.A., Šír, M.I.L.O.S.L.A.V. and Tesař, M.I.R.O.S.L.A.V., 2007. The impact of vegetation on hydraulic conductivity of sandy soil. Soil Water Res, 2, pp.59-66.

Ling, H.I., Leshchinsky, D. and Tatsuoka, F. eds., 2003. Reinforced soil engineering: advances in research and practice. CRC Press.

Liu, R., Liu, G., Yousaf, B. and Abbas, Q., 2018. Operating conditions-induced changes in product yield and characteristics during thermal-conversion of peanut shell to biochar in relation to economic analysis. Journal of cleaner production, 193, pp.479-490.

Liyanage, M.D.S., Jayasekara, K.S. and Fernandopulle, M.N., 1993. "Effects of application of coconut husk and coir dust on the yield of coconut." In Cocos 9: 15-22. https://doi.org/10.4038/cocos.v9i0.2125

Look, B.G., 2016.The weighted plasticity index in road design and construction. Australian Geomechanics. 5(3).

López-Vicente, M. and Álvarez, S., 2018. Influence of DEM resolution on modelling hydrological connectivity in a complex agricultural catchment with woody crops. Earth Surface Processes and Landforms, 43(7), pp.1403-1415.

Lu, S.G., Sun, F.F. and Zong, Y.T., 2014. Effect of rice husk biochar and coal fly ash on some physical properties of expansive clayey soil (Vertisol). Catena, 114, pp.37-44.

Madsen, M.D. and Chandler, D.G., 2007. Automation and use of mini disk infiltrometers. Soil Science Society of America Journal, 71(5), pp.1469-1472.

Mahamadi, C. and Nharingo, T., 2010. Utilization of water hyacinth weed (Eichhornia crassipes) for the removal of Pb (II), Cd (II) and Zn (II) from aquatic environments: an adsorption isotherm study. Environmental technology, 31(11), pp.1221-1228.

Maher, M.H. and Gray, D.H., 1990. Static response of sands reinforced with randomly distributed fibers. Journal of Geotechnical Engineering, 116(11), pp.1661-1677.

Maher, M.H. and Ho, Y.C., 1994. Mechanical properties of kaolinite/fiber soil composite. Journal of Geotechnical Engineering, 120(8), pp.1381-1393.

Malik, A., 2007. Environmental challenge vis a vis opportunity: the case of water hyacinth. Environment international, 33(1), pp.122-138.

Maneecharoen, J., Htwe, W., Bergado, D.T. and Baral, P., 2013. Ecological erosion control by limited life geotextiles (LLGs) as well as with Vetiver and Ruzi grasses. Indian Geotechnical Journal, 43(4), pp.388-406.

Marandi, S.M., Bagheripour, M.H., Rahgozar, R. and Zare, H., 2008. Strength and ductility of randomly distributed palm fibers reinforced silty-sand soils. American Journal of Applied Sciences, 5(3), pp.209-220.

Marschner, B. and Kalbitz, K., 2003. Controls of bioavailability and biodegradability of dissolved organic matter in soils". Geoderma, 113(3), pp.211-235.

Martins, A.P.S., Silva, F.A. and Toledo Filho, R.D., 2015. Mechanical behavior of self-compacting soil-cement-sisal fiber composites. In Key Engineering Materials (Vol. 634, pp. 421-432). Trans Tech Publications.

Martins, D.A.B., do Prado, H.F.A., Leite, R.S.R., Ferreira, H., de Souza Moretti, M.M., da Silva, R. and Gomes, E., 2011. Agroindustrial wastes as substrates for microbial enzymes production and source of sugar for bioethanol production. In Integrated Waste Management-Volume II. InTech.

Mattone, R., 2005. Sisal fibre reinforced soil with cement or cactus pulp in bahareque technique. Cement and Concrete Composites, 27(5), pp.611-616.

McKenzie, A.W. and Yuritta, J.P., 1979. Wood fibre reinforced polymers. Appita.

Meriles, J.M., Gil, S.V., Conforto, C., Figoni, G., Lovera, E., March, G.J. and Guzman, C.A., 2009. Soil microbial communities under different soybean cropping systems: characterization of microbial population dynamics, soil microbial activity, microbial biomass, and fatty acid profiles. Soil and Tillage Research, 103(2), pp.271-281.

Mesbah, A., Morel, J.C., Walker, P. and Ghavami, K., 2004. Development of a direct tensile test for compacted earth blocks reinforced with natural fibers. Journal of Materials in Civil Engineering, 16(1), pp.95-98.

Meshesha, D.T., Tsunekawa, A. and Haregeweyn, N., 2016. Determination of soil erodibility using fluid energy method and measurement of the eroded mass. Geoderma, 284, pp.13-21.

Methacanon, P., Weerawatsophon, U., Thainthongdee, M. and Lekpittaya, P., 2010. Optimum conditions for selective separation of kraft lignin. Kasetsart J.(Nat. Sci.), 44(4), pp.680-690.

Michalowski, R.L. and Zhao, A., 1996. Failure of fiber-reinforced granular soils. Journal of Geotechnical Engineering, 122(3), pp.226-234.

Miller, C.J. and Rifai, S., 2004. Fiber reinforcement for waste containment soil liners. Journal of Environmental Engineering, 130(8), pp.891-895. https://doi.org/10.1061/(asce)0733-9372(2004)130:8(891)

Miller, C.J., Mi, H. and Yesiller, N., 1998. Experimental analysis of desiccation crack propagation in clay liners 1. JAWRA Journal of the American Water Resources Association, 34(3), pp.677-686.

Millogo, Y., Aubert, J.E., Hamard, E. and Morel, J.C., 2015. How properties of kenaf fibers from Burkina Faso contribute to the reinforcement of earth blocks. Materials, 8(5), pp.2332-2345.

Mishra, S., Mohanty, A.K., Drzal, L.T., Misra, M., Parija, S., Nayak, S.K. and Tripathy, S.S., 2003. Studies on mechanical performance of biofibre/glass reinforced polyester hybrid composites. Composites Science and Technology, 63(10), pp.1377-1385.

Mitchell, A.R. and Van Genuchten, M.T., 1992. Shrinkage of bare and cultivated soil. Soil Science Society of America Journal, 56(4), pp.1036-1042.

Monteith, J.L., 1965. Evaporation and environment, in the state and movement of water in living organisms. In Symp. Soc. Exp. Biol. (pp. 205-234). Academic Press.

Moody, J.A., Kinner, D.A. and Úbeda, X., 2009. Linking hydraulic properties of fire-affected soils to infiltration and water repellency. Journal of Hydrology, 379(3-4), pp.291-303.

Moore, K.J. and Jung, H.J.G., 2001. Lignin and fiber digestion. Journal of range management, pp.420-430.

Morgan, R.P. and Rickson, R.J., 2003. Slope stabilization and erosion control: a bioengineering approach. Taylor & Francis.

Morris, P.H., Graham, J. and Williams, D.J., 1992. Cracking in drying soils. Canadian Geotechnical Journal. 29(2): 263-277. https://doi.org/10.1139/t92-030

Mwaikambo, L.Y. and Ansell, M.P., 2002. Chemical modification of hemp, sisal, jute, and kapok fibers by alkalization. Journal of applied polymer science, 84(12), pp.2222-2234.

Mwaikambo, L.Y., Tensile Properties of Alkalised Jute Fibres. BioResources, Vol. 4, No. 2, 2009, pp. 566–588.

Mwasha, A. and Petersen, A., 2010. Thinking outside the box: The time dependent behaviour of a reinforced embankment on soft soil. Materials & Design (1980-2015), 31(5), pp.2360-2367.

Mwasha, P.A., 2009. Coir fibre: a sustainable engineering material for the Caribbean environment. The College of the Bahamas Research Journal, 15, pp.36-44.

Namango, S.S., 2006. Development of Cost Effective Earthen Building Material for Housing Wall Construction: Investigations into the Properties of Compressed Earth Blocks Stabilized with Sisal Vegetable Fibres, Cassava Powder and Cement Compositions (Doctoral dissertation, Verlag nicht ermittelbar).

Ng, C.W.W. and Leung, A.K., 2011. Measurements of drying and wetting permeability functions using a new stress-controllable soil column. Journal of Geotechnical and Geoenvironmental Engineering, 138(1), pp.58-68.

Ng, C.W.W. and Menzies, B., 2014. Advanced unsaturated soil mechanics and engineering. CRC Press.

Ng, C.W.W., Leung, A.K. and Woon, K.X., 2013. Effects of soil density on grass-induced suction distributions in compacted soil subjected to rainfall. Canadian Geotechnical Journal, 51(3), pp.311-321.

Ng, C.W.W., Leung, A.K., Garg, A., Woon, K.X., Chu, L.M. and Hau, B.C.H., 2013, September. Soil suction induced by grass and tree in an atmospheric-controlled plant room. In Proceedings of the 18th International Conference on Soil Mechanics and Geotechnical Engineering, Paris (pp. 1167-1170).

Ng, C.W.W., Ni, J.J., Leung, A.K., Zhou, C. and Wang, Z.J., 2016. Effects of planting density on tree growth and induced soil suction. Géotechnique, 66(9), pp.711-724.

Ng, C.W.W., Woon, K.X., Leung, A.K. and Chu, L.M., 2013. Experimental investigation of induced suction distribution in a grass-covered soil. Ecological engineering, 52, pp.219-223.

Nguyen, T., Zavarin, E. and Barrall, E.M., 1981. Thermal Analysis of lignocellulosic materials: Part I. Unmodified materials. Journal of Macromolecular Science—Reviews in Macromolecular Chemistry, 20(1), pp.1-65.

Ni, J.J., Chen, X.W., Ng, C.W.W. and Guo, H.W., 2018. Effects of biochar on water retention and matric suction of vegetated soil. Géotechnique Letters, 8(2), pp.124-129.

Ni, J.J., Leung, A.K., Ng, C.W.W. and Shao, W., 2018. Modelling hydro-mechanical reinforcements of plants to slope stability. Computers and Geotechnics 95: 99-109. https://doi.org/10.1016/j.compgeo.2017.09.001

Ni, J.J., Leung, A.K., Ng, C.W.W. and So, P.S., 2016. Investigation of plant growth and transpiration-induced matric suction under mixed grass–tree conditions. Canadian Geotechnical Journal, 54(4), pp.561-573.

Nieber, J.L., 1982. Finite Element Analysis of Soil Moisture Flow and Moisture Stress in a Dessicating Soil. In Finite Elements in Water Resources (pp. 717-726). Springer, Berlin, Heidelberg.

Novak, V., Šimåunek, J. and Genuchten, M.T.V., 2000. Infiltration of water into soil with cracks. Journal of Irrigation and Drainage Engineering, 126(1), pp.41-47.

Novich, B.E., Maher, A. and Neubauer, J.A., PPG Industries Ohio Inc, 2000. Fiber-reinforced soil mixtures. U.S. Patent 6,042,305.

Nsiah, P.K. and Schaaf, W., 2018. The potentials of biological geotextiles in erosion and sediment control during gold mine reclamation in Ghana. Journal of Soils and Sediments, pp.1-12.

Paetsch, L., Mueller, C.W., K€ogel-Knabner, I., Lützow, M., Girardin, C., Rumpel, C., 2018. Effect of in-situ aged and fresh biochar on soil hydraulic conditions and microbial C use under drought conditions. Sci. Rep. 8 (1), 6852.

Pardo, G.S., Sarmah, A.K., Orense, R.P., 2018. Mechanism of improvement of biochar

Pauchard, L., Parisse, F. and Allain, C., 1999. Influence of salt content on crack patterns formed through colloidal suspension desiccation. Physical Review E, 59(3), p.3737.

Pejic, B.M., Kostic, M.M., Skundric, P.D. and Praskalo, J.Z., 2008. The effects of hemicelluloses and lignin removal on water uptake behavior of hemp fibers. Bioresource Technology, 99(15), pp.7152-7159.

Peng, X., Zhang, Z.B., Gan, L. and Yoshida, S., 2016. Linking soil shrinkage behavior and cracking in two paddy soils as affected by wetting and drying cycles. Soil Science Society of America Journal, 80(5), pp.1145-1156.

Penman, H.L., 1948. Natural evaporation from open water, bare soil and grass. Proceedings of the Royal Society of London. Series A. Mathematical and Physical Sciences, 193(1032), pp.120-145.

Pérez, J., Munoz-Dorado, J., De la Rubia, T.D.L.R. and Martinez, J., 2002. Biodegradation and biological treatments of cellulose, hemicellulose and lignin: an overview. International microbiology, 5(2), pp.53-63.

Peron, H., Hueckel, T., Laloui, L. and Hu, L., 2009. Fundamentals of desiccation cracking of fine-grained soils: experimental characterisation and mechanisms identification. Canadian Geotechnical Journal, 46(10), pp.1177-1201.

Perret, J.S., Al-Belushi, M.E. and Deadman, M., 2007. Non-destructive visualization and quantification of roots using computed tomography. Soil Biology and Biochemistry, 39(2), pp.391-399.

Peters, R.R., and Klavetter, E.A. 1988. “A continuum model for water movement in an unsaturated fractured rock mass.” Water Resour. Res. 24(3): 416–430. https://doi.org/10.1029/wr024i003p00416

Pham, H.Q. and Fredlund, D.G., 2008. Equations for the entire soil-water characteristic curve of a volume change soil. Canadian Geotechnical Journal, 45(4), pp.443-453.

Poë, S., Stovin, V. and Berretta, C., 2015. Parameters influencing the regeneration of a green roof’s retention capacity via evapotranspiration. Journal of Hydrology, 523, pp.356-367.

Pourakbar, S., Huat, B.B., Asadi, A. and Fasihnikoutalab, M.H., 2016. “Model study of alkali-activated waste binder for soil stabilization.” International Journal of Geosynthetics and Ground Engineering. 2(4): 35. https://doi.org/10.1007/s40891-016-0075-1

Prabakar, J. and Sridhar, R.S., 2002. Effect of random inclusion of sisal fibre on strength behaviour of soil. Construction and Building Materials, 16(2), pp.123-131.

Rai, R. and Shrivastva, B.K., 2012. “Effect of grass on soil reinforcement and shear strength.” Proceedings of the Institution of Civil Engineers-Ground Improvement, 165(3): 127-130. https://doi.org/10.1680/grim.10.00001

Ramaswamy, H.S., Ahuja, B.M. and Krishnamoorthy, S., 1983. Behaviour of concrete reinforced with jute, coir and bamboo fibres. International Journal of Cement Composites and Lightweight Concrete, 5(1), pp.3-13.

Ramesh, H.N., Manoj, K. and Mamatha, H.V., 2010. Compaction and strength behavior of lime-coir fiber treated Black Cotton soil. Geomechanics and Engineering, 2(1), pp.19-28.

Rasband, W.S., 2011. “ImageJ.” US National Institutes of Health, Bethesda, 616 Maryland, USA.

Rashdi, A.A.A., Sapuan, S.M., Ahmad, M.M.H.M. and Khalina, A., 2009. Water absorption and tensile properties of soil buried kenaf fibre reinforced unsaturated polyester composites (KFRUPC). Journal of food, agriculture & environment.

Rawal, A. and Sayeed, M.M.A., 2014. Tailoring the structure and properties of jute blended nonwoven geotextiles via alkali treatment of jute fibers. Materials & Design, 53, pp.701-705.

Rayhani, M.H.T., Yanful, E.K. and Fakher, A., 2008. “Physical modeling of desiccation cracking in plastic soils.” Eng. Geol. 97(1): 25-31. https://doi.org/10.1016/j.enggeo.2007.11.003

Reddy, K.R., Yaghoubi, P. and Yukselen-Aksoy, Y., 2015. Effects of biochar amendment on geotechnical properties of landfill cover soil. Waste Management & Research, 33(6), pp.524-532.

Reddy, N. and Yang, Y., 2005. Biofibers from agricultural byproducts for industrial applications. TRENDS in Biotechnology, 23(1), pp.22-27.

Reddy, V. and Jagadish, K.S., 1993. The static compaction of soils. Géotechnique, 43(2), pp.337-41.

Reynolds, W.D. and Elrick, D.E., 1991. Determination of hydraulic conductivity using a tension infiltrometer. Soil Science Society of America Journal, 55(3), pp.633-639.

Rezaei, M., Seuntjens, P., Joris, I., Boënne, W., Van Hoey, S., Campling, P. and Cornelis, W.M., 2015. Sensitivity of water stress in a two-layered sandy grassland soil to variations in groundwater depth and soil hydraulic parameters. Hydrology & Earth System Sciences Discussions, 12(7).

Rodríguez-Vila, A., Selwyn-Smith, H., Enunwa, L., Smail, I., Covelo, E.F. Sizmur, T., 2018. Predicting Cu and Zn sorption capacity of biochar from feedstock C/N ratio and pyrolysis temperature. Environ. Sci. Poll. Res. 25(8), 7730-7739.

Ross, P.J., 1990. Efficient numerical methods for infiltration using Richards' equation. Water Resources Research, 26(2), pp.279-290.

Roure, F., GECO INGENIERIE, 2013. Method and device for producing a nonwoven geotextile, and geotextile thus produced. U.S. Patent Application 14/003,930.

Rowell, R.M. and Banks, W.B., 1985. Water repellency and dimensional stability of wood. Gen. Tech. Rep. FPL-50. Madison, WI: US Department of Agriculture, Forest Service, Forest Products Laboratory; 1985: 24 pages, 50.

Rowell, R.M. and Stout, H.P., 2007. Jute and kenaf. Handbook of fiber chemistry. Boca Raton: CRC/Taylor & Francis, c2007. International fiber science and technology series; 16: Pages 409-456.

Rowell, R.M., 2000. Characterization and factors effecting fiber properties. Natural polymers and agrofibers based composites.

Sadasivam, B.Y., Reddy, K.R., 2015a. Adsorption and transport of methane in biochars derived from waste wood. Waste Manage. 43, 218-229.

Sadasivam, B.Y., Reddy, K.R., 2015b. Adsorption and transport of methane in landfill cover soil amended with waste-wood biochars. J Environ Manage. 158, 11-23.

Sapuan, S.M., Pua, F.L., El-Shekeil, Y.A. and AL-Oqla, F.M., 2013. Mechanical properties of soil buried kenaf fibre reinforced thermoplastic polyurethane composites. Materials & Design, 50, pp.467-470.

Saran, S., 2011. Reinforced soil and its engineering applications. IK International Pvt Ltd.

Sarika, D., Singh, J., Prasad, R., Vishan, I., Varma, V.S. and Kalamdhad, A.S., 2014. Study of physico-chemical and biochemical parameters during rotary drum composting of water hyacinth. International Journal of Recycling of Organic Waste in Agriculture, 3(3), p.9.

Sarsby, R.W., 2007. Use of 'Limited Life Geotextiles'(LLGs) for basal reinforcement of embankments built on soft clay. Geotextiles and Geomembranes, 25(4-5), pp.302-310.

Scallan, A.M., 1983. The effect of acidic groups on the swelling of pulps: a review. Tappi journal, 66(11), pp.73-75.

Scanlan, C.A. and Hinz, C., 2010, August. Insights into the processes and effects of root-induced changes to soil hydraulic properties. In Proceedings of the 19th world congress of soil science, soil solutions for a changing world, Brisbane, Australia (Vol. 2, pp. 41-44).

Schilling, K.H., Freeman, D. and McPherson, R.E., Grain Processing Corp, 2006. Dust suppressant and soil stabilization composition. U.S. Patent 7,070,709.

Schmidt, K.M., Roering, J.J., Stock, J.D., Dietrich, W.E., Montgomery, D.R. and Schaub, T., 2001. The variability of root cohesion as an influence on shallow landslide susceptibility in the Oregon Coast Range. Canadian Geotechnical Journal, 38(5), pp.995-1024.

Schneider, C.A., Rasband, W.S. and Eliceiri, K.W., 2012. NIH Image to ImageJ: 25 years of image analysis. Nature methods, 9(7), p.671.

Schnürer, J. and Rosswall, T., 1982. Fluorescein diacetate hydrolysis as a measure of total microbial activity in soil and litter. Appl. Environ. Microbiol., 43(6), pp.1256-1261.

Scholl, P., Leitner, D., Kammerer, G., Loiskandl, W., Kaul, H.P. and Bodner, G., 2014. Root induced changes of effective 1D hydraulic properties in a soil column. Plant and soil, 381(1-2), pp.193-213.

Scoffoni, C., Chatelet, D.S., Pasquet-kok, J., Rawls, M., Donoghue, M.J., Edwards, E.J. and Sack, L., 2016. Hydraulic basis for the evolution of photosynthetic productivity. Nature plants, 2(6), p.16072.

Sebastian, B., Cryus, S. and Jose, B.T., 2011, December. Effect of inclusion of coir fibre on the shear strength of marine clay. In Proceedings of Indian Geotechnical Conference, Dec(pp. 15-17).

Segetin, M., Jayaraman, K. and Xu, X., 2007. Harakeke reinforcement of soil–cement building materials: manufacturability and properties. Building and environment, 42(8), pp.3066-3079.

Shackley, S., Carter, S., Knowles, T., Middelink, E., Haefele, S., Sohi, S., Cross, A. and Haszeldine, S., 2012. Sustainable gasification–biochar systems? A case-study of rice-husk gasification in Cambodia, Part I: Context, chemical properties, environmental and health and safety issues. Energy Policy, 42, pp.49-58.

Sharma, R.B. and Verma, G.P., 1977. Characterization of shrinkage cracks in medium black clay soil of Madhya Pradesh. Plant and Soil, 48(2), pp.323-333.

Shen, L., Haufe, J. and Patel, M.K., 2009. Product overview and market projection of emerging bio-based plastics PRO-BIP 2009. Report for European polysaccharide network of excellence (EPNOE) and European bioplastics, 243.

Shen, T., Tang, Y., Lu, X.Y., Meng, Z., 2018. Mechanisms of copper stabilization by mineral constituents in sewage sludge biochar. J. Clean. Prod. 193, 185e193

Shin, H. and Santamarina, J.C., 2011. Desiccation cracks in saturated fine-grained soils: particle-level phenomena and effective-stress analysis. Géotechnique, 61(11), p.961.

Shoeb, F. and Singh, H.J., 2000. Kinetic studies of biogas evolved from water hyacinth. Proceedings of Agroenviron.

Shokri, N., Zhou, P. and Keshmiri, A., 2015. Patterns of desiccation cracks in saline bentonite layers. Transport in Porous Media, 110(2), pp.333-344.

Shuttleworth, W.J., 2007. Putting the" vap" into evaporation. Hydrology and Earth System Sciences Discussions, 11(1), pp.210-244.

Sinnathamby, G., Phillips, D.H., Sivakumar, V. and Paksy, A., 2014. Landfill cap models under simulated climate change precipitation: impacts of cracks and root growth. Géotechnique, 64(2), p.95.

Siqueira, G., Bras, J. and Dufresne, A., 2010. Cellulosic bionanocomposites: a review of preparation, properties and applications. Polymers, 2(4), pp.728-765.

Smethurst, J.A., Briggs, K.M., Powrie, W., Ridley, A. and Butcher, D.J.E., 2015. Mechanical and hydrological impacts of tree removal on a clay fill railway embankment. Géotechnique, 65(11), pp.869-882.

Smethurst, J.A., Clarke, D. and Powrie, W., 2006. Seasonal changes in pore water pressure in a grass covered cut slope in London Clay. Géotechnique, 56(8), pp.523-537.

Smettem, K.R.J. and Clothier, B.E., 1989. Measuring unsaturated sorptivity and hydraulic conductivity using multiple disc permeameters. Journal of Soil Science, 40(3), pp.563-568.

Song, L., Li, J.H., Zhou, T. and Fredlund, D.G., 2017. "Experimental study on unsaturated hydraulic properties of vegetated soil." Ecological Engineering 103: 207-216. https://doi.org/10.1016/j.ecoleng.2017.04.013

Song, W.K., Cui, Y.J., Tang, A.M., Ding, W.Q. and Wang, Q., 2016. Experimental study on water evaporation from compacted clay using environmental chamber. Canadian Geotechnical Journal, 53(8), pp.1293-1304.

Spiegelberg, H.L., 1966. The effect of hemicelluloses on the mechanical properties of individual pulp fibers (Doctoral dissertation, Georgia Institute of Technology).

Sreekala, M.S. and Thomas, S., 2003. "Effect of fibre surface modification on water-sorption characteristics of oil palm fibres." Composite Science Technology 63(6): 861-869. https://doi.org/10.1016/s0266-3538(02)00270-1

Stone, J.E. and Scallan, A.M., 1965. The Influence of Drying on the Pore Structure of the Cell Wall. Pulp and Paper Research Institute of Canada.

Subaida, E.A., Chandrakaran, S. and Sankar, N., 2008. Experimental investigations on tensile and pullout behaviour of woven coir geotextiles. Geotextiles and Geomembranes, 26(5), pp.384-392.

Subaida, E.A., Chandrakaran, S. and Sankar, N., 2009. Laboratory performance of unpaved roads reinforced with woven coir geotextiles. Geotextiles and Geomembranes, 27(3), pp.204-210.

Talbot, J.R. and Deal, C.E., 1993, April. Rehabilitation of cracked embankment dams. In Geotechnical Practice in Dam Rehabilitation (pp. 267-283). ASCE.

Taleisnik, E., Peyrano, G., Cordoba, A. and Arias, C., 1999. Water retention capacity in root segments differing in the degree of exodermis development. Annals of Botany, 83(1), pp.19-27.

Tang CS, Shi B, Zhao LZ. 2010. Interfacial shear strength of fiber reinforced soil. Geotextiles and Geomembranes. 28(1):54-62. https://doi.org/10.1016/j.geotexmem.2009.10.001

Tang, C., Shi, B., Gao, W., Chen, F. and Cai, Y., 2007. Strength and mechanical behavior of short polypropylene fiber reinforced and cement stabilized clayey soil. Geotextiles and Geomembranes, 25(3), pp.194-202.

Tang, C.S., Shi, B. and Zhao, L.Z., 2010. Interfacial shear strength of fiber reinforced soil. Geotextiles and Geomembranes, 28(1), pp.54-62.

Tang, C.S., Shi, B., Cui, Y.J., Liu, C. and Gu, K., 2012. Desiccation cracking behavior of polypropylene fiber–reinforced clayey soil. Canadian Geotechnical Journal, 49(9), pp.1088-1101.

Tang, C.S., Shi, B., Liu, C., Gao, L. and Inyang, H.I., 2010. Experimental investigation of the desiccation cracking behavior of soil layers during drying. Journal of Materials in Civil Engineering, 23(6), pp.873-878.

Tang, C.S., Wang, D.Y., Cui, Y.J., Shi, B. and Li, J., 2016. Tensile strength of fiber-reinforced soil. Journal of Materials in Civil Engineering, 28(7), p.04016031.

TAPPI T222 om-88, Acid-Insoluble Lignin in Wood and Pulp, Klason Lignin, TAPPI, Peachtree Corners, GA, 1996.

Tarantino, A. 2010. "Unsaturated soils: compacted versus reconstituted states." Proc. of 5th International Conference of Unsaturated Soils, Barcelona, Spain, 113 – 136. 6 – 8 Sep 2010. https://doi.org/10.1201/b10526-9

Thiruchitrambalam, M., Athijayamani, A., Sathiyamurthy, S. and Thaheer, A.S.A., 2010. A review on the natural fiber-reinforced polymer composites for the development of roselle fiber-reinforced polyester composite. Journal of Natural Fibers, 7(4), pp.307-323.

Thomas, G.W., 1982. Exchangeable cations. Methods of soil analysis. Part 2. Chemical and microbiological properties. Methodsofsoilan2 159e165.

Trabelsi, H., Jamei, M., Zenzri, H. and Olivella, S., 2012. Crack patterns in clayey soils: experiments and modeling. International Journal for Numerical and Analytical methods in geomechanics, 36(11), pp.1410-1433.

Traoré, O., Groleau-Renaud, V., Plantureux, S., Tubeileh, A. and Boeuf-Tremblay, V., 2000. Effect of root mucilage and modelled root exudates on soil structure. European journal of soil science, 51(4), pp.575-581.

Tripathy, S., Al-Khyat, S., Cleall, P.J., Baille, W. and Schanz, T., 2016. Soil suction measurement of unsaturated soils with a sensor using fixed-matrix porous ceramic discs. Indian Geotechnical Journal, 46(3), pp.252-260.

Ulyett, J., Sakrabani, R., Kibblewhite, M. and Hann, M., 2014. Impact of biochar addition on water retention, nitrification and carbon dioxide evolution from two sandy loam soils. European Journal of Soil Science, 65(1), pp.96-104.

Vadivambal, R., Vellaichamy, C., Jian, F. and Jayas, D., 2015. Tensile strength and elongation of hemp and sisal ropes at different temperatures. Can. Biosyst. Eng, 57(1).

Valadez-Gonzalez, A., Cervantes-Uc, J.M., Olayo, R.J.I.P. and Herrera-Franco, P.J., 1999. Effect of fiber surface treatment on the fiber–matrix bond strength of natural fiber reinforced composites. Composites Part B: Engineering, 30(3), pp.309-320.

Van der Walt, S., Schönberger, J.L., Nunez-Iglesias, J., Boulogne, F., Warner, J.D., Yager, N., Gouillart, E. and Yu, T., 2014. scikit-image: image processing in Python. PeerJ, 2, p.e453.

Van Genuchten, M.T., 1980. A closed-form equation for predicting the hydraulic conductivity of unsaturated soils 1. Soil science society of America journal, 44(5), pp.892-898.

Van Genuchten, M.T., Leij, F.J. and Yates, S.R., 1991. "The RETC code for quantifying the hydraulic functions of unsaturated soils." USDA, US Salinity Laboratory, Riverside, CA. United States Environmental Protection Agency. document EPA/600/2-91/065.

Vanapalli, S.K., Fredlund, D.G., Pufahl, D.E. and Clifton, A.W., 1996. Model for the prediction of shear strength with respect to soil suction. Canadian Geotechnical Journal, 33(3), pp.379-392.

Vanapalli, S.K., Sillers, W.S. and Fredlund, M.D., 1998, October. The meaning and relevance of residual state to unsaturated soils. In Proceedings of the 51st Canadian Geotechnical Conference, Edmonton, Alta (pp. 4-7).

Vandervaere, J.P., Vauclin, M. and Elrick, D.E., 2000a. Transient flow from tension infiltrometers I. The two-parameter equation. Soil Science Society of America Journal, 64(4), pp.1263-1272.

Vandervaere, J.P., Vauclin, M. and Elrick, D.E., 2000b. Transient flow from tension infiltrometers II. Four methods to determine sorptivity and conductivity. Soil Science Society of America Journal, 64(4), pp.1272-1284.

Vannoppen, W., Vanmaercke, M., De Baets, S. and Poesen, J., 2015. A review of the mechanical effects of plant roots on concentrated flow erosion rates. Earth-Science Reviews, 150, pp.666-678.

Vardhan H, Bordoloi S, Garg A, Garg A. 2017. "Compressive strength analysis of soil reinforced with fiber extracted from water hyacinth." Eng. Computation. 34(2): 330-342 https://doi.org/10.1108/ec-09-2015-0267

Ververis, C., Georghiou, K., Christodoulakis, N., Santas, P. and Santas, R., 2004. Fiber dimensions, lignin and cellulose content of various plant materials and their suitability for paper production. Industrial crops and products, 19(3), pp.245-254.

Vidal, H., The principle of reinforced earth. Highway research record, (282) 1969.

Vo, T.D., Pouya, A., Hemmati, S. and Tang, A.M., 2017. "Numerical modelling of desiccation cracking of clayey soil using a cohesive fracture method." Comput. Geotech. 85: 15-27. https://doi.org/10.1016/j.compgeo.2016.12.010

Wadell, H., 1935. Volume, shape, and roundness of quartz particles. The Journal of Geology, 43(3), pp.250-280.

Wambua, P., Ivens, J. and Verpoest, I., 2003. Natural fibres: can they replace glass in fibre reinforced plastics? Composites science and technology, 63(9), pp.1259-1264.

Wathén, R., 2006. Studies on fiber strength and its effect on paper properties.

Weber, K., & Quicker, P., 2018. Properties of biochar. Fuel. 217, 240-261

Weerawatsophon, U., Sumransin, N., Prahsarn, C. and Bergado, D.T., 2010. Properties and potential application of the selected natural fibers as limited life geotextiles. Carbohydrate Polymers, 82(4), pp.1090-1096.

Widdel, F. and Rabus, R., 2001. Anaerobic biodegradation of saturated and aromatic hydrocarbons. Current opinion in biotechnology, 12(3), pp.259-276.

Wong, J.T.F., Chen, Z., Chen, X., Ng, C.W.W. and Wong, M.H., 2017. Soil-water retention behavior of compacted biochar-amended clay: a novel landfill final cover material. Journal of soils and sediments, 17(3), pp.590-598.

Wong, J.T.F., Chen, Z., Ng, C.W.W. and Wong, M.H., 2016. Gas permeability of biochar-amended clay: potential alternative landfill final cover material. Environmental Science and Pollution Research, 23(8), pp.7126-7131.

Wong, J.T.F., Chen, Z., Wong, A.Y.Y., Ng, C.W.W. and Wong, M.H., 2018. Effects of biochar on hydraulic conductivity of compacted kaolin clay. Environmental Pollution, 234, pp.468-472.

Wooding, R.A., 1968. Steady infiltration from a shallow circular pond. Water resources research, 4(6), pp.1259-1273.

Wu, Y.K., Li, Y.B. and Niu, B., 2014. Investigation of mechanical properties of randomly distributed sisal fibre reinforced soil. Materials Research Innovations, 18(sup2), pp.S2-953.

Yalley, P.P. and Kwan, A.S.K., 2008. Use of waste and low energy materials in building block construction. In 25th Conference on Passive and Low Energy Architecture (PLEA), Dublin, 22nd to 24th October.

Yamaguchi, J. and Tanaka, A., 1990. Quantitative observation on the root system of various crops growing in the field. Soil Science and Plant Nutrition, 36(3), pp.483-493.

Yang, S., Li, B., Zheng, J. and Kankala, R.K., 2018. Biomass-to-Methanol by dual-stage entrained flow gasification: Design and techno-economic analysis based on system modeling. Journal of Cleaner Production, 205, pp.364-374.

Yargicoglu, E.N. and Reddy, K.R., 2017. Microbial abundance and activity in biochar-amended landfill cover soils: evidence from large-scale column and field experiments. Journal of Environmental Engineering, 143(9), p.04017058.

Yargicoglu, E.N., Reddy, K.R., 2015. Review of biological diagnostic tools and their applications in geoenvironmental engineering. Rev. Environ. Sci. Biotechnol. 14 (2), 161e194.

Yargicoglu, E.N., Reddy, K.R., 2017. Biochar-amended soil cover for microbial methane oxidation: effect of biochar amendment ratio and cover profile. J. Geotech. Geoenviron. Eng. 144 (3), 04017123.

Yesiller, N., Miller, C.J., Inci, G. and Yaldo, K., 2000. Desiccation and cracking behavior of three compacted landfill liner soils. Engineering Geology, 57(1-2), pp.105-121.

Yetimoglu, T. and Salbas, O., 2003. A study on shear strength of sands reinforced with randomly distributed discrete fibers. Geotextiles and Geomembranes, 21(2), pp.103-110.

Yetimoglu, T., Inanir, M. and Inanir, O.E., 2005. A study on bearing capacity of randomly distributed fiber-reinforced sand fills overlying soft clay. Geotextiles and Geomembranes, 23(2), pp.174-183.

Yong, R.N. and Warkentin, B.P., 1975. "Soil Properties and Behavior." Elsevier. New York.

Yoshida, S. and Adachi, K., 2001a. Analysis of generation of linear inter-row cracks using numerical model. Transactions of the Japanese Society of Irrigation, Drainage and Reclamation Engineering (Japan).

Yoshida, S. and Adachi, K., 2001b. Effects of cropping and puddling practices on the cracking patterns in paddy fields. Soil science and plant nutrition, 47(3), pp.519-532.

Yoshida, S. and Adachi, K., 2004. Numerical analysis of crack generation in saturated deformable soil under row-planted vegetation. Geoderma, 120(1-2), pp.63-74.

Yusoff, M.Z.M., Salit, M.S., Ismail, N. and Wirawan, R., 2010. Mechanical properties of short random oil palm fibre reinforced epoxy composites. Sains Malaysiana, 39(1), pp.87-92.

Zama, E.F., Reid, B.J., Arp, H.P.H., Sun, G.X., Yuan, H.Y. and Zhu, Y.G., 2018a. Advances in research on the use of biochar in soil for remediation: a review. Journal of Soils and Sediments, 18, pp.2433-2450.

Zama, E.F., Reid, B.J., Sun, G.X., Yuan, H.Y., Li, X.M., Zhu, Y.G., 2018b. Silicon (Si) biochar for the mitigation of arsenic (As) bioaccumulation in spinach (Spinacia oleracean) and improvement in the plant growth. Journal of Cleaner Production 189, 386e395

Zhan, T.L., Ng, C.W. and Fredlund, D.G., 2007. Field study of rainfall infiltration into a grassed unsaturated expansive soil slope. Canadian Geotechnical Journal, 44(4), pp.392-408.

Zhang, R., 1997a. Determination of soil sorptivity and hydraulic conductivity from the disk infiltrometer. Soil Science Society of America Journal, 61(4), pp.1024-1030.

Zhang, R., 1997b. Infiltration models for the disk infiltrometer. Soil Science Society of America Journal, 61(6), pp.1597-1603.

Zhang, X.D., Chen, Y.G., Ye, W.M., Cui, Y.J., Deng, Y.F. and Chen, B., 2017. Effect of salt concentration on desiccation cracking behavior of GMZ bentonite. Environmental Earth Sciences, 76(15), p.531.

Zhou, C. and Wu, Q., 2012. Recent development in applications of cellulose nanocrystals for advanced polymer-based nanocomposites by novel fabrication strategies. In Nanocrystals-synthesis, characterization and applications. Intech.

ZHOU, Y., CHEN, J. and WANG, X., 2009. Research on Resistance Cracking and Enhancement Mechanism of Plant Root in Slope Protection by Vegetation [J]. Journal of Wuhan University (Natural Science Edition), 5.

Zong, Y., Chen, D. and Lu, S., 2014. Impact of biochars on swell–shrinkage behavior, mechanical strength, and surface cracking of clayey soil. Journal of Plant Nutrition and Soil Science, 177(6), pp.920-926.

List of publications from this work

JOURNAL PUBLICATION ACCEPTED/PUBLISHED

1. **Bordoloi, S.,** Hussain, R., Gadi, V.K., Bora, H., Sahoo, L., Karangat, R., Garg, A., and Sreedeep S., Monitoring soil cracking and plant parameters for mixed grass species. **Geotechnique Letters,** 2018. Vol.8, Issue 1. **(ICE) (*Impact Factor: 2.05*) (H-Index: 18)** (**DOI: https://doi.org/10.1680/jgele.17.00145) (Q1 journal)**

2. **Bordoloi, S.,** Gadi, V.K., Hussain, R., Leung, A.K., Garg, A., and Sreedeep S., Water retention and desiccation potential of lignocellulose based fiber reinforced soil. **Journal of Geotechnical and Geo-Environmental Engineering, (ASCE) (*Impact Factor: 2.4*) (H-Index: 114) (Q1 journal) (*Accepted*) (Q1 journal)**

3. **Bordoloi,** S., Gadi, V.K., Hussain, R., Garg, A., Sreedeep S., Mei, G., and Poulsen, T. Influence of fiber from waste weed Eichhornia Crassipes on water retention and cracking characteristics of vegetated soils. **Geotechnique Letters**, 2018. **(ICE) (*Impact Factor: 2.05*) (H-Index: 18) (DOI: https://doi.org/10.1680/jgele.17.00181) (Q1 journal)**

4. **Bordoloi S**, Yamsani SK, Garg A, Sreedeep S. Critical assessment of infiltration measurements for soils with varying fine content using mini disk infiltrometer. **Journal of Testing and Evaluation**. 2018. May 3;47(2) (**ASTM**) **(*Impact Factor: 0.72*) (H-Index: 29) (DOI: 10.1520/jte20170328) (Q2 journal)**

5. **Bordoloi S**, Garg A, Sreedeep S, Peng L, Mei G. Investigation of cracking and water availability of soil-biochar composite synthesized from invasive weed water hyacinth. 2018 May 3. **Bioresource Technology. (Elsevier) (*Impact Factor: 5.98*) (H-Index: 229) (DOI: https://doi.org/10.1016/j.biortech.2018.05.011) (Q1 journal)**

6. Alammyan, A., Gadi, V; **Bordoloi, S**., Kothapalli, SK., Sreedeep. S., Mei, G., and Garg, A. An autonomous algorithm customized for evaluating surface cracks in an unsaturated soil in 1-D Column. **Journal of Testing and Evaluation**. (**ASTM**) **(*Impact Factor: 0.72*) (H-Index: 29) (doi:10.1520/JTE20180609) (Q2 journal)**

7. **Bordoloi S**, Yamsani SK, Garg A, Sreedeep S, Borah S. Study on the efficacy of harmful weed species Eicchornia crassipes for soil reinforcement. **Ecological Engineering**. 2015 Dec 31; 85:218-22. (**Elsevier**) **(*Impact Factor: 3.43*) (H-Index: 101) (DOI: https://doi.org/10.1016/j.ecoleng.2015.09.082) (Q1 journal)**

8. **Bordoloi S**, Garg A, Sreedeep S. Potential of Uncultivated, Harmful and Abundant Weed as a Natural Geo-Reinforcement Material. **Advances in Civil Engineering Materials**. 2016 Dec 28;5(1):276-88., (**ASTM**) **(*Impact Factor: 0.4)* (H-Index: 3) (DOI: https://doi.org/10.1520/ACEM20160012) (Q2 journal)**

9. **Bordoloi, S**., Garg, A., and Sekharan, S., A Review of Physio-Biochemical Properties of Natural Fibers and Their Application in Soil Reinforcement. **Advances in Civil Engineering Materials**, Vol. 6, No. 1, 2017, pp. 323–359 (**ASTM**) **(*Impact Factor: 0.4)* (H-Index: 3) (DOI: https://doi.org/10.1520/ACEM20160076) (Q2 journal)**

10. **Bordoloi, S**., Sen, S., Hussain, R., Garg, A., and Sreedeep S. Chemically Altered Natural Fiber Impregnated Soil for Improving Subgrade Strength of Pavements. **Advances in Civil Engineering Materials**. 2017 **(ASTM) (*Impact Factor: 0.4)* (H-Index: 3) (DOI: https://doi.org/10.1520/ACEM20170042) (Q2 journal)**

11. **Bordoloi S**, Kashyap V, Garg A, Sreedeep S, Wei L, Andriyas S. Measurement of mechanical characteristics of fiber from a novel invasive weed: A comprehensive comparison with fibers from agricultural crops. **Measurement**. 2018 Jan 1; 113:62-70.

(**Elsevier**) ***(Impact Factor: 2.3)*** **(H-Index:61) (DOI: https://doi.org/10.1016/j.measurement.2017.08.044) (Q1 journal)**

12. **Bordoloi S**, Hussain R, Garg A, Sreedeep S, Zhou WH. Infiltration characteristics of natural fiber reinforced soil. **Transportation Geotechnics**. 2017 Sep 1; 12:37-44. (**Elsevier**) ***(Impact Factor: 1.15)*** **(H-Index:11) (DOI: https://doi.org/10.1016/j.trgeo.2017.08.007) (Q1 journal)**

BOOK CHAPTER

1. Sreedeep S., Gadi, V.K., **Bordoloi, S.**, Saha, A., Kumar, H., Hazra, B., and Garg, A. Sustainable Geotechnics: A Bio-geotechnical Perspective. In "Frontiers in Geotechnical Engineering". **ISBN 978-981-13-5871-5 (Due: April 18, 2019)** (**Springer**)

2. **Bordoloi, S.**, Shaikh, J., Sreedeep S. and Garg, A. Biochar amended soil as surface cover soil for geo-environmental applications. In "Biochar: Fundamentals and Applications in Environmental Science and Remediation Technologies". Volume 6. (**Elsevier**) (***Under review***)

PATENT

- A novel use of a harmful invasive weed-water hyacinth for increasing the mechanical strength of rural road embankment (**Patent No.- 2018012201142190**)
- A new PYTHON Code for computing cracking in unsaturated soils (**Patent No.- 2018042401940100**)
- Synthesis of biochar from invasive weed for suppressing desiccation of soils (**Patent No.- 2018042501521500**)

PEER REVIEWED CONFERENCES

- **Bordoloi, S**., Patwa, D., Hussain, R., Garg, A., and Sreedeep S., Nano-Particle Coated Natural Fiber Impregnated Soil as a Sustainable Reinforcement Material. **ASCE India Conference 2017**, December,2017. (DOI: 10.1061/9780784482032.044)

- Hussain, R., **Bordoloi, S**., Gadi, V.K., Garg, A., Karangat, R., and Sreedeep S. Effect of filament type and biochemical composition of lignocellulose fiber in vegetation growth in early plant establishment period. **Indian Geotechnical Conference 2018**. December, 2018.